Alma Mater Studiorum – Università di Bologna

DOTTORATO DI RICERCA IN

Beni Culturali e Ambientali

Ciclo XXXVI

Settore Concorsuale: 03/A1 - CHIMICA ANALITICA

Settore Scientifico Disciplinare: CHIM/12 - CHIMICA DELL'AMBIENTE E DEI BENI CULTURALI

Radiocarbon and stable isotopes in the shell organic matrix: A new approach for the use of mollusk shells in the study of human evolution.

Presentata da: Dragana Paleček

Coordinatrice di Dottorato

Prof.ssa Donatella Restani

Supervisore

Prof.ssa Sahra Talamo

Co-Supervisore

Prof.ssa Silvia Prati

Esame finale anno 2024

ACKNOWLEDGEMENTS

This Ph. D. project is funded by the European Research Council under the European Union's Horizon 2020 Research and Innovation Programme (grant agreement no. 803147 RESOLUTION, https://site.unibo.it/resolution-erc/en) and the Departments of Environmental and cultural heritage and Chemistry "Giacomo Ciamician" of the University of Bologna.

This work wouldn't have been possible without my supervisor Prof. Sahra Talamo, who has been there every step of the way, giving me support and helping me learn and make this thesis the best it can be. Thank you so much for sticking with me through the good times and the bad, and for having my back even when you did not necessarily agree with me. You have helped build the person I am today in many ways, and I will always be grateful for all the opportunities you gave me.

I would also like to thank Dr. Dr. Bernd Kromer, for all the enthusiasm, help and willingness to share his knowledge and all the interesting and useful papers he would send throughout the years.

A big thank you also goes to all the members of the RESOLUTION team and our collaborators, especially Dr. Michael Friedrich and Dr. Lukas Wacker.

Many thanks to Dr. Stefania Milano, who welcomed me to the IZW institute in Berlin and taught me so much. Thank you for the help during my stay in Berlin, and afterwards throughout the process of writing the thesis chapter and manuscript.

I would like to thank all the co-authors on the thesis chapters/manuscripts for their contributions and support in performing the analyses and writing the manuscripts, Prof. Giuseppe Falini, Prof. Nuno Bicho, Dr. João Cascalheira, Prof. Marcello A. Mannino, Prof. Daniele Fabbri, Dr. Alessandro G. Rombolà and Prof. Igor Gutiérrez-Zugasti. Furthermore, I would like to thank Prof. Enrico Dinelli and Prof. Giorgio Gasparotto for lending me their sample mill to grind the shell samples used for this thesis.

A special thanks goes to my colleagues from the BRAVHO lab, Silvia Cercatillo, Laura Tassoni, Alice Zurzolo, Enrico Pelloni and Mike Thomas for their constant support and invaluable friendship in these years. Their help and care meant so much to me, and the love and friendships will stay with me for the rest of my life.

Silvia, you have been there from the beginning making every day better and helping me through the learning process when I was starting, giving me advice and support whenever I needed it. Thank you!

Laura, you have been my savior and advisor more times than I can count, and there are not enough words in any language to express how grateful I am for and to you.

Enrico, you brought so much joy and laughter to the team and were always there when I needed a hug. Your energy and presence were so refreshing, and I am so thankful for and to you.

Mike, our Belgian chocolate, maple syrup and all ‘round sweet guy, thank you for all the jokes, laughter and of course all the help with rephrasing and rewording the long and awkward sentences in this thesis.

Alice, thank you for the help and advice, the endless laughs, jokes, and support during these last months of my PhD journey. You brought a new energy to the lab, which I am happy to keep near me in the future.

Finally, I dedicate this thesis to my family who made arriving to this moment possible by allowing me to find my way, grow and learn. To my parents, brother, and grandparents, for their love and support, for always believing in me and being there to advise me on anything and everything. To David, who has shared all the ups and downs, the celebrations, and frustrations, and who has been my pillar, holding me up and pushing me to be the best I can be every day. To Shiro, who made every bad moment a good one, just by being there. To my soon-to-be in-laws and to all my friends, for their love and support.

Thank you!

ABSTRACT

This Ph.D. project has the aim of adding a contribution to the study of human evolution through the application of radiocarbon dating and stable isotope analyses to mollusk shells. The constant improvements to these techniques over the years have allowed archeologists and sclerochronologists to continuously obtain more precise information, allowing them to make better interpretations and reconstructions of the events taking place throughout the evolutionary history of ours, and other human species. Researchers use these techniques to obtain information about human activity through the combination of radiocarbon dates and environmental reconstructions obtained over large geographical and temporal ranges. The construction of radiocarbon chronologies and environmental estimates for a single archeological site allows for the interpretation of the timing of occupation and activities performed at the site and area in question. However, once such information is available over a large geographical scale, it is possible to interpret human migration patterns, their interactions, adaptations, and cultural exchange. The refinement of these methods is especially important for the transition from the Middle to the Upper Paleolithic when the first groups of *Homo sapiens* arrive and disperse into Europe encountering Neanderthal populations.

Mollusk shells are often found in archeological sites, given their great preservation potential and high value as a multipurpose resource. They are often the only available material to use for radiocarbon dating, due to a lack of well-preserved bones in many archeological sites, especially for the key period of the Middle to Upper Paleolithic transition. However, radiocarbon dating on mollusk shells is often regarded as less reliable compared to bones, wood, or charcoals due to the various factors influencing their radiocarbon content (e.g., Isotope fractionation, marine reservoir effect etc.). For the development of more accurate chronologies using shells, it is fundamental to continue improving the precision of the techniques applied, as has been done for other materials (wood and bones). Thus, improving the chemical pretreatment on mollusk shells might allow researchers to obtain more reliable radiocarbon determinations allowing for the construction of new radiocarbon chronologies in archeological sites where so far it has not been possible. Furthermore, mollusk shells can provide information on the climatic and environmental variables present during their growth. Using shells for paleoclimatic reconstruction adds more evidence helpful for the interpretation of scenarios of human migration, adaptation, and behavior. Standard methods for both radiocarbon and stable isotope studies use the carbonate fraction of the shell. However, being biogenic structures, mollusk shells also consist of a minor organic fraction. The shell organic matrix has an important role in the formation of the calcium carbonate structure and is still not fully understood. This thesis explores the potential of using the shell organic matrix for radiocarbon dating and paleoenvironmental studies.

In this thesis, the comparison of four chemical pretreatment methods for radiocarbon dating on mollusk shells is presented, with the introduction of two newly proposed methods for organic matrix extraction. The methods are applied first to modern shells, and then to archeological specimens from a well-known Upper Paleolithic site in Portugal, Vale Boi. The abundance of mollusk shells throughout the stratigraphic sequence of this site allowed for the selection and analysis of shells from five different archeological layers from the most complete stratigraphic sequence found in one of the several excavated areas of the site - the Terrace area. Mollusk shell samples from this area of the site have already been radiocarbon dated after using the standard pretreatment method, thus allowing a comparison not only among methods but to previous results as well. Additionally, the application and results of two different methods for the assessment of the shell material preservation are also presented, one focusing on the carbonate fraction (X – Ray Diffraction), and the other focusing on the organic matrix (Pyrolysis – Gas Chromatography – Mass Spectrometry).

Furthermore, one of the two proposed methods for organic matrix extraction was applied to modern shell specimens collected in three sites in Northern Spain. The three sites: Berria beach, Montehano (lower estuary) and Carasa (upper estuary) represent an environmental gradient which was used to evaluate the effect of different environmental parameters on changes in stable isotope ratios of oxygen and hydrogen in the shell organic matrix. Once extracted, the organic matrix was divided into the soluble and insoluble fraction which were analyzed separately, revealing significant differences in the isotopic signatures among them. Moreover, the comparison of stable isotope signatures among the three study sites is presented, revealing differences indicative of environmental influences on the isotope fractionation during the formation of the organic matrix. A comparison to previous data from the carbonate fraction of shells and water collected in the three study sites is also presented, revealing significant differences in fractionation mechanisms between the organic matrix and carbonates. These results demonstrate the high potential of both the soluble and insoluble organic matrix fractions for future (paleo) environmental reconstructions.

The present thesis constitutes a significant contribution to the research focusing on mollusk shells and their use for radiocarbon dating and (paleo) environmental reconstructions. The results of the work performed for this thesis represent a starting point for future research to build on, and further develop the approach and methodology proposed here.

CONTENTS

CHAPTER 1 - INTRODUCTION

1.1. INTRODUCTION TO RADIOCARBON DATING

In order to discuss the application of the radiocarbon dating technique, it is important to understand the production, distribution and decay of radiocarbon in nature. Understanding these basic principles helps scientists improve the method continuously, through the establishment of new measurement techniques, sample pretreatment protocols and statistical and calibration models, which all serve to provide the most accurate age determination possible (Talamo et al. 2023). This, in turn, allows for a better understanding and reconstruction of the evolutionary history of ours and other human species. This chapter will briefly summarize the basic principles and development of radiocarbon dating, as well as the improvements made to different aspects of the radiocarbon dating process over the years.

1.1.1. ORIGIN AND DISTRIBUTION OF RADIOCARBON IN THE ATMOSPHERE

Radiocarbon (^{14}C) is one of three naturally occurring carbon isotopes. It is present in all carbonaceous matter along with the two stable isotopes ^{12}C and ^{13}C. These isotopes are present in nature in different quantities reflecting their stability approximately as follows: ^{12}C (98,89 %), ^{13}C (1,11 %) and ^{14}C (10^{-10} %). ^{14}C is produced in the upper atmosphere in a nuclear reaction resulting from the formation of neutrons by cosmic rays (Figure 1). The reaction is triggered by the bombardment of nitrogen-14 (^{14}N) by thermal neutrons resulting in the formation of ^{14}C and a proton:

$$^{14}N + n \rightarrow ^{14}C + p$$

Subsequently ^{14}C reacts with hydroxyl radicals to form ^{14}CO and then $^{14}CO_2$ (Pandow et al. 1960), or less frequently forms $^{14}CO_2$ directly, in the following oxidizing reaction:

$$^{14}C + 2OH \rightarrow ^{14}CO_2 + H_2$$

Atmospheric $^{14}CO_2$ is well mixed due to rapid atmospheric circulation and thus causes a uniform distribution of ^{14}C in one hemisphere (Anderson and Libby 1951). However, there are some factors including variations in Earth's geomagnetic field, the carbon cycle and solar activity which can cause variations in the production of ^{14}C (Hughen et al. 2004; Stuiver 1961; Stuiver and Braziunas 1998; Stuiver and Quay 1980). Collisions between thermal neutrons and ^{14}N atoms are most likely to occur at around 15 km above the Earth's surface where the production rate of ^{14}C is the highest (Aitken 1990). The Earth's magnetic field deflects cosmic rays at a different rate at different latitudes, thus influencing the rate of ^{14}C

production. Latitudinal differences in production are mostly neutralized by atmospheric mixing, although leaving an offset between the two hemispheres. This offset is created by the large ocean area in the Southern hemisphere (flux of low ^{14}C CO2 to the atmosphere) and due to diverging winds present at the equator resulting in reduced atmospheric mixing between the Northern and Southern hemispheres and is accounted for by having separate calibration curves for each hemisphere (Hogg et al. 2020; Reimer et al. 2020). Calibration will be further discussed in the following paragraphs. Finally, magnetic fields created by solar activity will influence the production of ^{14}C (Stuiver 1961), which has periodical changes correlated to the variations in solar activity at different time scales.

1.1.2. INCORPORATION OF ^{14}C INTO THE BIOSPHERE AND HYDROSPHERE

Once it enters the carbon cycle, ^{14}C is stored in different reservoirs for various periods of time depending on the rate of exchange between them. This creates the need to consider the carbon cycle when determining the radiocarbon age of different samples. From the atmosphere to the biosphere and the surface layer of the ocean, it takes only years or decades for the exchange, while for other reservoirs such as carbonates in limestone, deep water masses and others it can take much longer (Bronk Ramsey 2008; Olsson 2009).The slower the exchange, the less ^{14}C there will be in the reservoir due to the radioactive decay and lack of ^{14}C renewal.

Atmospheric $^{14}CO_2$ is incorporated into the food web during the process of photosynthesis, in the terrestrial biosphere by terrestrial plants, and in the aquatic biosphere by phytoplankton and algae (Figure 1). It is then transported along the food web to heterotrophic organisms by ingestion of plants and other animals, becoming a part of the organic carbon load of the biosphere. It is important to consider the fractionation of carbon isotopes during these chemical and physical processes, which results in the enrichment in lighter isotopes. The lighter isotope ^{12}C is preferentially taken up during photosynthesis compared to the two heavier isotopes. The fractionation of ^{14}C compared to ^{12}C is twice as much as the fractionation of ^{13}C compared to ^{12}C. It also depends on the type of metabolic process, which in plants can be divided in two groups: C3 and C4 plants. Most terrestrial plants are C3 plants and have a higher fractionation of ^{13}C compared to C4 plants (tropical plants) resulting in different ratios among isotopes in these plants, and in animals preferentially feeding on one of the two types of plant. In radiocarbon dating, the ratio of the two stable isotopes (^{13}C /^{12}C) is used to correct for the ^{14}C /^{12}C fractionation. This is done by calculating a $\delta^{13}C$ value by comparing the ^{13}C /^{12}C ratio of the sample with that of a standard and using this value to correct for ^{14}C by creating a fractionation factor.

On the other hand, atmospheric $^{14}CO_2$ is incorporated into the inorganic carbon load of the ocean by gas exchange through the air-sea interface (Figure 1). Once in the surface waters, it follows the currents in the

so-called global ocean conveyor belt of thermohaline circulation towards the polar regions where the water cools down, becomes denser and sinks. This water mass then becomes part of the deep ocean where there is no other input of ^{14}C, there is only radioactive decay. At the end of this conveyor belt, the water finally reaches the surface once again due to upwelling. In the areas where this phenomenon occurs, the surface water becomes depleted in ^{14}C compared to the atmosphere (Broecker 1991; Gordon and Harkness 1992). This is the reason behind the difference in ^{14}C concentration between the atmosphere and the oceans called the reservoir effect (described more in detail in the following paragraphs). However, the ocean reservoir is very heterogeneous in terms of ^{14}C concentrations because of local changes in air-water exchange and different ocean mixing rates (Gordon and Harkness 1992).

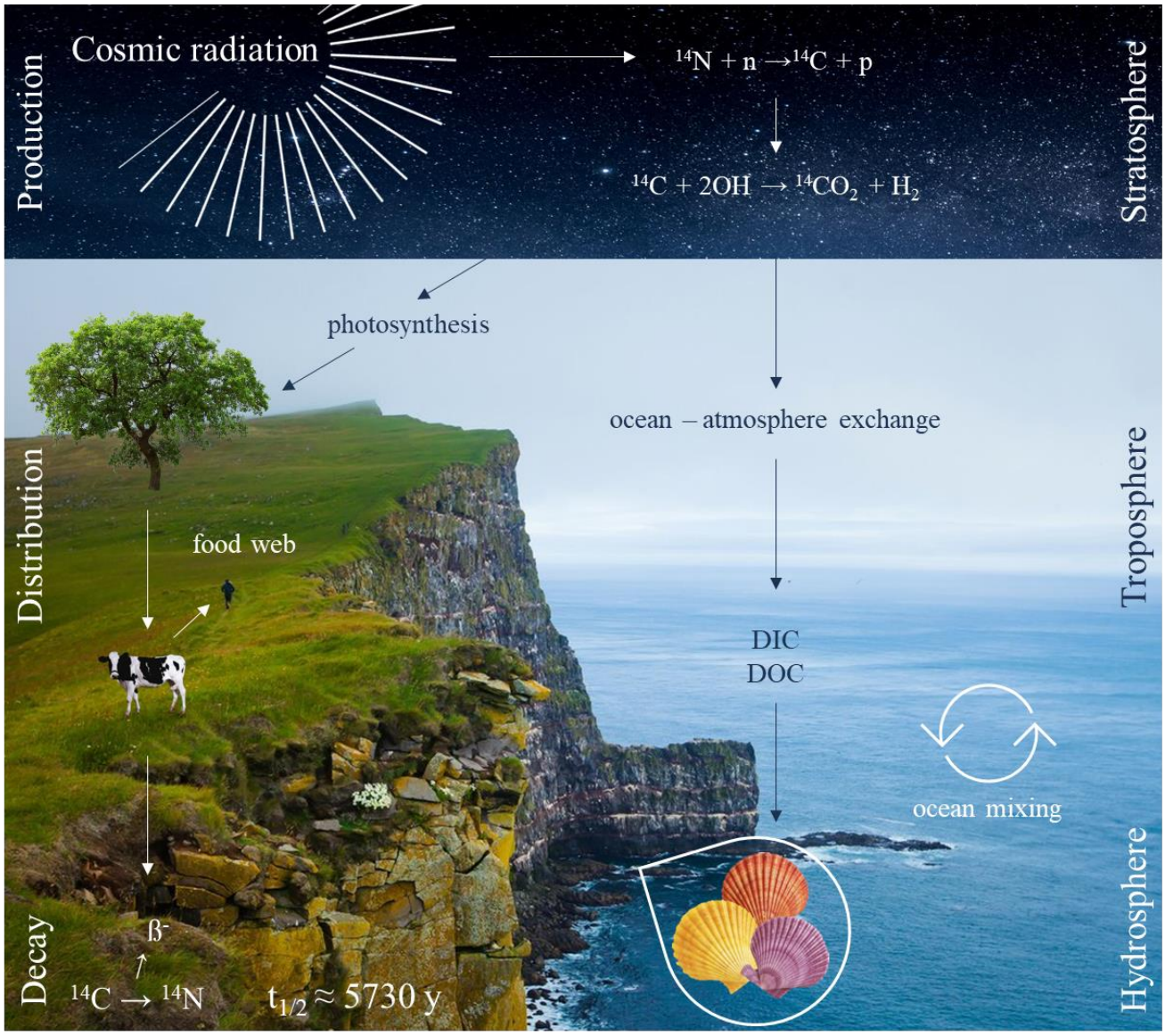

Figure 1. Production, distribution, and decay of radiocarbon in the global carbon cycle.

1.1.3. RADIOCARBON DATING

Radiocarbon dating was a revolutionary discovery for archaeology since it was first described in the late 1940s. It allowed for attribution of calendar ages to dated samples, and a better understanding of historical and prehistorical events despite the lack of written records. It is currently one of the main dating techniques used within archaeological research to establish absolute chronologies by dating both organic (e.g., bone, wood, charcoal) and inorganic materials (e.g., shell carbonates, corals, stalagmites). Radiocarbon dating is based on the notion that the ^{14}C activity remains constant in living organisms throughout their life and that only after death it starts decreasing exponentially in its radioactive decay (Figure 2). Radioactive decay is described with the following equations:

$$(1)\ A = A_0 e^{-\lambda t}$$

$$(2)\ t = -1/\lambda * \ln (A/A_0)$$

Where:

- t = the time since the sample material ceased to exchange carbon with the environment
- λ = decay constant
- A_0 = activity at time of death
- A = activity remaining in the sample "t" years after death

Knowing the rate of decay (half-life) and the initial ^{14}C activity of the living sample, we can calculate the time elapsed from the moment of death. Willard Libby won the Nobel Prize in Chemistry in 1960 for the development of the radiocarbon dating method. He determined a half-life of 5568 years (Libby 1955), however not long after a more precise value of 5730±40 years was established (Godwin 1962; Stuiver and Polach 1977). The half-life determined by Libby is still used to allow comparison with dates from before 1962. The decay takes around 8 to 10 half-lives to almost remove ^{14}C completely from the sample, rendering the limit of the method around 55,000 years.

In the early years, a complex procedure of coating amorphous carbon onto a metal screen was used to perform ^{14}C dating (Anderson et al. 1951). This procedure was susceptible to contamination from other beta-emitting nuclides during the period of atmospheric nuclear testing, and thus was later abandoned. A new method for ^{14}C measurements used gas proportional counting and scintillation counting, before arriving to the technique used today - accelerator mass spectrometry (AMS). AMS was first introduced in 1977 and it reduced the amount of carbon required for analysis from 1 g to 1 mg and decreased the analysis time from days to 30 min for the equivalent precision (Taylor and Bar-Yosef 2014). In the past two decades, this

amount decreased to micrograms thanks to constant method improvements (Fewlass et al. 2017; Fewlass et al. 2019b). For a more detailed history of the establishment of ^{14}C dating and a comparison of AMS dates with the early solid counting dates see Jull et al. (2018) and Olsson (2009).

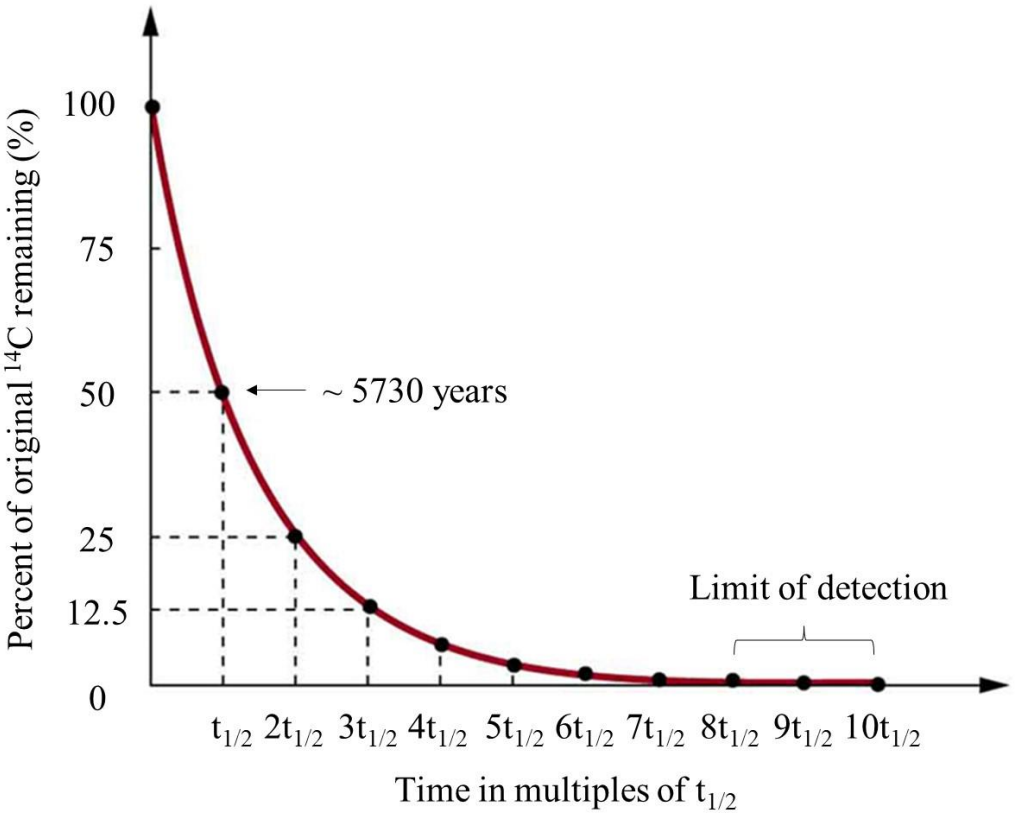

Figure 2. Exponential radioactive decay with the half-life shown as $t_{1/2}$

1.1.4. AMS

As opposed to decay counters (gas proportional counters and liquid scintillation counters) which indirectly measured ^{14}C activity by detecting and measuring ^{14}C beta decay events, the AMS uses direct carbon isotope ion counting, allowing to decrease drastically the amount of time and sample needed to perform the measurements. AMS systems typically use a two-step particle acceleration process relying on tandem electrostatic accelerators with negative ion sources (Taylor and Bar-Yosef 2014). Once introduced into the ion source, either in the form of graphite or CO_2 gas, the carbon atoms of the sample are ionized with a negative charge by cesium ion bombardment and accelerated into a beam. The electromagnetic field of the low-energy mass spectrometer changes the trajectory of the ions in the beam, discriminating the heavier ^{14}C isotopes from the lighter ^{13}C and ^{12}C isotopes. The tandem accelerator has a positive charge that attracts the negative ions, which are then stripped of their outer electrons changing their charge from negative to positive and repelling them from the tandem accelerator. A second magnetic field in the high-energy mass spectrometer accelerates the positive ion beam, separating the ^{12}C and ^{13}C ions which are measured in faraday cups, from the ^{14}C ions measured by a much more sensitive ion detector (Figure 3).

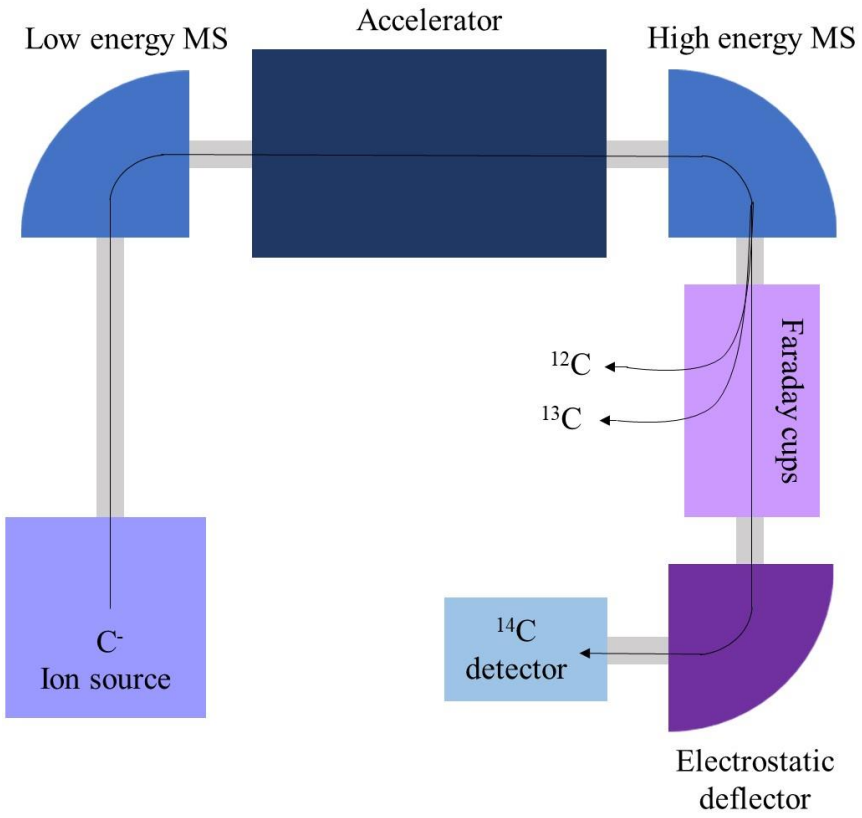

Figure 3. Simplified scheme of the AMS system components

The Bologna Radiocarbon Laboratory devoted to Human Evolution (BRAVHO lab) is equipped with an Elemental Analyzer (EA) and the AGE III graphitization system (Figure 4) which allows all pretreated samples to be combusted into CO_2 gas and then converted into a solid form by reducing them to graphite (Tassoni et al. 2023). The obtained graphite is then pressed into sample holders (targets, typically needing 500 - 1000 μg C) prior to shipment to an AMS lab for measurement. Graphite is preferred to CO_2 because it produces higher ion beam currents, allowing for a higher level of precision, and less memory effect in the ion source between samples. However, despite the lower precision the direct measurement of CO_2 gas is still used in many cases, since it requires a much smaller sample size (5 - 100 μg C) and the results are obtained in less time as the graphitization step is omitted (Ramsey and Hedges 1997). Furthermore, the precision for CO_2 samples was increased, due to improvements to the AMS system which allowed the production of higher ion beam currents. This improvement was possible thanks to the introduction of a more compact AMS system - the MIni CArbon DAting System (MICADAS), capable of accepting both solid and gas samples (Ruff et al. 2007; Wacker et al. 2010). This kind of technological improvements make it possible to date even small amounts of material, limiting the destruction of precious archaeological samples. However, this increases the need for rigorous pretreatment protocols, since the small sample size implies a higher susceptibility to modern contamination.

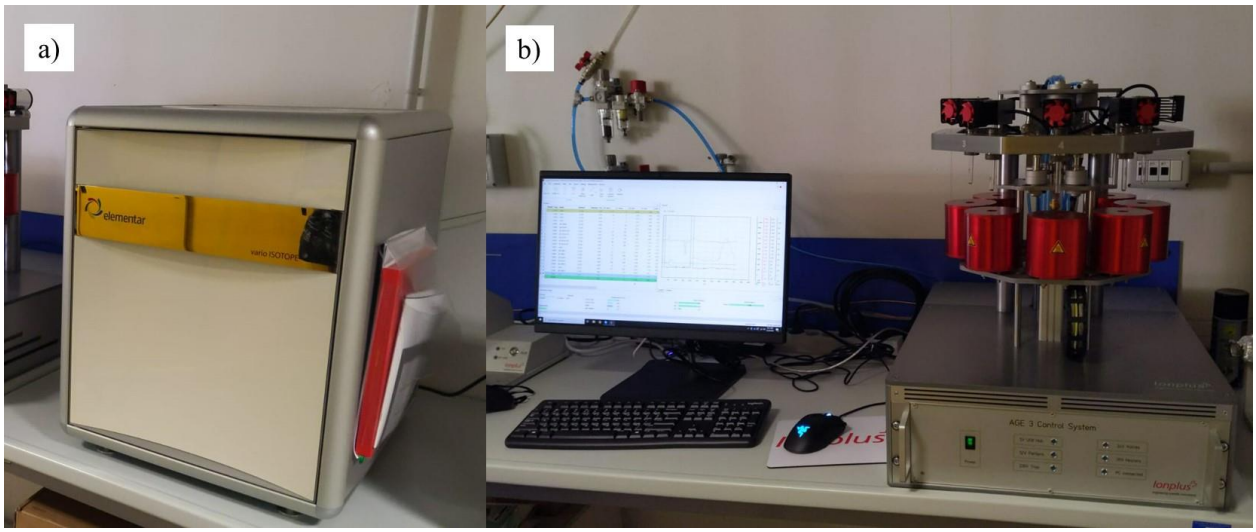

Figure 4. Equipment at the BRAVHO lab (a) elemental analyzer and (b) AGE III graphitization system

1.1.5. SAMPLE MATERIALS AND PRETREATMENT

The only samples which can be used for ^{14}C dating, are those containing organic or inorganic carbon. However, samples older than the limit of the method cannot be measured due to the complete decay of ^{14}C. A wide array of terrestrial, marine, and man-made materials are suitable for ^{14}C dating. The most commonly used materials include artefacts made using carbon containing materials such as bones, wood, charcoal and shells (tools and ornaments made out of wood, bone, shells; rope, pottery or paper). A list of materials used in archaeological studies is shown in Table 1. It is important to perform a careful sample material selection taking into account the research question, the availability and preservation of different sample materials and their correlation to human activity at the archaeological site. Various sample prescreening methods are employed to evaluate the preservation and presence of potential contaminants of different sample materials (visual inspection, inspection under UV light, with polarized light microscopy, scanning electron microscopy (Yates 1986), spectroscopy – infrared (Fewlass et al. 2019a; Lugli et al. 2021; Malegori et al. 2023; Sponheimer et al. 2019; Talamo et al. 2021a), X- ray diffraction or fluorescence, Raman (Quarta et al. 2020), pyrolysis–gas chromatography–mass spectrometry (Cersoy et al. 2018) and percentage of carbon and nitrogen (Ambrose 1990; Talamo et al. 2021a; van Klinken 1999).

Radiocarbon dating includes an especially crucial step prior to the AMS measurement - sample pretreatment. Physical and chemical pretreatment of different kinds of samples for ^{14}C dating aims at the removal of any potential exogenous carbon which could interfere with the sample age determination. Standards and blanks are used during sample preparation and processing to detect introduction of exogenous carbon into the sample. In the case of modern contamination, blanks or background standards which are devoid of ^{14}C (older than 55,000 years) are used. Modern samples of known age can be used as standards to detect contamination by old carbon. Processing blanks are chosen based on the material and pretreatment used and processed together with the sample of the same type and amount. The first step in the pretreatment process is a mechanical surface cleaning, which is performed for all material and sample types. However, different materials require distinct pretreatment methods to remove any contaminants added over time by natural processes or by sample handling. Chemical pretreatment methods for organic samples usually include a variation of a standard method using alternate washes in acid, base and again acid (ABA; wood – (Cercatillo et al. 2021), bones – (Talamo et al. 2021a; Talamo and Richards 2011), charcoal (Bird et al. 1999; Tassoni et al. 2023; Wood et al. 2012), ash, sediment, and plant fragments – (Bronk Ramsey 2008). The first acid step (usually hydrochloric acid) serves to remove the calcium carbonates present in the sample, while the base step (sodium hydroxide) removes the humic acids, which can have different origins and isotopic signatures, and for this reason are considered contaminating. The second acid step serves to remove the modern carbon dioxide (CO_2) which is taken up during the base step. For inorganic

samples, in most cases the pretreatment is performed only using acid, firstly to remove the outer surface of the sample which is exposed and thus potentially contaminated, and secondly to evolve the CO_2 from the calcium carbonate. Surface acid etching was found to remove about 30 – 80% of the initial weight of the sample (Douka et al. 2010; Lindauer and Kromer 2013). The methods for pretreatment are constantly being improved in order to achieve the most accurate age determinations. An example for such an improvement is the introduction of an ultrafiltration step in bone pretreatment to remove low molecular weight fractions which were found to be sources of contamination (Talamo et al. 2021a). Similarly, the introduction of an oxidation step to the ABA protocol for the pretreatment of charcoal was shown to improve the removal of modern contamination (Bird et al. 1999; Tassoni et al. 2023; Wood et al. 2012). Furthermore, a new protocol for carbonate pretreatment based on density separation using heavy liquids allows for the separation of calcite and aragonite, which was shown to improve radiocarbon dating of mollusk shells and corals and will be further discussed in Chapter 2 (Douka et al. 2010).

Table 1. List of different materials and the respective fractions extracted for radiocarbon dating.

Sample material	Selected datable fraction
Terrestrial	
Animal and human remains	Bone collagen
Fossil trees including charred wood and anthropogenic wood products	1) Charcoal & whole wood 2) Cellulose
Peat	1) Fine fraction of bulk (<150µ): humin and humic acid 2) Identifiable fragments of plants
Sedimentary records: fluvial, caves, lake deposits, soils, permafrost, loess, paleo soils	1) Fine fraction of bulk (<150µ): humin and humic acid 2) Identifiable fragments of plants 3) Earthworms droppings 4) Mesofauna
Remains of plants and animals	1) Fragments of plants 2) Insects 3) Pollen
Tufa (fresh water carbonate)	1) $CaCO_3$ 2) Organic inclusions
Marine	
Sedimentary records	Foraminifera
Fish, Corals, Mollusk shells	$CaCO_3$

Sample material	Selected datable fraction
Human history and collections of Flora and Fauna	
Human remains	1) Skin, hair 2) Bones 3) Cremated bones
Pottery	Whole bulk
Short lived charred and fresh vegetal material	1) Straw 2) Grains, seeds 3) Pits 4) Nuts
Collections of seeds, herbaria, museum specimens	1) Vegetal fragments/tissue 2) Bones 3) Other tissue: hair, skin
Anthropogenic products	
Buildings and constructions	1) Wood 2) Charcoal 3) Vegetal temper 4) Mortar
Art and written documents	1) Wood 2) Textiles 3) Paper, papyri and parchment 4) Binder 5) Pigments 6) Corals and pearls (carbonates)

1.1.6. CALIBRATION

In the early years of radiocarbon dating, a constant level of ^{14}C in the atmosphere and a rapid distribution in both hemispheres was assumed (Libby et al. 1949) implying that the radiocarbon years correspond to calendar years. However, in the early applications of radiocarbon dating the ^{14}C ages obtained did not match historical dates or tree-ring records because of variations in the atmospheric $^{14}C/^{12}C$ ratio through time and space (de Vries 1958; Stuiver and Suess 1966; Willis et al. 1960). Therefore, it was discovered that ^{14}C years are not equivalent to calendar years and they must be calibrated using temporal proxies (de Vries 1958; Stuiver and Suess 1966; Willis et al. 1960). Calibration allows us to determine the calendar age of dated samples by converting the radiocarbon results into years BC/AD or years BP (before present, where the present is the year 1950). It is important to distinguish them and thus the calibrated ages are marked as cal BC, cal AD, cal BP, whereas the uncalibrated results are marked with ^{14}C yrs BP. In order to perform this conversion, we need a calibration curve constructed using securely dated samples, employing an independent dating method. This is done by using U/Th dating, laminated sediment layers or annual tree rings with dendrochronological measurements. There are different calibration curves currently in use for the pre-bomb samples: the atmospheric calibration curves (IntCal for the northern hemisphere and SHCal for the southern hemisphere) and the marine calibration curve (MarineCal). Atmospheric ^{14}C concentrations doubled due to the nuclear tests starting in the late 1950s. Therefore, there is an additional calibration curve for the post-bomb period (Reimer and Reimer 2023).

A first approach to constructing a calibration curve was with Libby's "Curve of knowns" which was based off known-age samples of wood and represented the beginning of the calibration method (Jull et al. 2018). From these first attempts of calibration the calibration curve has improved substantially throughout the years, with method improvements and more data becoming available (Reimer 2021). The early versions of calibration curves were based on different records which were often inconsistent, especially with older ages and near the limit of the method. For example, the early versions of the calibration curve IntCal98 (Stuiver et al. 1998) and IntCal04 (Reimer 2004) only spanned the period until 24 and 26 ka respectively, and there was no unified recommendation for calibration beyond that age (Van Der Plicht et al. 2004). The older radiocarbon ages were calibrated using a range of different calibration curves making it difficult to compare the published calibrated ages (Reimer 2021). With new data becoming available through time and by incorporating it into the existing curve, some of the inconsistencies were resolved in the IntCal09 calibration curve (Reimer et al. 2009), which was further improved in the IntCal13 (Reimer et al. 2013). The latest updated calibration curve for the northern hemisphere is IntCal20, for which the dendro-based calibration curve extends back to 14.200 cal BP, with further extensions to 55,000 cal BP from other records such as laminated lake sediments, marine sediments, corals, and speleothems (Reimer et al. 2020). The difference

between the last two IntCal calibration curves in the oldest part of the curve is shown in Figure 5, compared to a theoretical line representing a perfect correspondence of ^{14}C and calendar (calibrated) ages. It is important to mention that there is a significant difference in terms of resolution and accuracy between the dendro-based curve and the rest, based on materials indirectly related to the atmospheric ^{14}C. The improvement of the efficiency and precision of the radiocarbon measurements due to newly developed MICADAS AMS machines contributed to the improvement and extension of the radiocarbon calibration curve. In recent years, a new method was developed linking variations in ^{14}C to variations in Beryllium 10 (^{10}Be) which could improve the calibration curve by anchoring the older floating tree ring chronologies by absolutely dating them (Adolphi et al. 2017; Muscheler et al. 2020).

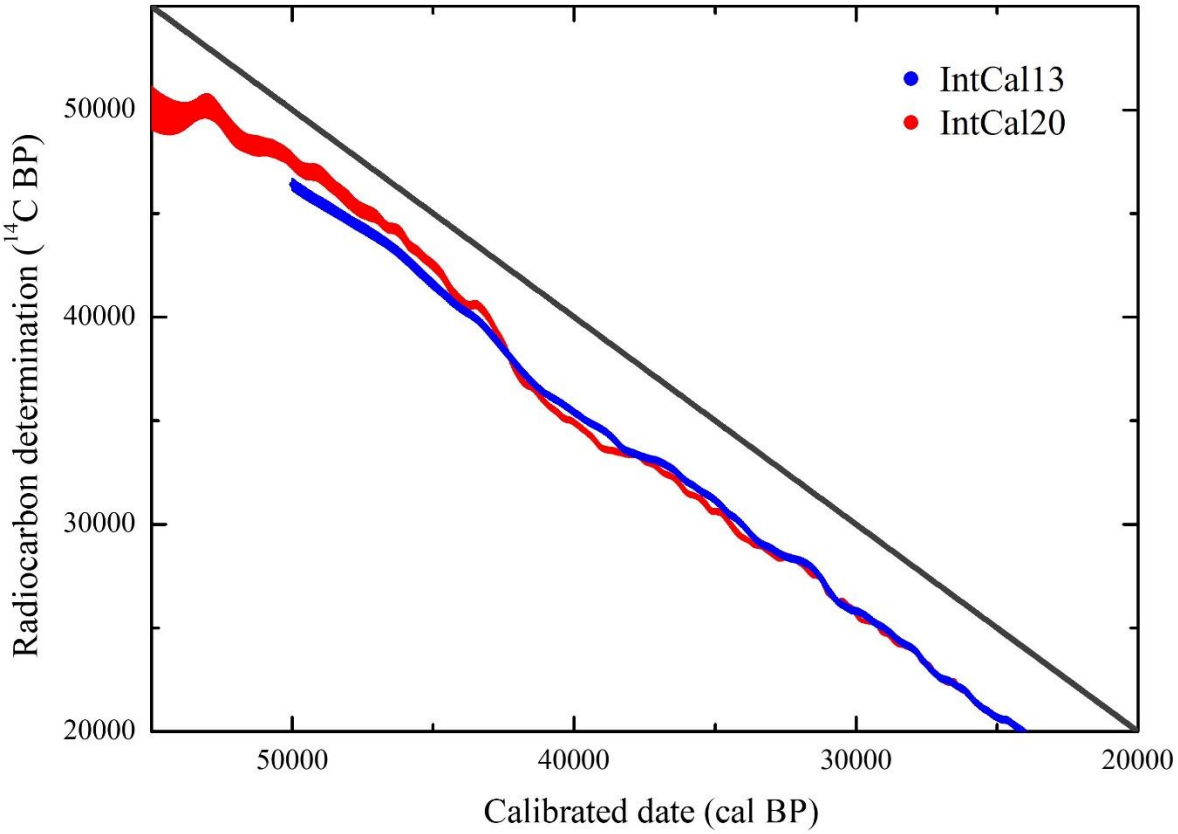

Figure 5. Comparison of the latest two calibration curves IntCal13 in blue (Reimer et al. 2013) and IntCal20 in red (Reimer et al. 2020), compared to a hypothetical constant atmospheric ^{14}C concentration over time which would make the ^{14}C age correspond to the calendar (calibrated age) represented by the gray line.

1.2. APPLICATION TO HUMAN EVOLUTION STUDIES

Radiocarbon analysis is applied in many different disciplines to study Earth's history in the past 55,000 years. With the increasingly interdisciplinary approaches, the number of possible applications of ^{14}C analysis is constantly growing. Some of the most frequent applications include archaeology, paleoclimatic research, environmental studies, cultural heritage, biomedicine, and forensic science, to name a few. However, the focus of this thesis will be the study of human evolution. The application of ^{14}C dating in archeology and human evolution studies is used not only to determine the time elapsed since a certain past event but to obtain information about human activity through the combination of dates obtained over large geographical and temporal ranges. The construction of radiocarbon chronologies for a single archeological site allows for the interpretation of the timing of occupation and activities performed at the site and area in question (Hublin et al. 2012; Talamo et al. 2016a; Talamo et al. 2014; Talamo et al. 2012b; Tátá et al. 2014). However, once numerous chronologies are available over a large geographical scale, it is possible to interpret human migration patterns, their interactions, adaptations, and cultural exchange (Hublin 2015; Picin et al. 2022). To reconstruct such large-scale contexts of human migration and population dynamics, a correct determination of the timing of human presence and activity is necessary. Therefore, when collecting samples for radiocarbon dating from an archeological site, it is important to have accurate information on the sampling location within the archaeological sequence. To achieve the best results and select the samples representative of the event of interest (usually human presence or activity), a close collaboration between archeologists and radiocarbon dating researchers is necessary. Interdisciplinary collaboration is crucial to achieve the best possible reconstruction of our evolutionary history. For example, paleoclimatic and paleoenvironmental studies are often combined with archeological research to obtain more information allowing for a better interpretation of past scenarios of human migrations, interactions, and cognitive and technological development (Álvarez-Fernández et al. 2020; Bicho and Haws 2008; Carrion et al. 2008; Finlayson and Carrión 2007; Leng and Lewis 2016; Linstädter et al. 2018; Mannino et al. 2003; Mannino et al. 2015; Milano et al. 2018a; Milano and Szymanek 2019; Schöne and Fiebig 2009; Talamo et al. 2023). The combination of radiocarbon dating and other analyses such as DNA, ZooMS (mass spectrometry for zooarchaeology) and stable isotope analysis has allowed for the determination of the sample species, diet, and ancestry even from fragmentary samples, thanks to interdisciplinary studies and the development of new techniques (Korlevic et al. 2018; Mannino et al. 2012; Talamo et al. 2016b; Talamo et al. 2021b). A new method for collagen detection and quantity estimation has been developed by a group of researchers including our team, to minimize the loss of precious archeological bones by scanning the samples with NIR (Near InfraRed spectroscopy) prior to collagen extraction (Malegori et al. 2023). This method allows researchers to scan the bones and precisely map out the collagen content determined within

each pixel of the image with an error of only 2% (Malegori et al. 2023). Furthermore, the application of Bayesian statistics and modelling has been a true revolution in radiocarbon research applied to studies of human evolution and population dynamics (Bayliss 2009; Bayliss and Bronk Ramsey 2004; Ramsey 2009). The collaboration among scientists from different fields combined with all the advances in the techniques used in radiocarbon dating (i.e., AMS, pretreatment methods, calibration, Bayesian modelling), have allowed for a higher resolution in the reconstruction of scenarios from human evolutionary history even near the limit of the method (Talamo et al. 2023). The importance of these improvements lies in the fact that the limit of the radiocarbon method coincides with one of the key periods in human evolution, the transition from the Middle to the Upper Paleolithic.

1.2.1. THE MIDDLE TO UPPER PALEOLITHIC TRANSITION

The refinement of the radiocarbon dating methods, and the decrease in measurement errors will allow for the revision and improvement of many previously constructed chronologies, which will be especially important for the transition from the Middle to the Upper Paleolithic - MUP (Talamo et al. 2023). This period is crucial for human evolution as it represents the arrival and dispersal of the Upper Paleolithic *Homo sapiens* into Europe, their encounter with *Homo neanderthalensis* (Neanderthals) and the subsequent disappearance of the latter. The archeological data so far indicate multiple consecutive waves of *Homo sapiens* migrations from the Levant along the Mediterranean coast and the Danube River. New cultural behaviors emerged in the European territories in association with these migrations including the development of novel lithic technologies, more efficient foraging strategies and the creation of personal adornments and art (Picin et al. 2022). The precise mechanisms which led to the behavioral changes occurring between ~44 and 39 ka BP, as well as the reasons behind the demise of Neanderthals are still unknown. There were several different hypotheses on how these cultural changes occurred. Some suggested that the behavior was species-specific, implying that the replacement of Middle Paleolithic technologies by Upper Paleolithic ones was directly equated with the replacement of Neanderthals by *Homo sapiens* (Bar-Yosef 1998). Others implied they had a trans-specific nature, where the behavioral changes were the result of Neanderthal endemic innovations or of cultural exchanges with *Homo sapiens* (D'Errico et al. 1998; Hublin et al. 1996; Mellars 1999). A reliable chronological framework defined by highly accurate stratigraphic records and chronometric age determinations is crucial for the elucidation of debates such as these.

To be able to fully understand the complex transition that took place in Europe between 50 and 35 ka cal BP, it is essential to accurately define the first occurrences of *Homo sapiens* and the latest occurrences of Neandertals in as many sites as possible. Obtaining this type of chronological information helps in

reconstructing the area and period in which the two species overlapped and interacted and their respective migration patterns. Additionally, in this type of archeological and chronological studies, lithic tool assemblages found in different archeological sites are associated with one species or the other and combined with direct or indirect chronological attributions to study their cultural and cognitive development and potential interactions that led to the exchange of knowledge. Three groups of lithic assemblages covering different time frames within the period from 50 to 35 ka cal BP have been assigned to the earliest *Homo sapiens* populations in Eurasia: The "Initial Upper Paleolithic" (IUP), "transitional assemblages" and Aurignacian assemblages (Figure 6 (Hublin 2015). Other authors include an "Early Upper Paleolithic" (EUP) group of assemblages encompassing the Aurignacian and several other regional EUP variants (Figure 6 (Picin et al. 2022). The current data supports a Levantine origin for the IUP where it was represented by the Emiran industry (Figure 6), although other dispersal routes for the IUP from Central Asia into Europe were also hypothesized (Picin et al. 2022). The first expansion of *Homo sapiens* at ~47 - 44 ka cal BP has been related to the spread of techno-complexes assigned to the IUP, and it reached Bulgaria where it is represented by the Bachokirian industry, Moravia as the Bohunician industry, as well as southern Europe where the Uluzzian technocomplexes are encountered (Figure 6 (Hublin 2015; Picin et al. 2022). The Uluzzian industry, among others, is still being extensively studied as its exact stratigraphic definition is still uncertain. It was originally assigned to Neanderthals and later to *Homo sapiens* (Benazzi et al. 2011), it was included in the group of transitional assemblages (Hublin 2015) although other authors argue it is fully an Upper Paleolithic assemblage with a potential direct African origin (Moroni et al. 2018). Furthermore, the Uluzzian assemblage is often considered the Italian counterpart of the Châtelperronian industry belonging to the group of transitional assemblages (Hublin 2015; Picin et al. 2022). The transitional assemblages are a heterogeneous group of assemblages thought to have been produced, at least in part, by autochthonous Neandertal populations surviving in Europe until c. 41 ka cal BP (Hublin 2015). This group encompasses the Szeletian found in Hungary, Czech Republic, Slovakia, and southern Poland, the Lincombian-Ranisian-Jerzmanowician (LRJ) which is found in Great Britain (Lincombian), Belgium, Germany (Ranisian) and Poland (Jerzmanowician) and lastly the Châtelperronian in Western France, the Cantabrian region and Catalonia (Figure 6). The scarcity of well-placed and well-preserved human remains associated with these industries leaves much room for debate over who their creators were and if they were a result of *Homo sapiens* influence on Neanderthals (Picin et al. 2022). Another wave of *Homo sapiens* migrations starting in the Levant area with a technological shift from IUP to EUP (Picin et al. 2022), caused the expansion of the earliest phases of the Aurignacian complex (Protoaurignacian and Early Aurignacian) throughout Europe and completed the colonization of the continent (Hublin 2015). The EUP is represented in the Levant by the Ahmarian which is a long lasting and widely distributed assemblage which has been thus divided into Southern and Northern Early Ahmarian, and Late Ahmarian, which was preceded by the

Levantine Aurignacian thought to have been brought by populations migrating back from Europe (Figure 6 (Picin et al. 2022). In Europe, the EUP is represented by the Aurignacian, which is usually found as two subsequent phases - Protoaurignacian and Early Aurignacian, the shift between the two was thought to have been caused by the Heinrich Stadial 4 (Picin et al. 2022). In Eastern Europe, technocomplexes different from the Western European ones are encountered in the EUP – the Streletskian and the Spitsynian (Figure 6), sparking debates over potential Central Asian or local climatic influences which might have caused them (Picin et al. 2022).

Although the rich paleontological and archeological records allowed for the definition of these industries and broad migration and behavior interpretations, it is still difficult to define the exact process of the replacement of Neandertals by *Homo sapiens* in Europe. There is still a lot of uncertainty regarding the precise mechanism and timing for the start of the various industries and the geological age of key specimens due to a number of issues. A lot of the uncertainty has been created by the lack of information during excavation of a large portion of the available materials. These excavations were conducted starting in the early 1900s, and the documentation about the stratigraphy and precise location of each sample is not up to present-day standards and often missing or lost. This leaves doubts on the possible intrusion of archaeological material from one layer into another and the stratigraphical attribution of the excavated samples. Furthermore, the radiocarbon dates used to construct these scenarios, which were performed on the human remains and the archaeological layers they came from, are also often a matter of controversy having been obtained before the advent of modern and advanced techniques. Therefore, having new, more precise chronologies might shed light on the precise timing and duration of the coexistence of Neanderthals and *Homo sapiens*, their interactions, cultural and genetic exchanges, and the reasons behind the demise of Neanderthals. Answering the many questions about events taking place during this period has long been a challenge for researchers for several reasons, and there have been substantial efforts to make dating this period more trustworthy. For example, the reliable application of radiocarbon dating during this period was questioned due to suspected large fluctuations in atmospheric ^{14}C levels (Conard and Bolus 2003; 2008). This hypothesis was shown to be erroneous as the large anomalies were revealed to be artefacts beyond plausible physical limits for their magnitude (Talamo et al. 2012a). Furthermore, the low ^{14}C activity near the limit of the method causes larger uncertainties and higher susceptibility to modern carbon contamination, which was addressed by the development of more efficient pretreatment protocols (Talamo et al. 2021a). Additionally, many archaeological sites are being revisited to construct more robust chronologies using state of the art methods (Douka et al. 2020; Fewlass et al. 2020; Hublin et al. 2012; Ruebens et al. 2022; Talamo et al. 2020; Talamo et al. 2023; Talamo et al. 2012b; Talamo et al. 2021b). However, the scarcity and often complete absence of well-preserved samples still remains a critical issue,

hindering researchers from fully understanding *Homo sapiens* – Neanderthal interactions during the MUP (Hublin 2015; Picin et al. 2022).

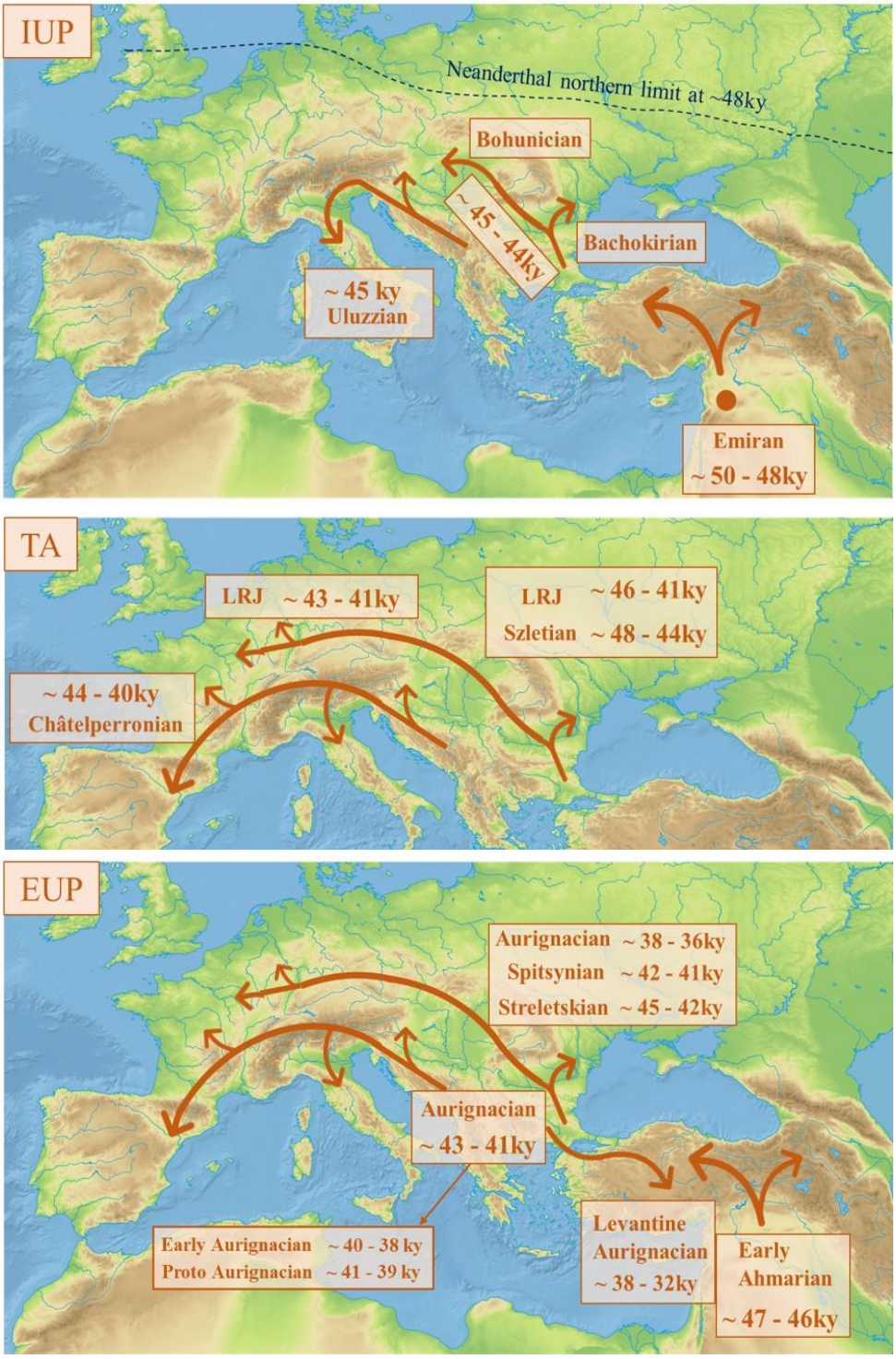

Figure 6. Simplified graphics of the spread of IUP, transitional assemblages (TA) and EUP in Europe with corresponding chronological estimates from Picin et al. 2022.

1.2.2. THE LEVANTINE CORRIDOR DEBATE

The migrations of *Homo sapiens* from Africa into Europe, whether they followed the Mediterranean coast or the Danube River, had started or passed through the Levant (Figure 7 (Hublin 2015; Mellars 2006a; 2006b; Picin et al. 2022). This makes studying this area of great importance in order to understand the mechanisms behind the emergence of new technologies and cognitive behavior associated with *Homo sapiens* in the MUP. As previously mentioned, one of the key issues in understanding the MUP is the lack of well-preserved fossils to use for radiocarbon dating, especially human remains. Researchers have thus had to find alternative, indirect ways of estimating the age of the rare human fossils that did get discovered in this area. An example of such indirect dating is found in the archeological site of Ksar Akil (Lebanon; Figure 7).

Figure 7. A map of the Mediterranean, showing the Levantine corridor and the Ksar Akil archeological site

The archeological site of Ksar Akil is one of the reference sites for the Upper Paleolithic in the Levant, with an archeological sequence including IUP and EUP layers in which *Homo sapiens* fossils were recovered (Figure 8). Two human fossils named 'Egbert' and 'Ethelruda' are rare examples of human fossils directly linked to early Upper Palaeolithic archaeological assemblages. 'Egbert' was uncovered in levels associated with the Early Ahmarian and comprises the skull and postcranial remains of a juvenile *Homo sapiens*, while 'Ethelruda' a partial maxilla of a ''Neandertaloid'' (*Homo sapiens* with Neanderthal features) female adult, was recovered from a level associated with the start of the IUP (Figure 8). Unfortunately, as often is the case with MUP remains, these fossils were too degraded and contained no collagen. Furthermore, there

were no charcoal samples available for radiocarbon dating. Therefore, it was necessary to use a different material. Since the assemblage at Ksar Akil was very rich in mollusk shells (~2000 specimens), most of which contained evidence of human use (perforation, burning, polishing, snapping, and ochre residues; Figure 8), they were used to construct the radiocarbon chronology for this site and to determine the age of the contexts from which 'Egbert' and 'Ethelruda' were recovered (Douka et al. 2013). Douka and colleagues dated marine shell beads, which are often regarded as indicators of behavioral modernity, to construct a chronostratigraphic framework for Ksar Akil using Bayesian modelling. They estimated the ages of 'Egbert' and 'Ethelruda' at 40.8–39.2 ka cal BP and 42.4–41.7 ka cal BP, indicating that they were roughly contemporaneous with the oldest directly dated *Homo sapiens* fossils from Europe. This led them to the conclusion that the MUP transition at Ksar Akil, and possibly in the wider northern Levant, occurred later than previously estimated, casting doubts on the Levantine corridor hypothesis.

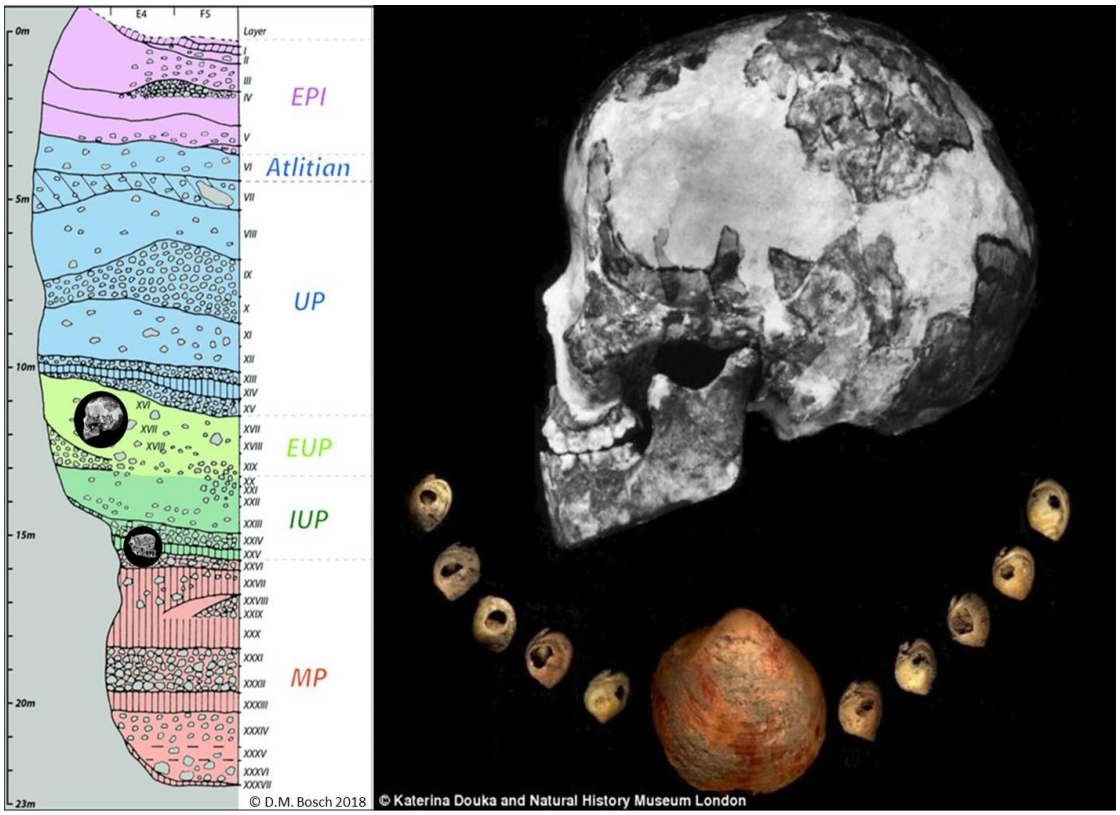

Figure 8. Stratigraphy of the Ksar Akil site showing the positions of 'Egbert and Ethelruda fossils in the EUP and IUP sequences respectively, and the 'Egbert' cranium together with shell samples from the site.

Two years later, another team of researchers revisited the Ksar Akil site to construct a new chronology, this time choosing shells of a very well-preserved marine gastropod associated with the human remains and stone tools present at the site (Bosch et al. 2015a). The shells chosen by Bosch and colleagues were collected

live and used as food, thus creating a tighter connection between the dated event (mollusk death) and the target event (human presence) compared to the previous study (Bosch et al. 2015a). Furthermore, apart from performing Bayesian modeling, Bosch et al. (2015) used amino acid racemization to evaluate the preservation state of the samples and compared their chronometric results to paleoclimatic data obtained using oxygen stable isotopes. Their results yielded a chronology which overlapped with the previous one in the upper part of the sequence but was significantly older in the lower part where the IUP and EUP layers are located (Bosch et al. 2015a; Douka et al. 2013). The new determinations were between 43.2 and 42.9 ka cal BP for 'Egbert' and older than ~45.9 ka cal BP for 'Ethelruda', falling in line with the chronologies of other Levantine sites and predating the European IUP and EUP counterparts (Bosch et al. 2015a). This leads the authors to conclude confirming the Levantine corridor hypothesis (Bosch et al. 2015a). They suggest several reasons for the discrepancy between the two chronologies including the sample selection (ornamental shells vs. live collected mollusks used for food), sample pretreatment (the CarDS protocol vs. the standard acid etching protocol) and the use of a different AMS laboratory to perform the radiocarbon dating (Oxford vs. Groningen) (Bosch et al. 2015a). Douka and colleagues soon published a letter, criticizing the work of Bosch et al. (2015), and stating that the new chronology cannot be valid, due to improper use of Bayesian statistics and poor understanding of the stratigraphical sequence of the site (Douka et al. 2015). Yet they considered the new radiocarbon determinations correct and the two AMS laboratories comparable (Douka et al. 2015). After applying the modifications and parameter changes suggested by Douka et al. (2015) to their Bayesian model, Bosch and colleagues obtained age ranges of 42.7–40.9 ka cal B.P. for 'Egbert', 49.9–44.1 ka cal BP for 'Ethelruda' and 44.9–43.6 ka cal B.P. for the start of the dated IUP, which did not change their original conclusions (Bosch et al. 2015b). 'Ethelruda' was still older than all European human fossils other than a sample from Cavallo cave (Italy), whose context was uncertain (Bosch et al. 2015b; Zilhão et al. 2015). The debate was concluded with the confirmation of Levantine corridor hypothesis by Bosch et al. (2015).

As attested by this debate, it is challenging to estimate the age of human remains when there isn't enough collagen for a direct radiocarbon determination. There are several issues when doing so using only mollusk shells, including the selection of samples not tightly related to the timing of human presence at the site, and the application of different sample pretreatment protocols. The determination of erroneously young ages can lead to conclusions casting doubt on important events in human evolution, such as the Levantine corridor hypothesis, which could have changed our understanding of the beginning of the MUP. This underlines the importance of obtaining reliable radiocarbon dates on mollusk shells by performing careful sample selection and adequate sample pretreatment. The use of mollusk shells in human evolution studies and radiocarbon dating is a multifaceted and complex issue with significant opportunities for improvement to which this thesis will be dedicated.

1.3. MOLLUSK SHELLS IN RADIOCARBON DATING AND HUMAN EVOLUTION STUDIES

In order to use marine mollusk shells for radiocarbon dating and in the reconstruction of human evolution scenarios, it is necessary to understand the many variables to consider when doing so. One of the main reasons for which using shells is such a complex issue is the sheer diversity of mollusk species. The phylum Mollusca is the second largest phylum of invertebrates and the largest marine phylum with over 80 thousand species in existence and at least 30 thousand fossil species from diverse habitats across the world (Ahyong et al. 2023). The World Register of Marine species (WoRMS) lists over 10 different classes out of which two are extinct (Ahyong et al. 2023). There are over a 100 thousand shell bearing species of mollusks, with rare exceptions where the shell is absent (i.e., Cephalopods, Caudofaveata, Solenogastres (Ahyong et al. 2023). They inhabit the oceans, seas, rivers, and land; some are mobile, while others live fixed to the substrate (Ahyong et al. 2023; Santhanam 2018a; 2018b). These diverse habitats have an effect on their diets, behavior, and morphology. Most mollusks are filter feeders and grazers, and their diet and way of feeding can influence the chemical composition of their soft and hard tissues. The diversity of this phylum is also reflected in the many different shapes, sizes, and colors of their carbonate shells. Mollusks grow their shells incrementally throughout their lifetime for support and protection, and their resistance gives them a high potential to be found within the archeological record. During their growth they faithfully record the physical and chemical conditions of the environment they are in, and how it changes through time, making them excellent paleoenvironmental archives. The study of changes in the chemical composition (i.e., stable isotopes and trace elements) and physical accretionary patterns of mollusk shells, used to produce paleoenvironmental reconstructions with extremely high resolution is called sclerochronology (Andrus 2011; Gillikin et al. 2019; Leng and Lewis 2016; Peharda et al. 2021; Schöne and Fiebig 2009; Yan et al. 2020). This field of research (described more in detail in the following paragraphs) is tightly intertwined with human evolution studies, as it can provide important information for the interpretation of past human behavior and facilitate the reconstruction of different scenarios of the past. This is one of the reasons for the great importance of mollusk shells for the study of human evolution. Another reason behind the significance of mollusk shells for human evolution studies is their diverse uses throughout the evolutionary history of ours and other human species (Bar-Yosef Mayer et al. 2009; Bicho et al. 2010; Cortés-Sánchez et al. 2011; Douka 2011; Douka and Spinapolice 2012; Joordens et al. 2015; Marean et al. 2007; Peresani et al. 2013; Ramos-Muñoz et al. 2016; Tátá et al. 2014; Wei et al. 2016; Zilhão et al. 2010). Anatomically modern humans have long used shellfish as an important dietary component due to their easy accessibility, reliable availability throughout the year and source of proteins and micronutrients essential for physical development (Bailey and Flemming 2008; Colonese et al. 2011; Fa et al. 2016; Marean et al.

2007). Furthermore, they have been often used for ornamental and utilitarian purposes, by both modern humans and Neanderthals, thus reflecting their symbolic thinking and cognitive development (Bicho and Haws 2008; Cortés-Sánchez et al. 2011; Douka 2011; Douka and Spinapolice 2012; Fa et al. 2016; Tátá et al. 2014; Wei et al. 2016; Will et al. 2019). Their diverse and frequent use, together with the mechanical and physical resistance of the calcium carbonate crystalline structure (Barthelat 2010), has made mollusk shells the most widespread marine material found in archaeological sites around the world, often found as accumulations up to several meters heigh called shell middens (Álvarez et al. 2011; Ambrose 1967; Hausmann et al. 2019; Lindauer et al. 2017a; Waselkov 1987). This abundance in the archeological record makes them a useful material to construct site chronologies, especially since mollusk shells are present even where other materials are absent or too degraded to be radiocarbon dated (e.g., especially in arid environments in the Arabian Peninsula such as the case of Ksar Akil and similar sites (Biagi 1994; Bosch et al. 2015a; Douka et al. 2013; Magee et al. 2009). Shells are thus frequently used to constrain chronologies from archaeological sites where other materials are unavailable, where it is crucial to consider the different variables affecting ^{14}C content in the shells before drawing important conclusions about human evolution. Some of these variables are briefly described in the following paragraphs.

1.3.1. RESERVOIR EFFECTS

Shells show an older radiocarbon age compared to contemporaneous terrestrial materials and this offset is known as the reservoir effect. It is caused by the slow diffusion of CO_2 through the ocean surface and the even slower circulation of deep oceanic water masses, which cause a higher depletion than replenishment of ^{14}C (Figure 9). Subsequently, the different global and local ocean currents influence the amount of ^{14}C depleted water at each location and the local reservoir effect. The current marine calibration curve (Marine20) that was developed to account for this offset in ^{14}C in the ocean, includes comparison to reservoir ages that have been determined using known-age specimens from museum collections, which were collected alive (during the pre-bomb era (Heaton et al. 2020). It should be noted that the nuclear bomb tests caused an enormous increase of atmospheric ^{14}C values, which were stored in the ocean reservoir in a large amount, causing a reduced or absent reservoir age in marine organisms nowadays compared to the pre-bomb period (Jenkins et al. 2010). The average pre-bomb period value of the marine reservoir offset is approximately 400 ^{14}C years for the global surface oceans in the Northern hemisphere (Stuiver and Braziunas 1993). However, as mentioned, the marine reservoir age values vary geographically and can range from about 400 ^{14}C years in subtropical oceans to over 1000 ^{14}C years near the poles (Reimer and Reimer 2001). These values are influenced by factors such as ocean currents, freshwater inputs and the presence of different upwelling intensities bringing ^{14}C depleted waters to the surface ocean, where they are incorporated into marine organisms (Alves et al. 2018). When performing ^{14}C calibration for marine

samples, the regional variation of the reservoir age has usually been taken into account by including a regional correction to the marine calibration curve called ΔR but the time dependence of both the reservoir age and ΔR has made marine calibration more uncertain than for terrestrial samples (Russell et al. 2011b). In 2001 an on-line marine reservoir correction database has been developed and updated through the years, to allow for the correct calibration of marine sample ages (Reimer and Reimer 2001), while more recently an on-line application for the calculation of ΔR offsets has also been developed (Reimer and Reimer 2017). However, the local reservoir effect also varies for different species and through time (Lindauer 2019). Some studies on the determination of species-specific reservoir effects are already available (Alves et al. 2015; Hadden and Cherkinsky 2017; Paterne et al. 2018; Russell et al. 2011a), although mean values irrespective of species are still being determined by some authors (Diaz et al. 2017). To establish reliable radiocarbon chronologies using shells, the reservoir effect must be determined considering both the location, period, and species of interest to avoid increasing the dating uncertainty and causing subsequent erroneous interpretations.

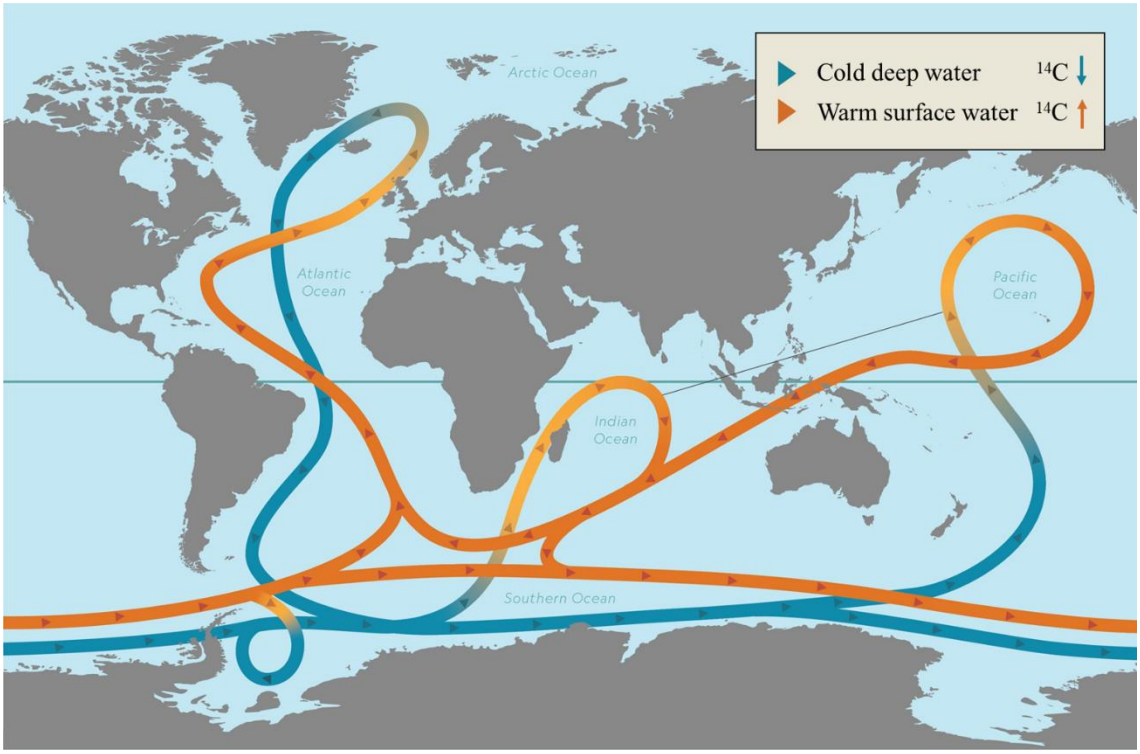

Figure 9. Schematic representation of the global termohaline circulation. Figure modified after National-Geographic-Society 2023.

The terrestrial equivalent of the reservoir effect is the hardwater effect, caused by the uptake of ^{14}C deprived carbon from limestones or carbonate-bearing rocks by organisms or via groundwater. The hardwater effect can be even larger than the reservoir effect and is important to consider when using freshwater or estuarine mollusk species for radiocarbon dating.

1.3.2. Habitat, Diet and Metabolism

Mollusk shells can provide high-resolution information about paleoenvironments over long periods of time, depending on the species (Andrus 2011; Hallmann et al. 2013; Lindauer 2019; Lindauer et al. 2017b). The shell material contains information about the environmental conditions and food resources throughout the mollusk's entire lifetime (Hallmann et al. 2013; Leng and Lewis 2016; Twaddle et al. 2016). However, even specimens of the same species can be exposed to different local conditions and food availability. The research so far has shown that there are radiocarbon offsets among specimens due to their habitat, food preference and availability, diet, and metabolic differences, as well as carbon uptake and incorporation changes due to stress or illness (Dye 1994; Fernandes et al. 2012; Ingram 1998; Keith and Anderson 1963; Kennett et al. 1997; Killingley and Berger 1979; Lindauer 2019; Wefer and Berger 1991). These offsets, especially among different species, clearly reflect the variable food resources and habitats (Lindauer 2019; Lindauer et al. 2017a). Therefore, before radiocarbon dating archeological specimens it is important to properly investigate the species diet and feeding, as well as shifts in their habitat conditions. Since these differences are mirrored in the ^{14}C content of the shells, we can detect them using stable isotope studies, which can be combined with radiocarbon dating to monitor environmental changes such as freshwater input in estuaries (Hadden et al. 2018; Webb et al. 2007).

1.3.3. Sclerochronology and Stable Isotopes

Numerous targeted and interdisciplinary studies on mollusk shells revealed the potential of using mollusk shells for paleoenvironmental studies with establishment of proxies for different environmental variables (Hallmann et al. 2013; Jones and Allmon 1995; Khim 2003; Lindauer et al. 2017b; Milano et al. 2018a; Milano et al. 2022; Milano et al. 2020; Peharda et al. 2021; Sadler et al. 2012). Mollusk shells incorporate trace elements and stable isotopes in their skeleton which grows in sequential increments, making them high-resolution temporally aligned geochemical records of past environmental conditions and climate changes (Schöne 2008; Schöne and Surge 2012). During suboptimal environmental conditions or other conditions of stress for the mollusk (e.g., spawning, lack of nutrients, extreme salinity, or temperature changes) the shell stops growing and thus no environmental condition is recorded. When conditions improve again and the calcium carbonate production resumes, a "growth line" is produced. The carbonate

deposition is typically periodic (daily or seasonal), and the material deposited between two growth lines called a growth increment. In this sense sclerochronology is comparable to dendrochronology (Figure 10). Both are based on the seasonal growth bands of these organisms which reflect the complex interactions of biological clocks and physiological processes with recurrent environmental pacemakers such as light/dark cycles, tidal exposure and diurnal or seasonal temperature variations (Butler et al. 2019). In fact, using cross dating derived from tree ring research, it is possible to assign precise ages to the growth increments and create absolutely dated chronologies. This allows for the creation of timelines of physical, geochemical, and genetic variability to study past environmental change in great detail. However, the growth hiatuses make the environmental record incomplete and cause a bias towards the physiological optimum of the animal. The conditions that cause changes in growth patterns due to different tolerances are genetically determined and species-specific (Schöne 2008). Furthermore, during aging the overall growth rates and the duration of growth seasons of mollusks decrease creating an ontogenetic trend (McConnaughey and Gillikin 2008; Schöne 2008).

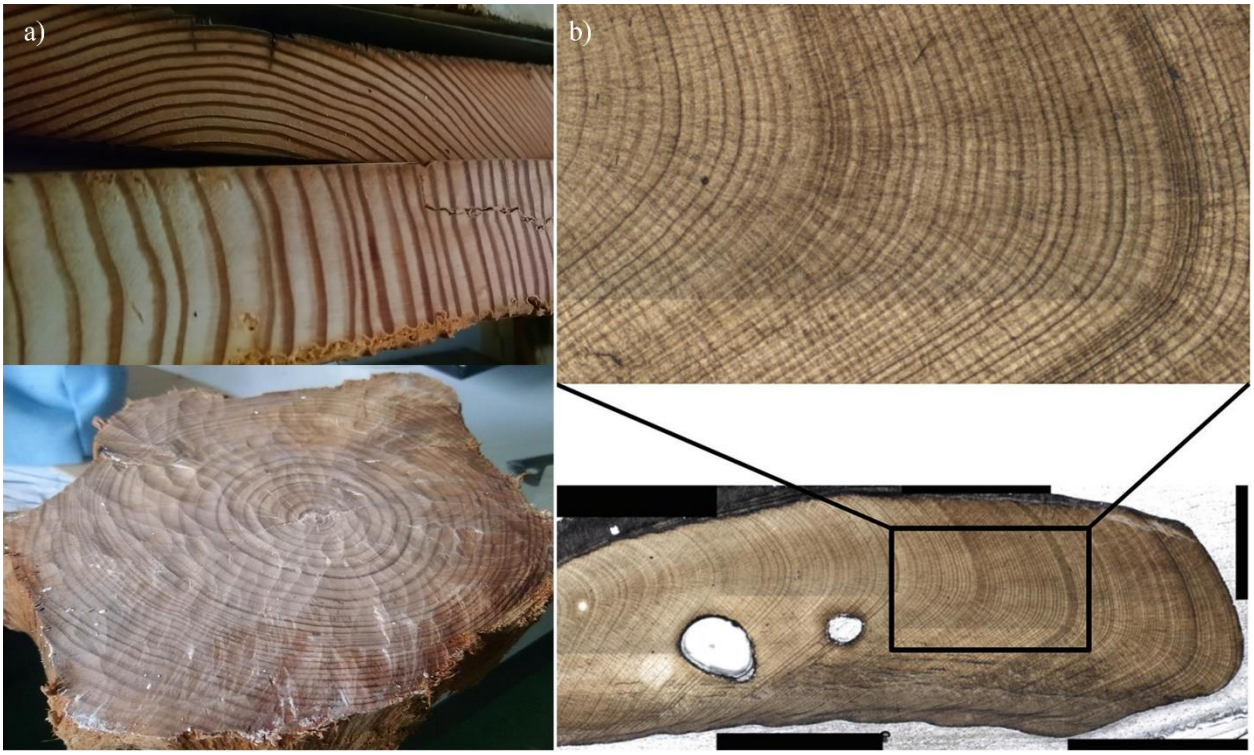

Figure 10. Comparison between the seasonal growth bands of a *Pinus* sp. (a) and of a *Glycymeris glycymeris* shell (b). Figure of *G. glycymeris* adapted from (Butler et al. 2019).

In sclerochronology, a number of proxies (i.e., stable isotopes and trace elements) are used to reconstruct different parameters of the paleoenvironment (Leng and Lewis 2016; McConnaughey and Gillikin 2008; Peharda et al. 2021). The use of stable isotopes as geochemical proxies relies on isotope fractionation during different chemical reactions (e.g., carbonate precipitation or respiration in mollusks) and the preservation of the resultant stable isotope ratio in the shell material. An example of a paleoenvironmental proxy which has been extensively studied, is the shell oxygen isotope content ($\delta^{18}O$), and it is routinely used as a (paleo)thermometer in sclerochronological and archeological studies (Goodwin et al. 2003; Grossman and Ku 1986; Leng and Lewis 2016; Mannino et al. 2008; Milano et al. 2020; Prendergast et al. 2013; Prendergast and Schöne 2017; Schöne et al. 2004). Most shells precipitate their oxygen in or close to equilibrium with the oxygen isotope composition of the ambient water with no known metabolic effects influencing their $\delta^{18}O$ (Wefer and Berger 1991), making it a reliable tracer for temperature and geochemical changes of the water. One of the first empirical paleotemperature equations for the equilibrium precipitation of carbonates was developed by (Grossman and Ku 1986):

$$t = 20.60 - 4.34(c - (w - 0.27))$$

Where:

- t = temperature (°C)
- c = $\delta^{18}O$ of carbonate (compared to Vienna – PeeDee belemnite standard (V-PDB) in ‰)
- w = $\delta^{18}O$ of water (compared to Vienna – standard mean oceanic water (V-SMOW) in ‰).

There are now several paleotemperature equations available for different mollusk species (Butler et al. 2019). Since the correlation between shell oxygen isotopes and temperature is negative (Grossman and Ku 1986); with a change of 1 ‰ in $\delta^{18}O$ corresponding to a change temperature of ca. 4.3 °C), more positive $\delta^{18}O$ values will indicate colder water and more negative $\delta^{18}O$ values warmer water temperatures (Schöne and Surge 2012). Using the shell $\delta^{18}O$ and growth lines, species-specific optimal temperature ranges can also be determined, due to the species-specific physiological tolerances influencing shell growth (Schöne 2008). Furthermore, combining $\delta^{18}O$ shell values with their growth patterns can help determine the periodicity of shell growth, and when temperatures are known it can be used to derive salinity variations in certain periods of time (Schöne and Surge 2012).

Stable isotopes of $\delta^{18}O$ and $\delta^{13}C$ are often measured together and usually along the shells growth direction to monitor changes throughout the lifetime of the mollusk (Milano et al. 2018a; Milano et al. 2022; Milano et al. 2020). Changes in freshwater input and salinity can be detected using both $\delta^{18}O$ and $\delta^{13}C$, given that freshwater and seawater have different isotopic signatures due to different amounts of precipitation and

terrestrial input (i.e., decomposition of terrestrial plants adds CO_2 and thus lighter isotopes to river water). Shells incorporate $\delta^{13}C$ mainly from dissolved inorganic carbon (DIC) in the water and to a minor extent metabolic CO_2 (McConnaughey and Gillikin 2008). Interpreting the $\delta^{13}C$ signal is very challenging due to the many factors influencing the isotopic composition of the shells such as physiological factors, food availability, or varying water DIC levels (including freshwater input (Culleton et al. 2006; McConnaughey and Gillikin 2008), which would also influence the apparent ^{14}C age and the local reservoir effect (e.g., (Culleton et al. 2006). As most of the carbon responsible for the $\delta^{13}C$ should have the same origin as ^{14}C in the shell, measuring radiocarbon along the shell might help to better interpret $\delta^{13}C$ data, and vice versa since the same origin can represent different influences on the respective signals. For example, incorporating carbon from limestone will shift $\delta^{13}C$ towards more positive values, but at the same time will be depleted in ^{14}C, hence shifting the signal towards older ages. Therefore, combining sclerochronology and stable isotope data with radiocarbon dating can shed light on local environmental conditions and how they change over time, helping elucidate certain events in human evolution.

1.3.4. HUMAN PROCESSING OF MOLLUSK SHELLS

Archaeological research has shown that the human processing of mollusk shells occurs not far from the place of collection in most cases, due to the high weight of the shell relative to that of the edible soft tissue (Waselkov 1987). Therefore, mollusk shells can be considered a reliable indicator of local coastal conditions near the site from which they were collected. However, shell foraging and processing often includes heating of shells that inflicts a transformation from aragonite to calcite and can also destroy the microstructural pattern of the shell material (Lindauer et al. 2018; Milano et al. 2018b; Milano and Nehrke 2018; Milano et al. 2016). Such shells cannot always be distinguished with certainty from non-heated ones during collection in the field, raising the question if the reservoir effect and stable isotope signatures are affected by the heat exposure. So far, the studies on heat exposure in shells have found that an exchange of oxygen isotopes with the surrounding environment occurs during heating and it drastically alters the initial shell isotopic composition (Milano et al. 2016). Even though the oxygen isotopes showed significant changes in burnt shells, it was discovered that the radiocarbon ages from heated shells show a narrower range of variability compared to unheated shells (Lindauer 2019; Lindauer et al. 2018). This is possibly due to a closure of the shell structures during heat exposure which prevents external carbon from entering the shell structure even when polymorphic transformation has occurred (Lindauer 2019; Lindauer et al. 2018). Although heat significantly alters the appearance and mineralogy of shells, ^{14}C AMS ages obtained on burnt shells showed agreement with the archeological context they were found in, indicating that reliable dates can be obtained even on heat processed shells (Lindauer 2019; Lindauer et al. 2018).

1.3.5. POST DEPOSITIONAL AND DIAGENETIC PROCESSES

Last, but certainly not least, it is necessary to consider all the processes affecting the shell after it is deposited at the archeological site. In shells, there is a complex organization of calcium carbonate ($CaCO_3$) units and organic compounds with extraordinary resistance to mechanical and chemical stresses (Barthelat 2010). Yet over long timescales, diagenesis can still alter their material properties. Diagenesis encompasses all physical and chemical processes occurring to the tissues after the death of the animal, which are important to consider in case of archeological remains for a correct interpretation of obtained results. Specimens from the same archaeological layer should have a comparable preservation state since they are subjected to similar environmental conditions after burial (i.e., depth, sediment composition and soil pH). The overall preservation state indicates whether natural diagenesis altered the shells, and any further deviation from it likely indicates additional processes which might have affected the shell. One of the most prominent diagenetic processes which can occur in mollusk shells is recrystallization, which can be present in significant detectable amounts or limited to small portions of the shells. During recrystallization the primary carbonate phase, often the less stable polymorph – aragonite, transforms into a secondary more stable phase, often calcite (Toffolo 2021). This process creates the potential for isotopic exchange and the incorporation of exogenous carbon that can alter the ^{14}C signal and therefore the resulting age (Loftus et al. 2015; Webb et al. 2007). Sand blasting and abrasion were thought to remove surface contamination and altered portions, assumed to also be concentrated mainly on the outer portion of the shells. Attempts have also been made to exclude diagenetically altered shell portions from ^{14}C dating through chemical etching, but this methodology was not successful due to the higher solubility of aragonite compared to calcite (Vita-Finzi and Roberts 1984). Shell mineralogical composition can be determined using several different techniques including Confocal Raman Microscopy (CRM (Nehrke and Nouet 2011; Toffolo 2021), Scanning Electron Microscopy (SEM (Dauphin 2008; Toffolo 2021), Fourier Transform Infrared Spectrometry (FTIR (Loftus et al. 2015; Toffolo 2021) and X-ray diffraction (XRD (Douka et al. 2010; Russo et al. 2010; Toffolo 2021) which can allow for the detection of recrystallization in certain cases. In 2010, a new pre-treatment protocol was developed to attempt the removal of diagenetically altered shell portions through density separation of aragonite and calcite, showing great potential for the improvement of ^{14}C dates in heavily recrystallized shells (Douka et al. 2010; Russo et al. 2010) and will be discussed more in Chapter 2. However, diagenetic processes can often occur without a change in carbonate polymorphs, meaning that aragonite cannot be automatically considered the primary phase and the mere determination of the carbonate polymorph is not indicative of the presence or amount of diagenesis in the sample (Guzmán et al. 2009; Perrin 2004; Toffolo 2021). Furthermore, variation in diagenetic effects among shell samples was hypothesized in a previous study after the application of both XRD and Scanning

electron microscopy which did not always show consistent results (Barton 2012). Additionally, some of the samples which were determined as well-preserved gave radiocarbon determinations which despite that were statistical outliers (Barton 2012).Therefore, to truly asses the preservation state of the shells there is a need for multiple lines of evidence, and the polymorph detection should be combined with other tests such as microscopic examination of the crystalline structure and the examination of the organic matter preservation (Guzmán et al. 2009; Perrin 2004; Toffolo 2021).

1.3.6. THE SHELL ORGANIC MATRIX

The radiocarbon and stable isotope research so far focused almost exclusively on the carbonate fraction of shells (Douka et al. 2010; Peharda et al. 2021; Russo et al. 2010). However, as shells are biogenic structures, they contain a small portion of organic matter as well (< 5 wt%) (Kobayashi and Samata 2006; LeBlanc 1989; Marin et al. 2012; Marin et al. 2007; Marin et al. 2013; Suzuki and Nagasawa 2013; Weiner 1979; 1984; Weiner and Hood 1975; Weiner and Traub 1980; Weiner et al. 1983; Wheeler et al. 1988; Wheeler and Sikes 1984). Biomineralization in mollusk shells constitutes of a series of organic matrix – mediated processes which result in the formation of the calcium carbonate structures (Falini et al. 1996; Weiner and Dove 2003). The functions performed by different matrix constituents in mollusk shells are still poorly understood, yet it is clear that they have important roles in biomineralization (Nudelman et al. 2006; Suzuki and Nagasawa 2013; Weiner 1979; Weiner and Hood 1975). The organic matrix is also thought to take part in cell signaling, enzymatic (Marin et al. 2012; Marin et al. 2007; Marin et al. 2013) and immunity functions (Arivalagan et al. 2017). It is often divided into two biochemically and functionally distinct units: a soluble and an insoluble fraction (Grégoire 1972; LeBlanc 1989; Lowenstam and Weiner 1989; Suzuki and Nagasawa 2013; Weiner 1984; Weiner and Hood 1975; Weiner and Traub 1980; Wheeler et al. 1988; Wheeler and Sikes 1984). In the insoluble fraction, glycine, alanine, phenylalanine and tyrosine are the main amino acids constituting the proteins, which are crosslinked by phenoloxidase making this fraction insoluble (Weiner et al. 1983). On the other hand, the proteins of the soluble matrix are rich in aspartic acid and to a lesser extent glutamic acid (Weiner 1979; Weiner et al. 1983). The insoluble matrix is thought to act as a structural framework, directing the calcium carbonate mineralization by regulating crystal nucleation, orientation, and polymorphism, while the soluble fraction was found to have a role in the binding of calcium ions regulating crystal growth and morphology (Suzuki and Nagasawa 2013; Weiner and Hood 1975; Weiner and Traub 1980; Weiner et al. 1983). A recent study found that the organic intracrystalline matrix also plays an important role in the diagenetic mineralogical transformation from aragonite to calcite (Milano and Nehrke 2018). Even though its composition and functions have been studied since the late 1900s, researchers have only recently started using the organic fraction for radiocarbon dating (Hadden et al. 2018; Hadden et al. 2019) and stable isotope studies (Carroll et al. 2006; Ellis et al. 2014; Misarti et al. 2017; O'Donnell et al. 2007; Whitney et al. 2019). Furthermore, it was demonstrated that the intracrystalline organic matrix represents a closed system that should be unaffected by diagenetic processes (Penkman et al. 2008). Therefore, investigating the ^{14}C of the organic matrix could allow us to potentially improve the accuracy of the chronometric results and to increase the reliability of shells as suitable dating materials. Additionally, the stable isotope composition of the shell organic matrix could be a useful addition to the suite of available paleoenvironmental proxies.

1.4. PROJECT AIM

The overall objective of this project is to make steps forwards, toward more reliable methods and a better understanding of mollusk shells and their use for radiocarbon dating and the study of human evolution. Due to a lack of well-preserved remains in many archeological sites, especially for the period of the MUP, mollusk shells are often the only available material to use for radiocarbon dating. Therefore, obtaining reliable radiocarbon determinations on mollusk shells might allow for the construction of new radiocarbon chronologies and add crucial information about the timing of human migrations, interactions, and cognitive development. Furthermore, the use of mollusk shells for paleoenvironmental reconstructions also makes them a useful resource for the study of human evolution as they provide additional evidence helpful for the interpretation of scenarios of human migration, adaptation, and behavior. However, using mollusk shells in the study of past environments and for radiocarbon dating is a complex issue and comes with many sources of uncertainty, leaving ample room for improvement. Chapters 2 and 3 of this thesis focus on establishing and applying novel methodological approaches concerning the pretreatment and measurement of radiocarbon and stable isotopes in archeological and modern mollusk shells. Standard methods for both radiocarbon and stable isotope studies focus on the carbonate fraction of the mollusk shell. However, the shell contains a minor organic fraction which has an important role in the biomineralization and is still not fully understood. This thesis explores the potential of the shell organic matrix for radiocarbon dating and paleoenvironmental studies.

1.4.1 CHAPTER 2 - CHEMICAL PRETREATMENT FOR RADIOCARBON DATING

The first chapter of this thesis explores the existing radiocarbon pretreatment protocols for mollusk shells and aims at introducing new solutions to attempt a better and more reliable age determination.

The standard acid etching pretreatment method for mollusk shells is the most used in many ^{14}C laboratories, although another pretreatment protocol known as CarDS (Carbonate Density Separation) was introduced just over a decade ago. We compare these two methods targeting the carbonate fraction, with two newly proposed methods aiming at extracting the intracellular organic fraction of the shell which has been largely overlooked by the radiocarbon community. We tested the methods on modern shell specimens first to make adjustments to the protocols if and when necessary. We then applied all four methods to samples selected from different archeological layers of the well-known Upper Paleolithic site of Vale Boi.

The results of this study have been accepted to the Radiocarbon journal for peer review in a manuscript titled "To date or not to date? A comparison of different ^{14}C pretreatment methods applied to archeological marine shells from Vale Boi (Portugal)." **Dragana Paleček**, Giuseppe Falini, Lukas Wacker, Marcello A. Mannino, Nuno Bicho, João Cascalheira, Alessandro G. Rombolà, Daniele Fabbri, Sahra Talamo.

1.4.2 CHAPTER 3 – STABLE ISOTOPE ANALYSIS IN THE SHELL ORGANIC MATRIX

The second chapter of this thesis investigates the use of oxygen and hydrogen stable isotope determinations from the shell organic matrix as proxies for environmental reconstructions.

As for radiocarbon dating, stable isotope studies focus mainly on the carbonate fraction of mollusk shells, leaving the organic fraction largely unexplored. After extraction and separation of the soluble and insoluble fractions of the organic matrix of modern *Mytilus galloprovincialis* shells, we measure their hydrogen and oxygen stable isotope compositions. The shells were collected from three sites in Cantabria, Northern Spain located along a coast–to-upper estuary environmental gradient, which allowed for a study of the effect of different environmental parameters on the stable isotope composition.

The results obtained in this study have been submitted for publication in Nature Communications Chemistry in a manuscript titled: "Stable isotopes in the shell organic matrix for (paleo)environmental reconstructions". **Dragana Paleček**, Stefania Milano, Igor Gutiérrez-Zugasti, Sahra Talamo.

1.4.3 CHAPTER 4 – CONCLUSIONS AND OUTLOOK

The final section of this dissertation will provide a brief conclusion of the outcomes of this PhD project and discuss the implications for future applications.

1.5. REFERENCES

Adolphi F, Muscheler R, Friedrich M, Güttler D, Wacker L, Talamo S, Kromer B. 2017. Radiocarbon calibration uncertainties during the last deglaciation: Insights from new floating tree-ring chronologies. Quaternary Science Reviews. 170:98-108.

Ahyong S, Boyko CB, Bailly N, Bernot J, Bieler R, Brandão SN, Daly M, De Grave S, Gofas S, Hernandez F et al. 2023. World register of marine species (worms). WoRMS Editorial Board.

Aitken MJ. 1990. Science-based dating in archaeology. Routledge.

Álvarez-Fernández E, Bécares J, Jordá Pardo JF, Agirre-Uribesalgo A, Álvarez-Alonso D, Aparicio MT, Barrera-Mellado I, Carral P, Carriol R-P, Cubas M et al. 2020. Palaeoenvironmental and chronological context of human occupations at el cierro cave (northern spain) during the transition from the late upper pleistocene to the early holocene. Journal of Archaeological Science: Reports. 29.

Álvarez M, Briz Godino I, Balbo A, Madella M. 2011. Shell middens as archives of past environments, human dispersal and specialized resource management. Quaternary International. 239(1):1-7.

Alves E, Macario K, Souza R, Aguilera O, Goulart AC, Scheel-Ybert R, Bachelet C, Carvalho C, Oliveira F, Douka K. 2015. Marine reservoir corrections on the southeastern coast of brazil: Paired samples from the saquarema shellmound. Radiocarbon. 57(4):517-525.

Alves EQ, Macario K, Ascough P, Christopher. 2018. The worldwide marine radiocarbon reservoir effect: Definitions, mechanisms, and prospects. Reviews of Geophysics. 56(1):278-305.

Ambrose SH. 1990. Preparation and characterization of bone and tooth collagen for isotopic analysis. Journal of Archaeological Science. 17(4):431-451.

Ambrose WR. 1967. Archaeology and shell middens. Archaeology & Physical Anthropology in Oceania. 2(3):169-187.

Anderson E, Arnold J, Libby W. 1951. Measurement of low level radiocarbon. Review of Scientific Instruments. 22(4):225-230.

Anderson EC, Libby WF. 1951. World-wide distribution of natural radiocarbon. Physical Review. 81(1):64.

Andrus CFT. 2011. Shell midden sclerochronology. Quaternary Science Reviews. 30(21):2892-2905.

Arivalagan J, Yarra T, Marie B, Sleight VA, Duvernois-Berthet E, Clark MS, Marie A, Berland S. 2017. Insights from the shell proteome: Biomineralization to adaptation. Molecular Biology and Evolution. 34(1):66-77.

Bailey G, Flemming N. 2008. Archaeology of the continental shelf: Marine resources, submerged landscapes and underwater archaeology. Quaternary Science Reviews. 27(23-24):2153-2165.

Bar-Yosef Mayer DE, Vandermeersch B, Bar-Yosef O. 2009. Shells and ochre in middle paleolithic qafzeh cave, israel: Indications for modern behavior. J Hum Evol. 56(3):307-314.

Bar-Yosef O. 1998. On the nature of transitions: The middle to upper palaeolithic and the neolithic revolution. Cambridge Archaeological Journal. 8(2):141-163.

Barthelat F. 2010. Nacre from mollusk shells: A model for high-performance structural materials. Bioinspiration & Biomimetics. 5(3):035001.

Barton R. 2012. Gibraltar neanderthals in context. A report of the 1995-98 excavations at gorham's and vanguard caves, gibraltar.

Bayliss A. 2009. Rolling out revolution: Using radiocarbon dating in archaeology. Radiocarbon. 51(1):123-147.

Bayliss A, Bronk Ramsey C. 2004. Pragmatic bayesians: A decade of integrating radiocarbon dates into chronological models. Tools for Constructing Chronologies: crossing disciplinary boundaries.25-41.

Benazzi S, Douka K, Fornai C, Bauer CC, Kullmer O, Svoboda J, Pap I, Mallegni F, Bayle P, Coquerelle M et al. 2011. Early dispersal of modern humans in europe and implications for neanderthal behaviour. Nature. 479(7374):525-528.

Biagi P. 1994. A radiocarbon chronology for the aceramic shell-middens of coastal oman. Arabian Archaeology and Epigraphy. 5(1):17-31.

Bicho N, Haws J. 2008. At the land's end: Marine resources and the importance of fluctuations in the coastline in the prehistoric hunter–gatherer economy of portugal. Quaternary Science Reviews. 27(23-24):2166-2175.

Bicho N, Umbelino C, Detry C, Pereira T. 2010. The emergence of muge mesolithic shell middens in central portugal and the 8200 cal yr bp cold event. The Journal of Island and Coastal Archaeology. 5(1):86-104.

Bird MI, Ayliffe LK, Fifield LK, Turney CSM, Cresswell RG, Barrows TT, David B. 1999. Radiocarbon dating of “old” charcoal using a wet oxidation, stepped-combustion procedure. Radiocarbon. 41(2):127-140.

Bosch MD, Mannino MA, Prendergast AL, O'Connell TC, Demarchi B, Taylor SM, Niven L, van der Plicht J, Hublin JJ. 2015a. New chronology for ksar 'akil (lebanon) supports levantine route of modern human dispersal into europe. Proc Natl Acad Sci U S A. 112(25):7683-7688.

Bosch MD, Mannino MA, Prendergast AL, O'Connell TC, Demarchi B, Taylor SM, Niven L, van der Plicht J, Hublin JJ. 2015b. Reply to douka et al.: Critical evaluation of the ksar 'akil chronologies. Proc Natl Acad Sci U S A. 112(51):E7035.

Broecker WS. 1991. The great ocean conveyor. Oceanography. 4(2):79-89.

Bronk Ramsey C. 2008. Radiocarbon dating: Revolutions in understanding. Archaeometry. 50(2):249-275.

Butler PG, Freitas PS, Burchell M, Chauvaud L. 2019. Archaeology and sclerochronology of marine bivalves. Goods and Services of Marine Bivalves.413-444.

Carrion J, Finlayson C, Fernandez S, Finlayson G, Allue E, Lopezsaez J, Lopezgarcia P, Gilromera G, Bailey G, Gonzalezsamperiz P. 2008. A coastal reservoir of biodiversity for upper pleistocene human populations: Palaeoecological investigations in gorham's cave (gibraltar) in the context of the iberian peninsula. Quaternary Science Reviews. 27(23-24):2118-2135.

Carroll M, Romanek C, Paddock L. 2006. The relationship between the hydrogen and oxygen isotopes of freshwater bivalve shells and their home streams. Chemical Geology. 234(3-4):211-222.

Cercatillo S, Friedrich M, Kromer B, Paleček D, Talamo S. 2021. Exploring different methods of cellulose extraction for 14c dating. New Journal of Chemistry. 45(20):8936-8941.

Cersoy S, Daheur G, Zazzo A, Zirah S, Sablier M. 2018. Pyrolysis comprehensive gas chromatography and mass spectrometry: A new tool to assess the purity of ancient collagen prior to radiocarbon dating. Analytica chimica acta. 1041:131-145.

Colonese AC, Mannino MA, Bar-Yosef Mayer DE, Fa DA, Finlayson JC, Lubell D, Stiner MC. 2011. Marine mollusc exploitation in mediterranean prehistory: An overview. Quaternary International. 239(1-2):86-103.

Conard NJ, Bolus M. 2003. Radiocarbon dating the appearance of modern humans and timing of cultural innovations in europe: New results and new challenges. Journal of Human Evolution. 44(3):331-371.

Conard NJ, Bolus M. 2008. Radiocarbon dating the late middle paleolithic and the aurignacian of the swabian jura. Journal of Human Evolution. 55(5):886-897.

Cortés-Sánchez M, Morales-Muñiz A, Simón-Vallejo MD, Lozano-Francisco MC, Vera-Peláez JL, Finlayson C, Rodríguez-Vidal J, Delgado-Huertas A, Jiménez-Espejo FJ, Martínez-Ruiz F et al. 2011. Earliest known use of marine resources by neanderthals. PLoS ONE. 6(9):e24026.

Culleton BJ, Kennett DJ, Ingram BL, Erlandson JM, Southon JR. 2006. Intrashell radiocarbon variability in marine mollusks. Radiocarbon. 48(3):387-400.

D'Errico F, Zilhão J, Julien M, Baffier D, Pelegrin J. 1998. Neanderthal acculturation in western europe? A critical review of the evidence and its interpretation. Current Anthropology. 39(S1):S1-S44.

Dauphin Y. 2008. The nanostructural unity of mollusc shells. Mineralogical Magazine. 72(1):243-246.

de Vries H. 1958. Variation in concentration of radiocarbon with time and location on earth. Proc Koninkl Nederl Akad Wetenschappen, B. 61:1-9.

Diaz M, Macario K, Gomes P, Álvarez-Lajonchere L, Aguilera O, Alves E. 2017. Radiocarbon marine reservoir effect on the northwestern coast of cuba. Radiocarbon. 59(2):333-341.

Douka K. 2011. An upper palaeolithic shell scraper from ksar akil (lebanon). Journal of Archaeological Science. 38(2):429-437.

Douka K, Bergman CA, Hedges RE, Wesselingh FP, Higham TF. 2013. Chronology of ksar akil (lebanon) and implications for the colonization of europe by anatomically modern humans. PLoS One. 8(9):e72931.

Douka K, Chiotti L, Nespoulet R, Higham T. 2020. A refined chronology for the gravettian sequence of abri pataud. Journal of Human Evolution. 141:102730.

Douka K, Hedges RE, Higham TFJR. 2010. Improved ams 14 c dating of shell carbonates using high-precision x-ray diffraction and a novel density separation protocol (cards). 52(2):735-751.

Douka K, Higham TF, Bergman CA. 2015. Statistical and archaeological errors invalidate the proposed chronology for the site of ksar akil. Proc Natl Acad Sci U S A. 112(51):E7034.

Douka K, Spinapolice EE. 2012. Neanderthal shell tool production: Evidence from middle palaeolithic italy and greece. Journal of World Prehistory. 25(2):45-79.

Dye T. 1994. Apparent ages of marine shells: Implications for archaeological dating in hawai'i. Radiocarbon. 36(1):51-57.

Ellis GS, Herbert G, Hollander D. 2014. Reconstructing carbon sources in a dynamic estuarine ecosystem using oyster amino acid δ¹³c values from shell and tissue. Journal of Shellfish Research. 33(1):217-225, 219.

Fa DA, Finlayson JC, Finlayson G, Giles-Pacheco F, Rodríguez-Vidal J, Gutiérrez-López JM. 2016. Marine mollusc exploitation as evidenced by the gorham's cave (gibraltar) excavations 1998–2005: The middle–upper palaeolithic transition. Quaternary International. 407:16-28.

Fernandes R, Bergemann S, Hartz S, Grootes PM, Nadeau M-J, Melzner F, Rakowski A, Hüls M. 2012. Mussels with meat: Bivalve tissue-shell radiocarbon age differences and archaeological implications. Radiocarbon. 54(3-4):953-965.

Fewlass H, Talamo S, Kromer B, Bard E, Tuna T, Fagault Y, Sponheimer M, Ryder C, Hublin J-J, Perri A et al. 2019a. Direct radiocarbon dates of mid upper palaeolithic human remains from dolní věstonice ii and pavlov i, czech republic. Journal of Archaeological Science: Reports. 27:102000.

Fewlass H, Talamo S, Tuna T, Fagault Y, Kromer B, Hoffmann H, Pangrazzi C, Hublin J-J, Bard E. 2017. Size matters: Radiocarbon dates of <200 µg ancient collagen samples with aixmicadas and its gas ion source. Radiocarbon. 60(2):425-439.

Fewlass H, Talamo S, Wacker L, Kromer B, Tuna T, Fagault Y, Bard E, McPherron SP, Aldeias V, Maria R. 2020. A 14c chronology for the middle to upper palaeolithic transition at bacho kiro cave, bulgaria. Nature ecology & evolution. 4(6):794-801.

Fewlass H, Tuna T, Fagault Y, Hublin JJ, Kromer B, Bard E, Talamo S. 2019b. Pretreatment and gaseous radiocarbon dating of 40-100 mg archaeological bone. Sci Rep. 9(1):5342.

Finlayson C, Carrión JS. 2007. Rapid ecological turnover and its impact on neanderthal and other human populations. Trends in Ecology & Evolution. 22(4):213-222.

Gillikin DP, Wanamaker AD, Andrus CFT. 2019. Chemical sclerochronology. Chemical Geology. 526:1-6.

Godwin H. 1962. Radiocarbon dating: Fifth international conference. Nature. 195:943-945.

Goodwin DH, Schone BR, Dettman DL. 2003. Resolution and fidelity of oxygen isotopes as paleotemperature proxies in bivalve mollusk shells: Models and observations. Palaios. 18(2):110-125.

Gordon JE, Harkness DD. 1992. Magnitude and geographic variation of the radiocarbon content in antarctic marine life: Implications for reservoir corrections in radiocarbon dating. Quaternary Science Reviews. 11(7-8):697-708.

Grégoire C. 1972. Structure of the molluscan shell. Chemical zoology. 7:45-102.

Grossman EL, Ku T-L. 1986. Oxygen and carbon isotope fractionation in biogenic aragonite: Temperature effects. Chemical Geology: Isotope Geoscience Section. 59:59-74.

Guzmán N, Dauphin Y, Cuif JP, Denis A, Ortlieb L. 2009. Diagenetic changes in concholepas concholepas shells (gastropoda, muricidae) in the hyper-arid conditions of northern chile – implications for palaeoenvironmental reconstructions. Biogeosciences. 6(2):197-207.

Hadden CS, Cherkinsky A. 2017. Carbon reservoir effects in eastern oyster from apalachicola bay, USA. Radiocarbon. 59(5):1497-1506.

Hadden CS, Loftis KM, Cherkinsky A. 2018. Carbon isotopes (δ13c and δ14c) in shell carbonate, conchiolin, and soft tissues in eastern oyster (crassostrea virginica). Radiocarbon. 60(4):1125-1137.

Hadden CS, Loftis KM, Cherkinsky A, Ritchison BT, Lulewicz IH, Thompson VD. 2019. Radiocarbon in marsh periwinkle (littorina irrorata) conchiolin: Applications for archaeology. Radiocarbon. 61(5):1489-1500.

Hallmann N, Burchell M, Brewster N, Martindale A, Schöne B. 2013. Holocene climate and seasonality of shell collection at the dundas islands group, northern british columbia, canada—a bivalve sclerochronological approach. Palaeogeography, Palaeoclimatology, Palaeoecology. 373:163-172.

Hausmann N, Meredith-Williams M, Douka K, Inglis RH, Bailey G. 2019. Quantifying spatial variability in shell midden formation in the farasan islands, saudi arabia. PLoS One. 14(6):e0217596.

Heaton TJ, Köhler P, Butzin M, Bard E, Reimer RW, Austin WEN, Bronk Ramsey C, Grootes PM, Hughen KA, Kromer B et al. 2020. Marine20—the marine radiocarbon age calibration curve (0–55,000 cal bp). Radiocarbon. 62(4):779-820.

Hogg AG, Heaton TJ, Hua Q, Palmer JG, Turney CS, Southon J, Bayliss A, Blackwell PG, Boswijk G, Ramsey CB. 2020. Shcal20 southern hemisphere calibration, 0–55,000 years cal bp. Radiocarbon. 62(4):759-778.

Hublin J-J. 2015. The modern human colonization of western eurasia: When and where? Quaternary Science Reviews. 118:194-210.

Hublin J-J, Spoor F, Braun M, Zonneveld F, Condemi S. 1996. A late neanderthal associated with upper palaeolithic artefacts. Nature. 381:224-226.

Hublin JJ, Talamo S, Julien M, David F, Connet N, Bodu P, Vandermeersch B, Richards MP. 2012. Radiocarbon dates from the grotte du renne and saint-cesaire support a neandertal origin for the chatelperronian. Proc Natl Acad Sci U S A. 109(46):18743-18748.

Hughen K, Lehman S, Southon J, Overpeck J, Marchal O, Herring C, Turnbull J. 2004. 14c activity and global carbon cycle changes over the past 50,000 years. Science. 303(5655):202-207.

Ingram BL. 1998. Differences in radiocarbon age between shell and charcoal from a holocene shellmound in northern california. Quaternary Research. 49(1):102-110.

Jenkins WJ, Elder KL, McNichol AP, Von Reden K. 2010. The passage of the bomb radiocarbon pulse into the pacific ocean. Radiocarbon. 52(3):1182-1190.

Jones DS, Allmon WD. 1995. Records of upwelling, seasonality and growth in stable-isotope profiles of pliocene mollusk shells from florida. Lethaia. 28(1):61-74.

Joordens JC, d'Errico F, Wesselingh FP, Munro S, de Vos J, Wallinga J, Ankjaergaard C, Reimann T, Wijbrans JR, Kuiper KF et al. 2015. Homo erectus at trinil on java used shells for tool production and engraving. Nature. 518(7538):228-231.

Jull A, Pearson C, Taylor RE, Southon J, Santos GM, Kohl C, Hajdas I, Molnar M, Baisan C, Lange TE. 2018. Radiocarbon dating and intercomparison of some early historical radiocarbon samples. Radiocarbon. 60(2):535-548.

Keith M, Anderson G. 1963. Radiocarbon dating: Fictitious results with mollusk shells. Science. 141(3581):634-637.

Kennett DJ, Ingram BL, Erlandson JM, Walker P. 1997. Evidence for temporal fluctuations in marine radiocarbon reservoir ages in the santa barbara channel, southern california. Journal of Archaeological Science. 24(11):1051-1059.

Khim B-K. 2003. Seasonal discharge of estuarine freshwater to the western chukchi sea shelf identified in stable isotope profiles of mollusk shells. Journal of Geophysical Research. 108(C9).

Killingley JS, Berger WH. 1979. Stable isotopes in a mollusk shell: Detection of upwelling events. Science. 205(4402):186-188.

Kobayashi I, Samata T. 2006. Bivalve shell structure and organic matrix. Materials Science and Engineering: C. 26(4):692-698.

Korlevic P, Talamo S, Meyer M. 2018. A combined method for DNA analysis and radiocarbon dating from a single sample. Sci Rep. 8(1):4127.

LeBlanc C. 1989. Terrestrial input to estuarine bivalves as measured by multiple stable isotopes tracers.

Leng MJ, Lewis JP. 2016. Oxygen isotopes in molluscan shell: Applications in environmental archaeology. Environmental Archaeology. 21(3):295-306.

Libby W. 1955. Radiocarbon dating, the university of chicago press. Chicago.

Libby WF, Anderson EC, Arnold JR. 1949. Age determination by radiocarbon content: World-wide assay of natural radiocarbon. Science. 109(2827):227-228.

Lindauer S. 2019. Radiocarbon reservoir effects on shells from se arabia in the context of paleoenvironmental studies. PhD thesis - Technical University Darmstadt.

Lindauer S, Kromer B. 2013. Carbonate sample preparation for 14c dating using an elemental analyzer. Radiocarbon. 55(2):364-372.

Lindauer S, Marali S, Schöne BR, Uerpmann H-P, Kromer B, Hinderer M. 2017a. Investigating the local reservoir age and stable isotopes of shells from southeast arabia. Radiocarbon. 59(2):355-372.

Lindauer S, Milano S, Steinhof A, Hinderer M. 2018. Heating mollusc shells-a radiocarbon and microstructure perspective from archaeological shells recovered from kalba, sharjah emirate, uae. Journal of Archaeological Science: Reports. 21:528-537.

Lindauer S, Santos GM, Steinhof A, Yousif E, Phillips C, Jasim SA, Uerpmann H-P, Hinderer M. 2017b. The local marine reservoir effect at kalba (uae) between the neolithic and bronze age: An indicator of sea level and climate changes. Quaternary Geochronology. 42:105-116.

Linstädter J, Broich M, Weninger B. 2018. Defining the early neolithic of the eastern rif, morocco – spatial distribution, chronological framework and impact of environmental changes. Quaternary International. 472:272-282.

Loftus E, Rogers K, Lee-Thorp J. 2015. A simple method to establish calcite:Aragonite ratios in archaeological mollusc shells. Journal of Quaternary Science. 30(8):731-735.

Lowenstam HA, Weiner S. 1989. On biomineralization. Oxford University Press on Demand.

Lugli F, Sciutto G, Oliveri P, Malegori C, Prati S, Gatti L, Silvestrini S, Romandini M, Catelli E, Casale M et al. 2021. Near-infrared hyperspectral imaging (nir-hsi) and normalized difference image (ndi) data processing: An advanced method to map collagen in archaeological bones. Talanta. 226:122126.

Magee P, Uerpmann HP, Uerpmann M, Jasim SA, Händel M, Barber D, Fritz C, Hammer E. 2009. Multi-disciplinary research on the past human ecology of the east arabian coast: Excavations at hamriya and tell abraq (emirate of sharjah, united arab emirates). Arabian Archaeology and Epigraphy. 20(1):18-29.

Malegori C, Sciutto G, Oliveri P, Prati S, Gatti L, Catelli E, Benazzi S, Cercatillo S, Paleček D, Mazzeo R. 2023. Near-infrared hyperspectral imaging to map collagen content in prehistoric bones for radiocarbon dating. Communications Chemistry. 6(1):54.

Mannino MA, Catalano G, Talamo S, Mannino G, Di Salvo R, Schimmenti V, Lalueza-Fox C, Messina A, Petruso D, Caramelli D et al. 2012. Origin and diet of the prehistoric hunter-gatherers on the mediterranean island of favignana (egadi islands, sicily). PLoS One. 7(11):e49802.

Mannino MA, Spiro BF, Thomas KD. 2003. Sampling shells for seasonality: Oxygen isotope analysis on shell carbonates of the inter-tidal gastropod monodonta lineata (da costa) from populations across its modern range and from a mesolithic site in southern britain. Journal of archaeological science. 30(6):667-679.

Mannino MA, Talamo S, Tagliacozzo A, Fiore I, Nehlich O, Piperno M, Tusa S, Collina C, Di Salvo R, Schimmenti V et al. 2015. Climate-driven environmental changes around 8,200 years ago favoured increases in cetacean strandings and mediterranean hunter-gatherers exploited them. Sci Rep. 5:16288.

Mannino MA, Thomas KD, Leng MJ, Sloane HJ. 2008. Shell growth and oxygen isotopes in the topshell osilinus turbinatus: Resolving past inshore sea surface temperatures. Geo-Marine Letters. 28(5-6):309-325.

Marean CW, Bar-Matthews M, Bernatchez J, Fisher E, Goldberg P, Herries AIR, Jacobs Z, Jerardino A, Karkanas P, Minichillo T et al. 2007. Early human use of marine resources and pigment in south africa during the middle pleistocene. Nature. 449(7164):905-908.

Marin F, Le Roy N, Marie B. 2012. The formation and mineralization of mollusk shell. Front Biosci. 4(1099):125.

Marin F, Luquet G, Marie B, Medakovic D. 2007. Molluscan shell proteins: Primary structure, origin, and evolution. Elsevier. p. 209-276.

Marin F, Marie B, Hamada SB, Ramos-Silva P, Le Roy N, Guichard N, Wolf SE, Montagnani C, Joubert C, Piquemal D. 2013. Shellome': Proteins involved in mollusk shell biomineralization-diversity, functions. Recent advances in pearl research. 149:168.

McConnaughey TA, Gillikin DP. 2008. Carbon isotopes in mollusk shell carbonates. Geo-Marine Letters. 28:287-299.

Mellars P. 1999. The neanderthal problem continued. Current Anthropology. 40(3):341-364.

Mellars P. 2006a. Archeology and the dispersal of modern humans in europe: Deconstructing the "aurignacian". Evolutionary Anthropology: Issues, News, and Reviews: Issues, News, and Reviews. 15(5):167-182.

Mellars P. 2006b. A new radiocarbon revolution and the dispersal of modern humans in eurasia. Nature. 439(7079):931-935.

Milano S, Demeter F, Hublin J-J, Duringer P, Patole-Edoumba E, Ponche J-L, Shackelford L, Boesch Q, Houng NTM, Lan LTP et al. 2018a. Environmental conditions framing the first evidence of modern humans at tam pà ling, laos: A stable isotope record from terrestrial gastropod carbonates. Palaeogeography, Palaeoclimatology, Palaeoecology. 511:352-363.

Milano S, Lindauer S, Prendergast AL, Hill EA, Hunt CO, Barker G, Schöne BR. 2018b. Mollusk carbonate thermal behaviour and its implications in understanding prehistoric fire events in shell middens. Journal of Archaeological Science: Reports. 20:443-457.

Milano S, Nehrke G. 2018. Microstructures in relation to temperature-induced aragonite-to-calcite transformation in the marine gastropod phorcus turbinatus. PLoS One. 13(10):e0204577.

Milano S, Prendergast AL, Schöne BR. 2016. Effects of cooking on mollusk shell structure and chemistry: Implications for archeology and paleoenvironmental reconstruction. Journal of Archaeological Science: Reports. 7:14-26.

Milano S, Schöne BR, González-Morales MR, Gutiérrez-Zugasti I. 2022. Temporal and spatial variability of prehistoric aquatic resource procurement: A case study from mesolithic northern iberia. Scientific Reports. 12(1).

Milano S, Schöne BR, Gutiérrez-Zugasti I. 2020. Oxygen and carbon stable isotopes of mytilus galloprovincialis lamarck, 1819 shells as environmental and provenance proxies. The Holocene. 30(1):65-76.

Milano S, Szymanek M. 2019. Lacustrine molluscan carbonates: An interspecific approach toward the understanding of palaeoenvironmental conditions during the holsteinian interglacial (mis 11) using δ18o and δ13c. Palaeogeography, Palaeoclimatology, Palaeoecology. 530:49-58.

Misarti N, Gier E, Finney B, Barnes K, McCarthy M. 2017. Compound-specific amino acid δ15n values in archaeological shell: Assessing diagenetic integrity and potential for isotopic baseline reconstruction. Rapid Communications in Mass Spectrometry. 31(22):1881-1891.

Moroni A, Ronchitelli A, Simona A, Aureli D, Bailey SE, Boscato P, Boschin F, Capecchi G, Crezzini J, Douka K. 2018. Grotta del cavallo (apulia–southern italy). The uluzzian in the mirror. Journal of Anthropological Sciences. 96:125-160.

Muscheler R, Adolphi F, Heaton TJ, Bronk Ramsey C, Svensson A, van der Plicht J, Reimer PJ. 2020. Testing and improving the intcal20 calibration curve with independent records. Radiocarbon. 62(4):1079-1094.

National-Geographic-Society. 2023. National geographic society is a 501 (c)(3) organization. ©. In: ©, editor. https://www.nationalgeographic.org/activity/circulation-seas/.

Nehrke G, Nouet J. 2011. Confocal raman microscope mapping as a tool to describe different mineral and organic phases at high spatial resolution within marine biogenic carbonates: Case study on <i>nerita undata</i> (gastropoda, neritopsina). Biogeosciences. 8(12):3761-3769.

Nudelman F, Gotliv BA, Addadi L, Weiner S. 2006. Mollusk shell formation: Mapping the distribution of organic matrix components underlying a single aragonitic tablet in nacre. Journal of Structural Biology. 153(2):176-187.

O'Donnell TH, Macko SA, Wehmiller JF. 2007. Stable carbon isotope composition of amino acids in modern and fossil mercenaria. Organic Geochemistry. 38(3):485-498.

Olsson IU. 2009. Radiocarbon dating history: Early days, questions, and problems met. Radiocarbon. 51(1):1-43.

Pandow M, MacKay C, Wolfgang R. 1960. The reaction of atomic carbon with oxygen: Significance for the natural radio-carbon cycle. Journal of Inorganic and Nuclear Chemistry. 14(3-4):153-158.

Paterne M, Feuillet N, Cabioch G, Cortijo E, Blamart D, Weill-Accardo J, Bonneau L, Colin C, Douville E, Pons-Branchu E. 2018. Reservoir ages in the western tropical north atlantic from one coral off martinique island (lesser antilles). Radiocarbon. 60(2):639-652.

Peharda M, Schoene BR, Black BA, Correge T. 2021. Advances of sclerochronology research in the last decade. Palaeogeography, Palaeoclimatology, Palaeoecology. 570:110371.

Penkman KEH, Kaufman DS, Maddy D, Collins MJ. 2008. Closed-system behaviour of the intra-crystalline fraction of amino acids in mollusc shells. Quaternary Geochronology. 3(1-2):2-25.

Peresani M, Vanhaeren M, Quaggiotto E, Queffelec A, d'Errico F. 2013. An ochered fossil marine shell from the mousterian of fumane cave, italy. PLoS One. 8(7):e68572.

Perrin C. 2004. Early diagenesis of carbonate biocrystals : Isomineralogical changes in aragonite coral skeletons. Bulletin de la Société Géologique de France. 175(2):95-106.

Picin A, Moroni A, Benazzi S. 2022. The arrival of homo sapiens in the near east and europe. Updating neanderthals. Elsevier. p. 321-347.

Prendergast A, Azzopardi M, O'connell T, Hunt C, Barker G, Stevens R. 2013. Oxygen isotopes from phorcus (osilinus) turbinatus shells as a proxy for sea surface temperature in the central mediterranean: A case study from malta. Chemical Geology. 345:77-86.

Prendergast A, Schöne B. 2017. Oxygen isotopes from limpet shells: Implications for palaeothermometry and seasonal shellfish foraging studies in the mediterranean. Palaeogeography, Palaeoclimatology, Palaeoecology. 484:33-47.

Quarta G, D'Elia M, Paparella S, Serra A, Calcagnile L. 2020. Characterisation of lead carbonate white pigments submitted to ams radiocarbon dating. Journal of Cultural Heritage. 46:102-107.

Ramos-Muñoz J, Cantillo-Duarte JJ, Bernal-Casasola D, Barrena-Tocino A, Domínguez-Bella S, Vijande-Vila E, Clemente-Conte I, Gutiérrez-Zugasti I, Soriguer-Escofet M, Almisas-Cruz S. 2016. Early use of marine resources by middle/upper pleistocene human societies: The case of benzú rockshelter (northern africa). Quaternary International. 407:6-15.

Ramsey CB. 2009. Bayesian analysis of radiocarbon dates. Radiocarbon. 51(1):337-360.

Ramsey CB, Hedges R. 1997. Hybrid ion sources: Radiocarbon measurements from microgram to milligram. Nuclear Instruments and Methods in Physics Research Section B: Beam Interactions with Materials and Atoms. 123(1-4):539-545.

Reimer PJ. 2004. Intcal04: Terestrial radiocarbon age calibration, 0-26 cal kyr bp. Radiocarbon. 46(3):1029-1058.

Reimer PJ. 2021. Evolution of radiocarbon calibration. Radiocarbon.1-17.

Reimer PJ, Austin WE, Bard E, Bayliss A, Blackwell PG, Ramsey CB, Butzin M, Cheng H, Edwards RL, Friedrich M. 2020. The intcal20 northern hemisphere radiocarbon age calibration curve (0–55 cal kbp). Radiocarbon. 62(4):725-757.

Reimer PJ, Baillie MG, Bard E, Bayliss A, Beck JW, Blackwell PG, Ramsey CB, Buck CE, Burr GS, Edwards RL. 2009. Intcal09 and marine09 radiocarbon age calibration curves, 0–50,000 years cal bp. Radiocarbon. 51(4):1111-1150.

Reimer PJ, Bard E, Bayliss A, Beck JW, Blackwell PG, Ramsey CB, Buck CE, Cheng H, Edwards RL, Friedrich M. 2013. Intcal13 and marine13 radiocarbon age calibration curves 0–50,000 years cal bp. radiocarbon. 55(4):1869-1887.

Reimer PJ, Reimer RW. 2001. A marine reservoir correction database and on-line interface. Radiocarbon. 43(2A):461-463.

Reimer RW, Reimer PJ. 2017. An online application for δr calculation. Radiocarbon. 59(5):1623-1627.

Calibomb [www program] at http://calib.Org. 2023. [accessed].

Ruebens K, Sinet-Mathiot V, Talamo S, Smith GM, Welker F, Hublin J-J, McPherron SP. 2022. The late middle palaeolithic occupation of abri du maras (layer 1, neronian, southeast france): Integrating lithic analyses, zooms and radiocarbon dating to reconstruct neanderthal hunting behaviour. Journal of Paleolithic Archaeology. 5(1).

Ruff M, Wacker L, Gäggeler HW, Suter M, Synal H-A, Szidat S. 2007. A gas ion source for radiocarbon measurements at 200 kv. Radiocarbon. 49(2):307-314.

Russell N, Cook GT, Ascough P, Barrett JH, Dugmore A. 2011a. Species specific marine radiocarbon reservoir effect: A comparison of δr values between patella vulgata (limpet) shell carbonate and gadus morhua (atlantic cod) bone collagen. Journal of Archaeological Science. 38(5):1008-1015.

Russell N, Cook GT, Ascough PL, Scott EM, Dugmore AJ. 2011b. Examining the inherent variability in δr: New methods of presenting δr values and implications for mre studies. Radiocarbon. 53(2):277-288.

Russo CM, Tripp JA, Douka K, Higham TFJR. 2010. A new radiocarbon pretreatment method for molluscan shell using density fractionation of carbonates in bromoform. 52(3):1301-1311.

Sadler J, Carré M, Azzoug M, Schauer AJ, Ledesma J, Cardenas F, Chase BM, Bentaleb I, Muller SD, Mandeng M et al. 2012. Reconstructing past upwelling intensity and the seasonal dynamics of primary productivity along the peruvian coastline from mollusk shell stable isotopes. Geochemistry, Geophysics, Geosystems. 13(1):n/a-n/a.

Santhanam R. 2018a. Biology and ecology of edible marine bivalve molluscs. CRC Press.

Santhanam R. 2018b. Biology and ecology of edible marine gastropod molluscs. CRC Press.

Schöne BR. 2008. The curse of physiology—challenges and opportunities in the interpretation of geochemical data from mollusk shells. Geo-Marine Letters. 28(5-6):269-285.

Schöne BR, Fiebig J. 2009. Seasonality in the north sea during the allerød and late medieval climate optimum using bivalve sclerochronology. International Journal of Earth Sciences. 98(1):83-98.

Schöne BR, Freyre Castro AD, Fiebig J, Houk SD, Oschmann W, Kröncke I. 2004. Sea surface water temperatures over the period 1884–1983 reconstructed from oxygen isotope ratios of a bivalve mollusk shell (arctica islandica, southern north sea). Palaeogeography, Palaeoclimatology, Palaeoecology. 212(3):215-232.

Schöne BR, Surge DM. 2012. Part n, revised, volume 1, chapter 14: Bivalve sclerochronology and geochemistry. Treatise online. 46:1-24.

Sponheimer M, Ryder CM, Fewlass H, Smith EK, Pestle WJ, Talamo S. 2019. Saving old bones: A non-destructive method for bone collagen prescreening. Sci Rep. 9(1):13928.

Stuiver M. 1961. Variations in radiocarbon concentration and sunspot activity. Journal of Geophysical Research. 66(1):273-276.

Stuiver M, Braziunas TF. 1993. Modeling atmospheric 14c influences and 14c ages of marine samples to 10,000 bc. Radiocarbon. 35(1):137-189.

Stuiver M, Braziunas TF. 1998. Anthropogenic and solar components of hemispheric 14c. Geophysical Research Letters. 25(3):329-332.

Stuiver M, Polach HA. 1977. Discussion reporting of ¹⁴c data. Radiocarbon. 19(3):355-363.

Stuiver M, Quay PD. 1980. Patterns of atmospheric 14c changes. Radiocarbon. 22(2):166-176.

Stuiver M, Reimer PJ, Bard E, Beck JW, Burr GS, Hughen KA, Kromer B, McCormac G, Van Der Plicht J, Spurk M. 1998. Intcal98 radiocarbon age calibration, 24,000–0 cal bp. Radiocarbon. 40(3):1041-1083.

Stuiver M, Suess HE. 1966. On the relationship between radiocarbon dates and true sample ages. Radiocarbon. 8:534-540.

Suzuki M, Nagasawa H. 2013. Mollusk shell structures and their formation mechanism. Canadian Journal of Zoology. 91(6):349-366.

Talamo S, Aldeias V, Goldberg P, Chiotti L, Dibble HL, Guérin G, Hublin JJ, Madelaine S, Maria R, Sandgathe D. 2020. The new 14c chronology for the palaeolithic site of la ferrassie, france: The disappearance of neanderthals and the arrival of homo sapiens in france. Journal of Quaternary Science. 35(7):961-973.

Talamo S, Blasco R, Rivals F, Picin A, Gema Chacón M, Iriarte E, Manuel López-García J, Blain H-A, Arilla M, Rufà A et al. 2016a. The radiocarbon approach to neanderthals in a carnivore den site: A well-defined chronology for teixoneres cave (moià, barcelona, spain). Radiocarbon. 58(2):247-265.

Talamo S, Fewlass H, Maria R, Jaouen K. 2021a. “Here we go again”: The inspection of collagen extraction protocols for 14c dating and palaeodietary analysis. STAR: Science & Technology of Archaeological Research. 7(1):62-77.

Talamo S, Hajdinjak M, Mannino MA, Fasani L, Welker F, Martini F, Romagnoli F, Zorzin R, Meyer M, Hublin JJ. 2016b. Direct radiocarbon dating and genetic analyses on the purported neanderthal mandible from the monti lessini (italy). Sci Rep. 6:29144.

Talamo S, Hughen KA, Kromer B, Reimer PJ. 2012a. Debates over palaeolithic chronology – the reliability of 14c is confirmed. Journal of Archaeological Science. 39(7):2464-2467.

Talamo S, Kromer B, Richards MP, Wacker L. 2023. Back to the future: The advantage of studying key events in human evolution using a new high resolution radiocarbon method. PLOS ONE. 18(2):e0280598.

Talamo S, Peresani M, Romandini M, Duches R, Jequier C, Nannini N, Pastoors A, Picin A, Vaquero M, Weniger GC et al. 2014. Detecting human presence at the border of the northeastern italian pre-

alps. 14c dating at rio secco cave as expression of the first gravettian and the late mousterian in the northern adriatic region. PLoS One. 9(4):e95376.

Talamo S, Richards M. 2011. A comparison of bone pretreatment methods for ams dating of samples >30,000 bp. Radiocarbon. 53(3):443-449.

Talamo S, Soressi M, Roussel M, Richards M, Hublin J-J. 2012b. A radiocarbon chronology for the complete middle to upper palaeolithic transitional sequence of les cottés (france). Journal of Archaeological Science. 39(1):175-183.

Talamo S, Urbanowski M, Picin A, Nowaczewska W, Vazzana A, Binkowski M, Cercatillo S, Diakowski M, Fewlass H, Marciszak A et al. 2021b. A 41,500 year-old decorated ivory pendant from stajnia cave (poland). Scientific Reports. 11(1).

Tassoni L, Kromer B, Friedrich R, Wacker L, Cattani M, Friedrich M, Paleček D, Pelloni E, Peng K, Thomas E M, Talamo S. (2023, in press) "Safe preparation and delivery of graphite targets for 14C analysis: Procedures of BRAVHO lab at Bologna University". Radiocarbon. 24th Radiocarbon Conference and 10th 14C & Archaeology Conference. Conference Proceeding.

Tátá F, Cascalheira J, Marreiros J, Pereira T, Bicho N. 2014. Shell bead production in the upper paleolithic of vale boi (sw portugal): An experimental perspective. Journal of Archaeological Science. 42:29-41.

Taylor R, Bar-Yosef O. 2014. Radiocarbon dating: An archaeological perspective. Left coast press. Walnut Creek, CA.

Toffolo MB. 2021. The significance of aragonite in the interpretation of the microscopic archaeological record. Geoarchaeology. 36(1):149-169.

Twaddle RW, Ulm S, Hinton J, Wurster CM, Bird MI. 2016. Sclerochronological analysis of archaeological mollusc assemblages: Methods, applications and future prospects. Archaeological and anthropological sciences. 8:359-379.

Van Der Plicht J, Beck JW, Bard E, Baillie MGL, Blackwell PG, Buck CE, Friedrich M, Guilderson TP, Hughen KA, Kromer B et al. 2004. Notcal04—comparison/calibration ¹⁴c records 26–50 cal kyr bp. Radiocarbon. 46(3):1225-1238.

van Klinken GJ. 1999. Bone collagen quality indicators for palaeodietary and radiocarbon measurements. Journal of Archaeological Science. 26(6):687-695.

Vita-Finzi C, Roberts N. 1984. Selective leaching of shells for 14c dating. Radiocarbon. 26(1):54-58.

Wacker L, Bonani G, Friedrich M, Hajdas I, Kromer34 B, NÏmec M, Ruff M, Suter M, Synal H, Vockenhuber C. 2010. Micadas: Routine and high-precision radiocarbon dating. Radiocarbon. 52(2-3):252-262.

Waselkov GA. 1987. 3 - shellfish gathering and shell midden archaeology. In: Schiffer MB, editor. Advances in archaeological method and theory. San Diego: Academic Press. p. 93-210.

Webb GE, Price GJ, Nothdurft LD, Deer L, Rintoul L. 2007. Cryptic meteoric diagenesis in freshwater bivalves: Implications for radiocarbon dating. Geology. 35(9):803-806.

Wefer G, Berger WH. 1991. Isotope paleontology: Growth and composition of extant calcareous species. Marine Geology. 100(1):207-248.

Wei Y, d'Errico F, Vanhaeren M, Li F, Gao X. 2016. An early instance of upper palaeolithic personal ornamentation from china: The freshwater shell bead from shuidonggou 2. PLoS One. 11(5):e0155847.

Weiner S. 1979. Aspartic acid-rich proteins: Major components of the soluble organic matrix of mollusk shells. Calcified Tissue International. 29(1):163-167.

Weiner S. 1984. Organization of organic matrix components in mineralized tissues. American Zoologist. 24(4):945-951.

Weiner S, Hood L. 1975. Soluble protein of the organic matrix of mollusk shells: A potential template for shell formation. Science. 190(4218):987-989.

Weiner S, Traub W. 1980. X-ray diffraction study of the insoluble organic matrix of mollusk shells. FEBS letters. 111(2):311-316.

Weiner S, Traub W, Lowenstam H A. 1983 Organic matrix in calcified exoskeletons. Biomineralization and Biological Metal Accumulation: Biological and Geological Perspectives Papers presented at the Fourth International Symposium on Biomineralization, Renesse, The Netherlands, June 2–5, 1982; 1983: Springer.

Wheeler AP, Rusenko KW, Swift DM, Sikes CS. 1988. Regulation of in vitro and in vivo caco3 crystallization by fractions of oyster shell organic matrix. Marine Biology. 98(1):71-80.

Wheeler AP, Sikes CS. 1984. Regulation of carbonate calcification by organic matrix. American Zoologist. 24(4):933-944.

Whitney NM, Johnson BJ, Dostie PT, Luzier K, Wanamaker AD. 2019. Paired bulk organic and individual amino acid δ15n analyses of bivalve shell periostracum: A paleoceanographic proxy for water source variability and nitrogen cycling processes. Geochimica et Cosmochimica Acta. 254:67-85.

Will M, Kandel AW, Conard NJ. 2019. Midden or molehill: The role of coastal adaptations in human evolution and dispersal. Journal of World Prehistory. 32(1):33-72.

Willis E, Tauber H, Münnich K. 1960. Variations in the atmospheric radiocarbon concentration over the past 1300 years. Radiocarbon. 2:1-4.

Wood R, Douka K, Boscato P, Haesaerts P, Sinitsyn A, Higham TF. 2012. Testing the abox-sc method: Dating known-age charcoals associated with the campanian ignimbrite. Quaternary Geochronology. 9:16-26.

Yan H, Liu C, An Z, Yang W, Yang Y, Huang P, Qiu S, Zhou P, Zhao N, Fei H et al. 2020. Extreme weather events recorded by daily to hourly resolution biogeochemical proxies of marine giant clam shells. Proc Natl Acad Sci U S A. 117(13):7038-7043.

Yates T. 1986. Studies of non-marine mollusks for the selection of shell samples for radiocarbon dating. Radiocarbon. 28(2A):457-463.

Zilhão J, Angelucci DE, Badal-García E, D'Errico F, Daniel F, Dayet L, Douka K, Higham TFG, Martínez-Sánchez MJ, Montes-Bernárdez R et al. 2010. Symbolic use of marine shells and mineral pigments by iberian neandertals. Proceedings of the National Academy of Sciences. 107(3):1023-1028.

Zilhão J, Banks WE, D'Errico F, Gioia P. 2015. Analysis of site formation and assemblage integrity does not support attribution of the uluzzian to modern humans at grotta del cavallo. PLOS ONE. 10(7):e0131181.

CHAPTER 2 - SHELL PRETREATMENT FOR RADIOCARBON DATING

2.1. STATE OF THE ART AND PROBLEM STATEMENT

As mentioned in the introduction of this thesis, mollusk shells are often found in archeological sites, given their great preservation potential and high value as a multipurpose resource. Some mollusk species were used as food, others to make tools such as scrapers or decorative beads for ornamental purposes (Bicho and Haws 2008; Cascalheira et al. 2012; Douka 2011; Tátá et al. 2014). Mollusk shells provide high-resolution records of past environmental conditions and fluctuations, which are reflected in the carbonate structure as variable growth rates and chemical properties (Schöne 2008). Shell stable isotopes have been used extensively in the literature to estimate and reconstruct paleoenvironmental conditions, namely temperature, precipitation-evaporation patterns, upwelling intensity, and primary productivity (Elliot et al. 2009; Jones and Allmon 1995; Milano et al. 2022; Milano et al. 2020; Sadler et al. 2012; Schöne et al. 2004). Apart from past environmental conditions, shell remains represent a record of the evolutionary history of different human populations, their adaptation strategies, dietary habits, and symbolic thinking (Ramos-Muñoz et al. 2016; Will et al. 2019; Zilhão et al. 2010). Due to the elevated preservation potential of the carbonate crystalline structure, shells can often be the only available materials at archeological sites useful for ^{14}C dating (Brumm et al. 2018; Douka et al. 2013; Ono et al. 2009). However, dating only shells can lead to misinterpretations due to various potential issues that can arise before and during sample analysis and calibration. Firstly, it is important to perform careful sample selection, both considering the preservation state in terms of diagenesis and time averaging, as well as species selection which could potentially create a difference between the target event and the dated event. Furthermore, there can be issues during sample pretreatment and dating, which can cause insufficient contamination removal or the introduction of exogenous contaminant carbon during analysis and processing. Finally, there are several corrections that are necessary to perform on the obtained radiocarbon date to have a calibrated age (such as isotope fractionation, the marine reservoir effect for marine species and the freshwater effect for riverine species). If all these issues are not considered when performing analysis on shells, it can lead to misinterpretations not only of the archeological context of the site, but also erroneous conclusions about migration events in human evolution. The debate on the site of Ksar Akil in Lebanon highlights the issue of using only shells when constructing a site chronology (Bosch et al. 2015; Douka et al. 2013). In Ksar Akil, the human remains and any other organic material, were too degraded to be able to perform ^{14}C dating, and the only other available material was mollusk shells (Bosch et al. 2015; Douka et al. 2013). The results from Douka et al. (2013) placed the specimens as roughly contemporaneous to the oldest corresponding remains in Europe, thus casting doubts on the Levant as the point of origin for the dispersal of Upper

Paleolithic culture into Europe. On the other hand, Bosch et al. (2015) showed that the human remains from Ksar Akil predate the European Upper Paleolithic as previously thought, confirming the hypothesis of the Levant as the starting dispersal point of Upper Paleolithic culture into Europe (Belfer-Cohen and Goring-Morris 2012; Bosch et al. 2015; Hublin 2012). The two studies used two different shell pretreatment methods and different sample selection criteria, which might have been part of the reason behind the discrepancy of the dates. The sample preservation state was also different, as one study used ornamental shells, while the other used shells collected for consumption (Bosch et al. 2015; Douka et al. 2013). As demonstrated by this debate, dates obtained only on shells can cause changes in important scenarios that can alter our understanding of events in human evolution. This emphasizes the crucial need to improve the accuracy of the chronometric results and to increase the reliability of shells as suitable dating materials.

Although the ^{14}C dating of shells has been improved over the years (Alves et al. 2018; Douka et al. 2010b; Faivre et al. 2015; Lindauer 2019; Philippsen 2013; Pigati 2002; Reimer and Reimer 2001; Reimer and Reimer 2017; Russell et al. 2011), there are still issues hindering the reliability of the chronometric data. In shells, there is a complex organization of calcium carbonate ($CaCO_3$) units and organic compounds with extraordinary resistance to mechanical and chemical stresses (Barthelat 2010). Yet, over long timescales, diagenesis can still alter their material properties. The primary carbonate phase, often aragonite, can recrystallize into secondary calcite after deposition. During the dissolution and precipitation of secondary calcite, there can be an incorporation of exogenous carbon into the sample. This is one of the processes which can cause a difference in the isotopic composition of the secondary phase compared to the primary one and alter the ^{14}C signal and therefore the resulting age (Douka et al. 2010a). Sand blasting and abrasion were thought to remove surface contamination and altered portions, assumed to also be concentrated mainly on the outer portion of the shells. Furthermore, chemical etching is used in attempts to remove shell portions altered by diagenesis from the ^{14}C dating analysis, which is performed on the entire carbonate fraction. This method has been widely used since the first applications of ^{14}C dating on marine shells, and variations of it are still applied in most laboratories around the world (Brock et al. 2010; Busschers et al. 2014; Chappell and Polach 1972; Dee et al. 2019; Gillespie et al. 1986; Santos et al. 2004). However, the brief acid etching of the shell surface is not entirely successful in removing altered portions of the shell due to the higher solubility of aragonite compared to calcite and the localized effect of the pretreatment. A novel pretreatment protocol using Carbonate Density Separation (CarDS) was developed by Douka and colleagues in 2010 (Douka et al. 2010a; Russo et al. 2010). This method showed promising results for the removal of secondary calcite from diagenetically altered corals and mollusk shells for ^{14}C dating, and it represents the most recent innovation in this area. This method aims to separate the primary and secondary phase based on their different densities, in order to remove all the potentially contaminated secondary carbonate, not just from the surface, thus obtaining a more accurate date for the sample (Douka et al. 2010a; Russo et al. 2010).

However, diagenetic processes can often occur without a change in carbonate polymorphs, meaning that aragonite cannot be automatically considered the primary phase and the mere determination of the carbonate polymorph is not indicative of the presence or amount of diagenesis in the sample (Guzmán et al. 2009; Perrin 2004; Toffolo 2021). Although there are studies focusing on the pretreatment of the mineral fraction of the shell, the organic fraction was largely overlooked as it represents a minor portion of the shell (Hadden et al. 2018; Hadden et al. 2019). A recent study found that the organic intracrystalline matrix plays an important role in the diagenetic mineralogical transformation (Milano and Nehrke 2018). Their results state that the amount and composition of the organic portion of the shell influence the temperature at which the thermally induced transformation from aragonite to calcite occurs. Furthermore, the intracrystalline organic matrix is a closed system that was found to be isolated from the environment (Penkman et al. 2008) making isotopic exchange between the atmosphere and the intracrystalline organic matrix after deposition unlikely. However, attempts to date the organic matrix fraction are scarce and on much younger shells (Hadden et al. 2018; Hadden et al. 2019). Therefore, investigating the ^{14}C signal output of the organic matrix and comparing the results with outputs of the established methods could allow us to potentially improve the accuracy of the chronometric results and increase the reliability of shells as suitable dating materials.

Here, we introduce two methods aiming to extract the intracellular organic matrix of the shell and compare them to the two previously mentioned methods from literature (Dee et al. 2019; Douka et al. 2010a; Russo et al. 2010). One of the methods for organic matrix extraction is based on a method routinely used on modern shells and coral samples in studies focusing on the intracellular proteins (Falini et al. 2013; Reggi et al. 2014). The advantage of this method is the use of a dialysis membrane, which allows to extract both the soluble and the insoluble organic matrix from the shell and minimizes the loss of organic material. The second method is quite similar, following mostly the same steps, although it does not include the use of a dialysis membrane. It was developed based on the collagen extraction method routinely used on bone samples for ^{14}C dating (Talamo et al. 2021; Talamo and Richards 2011). Comparing the ^{14}C dates obtained from all four methods we could determine the best method to routinely apply on mollusk shells, which would exclude pretreatment as an issue when considering the use of shells for radiocarbon dating. This will be one step towards achieving more reliable results and helping obtain trustworthy chronologies for sites where shells are the only available material for dating.

2.2. SITE UNDER INVESTIGATION

The archeological site of Vale Boi is a well-known Upper Paleolithic site in southwestern Portugal (Figure 11) rich in mollusk shells, making it a great site to use for such methodological experiments. This site is situated between two different environments: the Mediterranean and Atlantic coasts, and it represents the earliest recorded *Homo sapiens* occupation in southwestern Iberia, as attested by the Early Gravettian remains dated to c. 32 ka cal BP (Bicho et al. 2013). This site has a long stratigraphic sequence spanning from the early Gravettian, Proto-Solutrean, Solutrean, and Magdalenian (Cascalheira et al. 2012; Manne et al. 2012; Marreiros et al. 2015). Previous studies found evidence of multiple human occupations at this site, proving that it was most likely a seasonal residential camp with a combination of exogenous and regional cultural traits and a diversified use and processing of available resources including mollusk shells (Bicho and Haws 2008; Bicho et al. 2013; Cascalheira et al. 2012; Manne et al. 2012). Furthermore, there was an intense presence of inland and coastal foraging, hunting, and processing of various types and sizes of prey, possible processing of edible plants, as well as the production of various lithic and bone tools, ornaments and art including abundant shell beads (Bicho and Haws 2008; Bicho et al. 2013; Manne 2014; Manne et al. 2012; Marreiros et al. 2015; Pereira et al. 2016; Tátá et al. 2014). The presence of several mollusk species spans the different levels of the site proving the continued use and importance of mollusk shells as a resource throughout the stratigraphic sequence and allowing us to select and pretreat samples of different ages for comparison. Vale Boi has been excavated in three main areas – the Rockshelter, Slope and Terrace areas (Figure 12). Out of these three areas, the Terrace has the longest and most complete archeological sequence (Cascalheira et al. 2012; Manne et al. 2012; Marreiros et al. 2015). In previous studies, numerous ^{14}C dates were available from all areas of the site, including dates on mollusk shells from the Terrace area (Table 2). However, there were some problems with the dates in terms of agreement with the stratigraphic sequence that need further investigation (Cascalheira et al. 2012). Access to previous dates allows us to compare any new experimental results, which might also help clarify the stratigraphic incoherencies.

Figure 11. The location of the Vale Boi archeological site in Portugal, at the Southwestern tip of the Iberian Peninsula; on the bottom right two archeological shell specimens collected in the Terrace area of the site, *Pecten* sp. (top) and *Crassostrea* sp. (bottom).

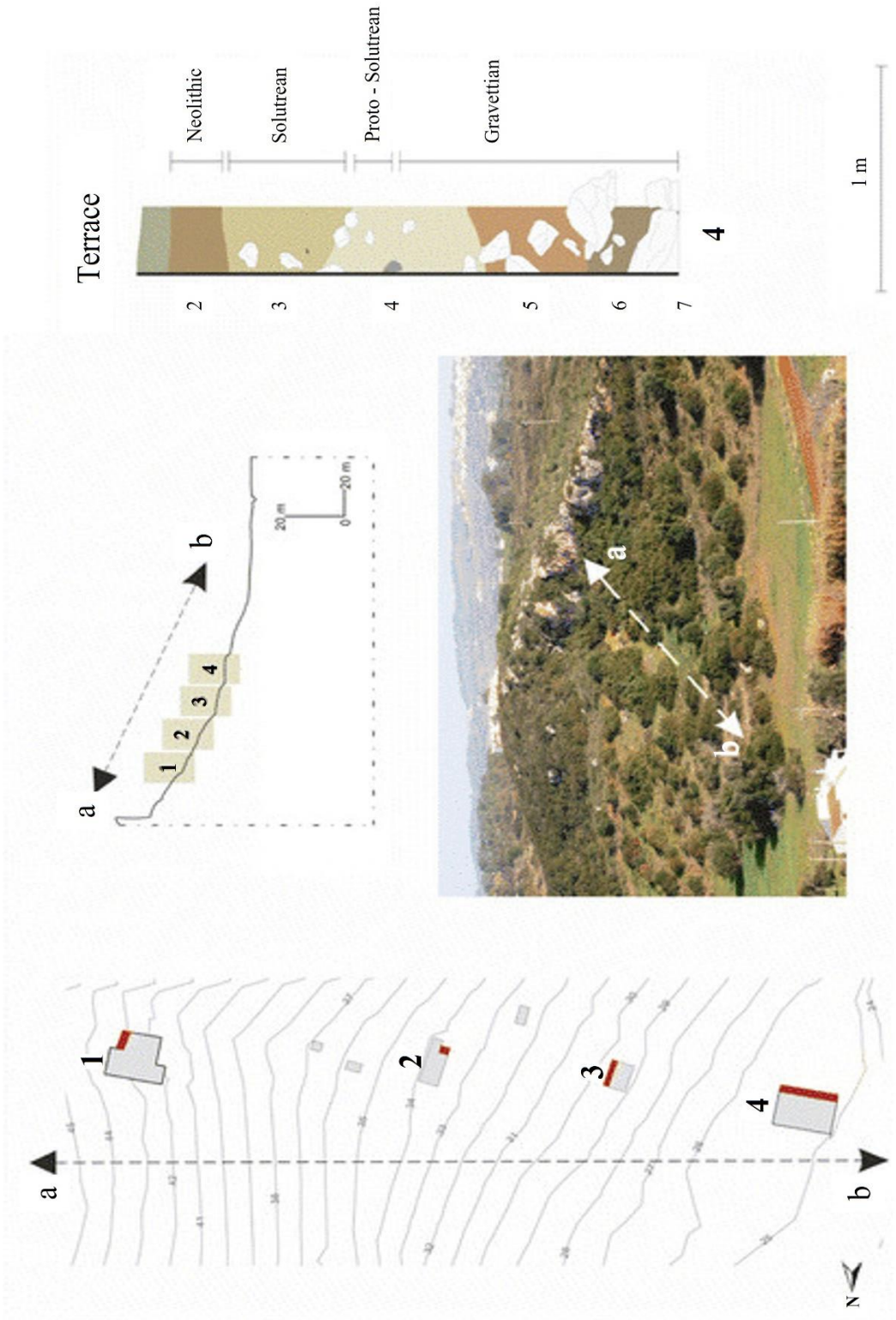

Figure 12. The Vale Boi excavation areas 1 – Rockshelter; 2 and 3 – Slope and 4 – Terrace (Figure modified after Cascalheira et al. 2012)

Table 2. Previous dates on samples from the Terrace area of the Vale Boi site.

Archeological attribution	Layer	Material	AMS code	^{14}C age	1σ err	Notes	Reference
Epipaleolithic	3	Charcoal	AA-63310	8696	54		Tàtà et al. 2014
Epipaleolithic	3	Charcoal	Wk-13685	8749	58		Tàtà et al. 2014
Epipaleolithic	3	Charcoal	AA-63305	8825	57		Tàtà et al. 2014
Epipaleolithic	3	Charcoal	Wk-24761	8886	30		Tàtà et al. 2014
Epipaleolithic	3	Olea	Wk-36256	8737	25		Tàtà et al. 2014
Epipaleolithic	3	Olea	Wk-36255	8664	25		Tàtà et al. 2014
Gravettian	5	Patella	Wk-32144	24381	258	Calcite	Tàtà et al. 2014
Gravettian	5	Bone	Wk-31090	24549	165	Min. age – low collagen	Tàtà et al. 2014
Gravettian	5	Charcoal	Wk-24762	24769	180		Tàtà et al. 2014
Gravettian	5	Patella	Wk-32144.2	23613	240	Aragonite	Tàtà et al. 2014
Proto-Solutrean	5	Patella	Wk-50390	20554	75		Tàtà et al. 2014
Proto-Solutrean	5	Shell	Wk-42831	20329	90		Cascalheira et al. 2017
Proto-Solutrean	5	Charcoal	Wk-42830	20818	107		Cascalheira et al. 2017
Gravettian	5	Littorina littorea	Wk-44416	22358	80		Belmiro et al. 2021
Gravettian	5	Bone	Wk-31089	24183	161	Min. age – low collagen	Tàtà et al. 2014
Gravettian	5	Patella	OxA-25710	25050	100	Calcite	Tàtà et al. 2014
Gravettian	5	Pecten	Wk-32145	25181	293	Min. age – burnt	Tàtà et al. 2014
Gravettian	5	Patella	Wk-30677	25196	103	Calcite	Tàtà et al. 2014
Gravettian	5	Patella	Wk-30679	25317	99	Calcite	Tàtà et al. 2014
Gravettian	5	Charcoal	Wk-26801	27720	370		Tàtà et al. 2014
Gravettian	5	Patella	Wk-30677.2	22235	173	Aragonite	Tàtà et al. 2014
Gravettian	5	Patella	Wk-30679.2	25390	255	Aragonite	Tàtà et al. 2014
Early Gravettian	6	Patella	Wk-30678	25579	98	Calcite	Tàtà et al. 2014
Early Gravettian	7	Nassarius	Wk-35714	25964	110	Calcite	Tàtà et al. 2014
Early Gravettian	6	Pecten	Wk-35712	26026	114		Tàtà et al. 2014
Early Gravettian	6	Pecten	Wk-35713	25930	122	Aragonite	Tàtà et al. 2014
Early Gravettian	7	Acanthocardia	Wk-32147	27141	365	Aragonite	Tàtà et al. 2014
Early Gravettian	6	Charcoal	Wk-35717	28012	192	Arbutus	Tàtà et al. 2014
Early Gravettian	6	Pecten	Wk-32146	28321	422	Calcite	Tàtà et al. 2014
Early Gravettian	6	Pecten	Wk-50396	41384	998		Tàtà et al. 2014
Early Gravettian	7	Patella	Wk-30676	24318	90	Calcite	Tàtà et al. 2014
Early Gravettian	7	Patella	Wk-30676.2	26353	284	Aragonite	Tàtà et al. 2014
Early Gravettian	7	Pecten	Wk-50394	26403	149		Tàtà et al. 2014
Early Gravettian	8	Pecten	Wk-50393	27349	172		Unpublished

2.3. MATERIALS AND METHODS

We performed analysis and ^{14}C dating on a total of 10 shell samples, collected from Layers 3 to 7 at the Terrace area of Vale Boi. Some of the samples were divided into several pieces to perform the different pretreatment methods. In addition to the shell samples, two bone samples from Layer 6 in the Terrace area of Vale Boi were dated.

The bone samples were pretreated following the standard acid-base-acid method followed by ultrafiltration (Talamo et al. 2021; Talamo and Richards 2011) at the Department of Human Evolution at the Max Planck Institute for Evolutionary Anthropology (Leipzig, Germany). The Accelerator Mass Spectrometry (AMS) dates were obtained at the at the Klaus-Tschira AMS laboratory of the Curt-Engelhom-Centre for Achaeometry (CEZA; Mannheim, Germany).

All selected shell samples were given the unique identifying BRAVHO lab number (BRA n°) and their stratigraphic position is shown in Figure 13.

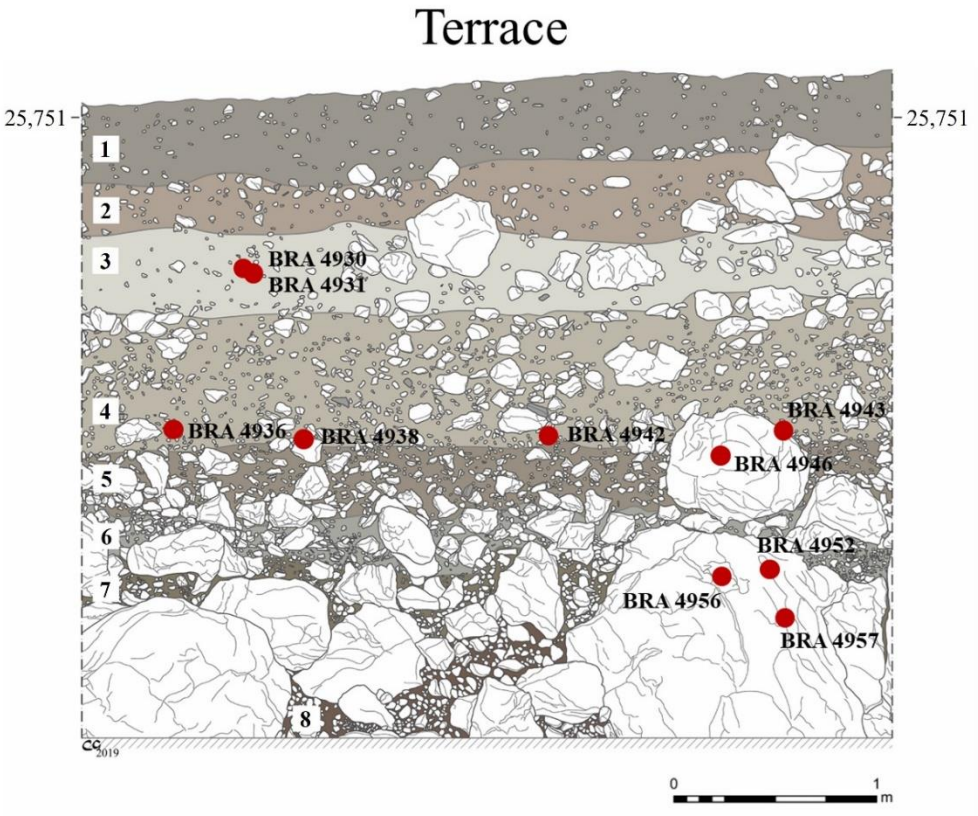

Figure 13. The samples used in this study shown as red dots in their sampling positions within each archeological layer in the Terrace area of the Vale Boi site.

2.3.1. SHELL PRETREATMENT METHODS

The shell samples were pretreated using four different methods. Method A was based on a protocol routinely used in organic matrix extraction from modern coral and mollusk samples (Falini et al. 2013; Reggi et al. 2014). Method B was developed based on the routine collagen extraction protocol used in the BRAVHO ^{14}C laboratory (Bologna Radiocarbon Laboratory Devoted to Human Evolution). Method C corresponds to the CarDS protocol (Douka et al. 2010a; Russo et al. 2010) and Method D to the standard acid etching pretreatment used in most laboratories across the world (Dee et al. 2019).

Method A - Organic matrix extraction via a dialysis process: The shell samples were first cleaned with a mechanical drill to remove any sediment that might have been adhered to the shell surface, after which they were further cleaned of impurities by leaving them in a 5 vol.% sodium hypochlorite solution overnight. This bleaching step is aimed at removing external organic matter from the sample, as it can be contaminating (Penkman et al. 2008). After these cleaning steps, the shells were rinsed in deionized water several times to wash off the sodium hypochlorite and any loose debris and left to air-dry before hand-crushing them to powder in an agate mortar (Figure 14). Then the crushed shells were further crushed in an automatic mill to obtain a finer powder (Figure 14). The obtained powder was sieved with a 150 µm mesh stainless steel sieve (Figure 14), and 2.5 g of each sample were put into labelled glass tubes. The powdered samples were once again left in 5 vol.% sodium hypochlorite solution overnight for a thorough removal of non-intracrystalline organic material, rinsed three times with deionized water and dried out in the oven for two days at 60 °C. The powder was then transferred into regenerated cellulose membranes for dialysis (MWCO = 3.5 kDa) and dispersed with 5 ml of deionized water. The sealed membranes were then put into 1 L of a 0.1 M CH_3COOH solution under stirring (Figure 15). The solution was changed every five days until the samples were decalcified, subsequently it was replaced by deionized water to reach a pH value of around 6. The obtained dispersion containing organic matter was centrifuged at 3500 rpm (2301 x g) for 5 min to separate the soluble (liquid) and insoluble (solid) fractions. Both fractions were then lyophilized and weighed.

Method B - Organic matrix extraction (as for collagen extraction): After an initial mechanical cleaning of the shell surface, the samples were ground to a fine powder and sieved in a stainless steel 150 µm mesh as described for Method A. The powder was then inserted into labelled test tubes together with a defined volume of a 0.5 M HCl solution. The solution was periodically changed until the powder stopped producing effervescence. Then, the acid was pipetted away, and the samples were washed in deionized water three times before proceeding with another 15 min HCl (0.5 M) step. Then the samples were washed in deionized water three times again before being put in a pH 3 (0.001 M) HCl solution in a heater block at 70 °C

overnight. After taking the samples out of the heater block and letting them cool down, each sample was filtered using an Elkey labs Eeze filter, to separate the soluble and insoluble fractions and transferred into glass vials to be frozen and lyophilized. This method was based on (Talamo et al. 2021), with modifications to account for the different material types. Alternatively, centrifugation can also be used to separate the two fractions, as described for Method A. As opposed to Method A, the soluble fraction is mostly lost during pretreatment in this case as it is not protected by the dialysis membrane.

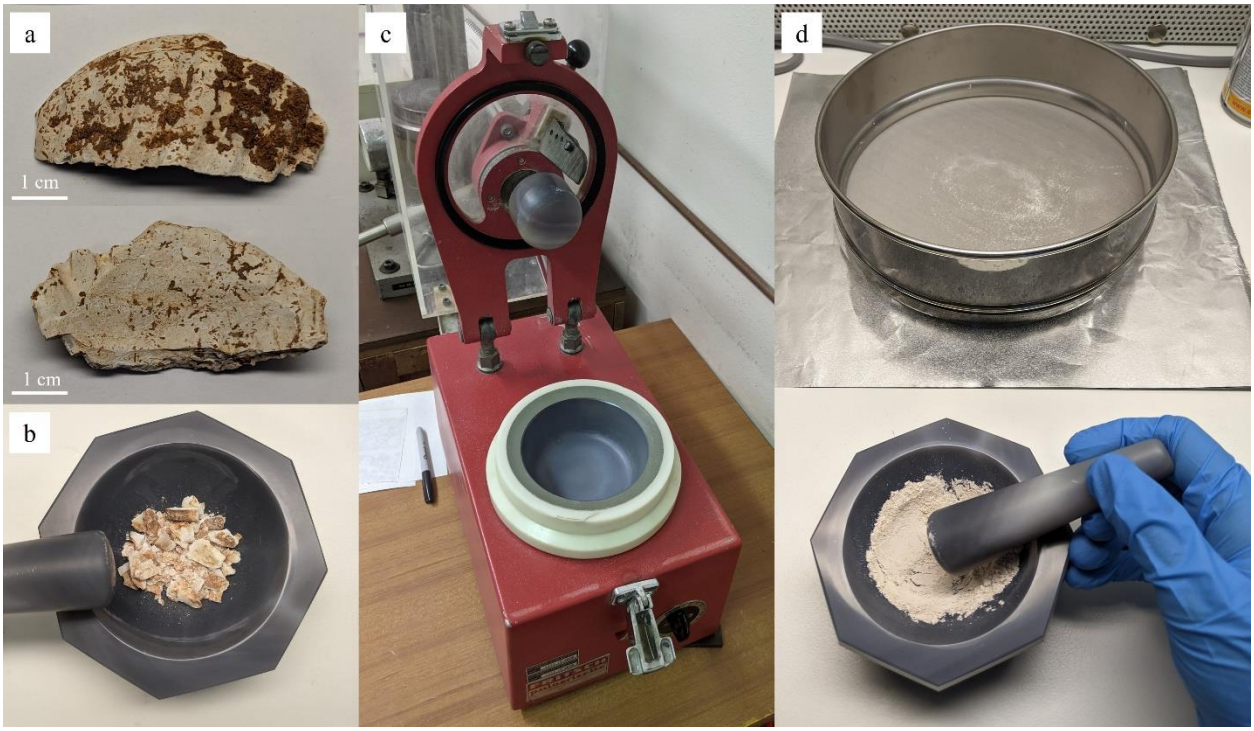

Figure 14. (a) Shell specimen before cleaning, front (top) and back (bottom); (b) roughly crushed sample after cleaning; (c) automatic mill used to crush the samples into fine powder; (d) the sieve used to obtain a homogeneous powder seen in the mortar underneath.

Method C - Carbonate Density Separation (CarDS): After the initial mechanical cleaning steps, the shells were soaked in a 50 % NaOH solution overnight to remove the external organic protein fraction. The samples were then ground to a fine powder and sieved with a 150 µm mesh stainless steel sieve as for the previous methods. An X–ray Diffraction (XRD) analysis was performed on the powder to identify the proportions of aragonite and calcite before proceeding with the separation protocol. A portion of 100 – 800 mg of powder was then inserted into a 10 ml test tube where 4 ml of 99 % bromoform solution and 250 – 350 µl of toluene were added. The mixture was then centrifuged for 20 min at 3500 rpm to separate the two polymorphs. The supernatant (presumable calcite) fraction was carefully pipetted into another glass tube, and both fractions were washed in dichloromethane and deionized water before freezing and lyophilization. This method was based on previous work by different authors (Douka et al. 2010a; Russo et al. 2010).

Method D – Acid etching: This pretreatment consisted of mechanical surface cleaning followed by an acid etching of the shell surface to remove the outermost layer. In the case of the shells used for these experiments, the etching duration was from 3 to 5 minutes. The shells were then ground into a fine powder and sieved with a stainless steel 150 µm mesh as for the other methods. The obtained powders were then sent for AMS dating. For this method, we followed the protocol described in (Dee et al. 2019).

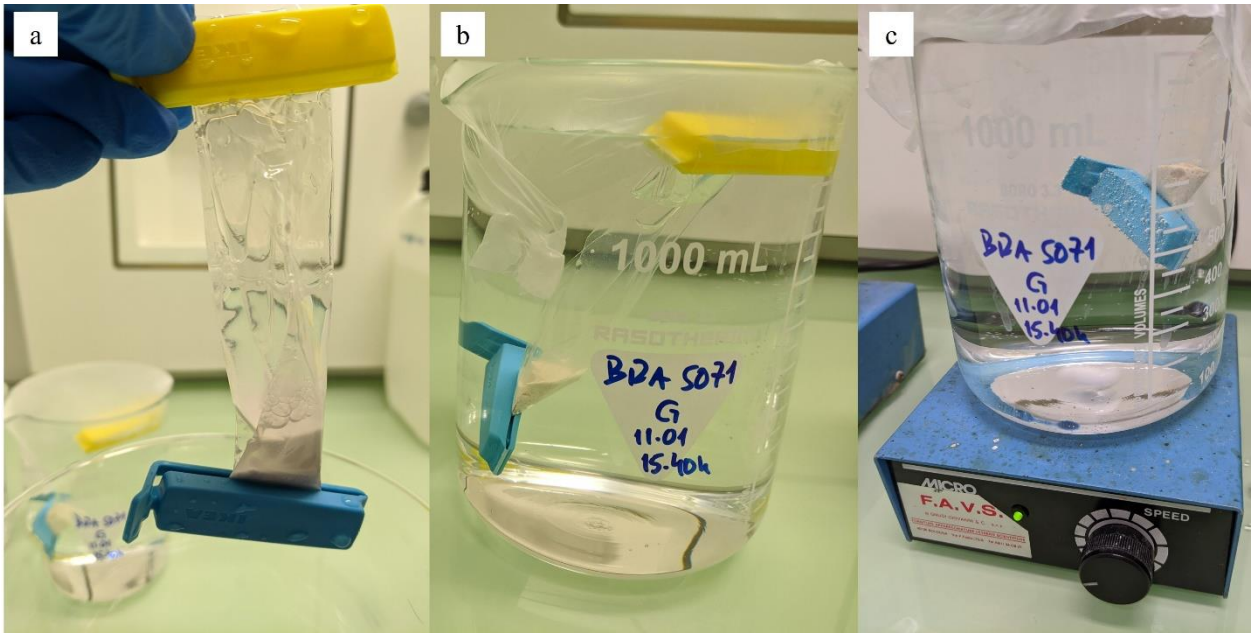

Figure 15. (a) dialysis membrane with the shell powder and deionized water; (b) inserted into 1000 ml of acetic acid and (c) put under stirring with a magnetic stirrer.

2.3.2. X-RAY DIFFRACTION (XRD) ANALYSES

For samples prepared using the Method C it was necessary to perform X-ray powder Diffraction analyses of the powdered shell material. All the analyses were performed using a PANalytical X'Pert Pro MRD X-ray diffractometer (Figure 16). This allowed to detect the presence and the relative content of calcite and aragonite before the pretreatment was performed and after, to see if the mineral phase separation was successful. Furthermore, XRD patterns were collected on all samples after the pretreatment was finished. For Method A and B, it was done to check if there was any mineral left in the extracted organic matrix, for method C to verify that the calcite-aragonite separation was complete and for Method D to have information on the composition of the powder, which could help to interpret the ^{14}C date or the potential differences in age among specimens. The raw XRD pattern files have been processed using the Profex 4.3.2a software (Döbelin and Kleeberg 2015) to determine the phases present in the powders (i.e., presence of aragonite/calcite) and their relative quantity.

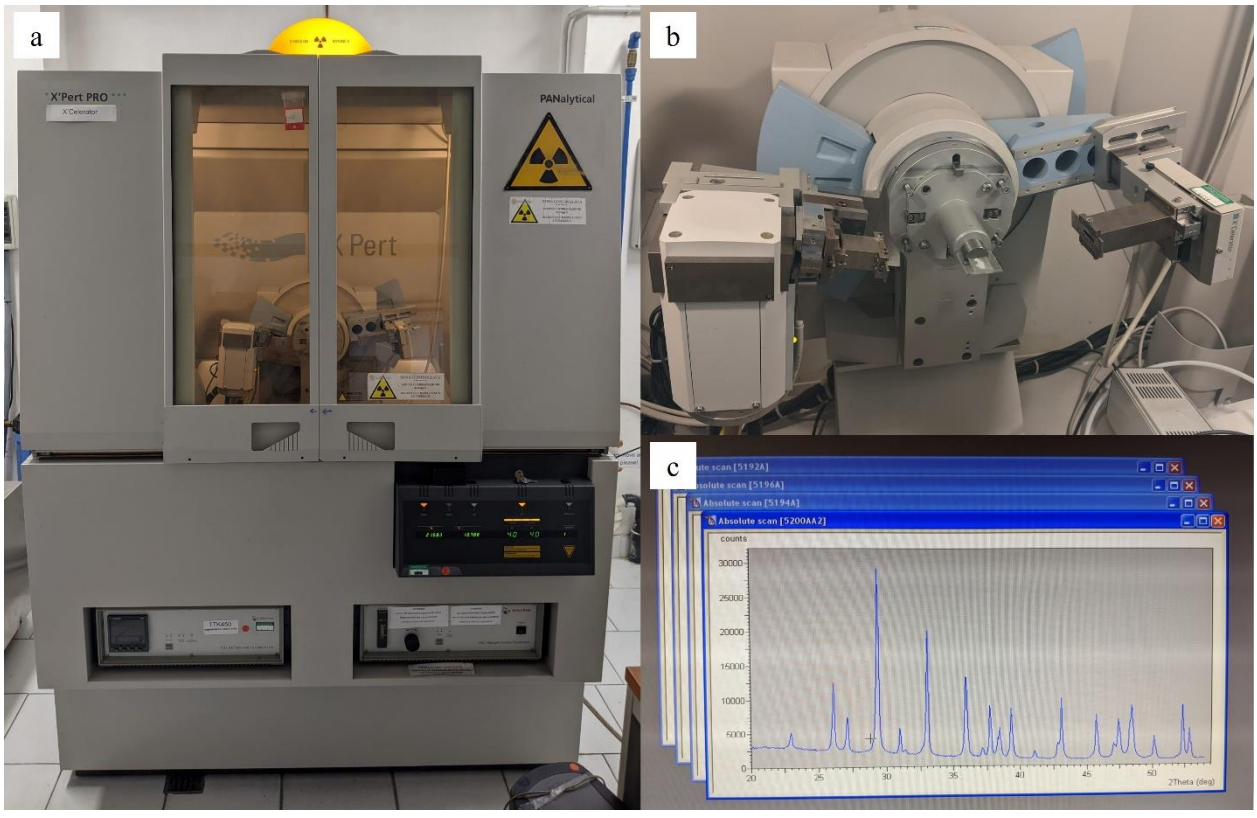

Figure 16. (a) X'Pert PRO X-ray diffractometer with (b) the X-ray tube (left) and detector (right) goniometers with a glass plate holding the sample powder (center) and (c) the raw XRD pattern file output.

2.3.2.1. BASIC NOTIONS FOR THE XRD GRAPH CREATION AND INTERPRETATIONS

After opening a raw scan file, we can search for the different phases we expect to find in our material, by selecting them from the reference materials database and adding them to the control file. When we are satisfied with the added phases, we can proceed to run the refinement using these selected reference phases. Once the refinement is complete, we can observe parameters such as the reference material peak positions shown as different colored tacks at the top of the graph (Figure 17), with each color representing one of the reference materials we searched for (In our case aragonite, calcite, and in some cases quartz). The peak positions let us identify the phases present in our measured material. The typical Profex software output graphs show us several different variables. Some of the important parameters shown are the observed, calculated, background, and difference patterns given by the software by default in black, red, blue, and gray color respectively (Figure 17). Usually, the observed, and calculated patterns should overlap, with the only difference being that the calculated result is smoother compared to the observed diffraction values, which represent the actual measured pattern of our material. On the other hand, the difference pattern in gray, shown at the bottom of each graph represents the difference between the observed, measured pattern and the calculated pattern which shows the peaks of our selected target phases (Figure 17). Ideally, the difference should only show background noise, with no significant peaks. We can have some difference showing based on the shape and intensity of the peaks, which can indicate a slightly different chemical composition than that of the reference material, or an alteration of the crystalline structure. If the difference is very high or showing peaks in positions other than our target phases, we can suppose that there is an additional phase present in our sample which we didn't include in the search. If there are no crystalline phases present in the material we are analyzing, such as in the case of organic matter, there will be no peaks present in the pattern, and often we will see a bulge formed at the beginning of the graph, which can also happen in case our material is scarce or not well distributed on the glass slide inserted into the XRD machine. In these cases, we can see the diffraction of the glass slide itself, which is amorphous. If we search our phases in these patterns, the program will give us a result indicating the relative proportions of the target phases. These results will not be very accurate since they indicate the proportions of the crystalline phases only, which in these cases are only present in traces.

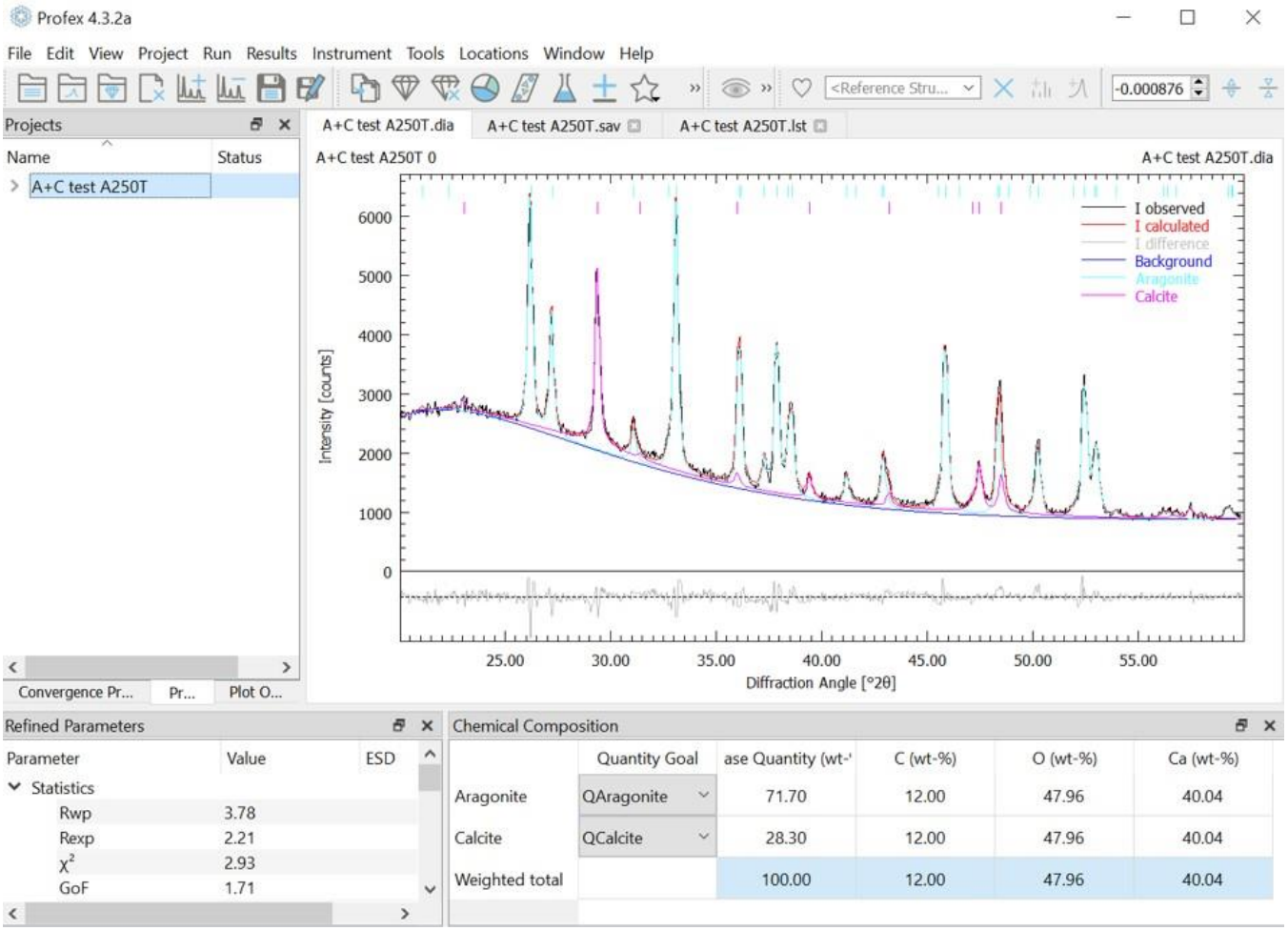

Figure 17. Profex 4.3.2a software interface showing the refinement file of a powder mixture of aragonite and calcite, showing the observed, calculated, background, and difference patterns along with the two target phases. The statistical parameters showing the degree of agreement to the reference database are shown on the bottom left and the chemical composition in percentages of the two phases is shown on the bottom right.

2.3.3. GRAPHITIZATION AND CO_2 AMS DATES

All shell samples were sent to the ETH laboratory in Zurich, Switzerland for AMS dating in the ETH MICADAS (Mini Radiocarbon Dating System, (Wacker et al. 2010). In the case of samples from Method A and B with a very low weight yield, CO_2 extraction was performed before injecting it into the AMS system (Fewlass et al. 2019; Wacker et al. 2013). For the organic matter extracted with methods A and B with a sufficient weight yield, the analysis was set up as for other organic samples (i.e., collagen and cellulose) with graphitization of the samples at the BRAVHO laboratory of the University of Bologna, and the pressing of the obtained graphite into AMS targets (sample holders; Tassoni et al. 2023). To be able to convert CO_2 to graphite in the AGE III graphitization system we need iron as catalyst, which results in a mixture of graphite and iron (more iron than graphite) in the target. In the ion source of the AMS a cesium beam is directed to the target creating carbon ions, and this process is diluted by the iron present in the target. The more iron is present, the lower the ion yield and thus the current will be. In the AGE, graphitization requires at least 3 mg of Fe for 1 mg of C. If the sample contains less than 1mg of C, the ratio of Fe:C will increase, so current will decrease. Thus, for four of the samples with lower weight yields, only 2mg of Fe was used during graphitization in order to allow for sufficient AMS ion current. Furthermore, samples of oxalic acid were graphitized with all the shell samples with the according iron amounts. Finally, for the carbonate fractions treated with Methods C and D the samples were sent directly to the ETH in gas chromatography (GC) vials to be dated. For all samples dated, phthalic acid blanks graphitized in the BRAVHO laboratory were included in order to correct the resulting ages.

2.3.4. TWO PRETREATMENT STEPS

All four methods were tested on modern shell specimens to help evaluate the materials and time needed for each method and the quantity of sample material resulting from the different methods. Moreover, for the organic matrix samples resulting from methods A and B, a graphitization test at the BRAVHO lab, in Bologna, was performed to measure the average carbon content and estimate the amount of sample needed in case of archeological samples, as well as to adjust the amount of Fe for graphitization if needed.

2.3.4.1. STEP 1 – MODERN SPECIMENS

The first step aimed to establish the protocols for each method and was completed using modern specimens of four different species of shells: *Pecten maximus; Crassostrea gigas; Mytilus* sp.*; Ruditapes philippinarum* (Table 3). The initial experiments in this step served as a trial for the application of the four different methods: Method A, B, C and D summarized in Figure 18.

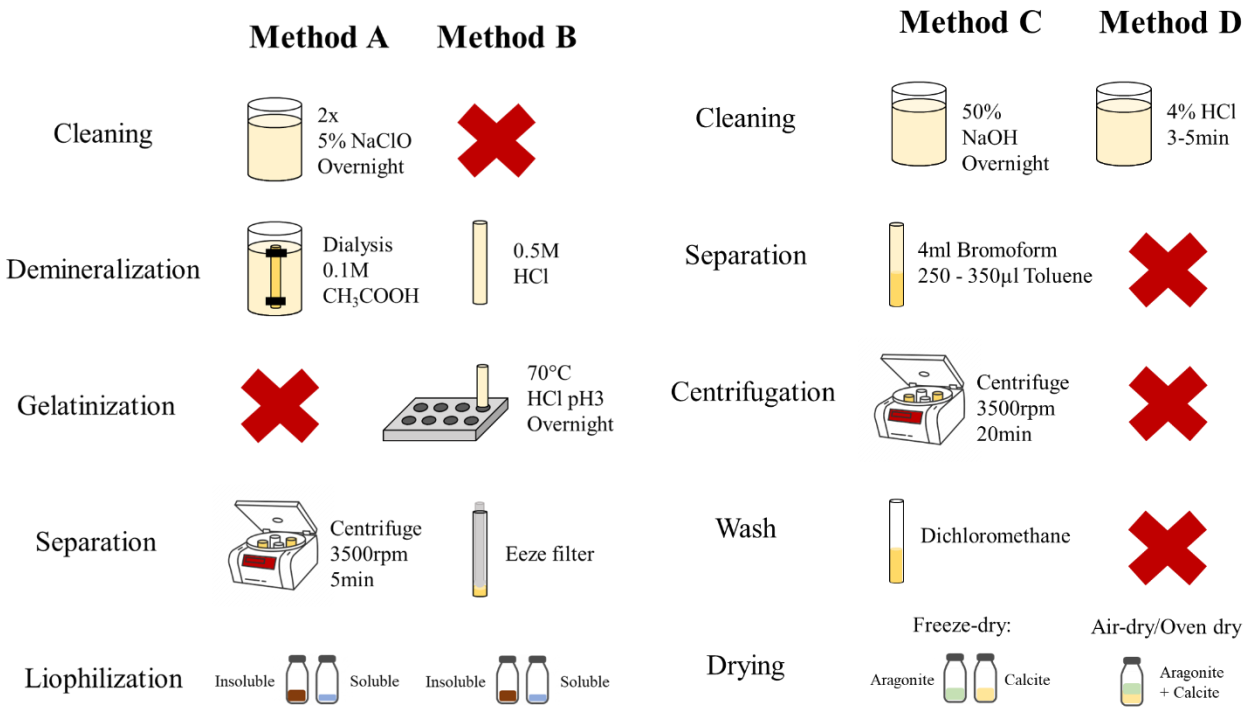

Figure 18: Summary and comparison of the four methods tested, with red crosses for steps not performed.

Table 3. Information on the Modern samples used in the experiments. The end weight is shown as the Soluble/Insoluble fraction for Methods A and B, and as Aragonite/Calcite for Method C.

Experimantal Step 1 - Modern specimens							
BRAVHO lab code	**Species**	**Area of origin**	**Method**	**Start weight (mg)**	**End weight (mg)**		**Comment**
					Soluble/ Aragonite	Insoluble /Calcite	
BRA 5070.1	*R. philippinarum*	Chioggia	A	2522	0.5	1.1	
BRA 5071.1	*R. philippinarum*	Chioggia	A	2638	0.9	18.4	
BRA 5072.1	*C. gigas*	St. Antioco	A	2562	29.6	3.5	
BRA 5104	*P. maximus*	N. Atlantic	A	2486	1.1	6.1	
BRA 5070.2	*R. philippinarum*	Chioggia	A	2594	0.8	50.2	
BRA 5071.2	*R. philippinarum*	Chioggia	A	2391	0.5	1.8	
BRA 5072.2	*C. gigas*	St. Antioco	A	2533	2.1	2.2	
BRA 5200.1	*Mytilus* sp.	Chioggia	A	2497	1.6	1.8	Cleaning step in fridge
BRA 5200.2	*Mytilus* sp.	Chioggia	A	2686	0.3	2.6	Cleaning step at RT
BRA 5194.1	*Mytilus* sp.	Chioggia	A	2645	1.2	6.5	Cleaning step in fridge
BRA 5194.2	*Mytilus* sp.	Chioggia	A	2977	0.2	3.0	Cleaning step at RT
BRA 5211	*Mytilus* sp.	Chioggia	A	7242	3.4	19.1	Whole shell used - fridge
BRA 5191	*Mytilus* sp.	Chioggia	A	5141	1.8	4.6	Whole shell used - fridge
BRA 5201	*Mytilus* sp.	Chioggia	B	6913	3.1	77.1	
BRA 5193	*Mytilus* sp.	Chioggia	B	4896	1.9	53.9	
BRA 5200	*Mytilus* sp.	Chioggia	B	290	0.5	0.6	Sticky material not usable
BRA 5200	*Mytilus* sp.	Chioggia	C	574	102.3	164.2	
BRA 5194	*Mytilus* sp.	Chioggia	C	466	37.3	292.1	
BRA 5196	*Mytilus* sp.	Chioggia	C	2012	498 + 457.7	604.1	Two separations done
BRA 5192	*Mytilus* sp.	Chioggia	C	2220	845.2 + 33.1	926.0	Two separations done
BRA 5200	*Mytilus* sp.	Chioggia	D	290	90.0		<3min
BRA 5192	*Mytilus* sp.	Chioggia	D	2615	1409.0		<3min
BRA 5196	*Mytilus* sp.	Chioggia	D	2676	910.0		5min

Method A - The first experiments using Method A were performed on modern specimens of *R. philippinarum, C. gigas, Mytilus* sp. and *P. maximus* and were repeated to verify reproducibility. These species were selected based on their occurrence in archeological sites and the easy access to modern specimens of each species. Two experiments were performed to improve the method. First, an experiment using the parameters from the original protocol was performed, and secondly the sample treatment with sodium hypochlorite was done in the fridge and at room temperature, to determine if it influences the weight yield. Furthermore, different initial amounts of powdered shells were used to determine the best option for an optimal extraction of the organic matrix.

Method B – As for Method A, different initial amounts of powdered shells were used during the initial tests for Method B. The tests performed on modern shells using Method B resulted in higher weight yields compared to Method A, especially for the insoluble fraction. However, the dissolution of the carbonates took longer to complete even with frequent acid changes. This was probably due to the dissolution in test tubes as opposed to Method A, where the dissolution was performed in dialysis membranes inside large beakers.

Method C - Before applying Method C to modern shells, a test with pure aragonite and pure calcite powders (99 %) was performed to evaluate the quantity of toluene needed in the intermediate density solution for the separation to be successful. In the first part of this experiment, three subsamples of pure aragonite and three subsamples of pure calcite were used with different amounts of toluene added to the powders. This was done to ascertain that calcite will float in the intermediate density solution, and aragonite will deposit. Russo and colleagues (Russo et al. 2010) used a range from 250 to 350 µl of toluene and 4 ml of 99 % bromoform solution for this method. In the initial experiment, three quantities from this range were used: 250, 300 and 350 µl. Subsequently, the pure polymorph powders were mixed in three subsamples with around 20 % of aragonite and 80 % of calcite to see if the method was still successful with a mixed sample. These mixed subsamples were treated with the same three toluene quantities as for the previous step.
Modern specimens of *Mytilus* sp. were also used to verify the efficacy of Method C since this species naturally presents both calcite and aragonite.

Method D – The tests on modern specimens performed using Method D served to determine the time necessary to remove the outer portion of the shell, without losing too much material. Three samples, two of which had a similar initial weight were put in acid simultaneously. The smallest sample had to be taken out and washed after just over two minutes to avoid losing the entire sample. Right after that, one of the other two samples was also taken out, while the other was left in the acid for 5 minutes to see the difference

in weight yield. For archeological samples, it will be necessary to observe each sample and monitor the rate of dissolution to be able to take them out of acid before losing the sample.

2.3.4.2. STEP 2 – ARCHEOLOGICAL SPECIMENS

The second step aimed to apply the four different methods to specimens from the Terrace area of the archeological site of Vale Boi. The selected samples in this context were *Crassostrea* sp. and *Pecten* sp. (Table 4), as these were the only two species present in different archeological layers with enough material to be used for four different pretreatment methods.

These specimens were selected based on their weight since the goal was to perform the different methods on the same specimen when possible. In case enough material from the same specimen was not available for all the methods, we selected a specimen from the same layer and same species to be able to compare the ^{14}C dates resulting from the different methods.

Table 4. Information on the Archeological samples used in the experiments. The end weight is shown as the Soluble/Insoluble fraction for Methods A and B, and as Aragonite/Calcite for Method C.

Experimantal Step 2 - Archeological specimens from Vale Boi (Portugal)						
BRAVHO lab code	**Species**	**Method**	**SU**	**Start weight (mg)**	**End weight (mg)**	
					Soluble/Aragonite	Insoluble/Calcite
BRA 4930	*Crassostrea sp.*	A	3	6609	4.2	14.1
BRA 4942	*P. maximus*	A	4	7430	2.6	56.4
BRA 4946	*P. maximus*	A	5	1582	1.6	3.7
BRA 4952	*P. maximus*	A	6	4527	1.9	6.7
BRA 4957	*P. maximus*	A	7	2861	2.3	20.8
BRA 4930	*Crassostrea sp.*	B	3	6385	1.7	47.8
BRA 4938	*P. maximus*	B	4	5577	2.0	31.2
BRA 4946	*P. maximus*	B	5	1546	0.6	2.0
BRA 4952	*P. maximus*	B	6	4514	1.9	20.6
BRA 4956	*P. maximus*	B	7	2413	1.8	33.9
BRA 4931	*Crassostrea sp.*	C	3	761	0.0	572.4
BRA 4943	*P. maximus*	C	4	886	131.9	454.2
BRA 4946	*P. maximus*	C	5	262	32.0	99.3
BRA 4952	*P. maximus*	C	6	431	343.8	0.0
BRA 4957	*P. maximus*	C	7	235	43.8	97.3
BRA 4931	*Crassostrea sp.*	D	3	724	134.0	
BRA 4936	*P. maximus*	D	4	2285	1107.0	
BRA 4946	*P. maximus*	D	5	294	155.7	
BRA 4952	*P. maximus*	D	6	415	119.9	
BRA 4957	*P. maximus*	D	7	205	25.1	

2.3.5. PYROLYSIS - GAS CHROMATOGRAPHY - MASS SPECTROMETRY (PY – GC - MS)

Analytical pyrolysis is a powerful technique capable to provide chemical information of the organic matter at a molecular level. The use of Py-GC-MS to characterize the chemical composition of natural organic matter has been reported in studies related to differences in ^{14}C ages (Ferro-Vázquez et al. 2019). Furthermore, Py-GC-MS was used to identify possible changes in the composition of fresh mussels (*M. galloprovincialis*) after exposure to cyanotoxins (Diez-Quijada et al. 2020). Analytical pyrolysis has also been applied to the characterization of the intra-skeletal organic matrix in hard corals (Adamiano et al. 2014).

For this study, analyses by Py-GC-MS were performed in order to determine if the insoluble materials extracted with Methods A and B were consistent to the chemical characteristics of the organic matrix of the shell and checking for the occurrence of any external material in the samples. Py-GC-MS analysis was performed using an EGA/PY-3030D micro-furnace pyrolyser (Frontier Laboratories Ltd., Japan) coupled with a 7890 Agilent HP gas chromatograph (GC) connected to a 5977 Agilent HP quadrupole mass spectrometer (MS) (Agilent Technologies, USA; Figure 19). A small crucible capsule containing weighed shell sample (2-4 mg) was introduced into the furnace and then pyrolyzed at 600 °C for 100 s using helium as carrier gas (1 mL min^{-1}) and an interface temperature of 280 °C. The evolved gases were then directly injected into the GC-MS for analysis. The GC injector was operated in split mode with a 10:1 ratio at 280 °C. Pyrolysis products were separated by a HP-5MS fused silica capillary column (stationary phase poly[5% diphenyl/95% dimethyl]siloxane, 30 m × 0.25 mm i.d., 0.25 μm film thickness, Agilent Technologies, USA) with the following temperature program: 50 °C to 300 °C at 10 °C min^{-1}, then hold for 10 min at 300 °C, using helium as carrier gas (1 mL min^{-1}). The MS was operated in EI positive mode (70eV, scanning 45–500 m/z) with transfer line temperature 250 °C, ion source temperature 230 °C and quadrupole temperature 150 °C. Tentative identification of the pyrolysis products was performed by comparison with MS library and published studies.

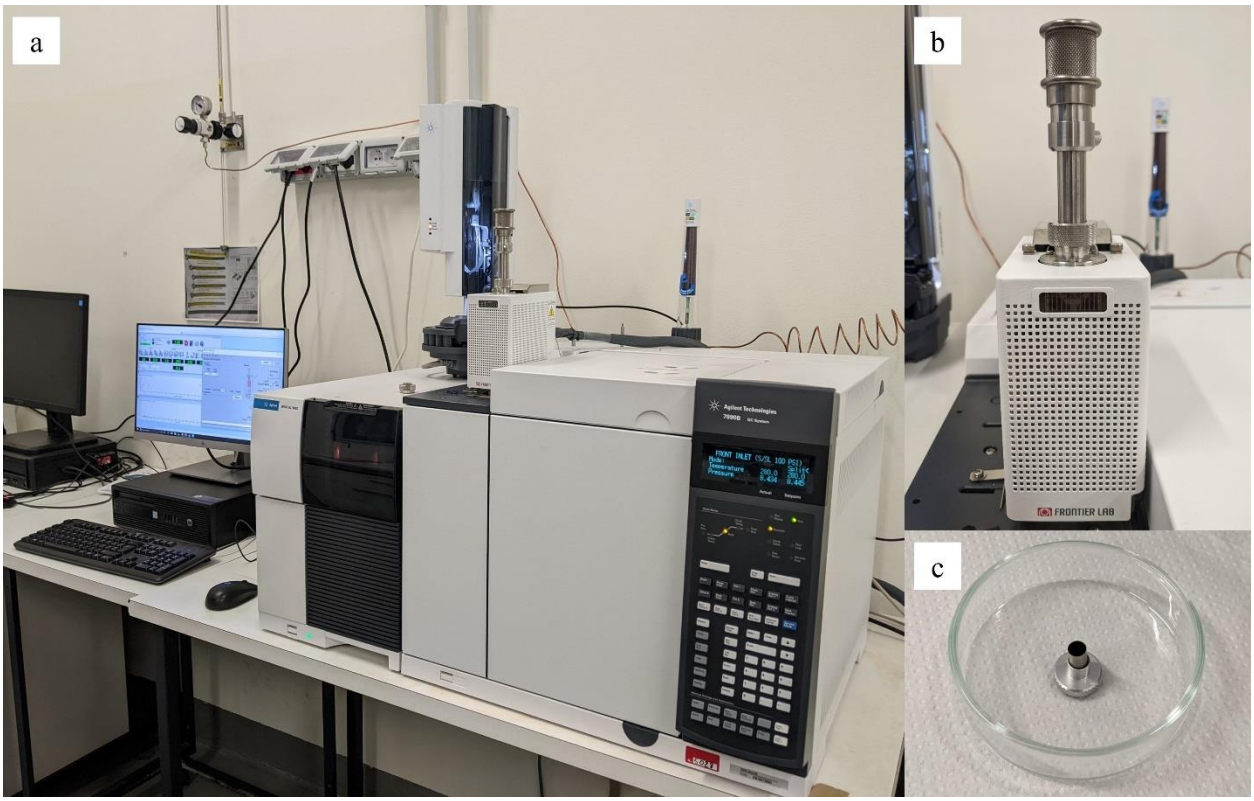

Figure 19. (a) The Py – GC – MS coupling setup; (b) a close-up view of the pyrolizer column where the (c) sample capsule is inserted.

2.4. RESULTS

In terms of complexity, time and equipment required for performing the methods, the simplest and quickest of the methods performed was Method D. Methods A and B required the longest time to complete, however the procedures were relatively simple. Method C on the other hand, was the most complicated to perform successfully and it required working with bromoform and toluene, both highly hazardous substances.

2.4.1. WEIGHT YIELDS

The final weight of all samples pretreated using the four selected methods is shown in Table 3 and 4. All four methods lead to the reduction of the initial sample weight, resulting in weights ranging from 0.1 wt.% to 81.3 wt.% of the initial sample weight (Table 5). The most substantial loss of material was seen in the case of Methods A and B, as for both methods only the organic matter was extracted, dissolving the carbonate fraction entirely. The resulting organic fraction ranged from a minimum of 0.1 wt.% to a maximum of 2.0 wt.% of the initial shell weight, with the mean value of 0.4 wt.% for modern shells and 0.5 wt.% for archeological shells for Method A, and: 0.9 wt.% and 0.7 wt.% for modern and archeological shells respectively for Method B. Considering that the organic matter content in mollusk shells makes up for 0.01 - 5% of the shell weight (Berger et al. 1964; Hadden et al. 2018; Hadden et al. 2019; Marin et al. 2012), and that the different steps of all pretreatment procedures entail some loss of material, it was expected to obtain such low values. Furthermore, the archeological shells on average show slightly lower yields, which is also expected due to degradation of the sample through time, even though the organic matrix in the shell is considered to remain well preserved (Berger et al. 1964). The difference in yield between the two methods could be due to a better dissolution in Method A of the carbonate fraction. A higher proportion of soluble organic matter is maintained in the sample due to the use of the dialysis technique as opposed to direct dissolution used in Method B, which causes most of the soluble fraction to be lost during pretreatment. For methods C and D, the carbonate fraction is used, thus resulting in a higher weight yield after pretreatment (from 12.2 wt.% to 81.3 wt.% of the initial weight). The mean weight yield for Method C was 69 wt. % for modern shells, and 66.3 wt.% for archeological shells, while for Method D the mean values were 39.6 wt.% and 32.2 wt.% for modern and archeological shells respectively. In the case of Method C, the material lost is mostly due to the various steps of pretreatment, as this method doesn't imply the use of acid to dissolve the shell. This explains the yield difference between Methods C and D since the latter uses an acid to purposefully dissolve the outer portion of the shell. As the authors of Method C (Douka et al. 2010a) also stated, the loss of material using acid etching usually varies from 30 to 80% of the initial weight. As for the first two methods, the yield is slightly lower for archeological shells, as the partially degraded material is more reactive.

Table 5. Weight yields for all four methods, and for modern and archeological samples.

Modern specimens			Archeological specimens		
BRAVHO lab code	**Method**	**Yield (wt.% of initial weight)**	**BRAVHO lab code**	**Method**	**Yield (wt.% of initial weight)**
BRA 5070.1	A	0.1	BRA 4930	A	0.3
BRA 5071.1	A	0.7	BRA 4942	A	0.8
BRA 5072.1	A	1.3	BRA 4946	A	0.3
BRA 5104	A	0.3	BRA 4952	A	0.2
BRA 5070.2	A	2.0	BRA 4957	A	0.8
BRA 5071.2	A	0.1	BRA 4930	B	0.8
BRA 5072.2	A	0.2	BRA 4938	B	0.6
BRA 5200.1	A	0.1	BRA 4946	B	0.2
BRA 5200.2	A	0.1	BRA 4952	B	0.5
BRA 5194.1	A	0.3	BRA 4956	B	1.5
BRA 5194.2	A	0.1	BRA 4931	C	75.2
BRA 5211	A	0.3	BRA 4943	C	66.2
BRA 5191	A	0.1	BRA 4946	C	50.1
BRA 5201	B	1.2	BRA 4952	C	79.7
BRA 5193	B	1.1	BRA 4957	C	60.1
BRA 5200	B	0.4	BRA 4931	D	18.5
BRA 5200	C	46.4	BRA 4936	D	48.4
BRA 5194	C	70.7	BRA 4946	D	53.0
BRA 5196	C	77.5	BRA 4952	D	28.9
BRA 5192	C	81.3	BRA 4957	D	12.2
BRA 5200	D	31.0			
BRA 5192	D	53.9			
BRA 5196	D	34.0			

2.4.2. XRD ANALYSES

For Methods A and B, the XRD analysis was performed after pretreatment on both the soluble and insoluble fractions. The results obtained were in line with the expectations, as the soluble organic matrix fraction did not contain any carbonates, while the insoluble one had traces of carbonates in some cases where the dissolution was not complete, as well as traces of quartz in some other cases (Figure 20). Presumably the traces of quartz derive from contamination in the seashells.

Method A results in two fractions of organic matter: Soluble and Insoluble. We performed XRD scans of both the fractions extracted. We expected to find no peaks for the soluble fraction, as all the carbonates should be dissolved leaving a fully amorphous organic fraction. In the insoluble fraction it was still possible to see some leftover carbonates, and thus the corresponding peaks as well. In most cases this was found to be true, but for some samples the dissolution was complete and even in the insoluble fraction there were no peaks present. In cases of amorphous samples, the scale of intensity is much lower compared to that of partially crystalline samples as the diffraction is barely present at all, thus eventual deviations from the background values might appear larger.

In the case of sample BRA 5070.1, we found no significant peaks in either the soluble or the insoluble fraction indicating a complete dissolution of the carbonates (Figure 21). The bulging of the graphs, or deviation from the zero of the background value shows an amorphous nature of the sample. The difference values for these graphs are not high, although there are some unidentified peaks in both fractions which would require further investigation in case of archeological samples.

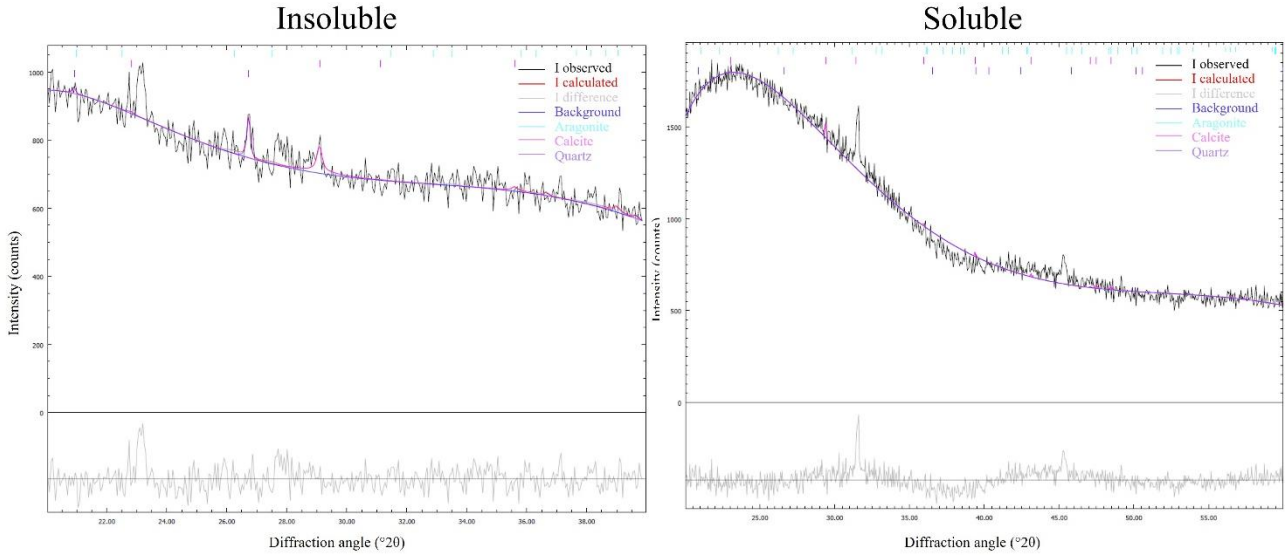

Figure 20. XRD graphs of the insoluble and soluble fractions extracted from sample BRA 5070.1.

Sample 5070.2 is a good example of what our expectations for most samples was, which is to find the soluble fraction free of carbonates and thus free of peaks, and the insoluble fraction still containing some (Figure 21). In this case we have some aragonite left in the insoluble fraction of the organic matrix as shown by the turquoise-colored peaks, in correspondence with the turquoise reference points shown at the top of the graph representing the typical peak positions of reference aragonite. In this sample the difference is very low so we can assume to have discovered all present phases in these samples.

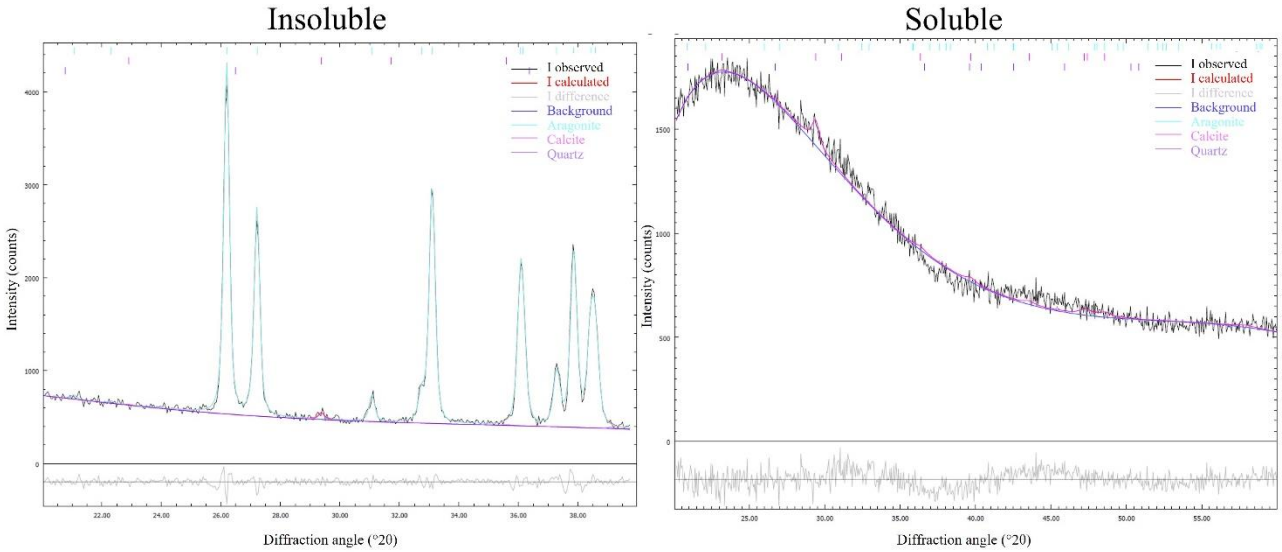

Figure 21. XRD graphs of the insoluble and soluble fractions extracted from sample BRA 5070.2.

Sample 5071.1 is another good example of what our expectations for most samples was. In this case, as the previous one we have some aragonite left in the insoluble fraction of the organic matrix (Figure 22). The difference from BRA 5070.2 is that in this case our Insoluble fraction shows to be more amorphous, which is evidenced by the bulging in the first part of the graph, like in the soluble fraction graph.

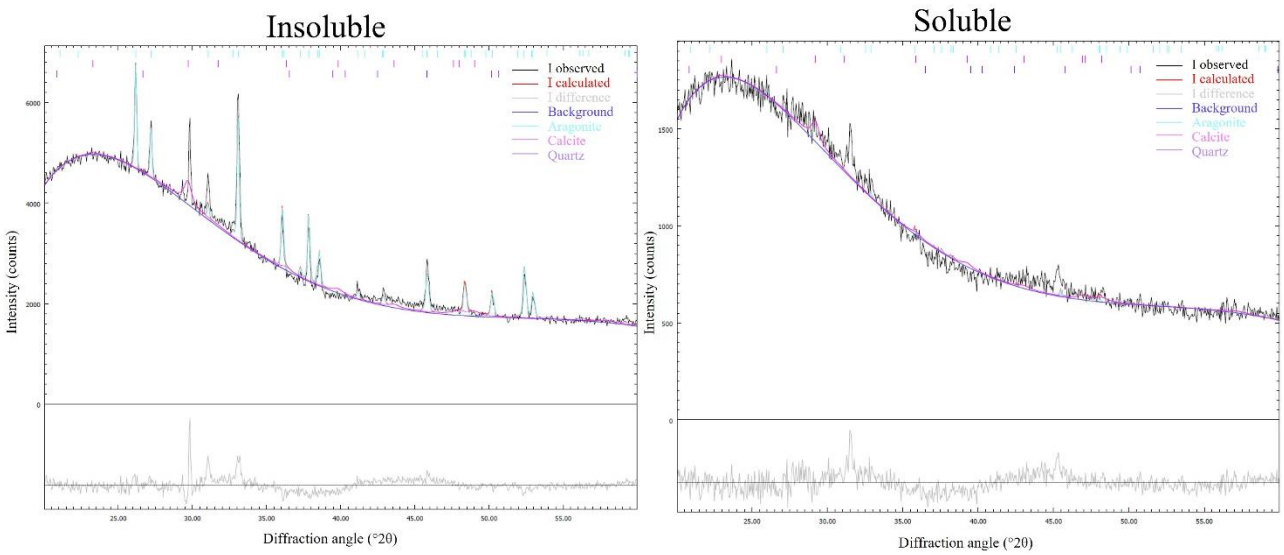

Figure 22. XRD graphs of the insoluble and soluble fractions extracted from sample BRA 5071.1.

Consistently to sample BRA 5070.1 where we found no peaks in either fraction, sample BRA 5071.2 shows the same situation with no peaks and a completely amorphous insoluble and soluble fraction, showing very similar graphs both in scale and in shape (Figure 23).

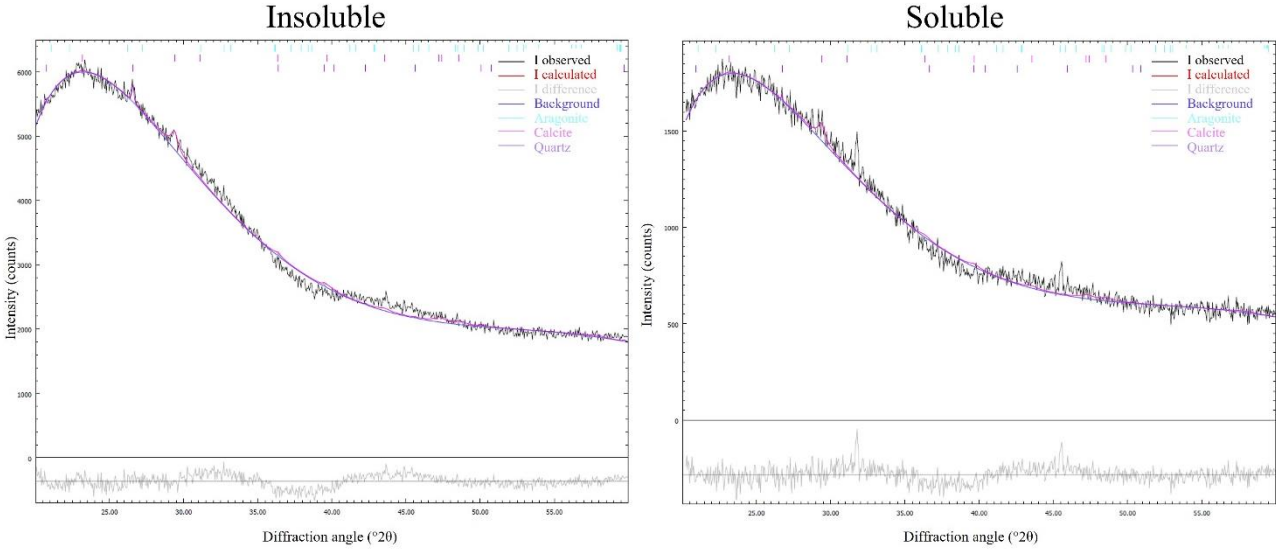

Figure 23. XRD graphs of the insoluble and soluble fractions extracted from sample BRA 5071.2.

Sample BRA 5072.1 contains a crystalline phase in the insoluble fraction as evidenced by the presence of an intense and several lesser peaks corresponding to reference peaks of quartz (shown in violet, Figure 24). There is a slight difference corresponding to the quartz peaks indicating minor deviations from the reference peaks in terms of shape and intensity. The presence of quartz could be the remnants of the agate mortar and pestle that was used to crush the shells. In the soluble fraction we have an unidentified peak present at the diffraction angle of 32°2θ, which is also seen in the difference portion of the graph. This would require further investigation in case of archeological samples as it might indicate the presence of another phase in the sample. However, given the low intensity of this peak it should not affect the further analysis of the sample.

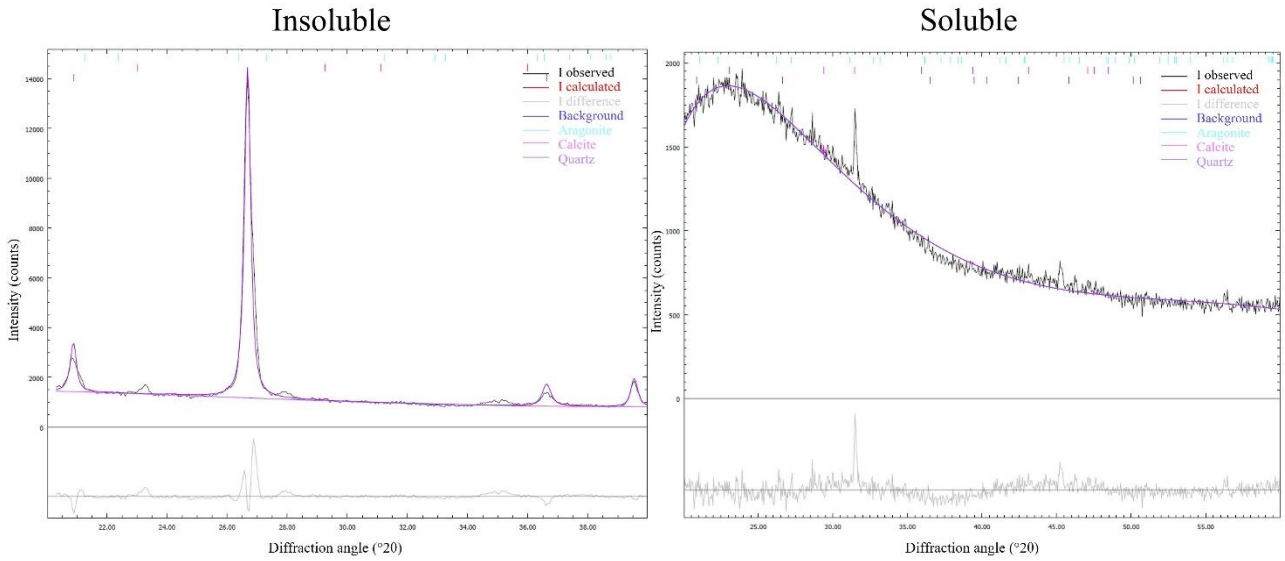

Figure 24. XRD graphs of the insoluble and soluble fractions extracted from sample BRA 5072.1.

Sample BRA 5072.2 shows two very similar graphs for both fractions, presenting amorphous with the presence of quartz peaks in both fractions (Figure 25). A small unidentified peak around the diffraction angle of 32°2θ is seen, which corresponds to the unidentified peak positions found in previous samples which are also present at that position and of similar intensity.

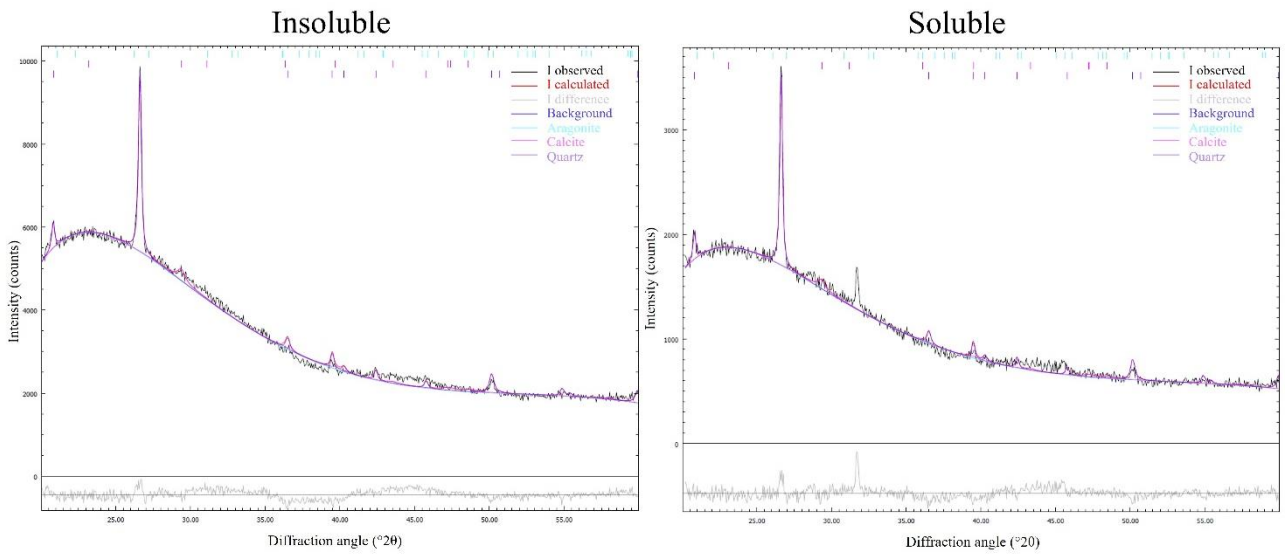

Figure 25. XRD graphs of the insoluble and soluble fractions extracted from sample BRA 5072.2.

Like sample BRA 5072.1, sample BRA 5104 has a small quartz fraction present, slightly deviating from the reference quartz as seen in the difference pattern (Figure 26). In the soluble fraction we have no peaks present indicating a completely amorphous sample, as was expected.

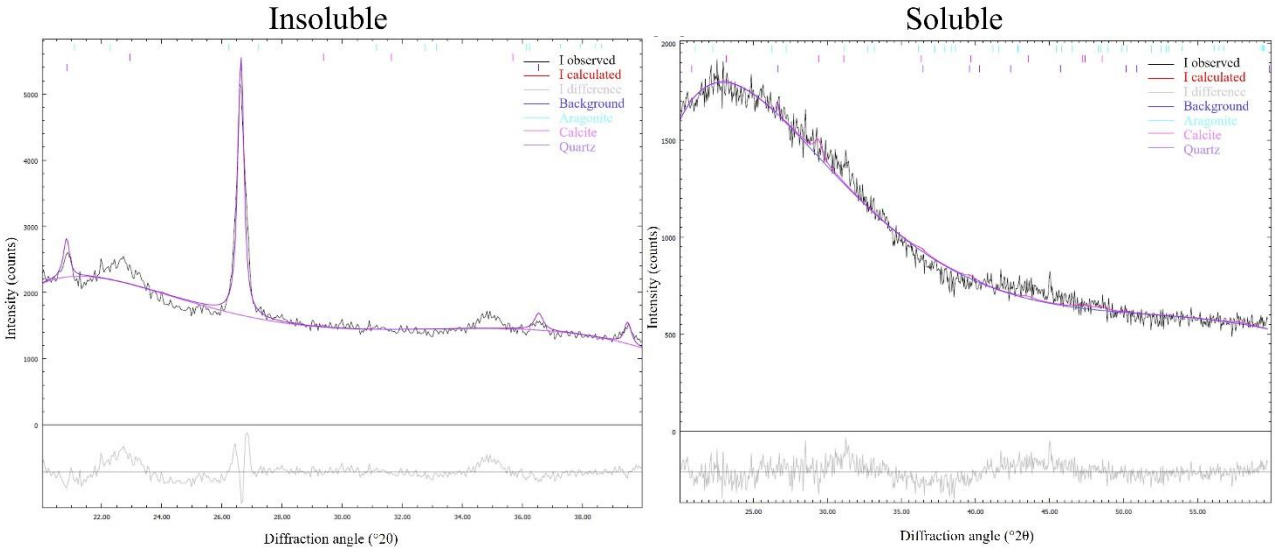

Figure 26. XRD graphs of the insoluble and soluble fractions extracted from sample BRA 5104.

Sample BRA 5191 shows several low intensity peaks in the insoluble fraction, some of which are unidentified and shown in the difference portion of the graph (Figure 27). Only the peak present at a diffraction angle 23°2θ could be relevant in the case of archeological samples. The soluble fraction shows a completely amorphous phase with no relevant peaks present.

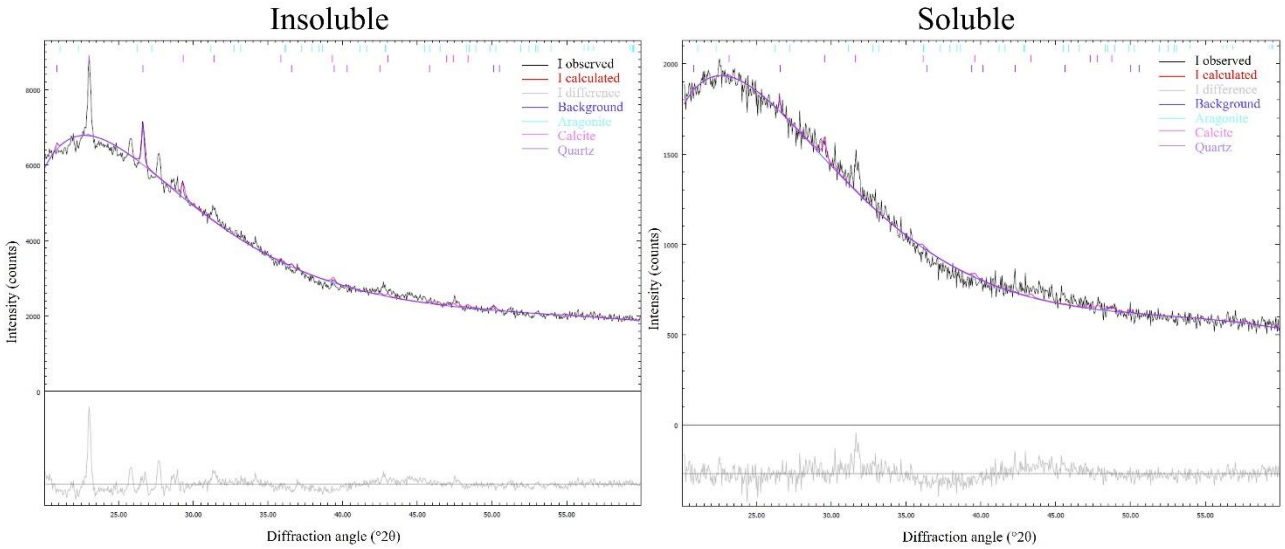

Figure 27. XRD graphs of the insoluble and soluble fractions extracted from sample BRA 5191.

Sample BRA 5211 also shows several unidentified low intensity peaks in the insoluble fraction (Figure 28). As for BRA 5191 only the peak present at a diffraction angle 23°2θ could be relevant in the case of archeological samples. The only other peak present was identified as quartz. The soluble fraction once again shows a completely amorphous phase with no relevant peaks present.

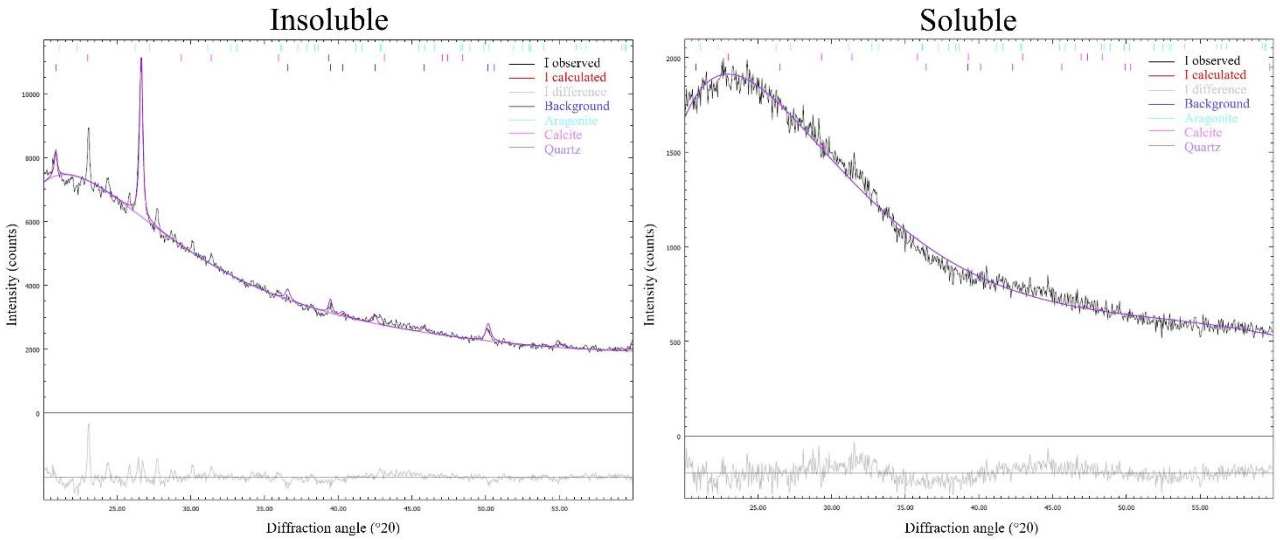

Figure 28. XRD graphs of the insoluble and soluble fractions extracted from sample BRA 5211.

Sample BRA 5200 was split into two subsamples to be treated with a 5% Hypochlorite solution in the fridge and at room temperature to see if there is any difference in the results. For sample BRA 5200.1 treated in the fridge, both fractions are amorphous with no significant peaks showing (Figure 29).

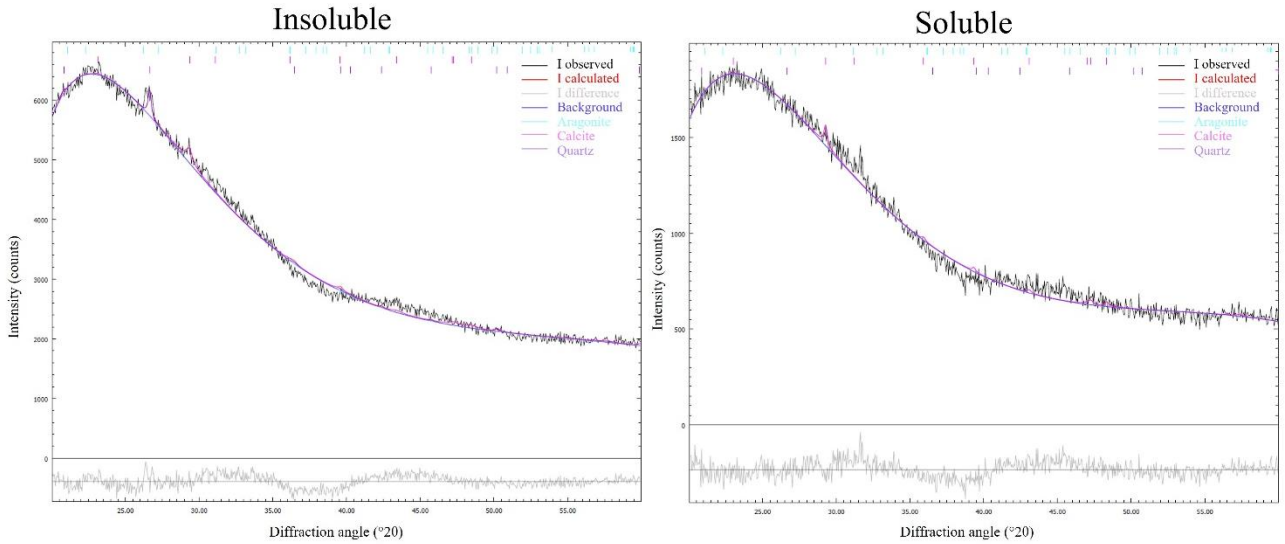

Figure 29. XRD graphs of the insoluble and soluble fractions extracted from sample BRA 5200.1.

Sample BRA 5200.2 treated with a 5% Hypochlorite solution at room temperature, also shows both fractions as amorphous (Figure 30). However, in this case as opposed to the sample treated in the fridge, we can see some low intensity peaks in both fractions, several of which are unidentified and would need further investigation if present in archeological samples destined for radiocarbon dating.

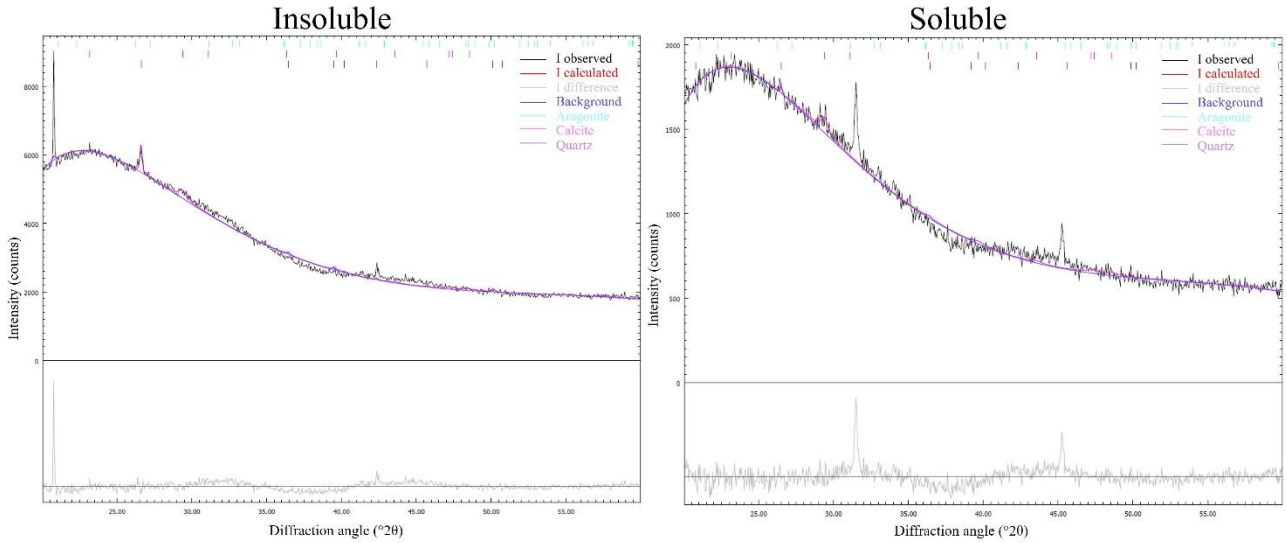

Figure 30. XRD graphs of the insoluble and soluble fractions extracted from sample BRA 5200.2.

As for sample BRA 5200, sample BRA 5194 was also split in two subsamples and treated with a 5% Hypochlorite solution in the fridge and at room temperature. Sample BRA 5194.1 treated in the fridge shows presence of calcite in the insoluble fraction and some traces of quartz, and the soluble fraction is shown as amorphous with no significant peaks showing (Figure 31).

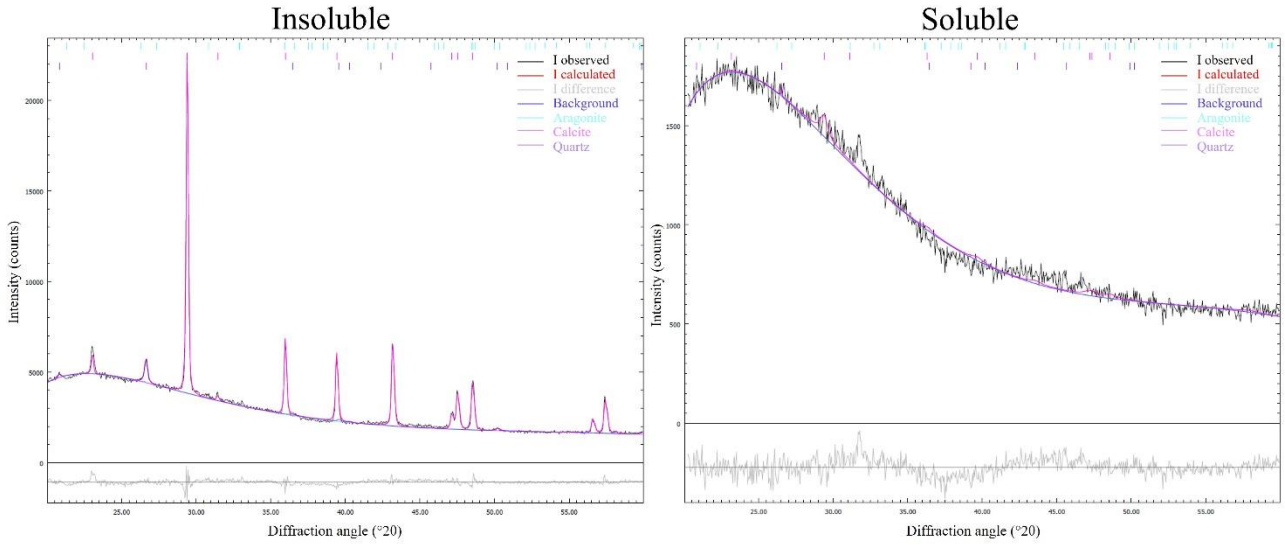

Figure 31. XRD graphs of the insoluble and soluble fractions extracted from sample BRA 5194.1.

Sample BRA 5194.1 treated at room temperature shows presence of quartz in the insoluble fraction, and the soluble fraction is shown as amorphous with no significant peaks showing (Figure 32). However, we see a low intensity unidentified peak around the diffraction angle of 32°2θ as in some previously analyzed samples.

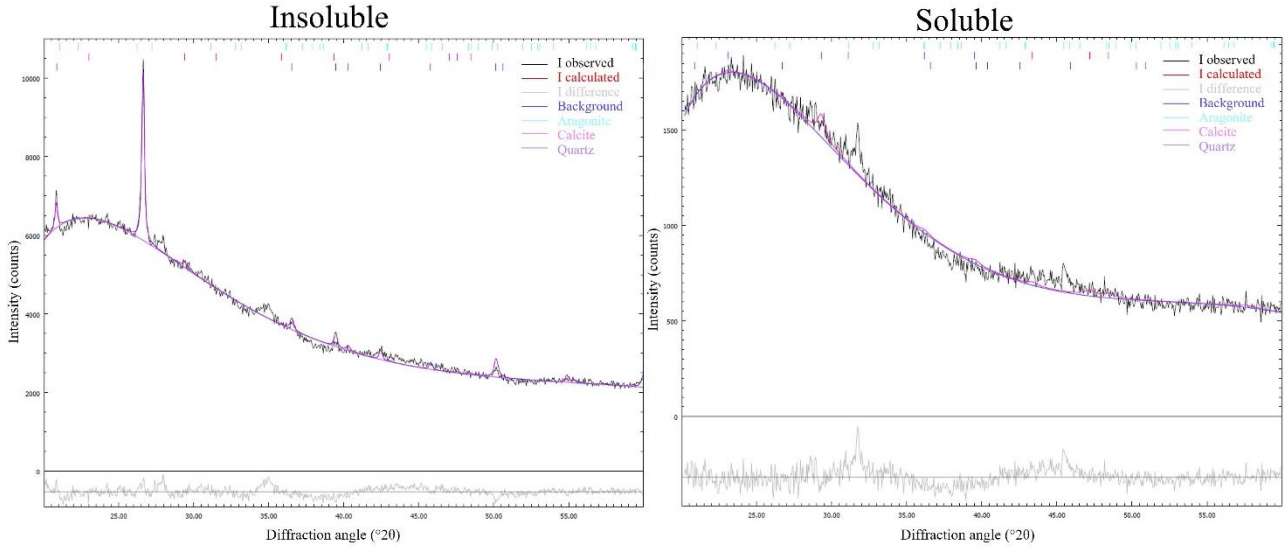

Figure 32. XRD graphs of the insoluble and soluble fractions extracted from sample BRA 5194.2.

The two graphs in Figure 33 show the insoluble fraction on the left and the soluble fraction on the right, extracted from all modern samples treated with Method B. These graphs do not show all the parameters shown in the single sample graphs, since the refinement is not shown in graphs with multiple samples. However, in this case, we can clearly see that none of these samples present any significant peaks and are amorphous in both their insoluble and soluble fractions. In the insoluble fraction of sample BRA 5193 we can see a small quartz peak around the diffraction angle of 26°2θ, and for sample BRA 5200 we can see a small peak around the diffraction angle of 32°2θ which is an unidentified phase present in some samples treated with Method A as well. The soluble fraction extracted from sample BRA 5200 was insufficient to perform XRD analysis and is thus missing from the graph.

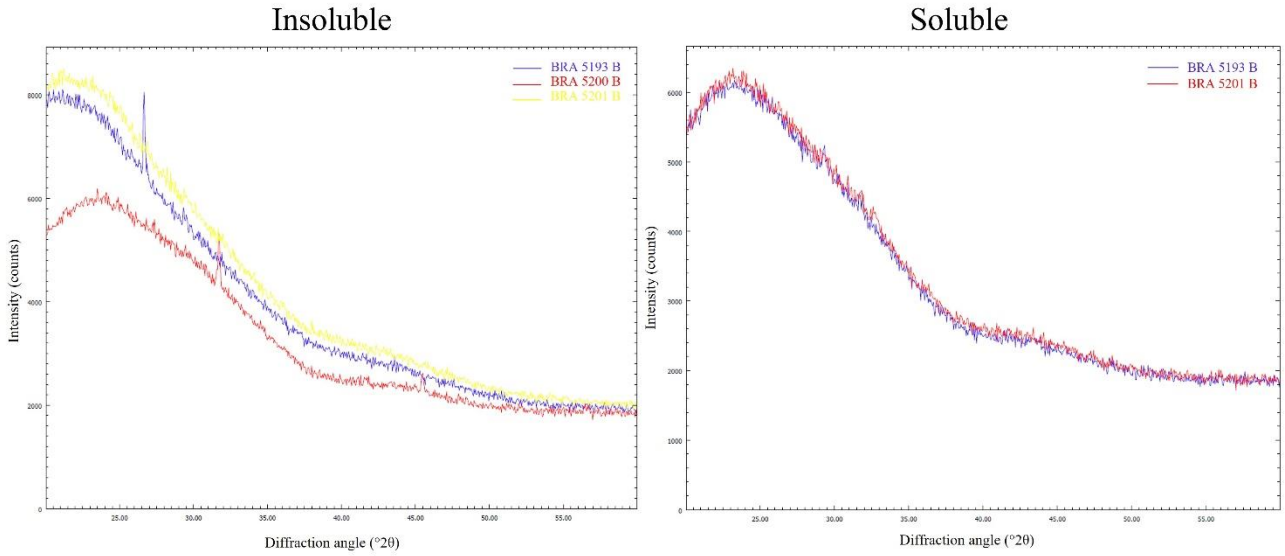

Figure 33. XRD graphs of the insoluble and soluble fractions extracted from all modern samples treated with Method B.

All toluene volumes used in this experiment were successful in making the pure aragonite deposit and the pure calcite float (Figure 34). The separation seemed successful once again with mixed calcite and aragonite samples, as there was a clear separation of the floating and the deposited fraction. However, the XRD analysis of the separated fractions showed that the separation was not complete. Both the aragonitic and calcite fractions presented a small amount of the other polymorph (Table 6).

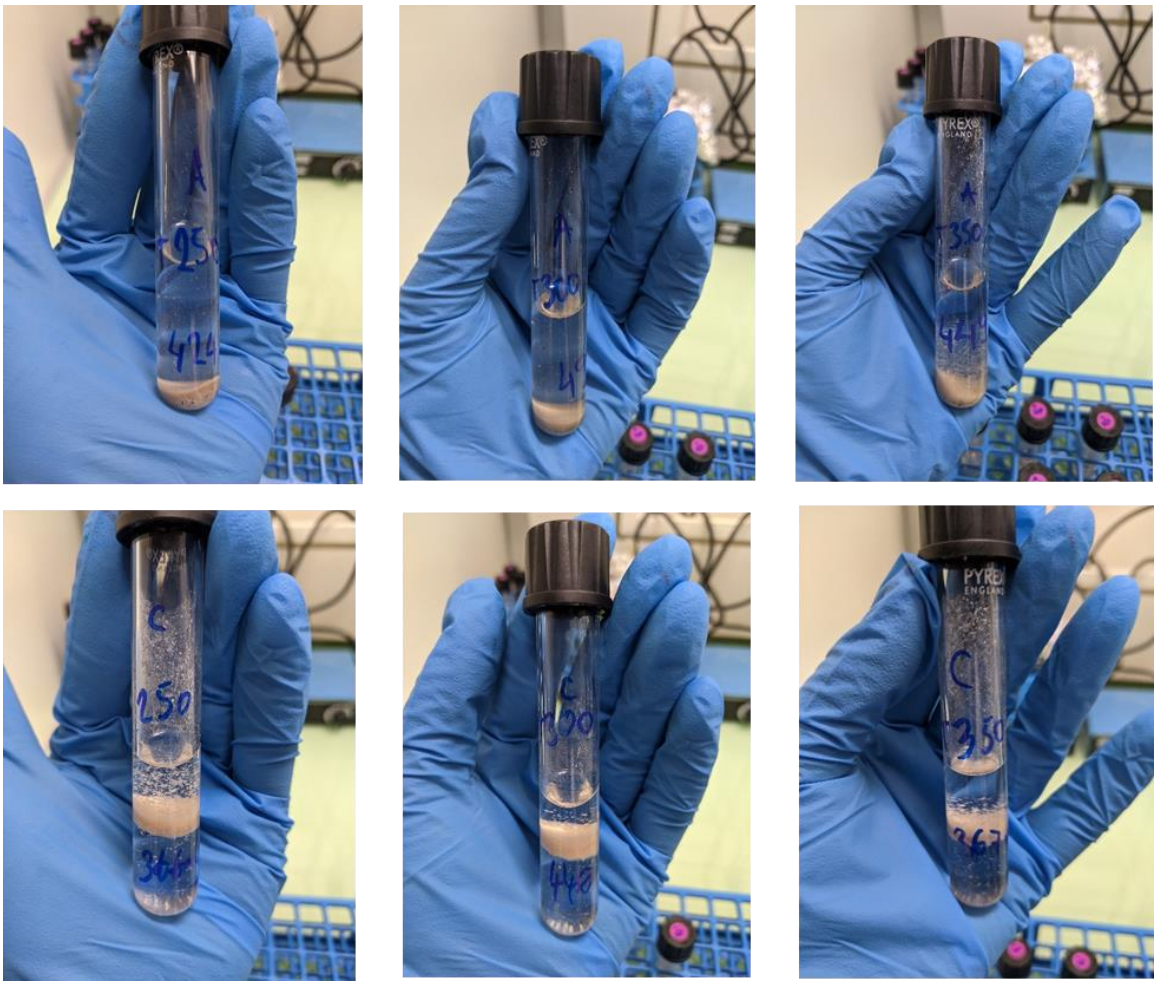

Figure 34. Top row: Pure aragonite powders; Bottom row: Pure calcite powders; Both in three different intermediate density solutions using 250, 300, and 350 µl of toluene in 4ml of bromoform (left to right).

Table 6. Percentages of calcite and aragonite after the application of Method C on three identical mixtures of pure powders

Initial proportions:		80%	20%
Separated fraction	Toluene used (µl)	Calcite (%)	Aragonite (%)
Aragonite	250	28.3	71.7
Aragonite	300	19.0	81.0
Aragonite	350	44.9	55.1
Calcite	250	74.6	25.4
Calcite	300	84.3	15.8
Calcite	350	91.5	8.5

The X-ray diffraction patterns from powders obtained from the Method C test (initial proportions: 80 wt.% calcite / 20 wt.% aragonite), which was applied using the lowest volume of toluene (250 µl in the 4 ml bromoform solution) producing an intermediate density solution, showed in the "aragonite fraction" 71.7 wt.% of aragonite and 28.3 wt.% of calcite, while in the "calcite fraction" it showed 74.61 wt.% of calcite and 25.39 wt.% of aragonite (Table 6). Even though the aragonite fraction did contain mostly aragonite, and the calcite fraction mostly calcite, the separation was not complete as evidenced by the presence of both aragonite and calcite peaks in the XRD graphs of both fractions (Figure 35).

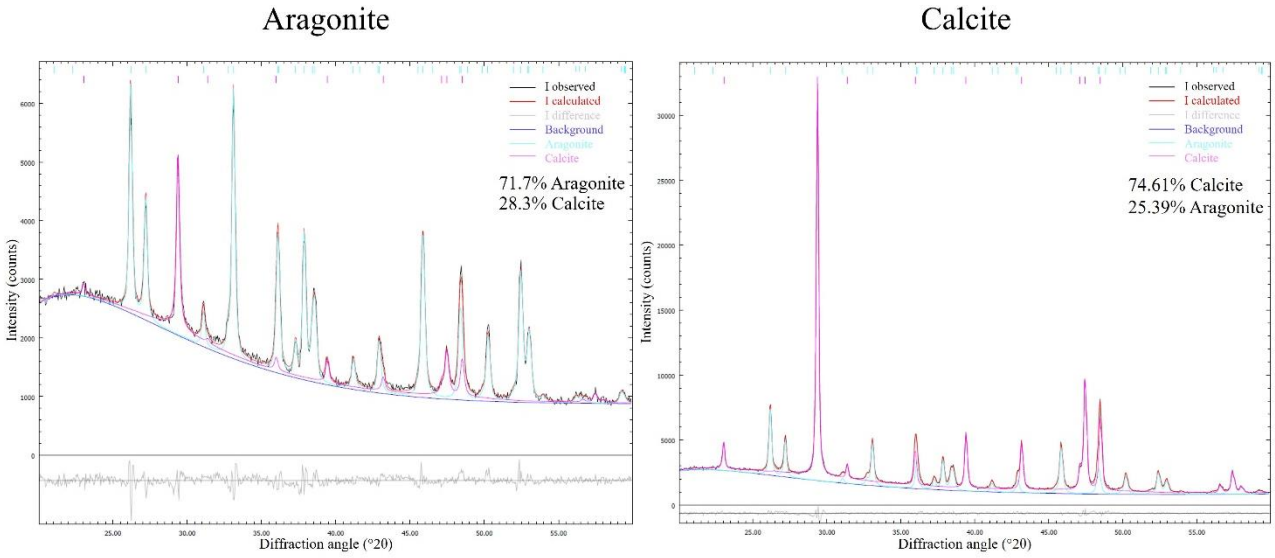

Figure 35. The aragonite and calcite fractions after the application of Method C using 250µl of toluene.

Using the intermediate toluene volume of 300 µl, in the resulting "aragonite fraction" we measured 81 wt.% of aragonite and 19 wt.% of calcite, while the "calcite fraction" contained 84.25 wt.% of calcite and 15.75 wt.% of aragonite. As in the previous case, the separation was not complete, and we found both calcite and aragonite peaks in both XRD graphs (Figure 36). However, using this volume of toluene caused a better separation compared to the previous one.

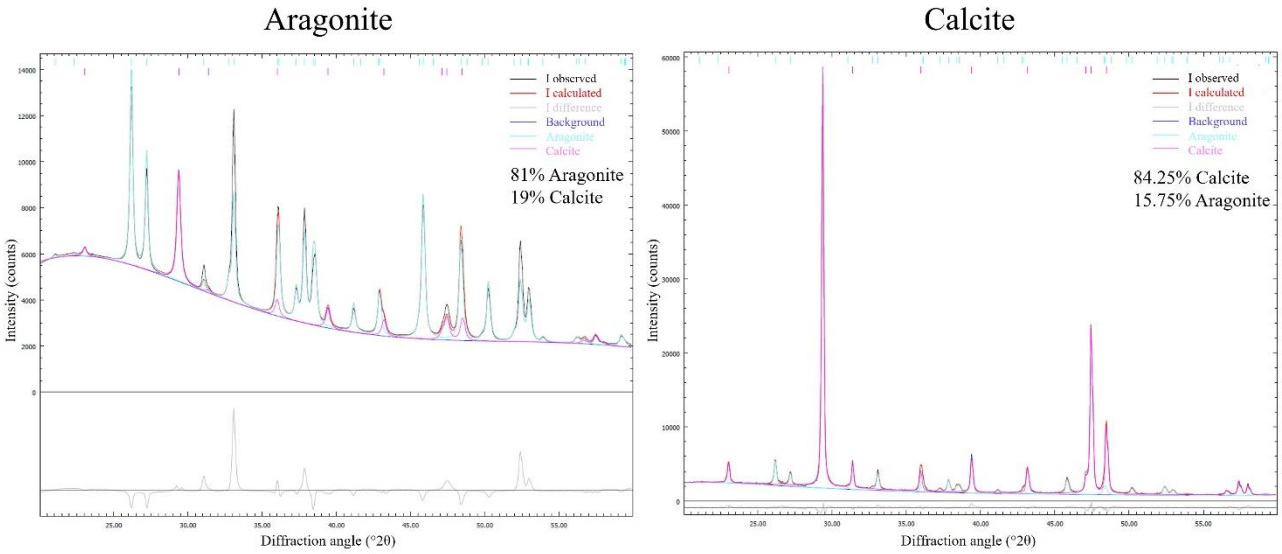

Figure 36. The aragonite and calcite fractions after the application of Method C using 300µl of toluene.

Finally, using the highest toluene volume from the test range (350 µl) the "aragonite fraction" contained 55.11 wt.% of aragonite and 44.89 wt.% of calcite, and the "calcite fraction" contained 91.46 wt.% of calcite and 8.54 wt.% of aragonite. This volume of toluene was more useful to purify the calcite fraction compared to the aragonite one, which still contained a high proportion of calcite after separation (44.89% calcite; Figure 37). This test demonstrated that a complete separation of pure aragonite and calcite powders after the application of Method C was not achieved, even though the separation of the two fractions after centrifugation appeared complete using all three concentrations (Figure 38). There was a clear difference in the efficiency of the three toluene quantities tested, with the most efficient option being the intermediate volume of 300 µl when considering both fractions, as was stated by Russo et al. (2010).

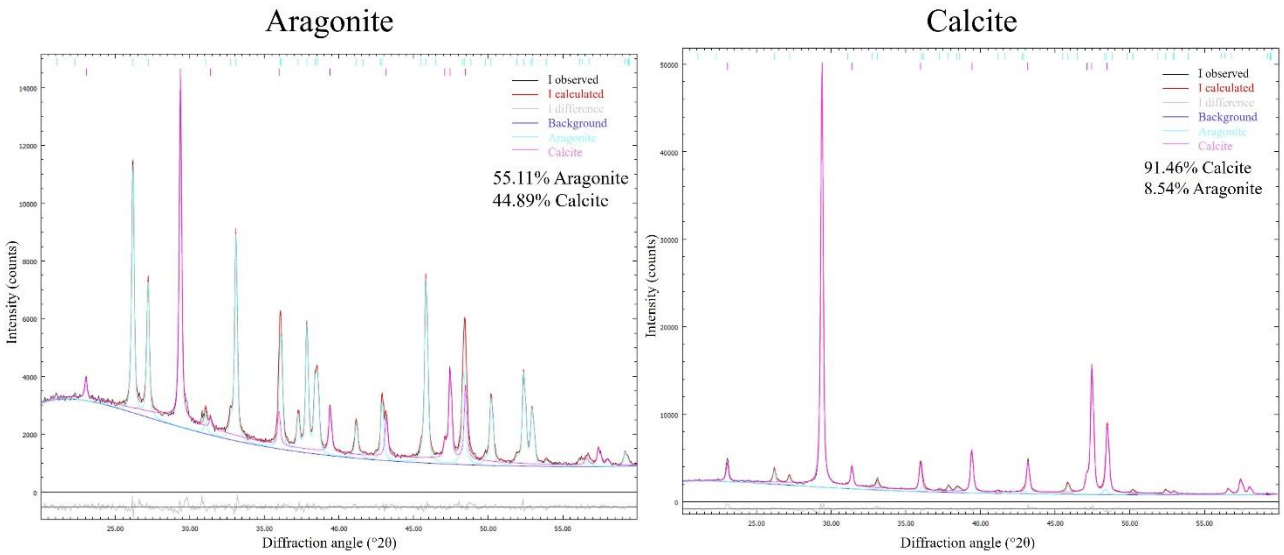

Figure 37. The aragonite and calcite fractions after the application of Method C using 350µl of toluene.

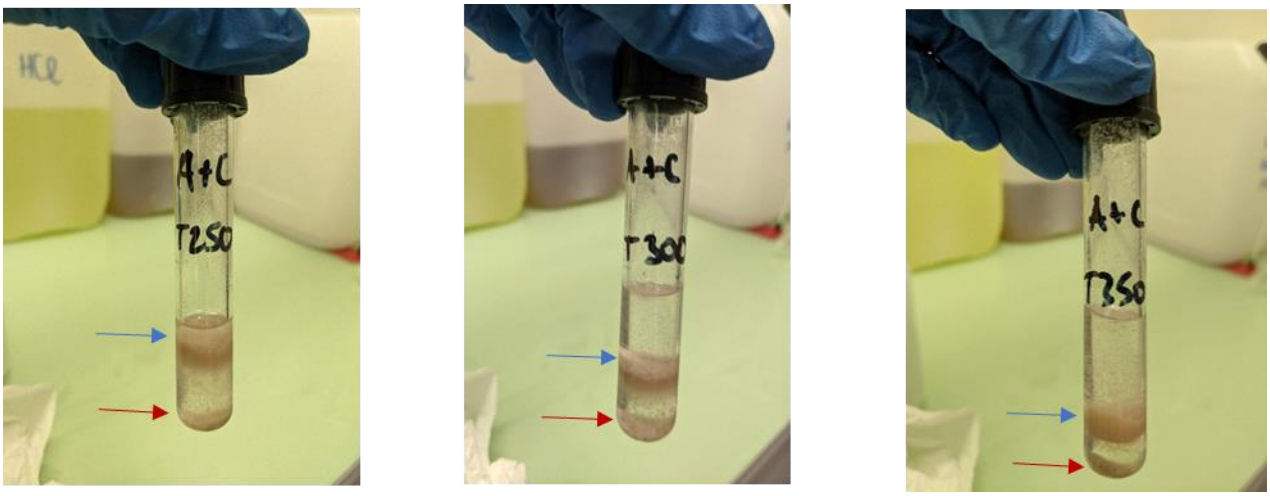

Figure 38: Three identical mixtures of 20% pure aragonite and 80% pure calcite powders in the three different intermediate density solutions using 250, 300, and 350 µl of Toluene in 4ml of Bromoform (from left to right). Blue arrows indicate the calcite fraction, and red arrows indicate the aragonite fraction.

All modern samples pretreated with Method C were made up mostly of calcite and only had a small fraction of aragonite (Table 7, Figure 39; 40).

The graph in Figure 39 shows all modern samples before applying the pretreatment with Method C. These samples show the typical peaks of calcite and aragonite, and the relative proportions of the two phases in the whole shell, before separation are present in Table 7.

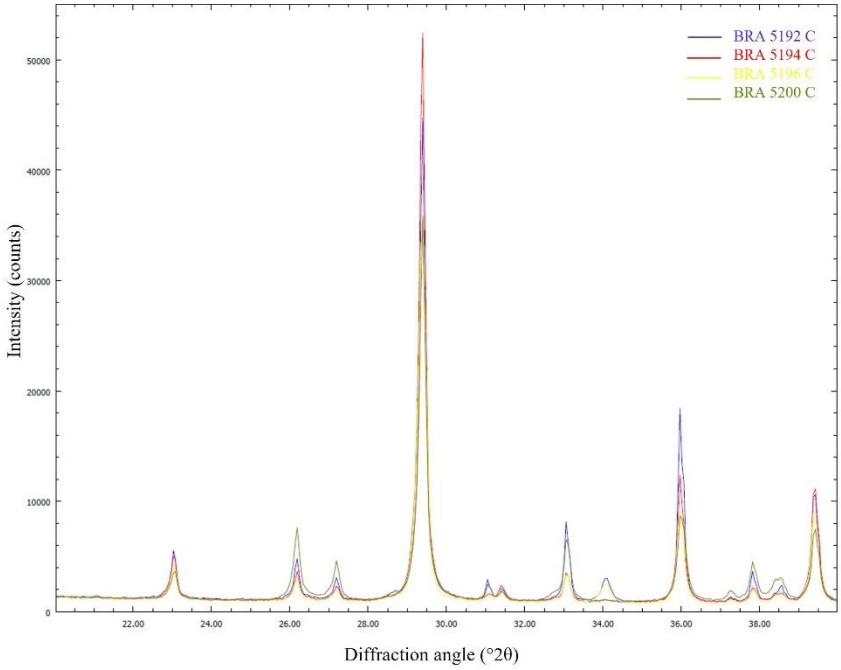

Figure 39. XRD graphs of the modern shells before applying Method C.

Since Method C results in two fractions, the results of the XRD scans after pretreatment are shown in two graphs, one of the calcite, and one of the aragonite fraction. The difference between calcite and aragonite fractions is visible from these graphs in Figure 40, as the peak intensities differ among them. However, the separation was unclear compared to the separation of the pure aragonite and pure calcite samples. It was difficult to separate the two phases, as there was an intermediate area where the phases seemed to be mixed.

Therefore, for modern shells the separation was not complete resulting in “aragonite” fractions still containing from 39.06 to 88.44% of calcite, even after two separations (Table 7). In Figure 40 it is also visible that neither fraction is pure, as both calcite and aragonite peaks are present in both fractions demonstrating that the separation of calcite and aragonite was not complete.

Table 7. Percentages of calcite and aragonite before and after the application of Method C to modern shells. Whole – percentages before separation; Aragonite/Calcite – the two resulting fractions; Aragonite 2 – resulting fraction after two centrifugations.

Method C			
BRAVHO lab code	Fraction	Calcite (%)	Aragonite (%)
BRA 5200	Whole	63.69	35.79
BRA 5200	Aragonite	50.21	49.79
BRA 5200	Calcite	72.19	27.58
BRA 5192	Whole	79.10	20.50
BRA 5192	Aragonite	80.82	19.18
BRA 5192	Calcite	85.60	14.09
BRA 5192	Aragonite 2	88.44	11.39
BRA 5196	Whole	84.74	15.20
BRA 5196	Aragonite	87.81	11.97
BRA 5196	Calcite	92.68	6.99
BRA 5196	Aragonite 2	75.60	24.10
BRA 5194	Whole	88.03	11.81
BRA 5194	Aragonite	39.06	60.94
BRA 5194	Calcite	92.62	7.27

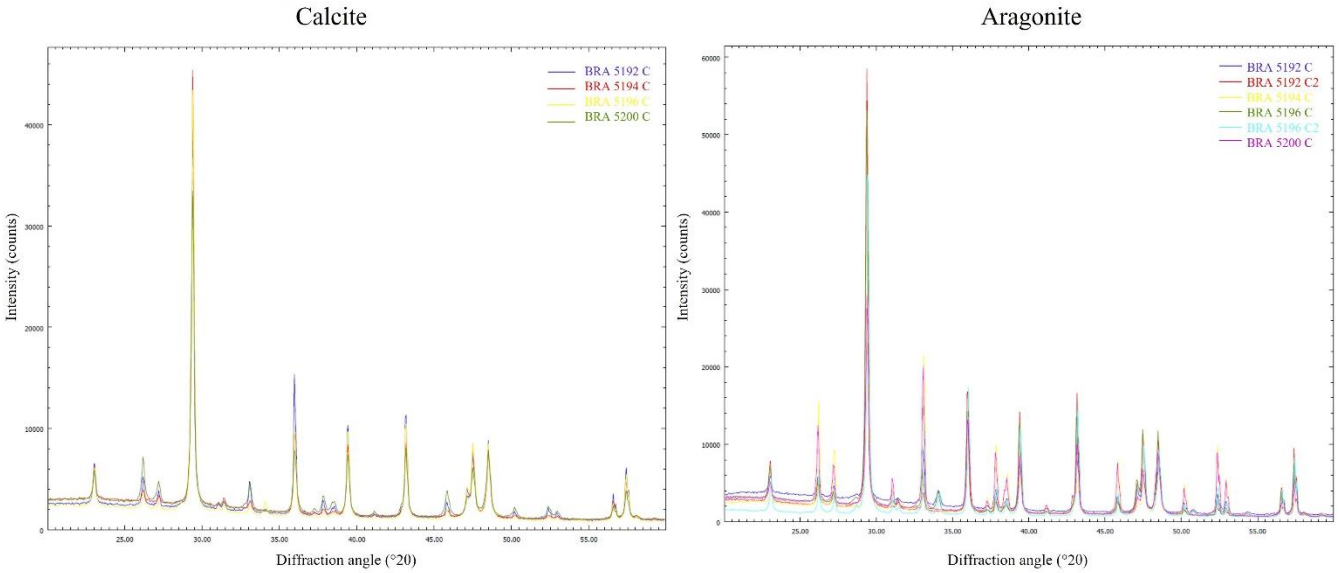

Figure 40. XRD graphs of the two resulting fractions of the modern shells after applying Method C.

The modern samples pretreated using Method D show a mixture of calcite and aragonite in similar proportions among all analyzed samples (Table 8, Figure 41). When comparing the graphs of the shell powder before pretreatment to the ones after pretreatment with Method D we can see not much has changed, even though there is a slightly higher proportion of calcite after the application of Method D. This could be due to the preferential dissolution of aragonite that was found to occur during the acid etching of shells (Vita Fanzi 1984)

Table 8. Percentages of calcite and aragonite after the application of Method D on modern shells

Method D		
BRAVHO lab code	Calcite (%)	Aragonite (%)
BRA 5200	75.93	23.71
BRA 5192	85.55	14.16
BRA 5196	85.79	13.74

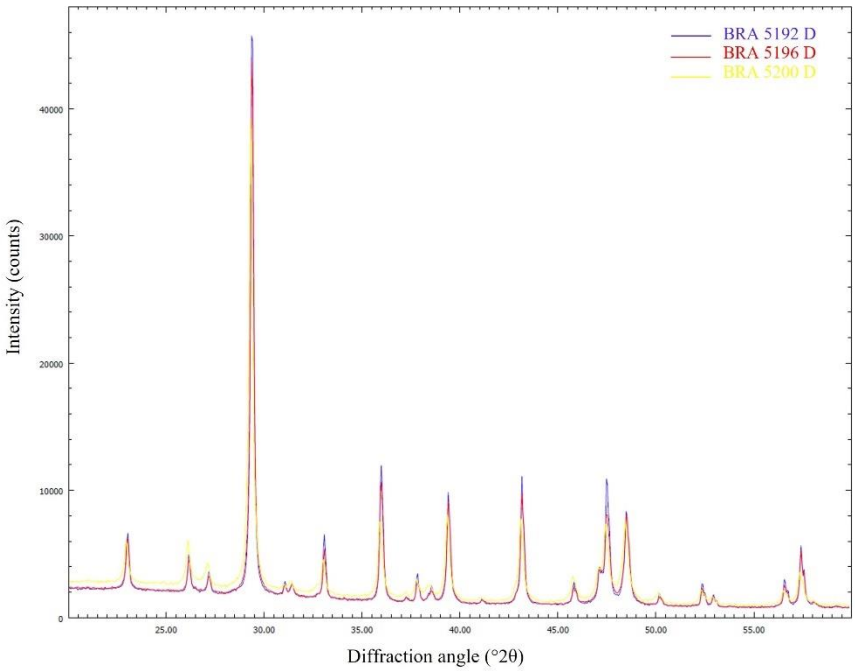

Figure 41. XRD graphs of the modern shells after applying Method D.

The archeological samples showed similar XRD results with all pretreatments as the ones obtained from modern shells. Most samples pretreated with Methods A and B show traces of quartz in the insoluble fraction while the soluble fraction is amorphous with no significant peaks (Figure 42). Both fractions are shown at two different levels of intensity as the measurements were performed at two times, thus potentially resulting from a displacement of the glass plate in the XRD machine, or a different quantity of material being placed on the glass plate. Note that the intensity scale is different among the two graphs, so the difference between the two levels is roughly the same in both graphs.

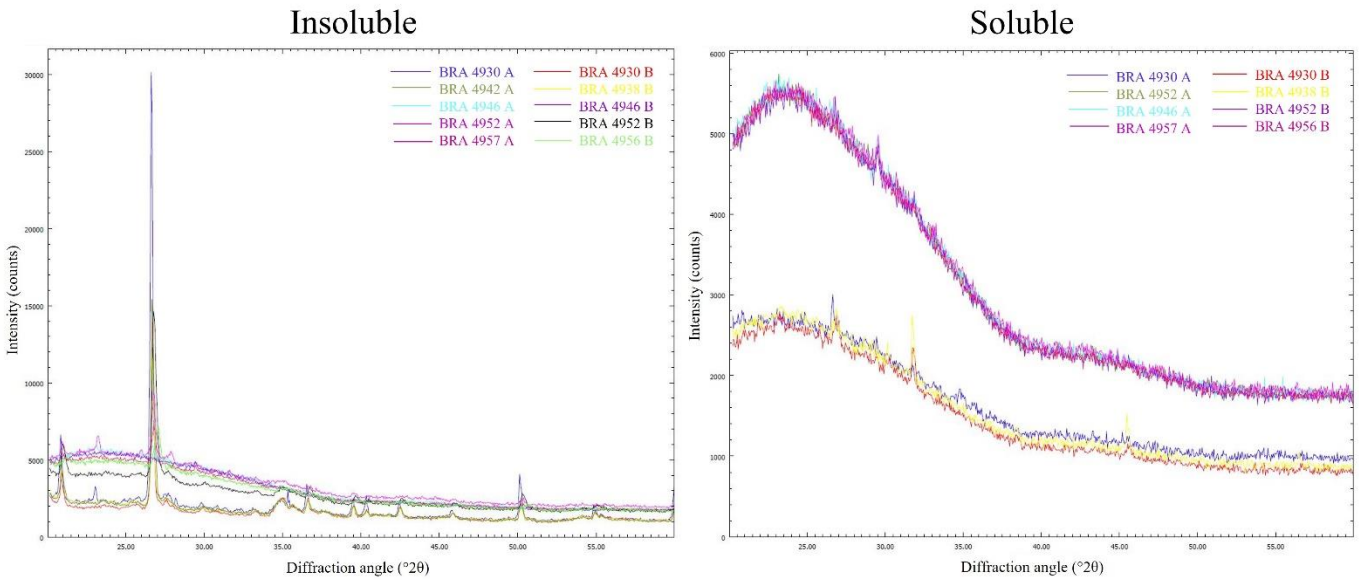

Figure 42. XRD graphs of the insoluble and soluble fractions extracted from the archeological shells using Method A and B.

As for modern shells, we analyzed the archeological specimens with XRD before and after pretreatment with Method C (Figure 43 and 44). Before pretreatment all specimens showed mostly calcite, while sample BRA 4952 showed mostly aragonite (Table 9).

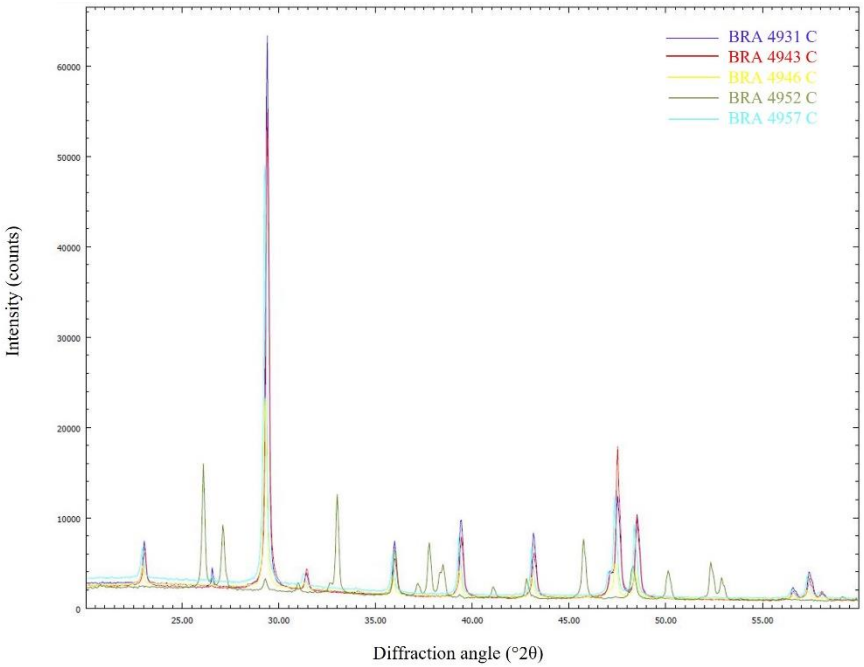

Figure 43. XRD graphs of the archeological shells before applying Method C.

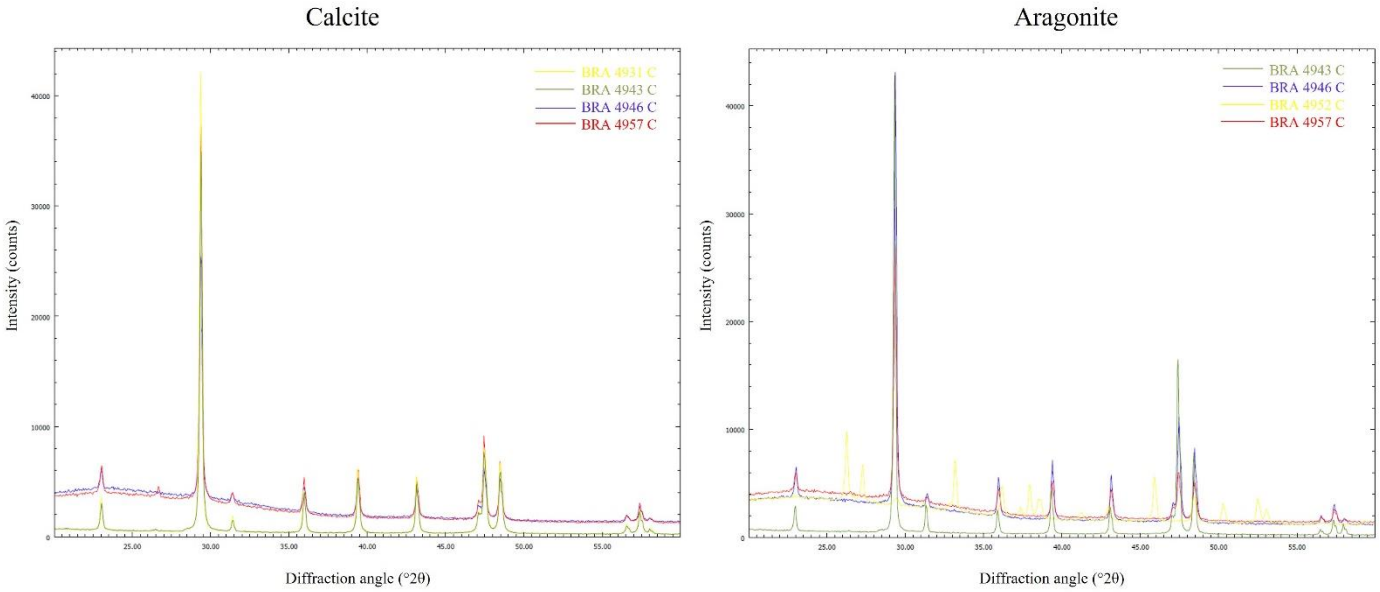

Figure 44. XRD graphs of the two resulting fractions of archeological shells after applying Method C.

The archeological samples pretreated with Method C, similarly to the modern specimens, were mostly made up of calcite and only had a small fraction of aragonite (Table 9; Figures 43 and 44). The only aragonite sample, containing over 90% of aragonite, was the archeological sample BRA 4952 (Table 9). In the case of archeological shells, all samples apart from BRA 4952 were over 99% calcite, thus we proceeded with a single separation to tentatively separate high Mg calcite (HMC) from low Mg calcite (LMC) in these samples, as was stated possible by the authors of the method (Douka et al. 2010a). Sample BRA 4952 resulted in a slightly higher aragonite proportion than the whole sample (Table 9), while the calcite samples in some cases showed traces of aragonite that were not detected in the whole sample. Furthermore, we were unable to detect differences between the calcite before and after the separation in terms of Mg content. The XRD patterns showed lattice parameters that did not differ from one another indicating no differences in average Mg content (Figures 39; 40; 43 and 44). This method would be more useful and successful in cases where there is a relatively high proportion of both polymorphs and in cases when there are high variations in the Mg content in the shell.

Table 9. Percentages of calcite and aragonite before and after the application of Method C to archeological shells. Whole – percentages before separation; Aragonite/Calcite – the two resulting fractions.

Method C			
BRAVHO lab code	Fraction	Calcite (wt.%)	Aragonite (wt.%)
BRA 4931	Whole	99.06	0.00
BRA 4931	Calcite	99.74	0.15
BRA 4943	Whole	100.00	0.00
BRA 4943	Calcite	99.47	0.40
BRA 4943	Aragonite	99.83	0.17
BRA 4946	Whole	99.98	0.00
BRA 4946	Calcite	100.00	0.00
BRA 4946	Aragonite	99.95	0.04
BRA 4952	Whole	7.24	91.15
BRA 4952	Aragonite	6.48	92.55
BRA 4957	Whole	99.29	0.20
BRA 4957	Calcite	99.11	0.00
BRA 4957	Aragonite	99.77	0.00

Archeological samples treated with Method D showed similar proportions of calcite and aragonite before and after applying the protocol. Interestingly, archeological sample BRA 4952 contained a higher amount of aragonite in the portion pretreated with Method D compared to the portion pretreated with Method C.

Furthermore, the results obtained from the XRD analysis revealed little to no change in the mineral phase composition in the carbonate samples pretreated for this study, which could indicate that the samples most likely have not been subjected to heavy recrystallization. However, to truly assess the preservation state of the shells, a simple polymorph determination is not enough, and should be combined with other tests such as microscopic examination of the crystalline structure, or the examination of the organic matter preservation (Guzmán et al. 2009; Perrin 2004; Toffolo 2021). Some of the differences in the XRD results could also be explained by differences in original polymorph proportions which can vary due to shell ontogeny and thickness, as well as due to the climatic and environmental conditions in which the mollusks secreted their exoskeletons. Moreover, the portions analyzed for each method were different fragments taken from the same shells, which may contain variable proportions of the two polymorphs. In order to avoid this in future experiments, the shells could be ground to powder whole and only then separated for pretreatment with the different methods.

2.4.3. RADIOCARBON AMS DATES

2.4.3.1. SHELL DATES

The radiocarbon ages of all the samples are shown in Table 10. All results are reported as uncalibrated dates and expressed in BP (years before 1950). Results from Method A and B were expected to overlap and mostly did so in Layers 3 and 4, while in Layers 5, 6 and 7 Method B resulted in even younger ages compared to Method A. In Layer 3 the carbonate fractions from Methods C and D overlap with the dates on the organic fraction from both Method A and B. However, for all the remaining layers, the carbonate fractions resulted in much older ages.

Table 10. AMS results for all four methods performed on samples from 5 different layers of the Terrace area of the Vale Boi site.

Method A					**Method B**				
Layer	**Sample**	**14C y BP**	**Error**	**Fraction**	**Layer**	**Sample**	**14C y BP**	**Error**	**Fraction**
3	BRA-4930	5260	30	Insoluble	3	BRA-4930	5409	22	Insoluble
3	BRA- 4930	3309	72	Soluble	4	BRA-4938	8275	23	Insoluble
4	BRA-4942	8318	25	Insoluble	5	BRA-4946	5054	77	Insoluble
4	BRA-4942	7704	93	Soluble	6	BRA-4952	8609	23	Insoluble
5	BRA-4946	6781	87	Insoluble	7	BRA-4956	4555	21	Insoluble
6	BRA-4952	15617	153	Soluble	7	BRA-4956	858	83	Soluble
6	BRA-4952	12975	123	Insoluble					
7	BRA-4957	5428	21	Insoluble					
Method C					**Method D**				
Layer	**Sample**	**14C y BP**	**Error**	**Fraction**	**Layer**	**Sample**	**14C y BP**	**Error**	**Fraction**
3	BRA-4931	4596	23	Calcite	3	BRA-4931	5522	24	Mix
4	BRA-4943	25102	95	Aragonite	4	BRA-4936	22499	74	Mix
4	BRA-4943	22266	70	Calcite	5	BRA-4946	20562	61	Mix
5	BRA-4946	19153	54	Aragonite	6	BRA-4952	33416	240	Mix
5	BRA-4946	18927	54	Calcite	7	BRA-4957	25091	96	Mix
6	BRA-4952	27374	121	Aragonite					
7	BRA-4957	20839	62	Aragonite					
7	BRA-4957	20632	61	Calcite					

Method A - The shells treated with Method A gave ages ranging from 15,617±153 to 3,309±72 BP. Both the insoluble and soluble fractions from Method A gave very young dates with no clear trend. Only three of the extracted soluble fractions resulted in enough material to obtain reliable radiocarbon measurements. In two cases, for samples BRA 4930 and BRA 4942, the soluble fraction was significantly younger than the insoluble fraction extracted from the same shell. On the other hand, the soluble fraction from sample BRA 4952 resulted significantly older than the insoluble fraction from the same shell.

Method B - Method B gave similar results to those from Method A, giving even younger ages ranging from 8,609±23 to 858±83 BP. This method resulted only in insoluble fractions, with one exception, as the soluble fractions were mostly lost during pretreatment. The only sample resulting in enough soluble organic matrix to be dated was BRA 4956 from Layer 7, and it was an outlier with an extremely young age of 858±83 BP.

Method C - The radiocarbon ages resulting from shells treated with Method C ranged from 27,374±121 to 4,596±23 BP. The aragonite fractions were consistently older compared to the calcite fractions resulting from the same shell even though the differences were not substantial in two out of three cases resulting in 226- and 207-years difference in Layers 5 and 7, BRA 4946 and BRA 4957 respectively. The only major difference between the calcite and aragonite fractions was 2,836 years in sample BRA 4943 from Layer 4.

Method D - Method D resulted in an age range from 33,416±240 to 5,522±24 BP. The age obtained for sample BRA 4931 from Layer 3 is similar to the results for this Layer obtained by the other methods. In Layer 4, the age obtained for sample BRA 4936 was close to the age obtained from Method C for the calcite fraction of sample BRA 4943 from the same Layer, while resulting significantly younger than the aragonite fraction from the same shell. The ages obtained for shells from Layers 5, 6 and 7 were older than those resulting from Method C both from aragonite and calcite fractions.

Comparison with previous results - Based on previous results on charcoal samples (Tátá et al. 2014) the expected ^{14}C age for samples from Layer 3 was from ~8,660 to ~8,880 BP (Table 2). However, on the shells used in this study for all four methods we obtained younger ages, even though a direct comparison of different materials and species can cause errors in interpretation. Ages obtained with Method C and D for samples from Layer 4 fell within the same range of expected ages for Layer 5 (Table 2). However, compared to the ages obtained with Method C and D for Layer 5, those from Layer 4 were older. The expected ages for Layer 5 based on previous results are ~20,300 – 25,400 BP (Table 2). While the obtained ages for Methods A and B on the same sample result significantly younger than expected with 6,781±87 and 5,054±77 BP respectively, the resulting ages for Methods C and D are similar to those expected with ~19 – 20,000 BP (Table 2). The sample pretreated with Method D falls within the range of previous dates, while

both aragonite and calcite from Method C give a slightly younger age. Layer 6 resulted in a higher variability of ages, both considering the previous ^{14}C dates on shells and the ^{14}C dates obtained in this study. Previous results include an age of 41,384±998 BP along with most other dates on shells resulting in ^{14}C ages ~26-28,000 BP (Table 2). The carbonate fractions from the same sample collected in this layer resulted in ages of 27,374±121 BP for Method C, and 33,416±240 BP for Method D. The two dates on bones from Layer 6 of the Terrace area resulted in two considerably different dates of 27,600±140 for sample MAMS-19366 and 20,260±80 BP for sample MAMS-19367. In Layer 6 the aragonite fraction mostly agrees with the previous results on shells. However, there is a significant variability of dates for this layer. For Layer 7, the expected ^{14}C age range was around 24,300 - 27,100 BP based on previous shell dates (Table 2). The age obtained for the sample from this layer pretreated with Method D falls within this range at around 25,000 BP, while the ages obtained for the same sample pretreated with Method C gave ages around 21,000 BP. In Layer 6 and 7 the sample pretreated with method D gave the oldest date, resulting ~5,000 years older than the dates from the same shells pretreated with Method C. However, some of the previous shell dates were even older (Table 2). When considering only dates obtained on *Pecten* sp. for layers 5 – 7, our dates from Method C are considerably younger, with Method D showing closer, yet still younger ages.

2.4.3.2. BONE DATES

The two dates on bones from Layer 6 of the Terrace area resulted in two considerably different dates of 27,600±140 for sample MAMS-19366 and 20,260±80 BP for sample MAMS-19367.

2.4.4. PYROLYSIS - GAS CHROMATOGRAPHY - MASS SPECTROMETRY (PY-GC-MS)

In this study, only the insoluble fractions of the extracted organic matrix were analyzed as the soluble fractions resulted insufficient to perform Py-GC-MS. The pyrograms of the archaeological samples (Figure 45) were characterized by a variety of pyrolysis products that included (1) aliphatic hydrocarbons, mainly n-alkanes from n-decane to n-tetratiacontane, (2) aromatic hydrocarbons principally diphenyl, monocyclic (from benzene to C4-benzenes) and polyaromatic hydrocarbons (PAHs, indenes, naphthalenes, phenanthrene and alkylated forms), (3) nitrogen-containing compounds (pyrroles, pyridines, aromatic and long chain aliphatic nitriles), (4) aliphatic (fatty acids, palmitic and oleic acids) and aromatic oxygenated compounds (furaldehydes, phenols, benzofurans).

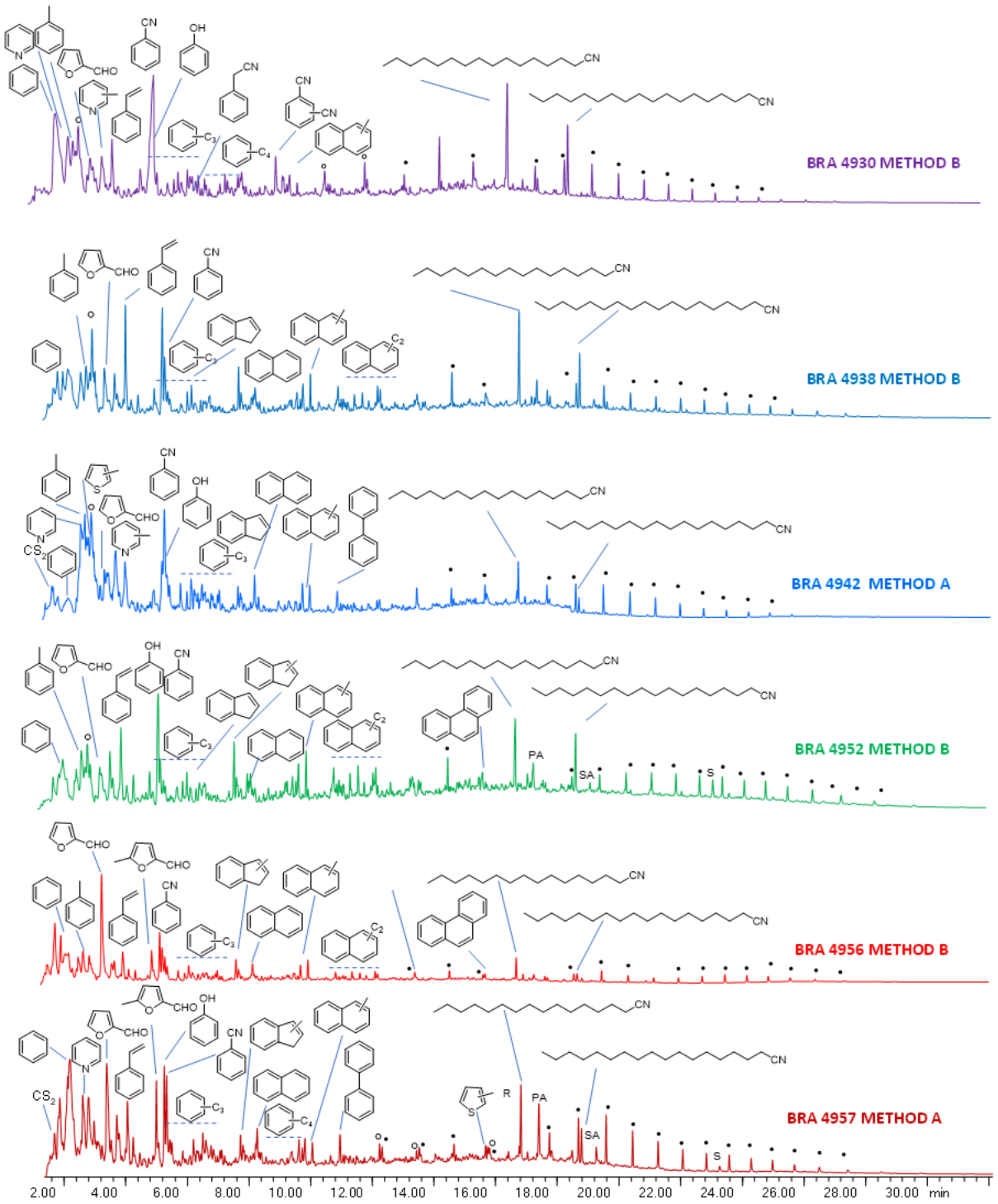

Figure 45. MS-pyrograms from Py-GC-MS of the insoluble fraction of archaeological samples. The molecular structures were reported for some of the most intense peaks. CS_2: carbon disulphide; PA: palmitic acid; SA: stearic acid; S: squalene; (o): alkenes; (▪): alkanes.

2.5. DISCUSSION

The weight yields obtained for Methods A and B were in line with the expectations based on literature and previous results (Berger et al. 1964; Hadden et al. 2018; Hadden et al. 2019; Marin et al. 2012). However, the weight yields obtained in this study for archeological shells did not significantly differ from those obtained for the modern shells, indicating that the organic matter fraction is indeed protected by the carbonate crystalline structure and remains relatively constant after the formation of the shell (Figure 46). Furthermore, it is important to acknowledge the high amount of material needed to perform Methods A and B compared to Methods C and D, considering the low yield both in terms of weight and in terms of carbon content, as seen during sample graphitization. This makes it difficult to choose to perform Method A or B instead of Method C or D, since the amount of material available for pretreatment can often be scarce. Furthermore, having a lower yield makes the extracted material more susceptible to contamination, the effect of which, if present, will be much greater than in a higher yield sample. For example, the same quantity of modern carbon introduced in a sample of 1mg would have a much more significant effect on the radiocarbon age than in a sample of 100mg.

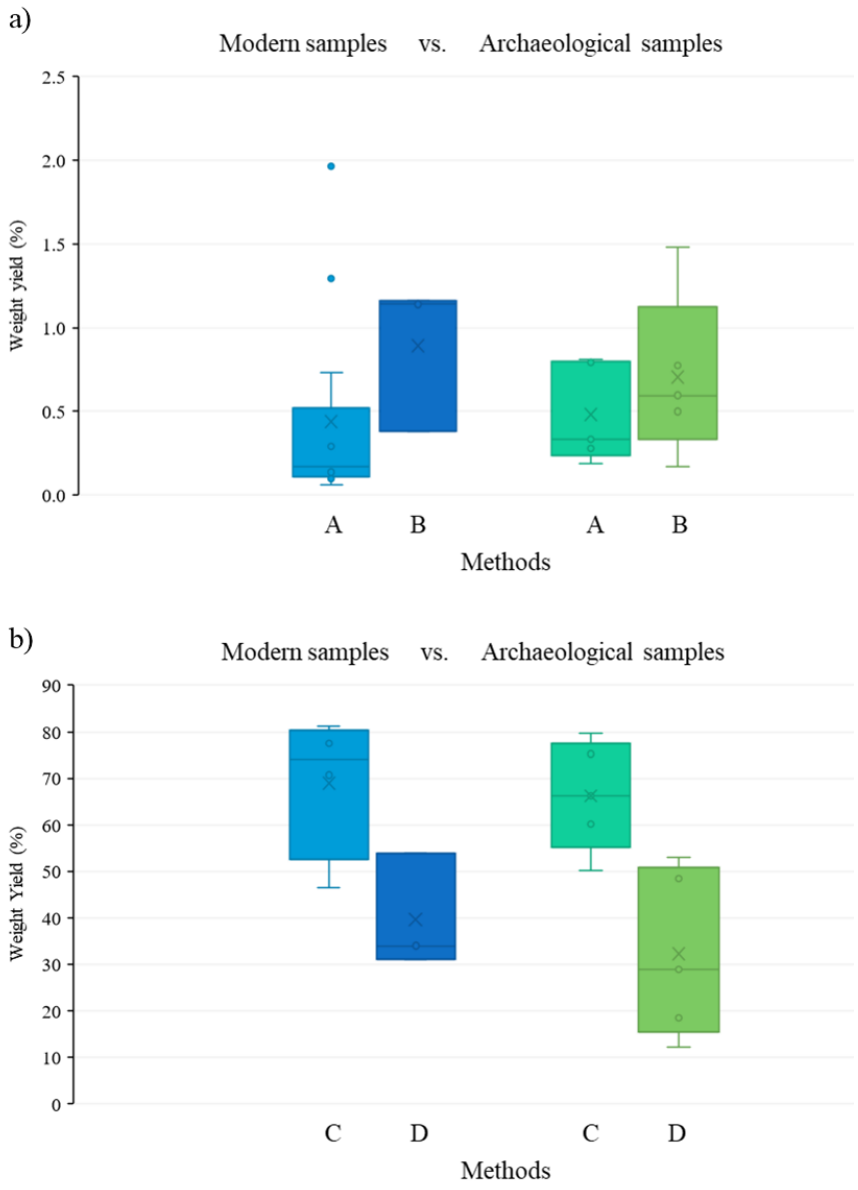

Figure 46: (a) Box plots showing the weight yields (% of initial weight) for Method A and B performed on modern (blue) and archeological (green) samples. (b) Box plots showing the weight yields (% of initial weight) for Method C and D performed on modern (blue) and archeological (green) samples.

The soluble fractions were expected to give the most reliable date, as this fraction is isolated from external influences and contained no more carbonate. However, the soluble fractions from Method A resulted younger than the insoluble fractions in most cases and the only soluble fraction resulting from Method B was an outlier and extremely young for an early Gravettian layer (Figure 47) possibly indicating that the soluble fraction is more susceptible to modern contamination. However, it could also be due to the very small amount of the soluble fraction that was extracted, which would be more affected by any potential contamination. The lack of overlap between the carbonate fractions with the organic matrix in all layers except Layer 3 could be due to the use of a different species, since for Layer 3 *C. gigas* was used and for all the other layers *P. maximus* was used. In previous studies, some of the *P. maximus* samples collected were heavily abraded and since they live at depths of 10 – 110 meters, they were almost certainly collected from the beach, thus possibly giving older ages than the age of their use at the site (Manne et al. 2012). The differences between the dates on *P. maximus* from previous studies compared to the results presented here could be partly explained by "shelf life" in beach deposits as well as variable preservation and taphonomy. However, this does not explain the differences among methods applied to the same shell (Figure 47).

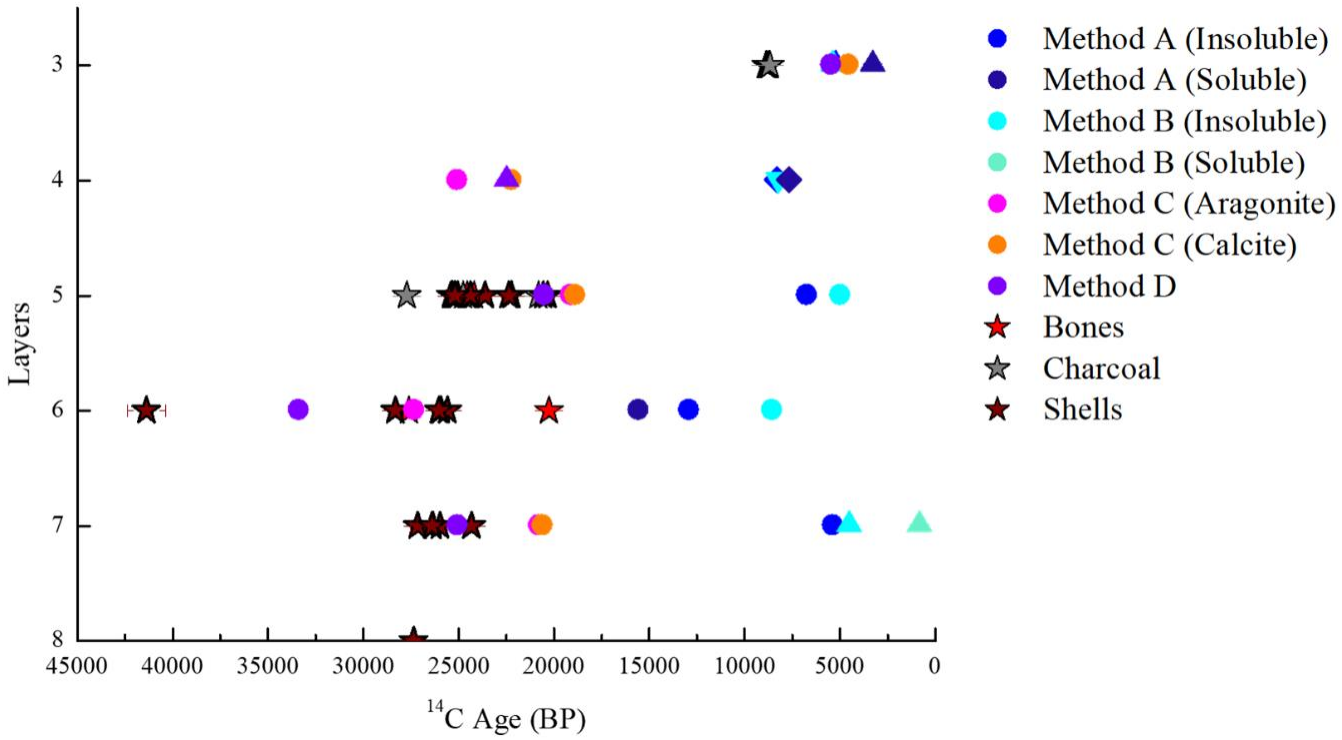

Figure 47: A graph showing the radiocarbon age (X axis) resulting from the four different methods applied on shells with different shapes indicating different shell samples used, and previous results from charcoal, bones, and shells (stars) from five different archeological layers (Y axis).

For Layers 5 and 7 the differences in age between aragonite and calcite, separated with Method C, were not substantial, which was expected since both fractions contained similar percentages of calcite and aragonite. Given the differences in age between the calcite and aragonite fractions in Layer 4, it is possible that there was some diagenetic alteration of the calcium carbonate. This could have occurred with potential incorporation of exogenous carbon into the sample and no change in the crystalline structure given the prevalence of one of the two polymorphs in all samples. Furthermore, intrashell variation in diagenetic effects was hypothesized in a previous study after the application of both XRD and Scanning electron microscopy which did not always show consistent results (Barton 2012). Additionally, some of the samples which were determined as well-preserved gave radiocarbon determinations which despite that were statistical outliers (Barton 2012). This confirms the hypothesis of diagenetic effects which cannot be detected merely by examining the carbonate polymorphs present in the sample. Therefore, it is necessary to perform multiple lines of analysis in order to confirm the preservation state of shell samples prior to radiocarbon dating.

The pyrolysis products we obtained for the insoluble organic matrix of the archeological samples pretreated with Method A and B are normally detected upon Py-GC-MS of diagenetically degraded natural organic matter (Brown et al. 2000). A similar suite of pyrolysis products was reported for the sedimentary matrix of samples of the Upper Paleolithic sequence of Abri Pataud that were attributed to charred organic matter mixed to other organic materials (Braadbaart et al. 2020).

The comparison of the pyrolytic patterns with those from modern samples evidenced changes indicative of degradative processes related to diagenesis. In fact, the set of compounds found in the pyrograms of the modern sample from *R.philippinarum* (BRA 5070) was dominated by pyrolysis products of proteins, (e.g. 4-methylphenol, benzylnitrile, indole) including the specific cyclic dipeptides (diketopiperazines) (Fabbri et al. 2012). Their absence in archaeological samples supported the degradation of proteins in the deposition environment. Nonetheless, the presence of proteinaceous matter remains was confirmed by the occurrence of nitrogen-containing pyrolysis products, as for instance pyrrole, pyridine and benzonitrile. Benzonitrile along with hydrocarbons were associated to recalcitrant organic matter that survived degradation (Ferro-Vázquez et al. 2019). Long chain alkylnitriles were indicative for the presence of fatty acids that reacted pyrolytically with proteinaceous materials (Nierop and van Bergen 2002). The presence of furaldehyde and the absence of anhydrosugars (levoglucosan) in the pyrolysates of archaeological samples, but the presence of levoglucosan in modern samples, suggested the occurrence of diagenetically altered carbohydrate precursors (Ferro-Vázquez et al. 2019).

It is worth noting that the samples obtained from method A (BRA 4930, BRA 4942, BRA 4957) generated Py-GC-MS traces featured by a suite of peaks tentatively identified as sulphur-containing compounds. In particular, carbon disulphide, alkyl tiophenes, benzotiophenes and a broad peak at the central part of the chromatogram attributed to S_8. The presence of tiophenes was typically encountered in the pyrograms of natural organic matter degraded under anoxic conditions (Çoban-Yıldız et al. 2006). The samples used in this study could have spent a significant amount of time in this type of conditions in marine sediments, given the fact that they were most likely collected from the beach. However, tiophenes could be formed as artefacts during pyrolysis by the reaction of elemental sulfur with fatty acids (Saiz-Jimenez 1995). Besides, the presence of sulfur compounds was also observed in the pyrogram of the modern samples and the sample BRA 4930 treated with method A suggesting differences in the pyrolytic pattern caused by sample treatment. This would support the hypothesis that the extraction protocol might have an effect on the obtained organic matrix.

It is important to note that the shell dates were not corrected for the marine reservoir effect, thus a direct comparison with bone dates from Layer 6, and among the different species will only be reliable once the correction of the marine reservoir effect is applied. Nonetheless, based on the ^{14}C ages all the results in Layer 6 are inconsistent and the differences are larger than the correction would be (Figure 47). Previous results from Layer 6 indicated two sets of human occupation around 3000 years apart from one another (Bicho et al. 2013), which could correspond to the dates we obtained. Furthermore, since the bone pretreatment method is well-established, proven to eliminate exogenous contaminant carbon from the sample (Talamo et al. 2021), these differences in Layer 6 might also be due to vertical movement and mixing within and between the layers which were also identified in previous work (Bicho et al. 2013). This could also explain why we obtained younger ages for Layer 5 compared to Layer 4, and those from Layer 7, compared to Layer 6. However, it does not explain the difference between the dates obtained for Layer 6 from the same shell (Figure 47). In previous work, heavy recrystallization was detected in some of the shell samples (Bicho et al. 2013). In this case, the carbonates resulting from Methods C and D come from different pieces of the same shell, so the differences might indicate more severe recrystallization in one fragment compared to the other. Even though our XRD results do not attest such differences in terms of aragonite to calcite transformations, there could have been some diagenetic alterations without a change in crystalline structure which were not detected. To improve the comparison of the two methods in the case of localized transformations, the shells could be grinded and thus homogenized before separating the pieces for pretreatment. Furthermore, analysis of the shell crystalline structure would help identify possible diagenetic alterations which did not result in change in the carbonate polymorph to improve the sample selection in cases where shells are used to construct site chronologies.

The ages obtained from Methods A and B were considerably younger than the expected ages for the archeological Layers 3 - 7 in the Terrace area of the Vale Boi site (Figure 47), as well as considering the lithic culture attributed for each layer (Figure 48). Given the consistency of the results obtained for both methods, the systematic error in dates is likely related to the process of organic matrix extraction irrespective of the specific methods used or possible contamination during pretreatment. Considering the ages of the samples pretreated with Methods A and B, in case it was modern contamination, half or more of each sample would have to be modern to obtain such results. Given the low weight yield of the organic matrix extracted and its low carbon content, even a small amount of modern contamination could have affected the results in such a way. Since the ages obtained from Methods C and D resulted in much older ages for all layers except Layer 3, it is possible that the contamination is specific to the organic matrix fractions and possibly species specific. In further research, the effect of the species used should be examined to determine if the organic matrix of different species from the same layers gives variable results, given the natural differences among species in terms of habitat, diet and even polymorph proportions. The overlap with the ages from the carbonate fractions in Layer 3 could also be explained by the smaller effect of modern contamination on younger samples (Talamo et al. 2021). Moreover, fungi and/or microorganisms have been found to introduce younger contamination into the organic fractions of a sample during storage and preparation (Wohlfarth 1998). Furthermore, another way to introduce younger contamination after shell deposition is the development of inorganic intracrystalline carbonate cement within a shell structure (Douka et al. 2010a; Webb et al. 2007). This fraction would be removed in Methods A and B, together with the rest of the carbonate fraction. Nonetheless, the formation of a secondary carbonate precipitate can occur in the presence of microorganisms which can leave carbonate, but also fatty acid signatures in the intracrystalline structure of the shells (Busschers et al. 2014), which would be maintained in the sample after pretreatment. Given the differences in age between the organic matrix and the carbonate fractions from our shells, microbially induced recrystallization could explain these results as it could have occurred with no change in the polymorphic state of the carbonates as seen in the XRD results for the samples used in this study. Even though the intracrystalline organic matrix has been shown to be a closed system (Penkman et al. 2008), what this entails in terms of radiocarbon analysis is yet to be understood. Since the carbonate fractions were unaffected, or significantly less affected by the contamination, this would mean that the organic matrix might be more susceptible to it.

All four methods gave ages inconsistent with the stratigraphical attribution of the samples and the expected age for the respective archeological layers given the associated lithic culture (Figure 48). Samples from Layer 6 gave the oldest ages for all four methods, and the samples from Layer 4 were consistently older than those from Layer 5, for all four methods. Most of the previous results on shells come from dates on *Patella* sp. which is a grazing species feeding on algae by scraping them off the rocky substrate (Santhanam 2018). This might cause age distortions by the introduction of older carbon from the limestone rocks present in the Vale Boi area (Bicho et al. 2013; Tátá et al. 2014). It is worth noting that the use of different mollusk species might cause large discrepancies in the results. On one hand due to the influence of variable diets, climatic and environmental conditions of each species which influences their initial biochemical composition, and on the other hand due to their different uses at the site. A previous study found differences among shell dates of up to 2000 years which they attributed mainly to heavy recrystallization, but also mentioned vertical sample movement as a potential issue (Bicho et al. 2013). This underlines the need of securing the stratigraphical attribution of the samples and further studying the potential disturbances and bioturbation in the stratigraphical units of the site. Furthermore, it is necessary to perform experiments using more samples to evaluate differences among the results when using different species from the same layer in a secure stratigraphical context.

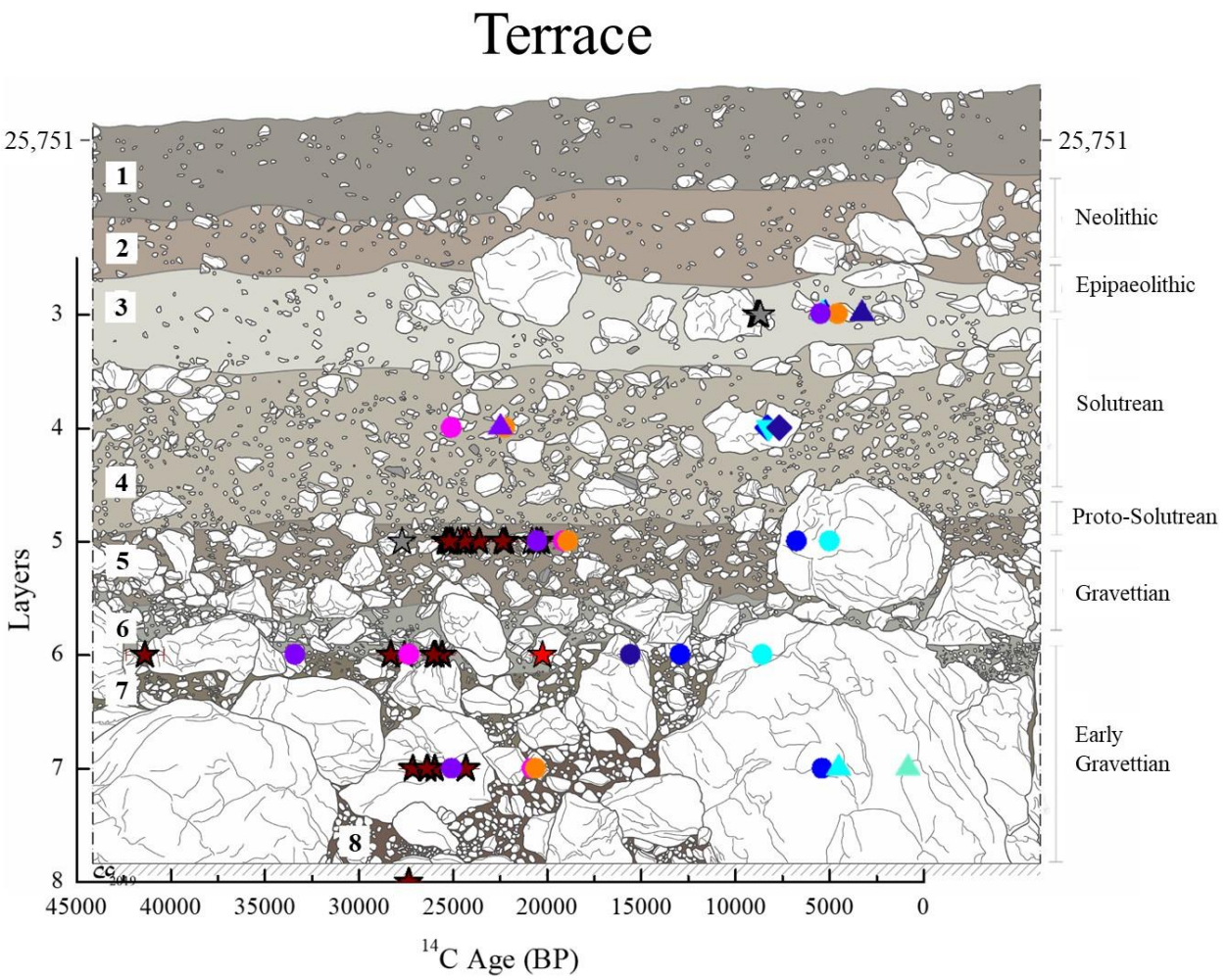

Figure 48: All previous dates and dates obtained in this study as shown in Figure 47 overlayed on the stratigraphic representation of the layers the samples were collected from and indicated on the right side the lithic culture associated to each layer.

2.6. CONCLUSIONS

The extraction of the organic matrix of the shells in theory could be a potentially useful method for radiocarbon dating, given that the intracrystalline organic matrix of the shell is protected from the surrounding environment in a closed system. However, after the application, the weight and carbon yields were very low for both method A and B, and the resulting ages were significantly younger than those resulting from carbonate fractions of the same shell specimens. This means that further research is needed to explore ways to perform the organic matter extraction without risk of contamination, such as was discovered here. Moreover, it is important to take into consideration the large amount of material needed to perform the organic matrix extraction (Method A and B) compared to the amount needed for the carbonate pretreatment (Method C and D). Method C is a useful method for aragonite and calcite separation in shells presenting both calcium carbonate polymorphs in significant amounts. However, in this study most of the samples consisted of one of the two polymorphs and the traces of the other polymorph were difficult to remove, therefore the method did not have enough of an effect to justify the effort of performing the pretreatment. Furthermore, there could be diagenetic effects that occur without aragonite to calcite transformations, which would not be detected by XRD nor removed by Method C. In fact, the pyrolysis results showed signs of degradation of the organic matter extracted using both Methods A and B. Method D is the quickest and simplest method performed, and it gave satisfactory results in terms of expected compared to obtained ages in most cases.

Overall, all the results were inconsistent both for shells and for the two bones analyzed in the Terrace area of Vale Boi in comparison with the previous results and with the archeological attribution. Given the complexities of the Vale Boi archeological site and the potential mixing in the stratigraphical sequence, it is likely that some of the inconsistencies in ages obtained from the different layers are due to factors not directly linked to dating shells. However, dates obtained from the same individuals using different methods showed significant differences, highlighting the importance of using efficient pretreatment protocols. The results of this study underline the difficulty of obtaining reliable radiocarbon dates on marine mollusk shells, and the need for additional method improvements for their pretreatment and contamination removal.

2.7. REFERENCES

Adamiano A, Goffredo S, Dubinsky Z, Levy O, Fermani S, Fabbri D, Falini G. 2014. Analytical pyrolysis-based study on intra-skeletal organic matrices from mediterranean corals. Analytical and Bioanalytical Chemistry. 406(24):6021-6033.

Alves EQ, Macario K, Ascough P, Christopher. 2018. The worldwide marine radiocarbon reservoir effect: Definitions, mechanisms, and prospects. Reviews of Geophysics. 56(1):278-305.

Barthelat F. 2010. Nacre from mollusk shells: A model for high-performance structural materials. Bioinspiration & Biomimetics. 5(3):035001.

Barton R. 2012. Gibraltar neanderthals in context. A report of the 1995-98 excavations at gorham's and vanguard caves, gibraltar.

Belfer-Cohen A, Goring-Morris N. 2012. Vi-the earlier upper palaeolithic: A view from the southern levant. L'Aurignacien de La Grotte Yafteh et Son Contexte (Fouilles 2005-2008)/The Aurignacian of Yafteh Cave and Its Context (2005-2008 Excavations) Liège.127-136.

Berger R, Horney AG, Libby WF. 1964. Radiocarbon dating of bone and shell from their organic components. Science. Vol. 144(No. 3621):pp. 999-1001.

Bicho N, Haws J. 2008. At the land's end: Marine resources and the importance of fluctuations in the coastline in the prehistoric hunter–gatherer economy of portugal. Quaternary Science Reviews. 27(23-24):2166-2175.

Bicho N, Manne T, Marreiros J, Cascalheira J, Pereira T, Tátá F, Évora M, Gonçalves C, Infantini L. 2013. The ecodynamics of the first modern humans in southwestern iberia: The case of vale boi, portugal. Quaternary International. 318:102-116.

Bosch MD, Mannino MA, Prendergast AL, O'Connell TC, Demarchi B, Taylor SM, Niven L, van der Plicht J, Hublin JJ. 2015. New chronology for ksar 'akil (lebanon) supports levantine route of modern human dispersal into europe. Proc Natl Acad Sci U S A. 112(25):7683-7688.

Braadbaart F, Reidsma FH, Roebroeks W, Chiotti L, Slon V, Meyer M, Théry-Parisot I, van Hoesel A, Nierop KGJ, Kaal J et al. 2020. Heating histories and taphonomy of ancient fireplaces: A multi-proxy case study from the upper palaeolithic sequence of abri pataud (les eyzies-de-tayac, france). Journal of Archaeological Science: Reports. 33:102468.

Brock F, Higham T, Ditchfield P, Ramsey CB. 2010. Current pretreatment methods for ams radiocarbon dating at the oxford radiocarbon accelerator unit (orau). Radiocarbon. 52(1):103-112.

Brown SD, Chiavari G, Ediger V, Fabbri D, Gaines AF, Galletti G, Karayigit AI, Love GD, Snape CE, Sirkecioglu O et al. 2000. Black sea sapropels: Relationship to kerogens and fossil fuel precursors. Fuel. 79(14):1725-1742.

Brumm A, Hakim B, Ramli M, Aubert M, van den Bergh GD, Li B, Burhan B, Saiful AM, Siagian L, Sardi R et al. 2018. A reassessment of the early archaeological record at leang burung 2, a late pleistocene rock-shelter site on the indonesian island of sulawesi. PLoS One. 13(4):e0193025.

Busschers F, Wesselingh F, Kars R, Versluijs-Helder M, Wallinga J, Bosch J, Timmner J, Nierop K, Meijer T, Bunnik F. 2014. Radiocarbon dating of late pleistocene marine shells from the southern north sea. Radiocarbon. 56(3):1151-1166.

Cascalheira J, Bicho N, Marreiros J, Pereira T, Évora M, Cortés M, Gibaja Bao JF, Manne T, Regala F, Gonçalves C. 2012. Vale boi (algarve, portugal) and the solutrean in southwestern iberia= vale boi (algarve, portugal) y el solutrense en el suroeste de la península ibérica.

Chappell J, Polach HA. 1972. Some effects of partial recrystallisation on 14c dating late pleistocene corals and molluscs. Quaternary Research. 2(2):244-252.

Çoban-Yıldız Y, Fabbri D, Baravelli V, Vassura I, Yılmaz A, Tuğrul S, Eker-Develi E. 2006. Analytical pyrolysis of suspended particulate organic matter from the black sea water column. Deep Sea Research Part II: Topical Studies in Oceanography. 53(17):1856-1874.

Dee MW, Palstra SWL, Aerts-Bijma AT, Bleeker MO, de Bruijn S, Ghebru F, Jansen HG, Kuitems M, Paul D, Richie RR et al. 2019. Radiocarbon dating at groningen: New and updated chemical pretreatment procedures. Radiocarbon. 62(1):63-74.

Diez-Quijada L, De Oliveira FL, Jos Á, Cameán AM, Aparicio-Ruiz R, Vasconcelos V, Campos A, González-Vila FJ, González-Pérez JA. 2020. Alterations in mediterranean mussel (mytilus galloprovincialis) composition exposed to cyanotoxins as revealed by analytical pyrolysis. Journal of Analytical and Applied Pyrolysis. 152:104970.

Döbelin N, Kleeberg R. 2015. "Profex: A graphical user interface for the rietveld refinement program bgmn" Journal of Applied Crystallography. p. 1573-1580.

Douka K. 2011. An upper palaeolithic shell scraper from ksar akil (lebanon). Journal of Archaeological Science. 38(2):429-437.

Douka K, Bergman CA, Hedges RE, Wesselingh FP, Higham TF. 2013. Chronology of ksar akil (lebanon) and implications for the colonization of europe by anatomically modern humans. PLoS One. 8(9):e72931.

Douka K, Hedges RE, Higham TFJR. 2010a. Improved ams 14 c dating of shell carbonates using high-precision x-ray diffraction and a novel density separation protocol (cards). 52(2):735-751.

Douka K, Higham TF, Hedges RE. 2010b. Radiocarbon dating of shell carbonates: Old problems and new solutions. Munibe. 31:18-27.

Elliot M, Welsh K, Chilcott C, McCulloch M, Chappell J, Ayling B. 2009. Profiles of trace elements and stable isotopes derived from giant long-lived tridacna gigas bivalves: Potential applications in paleoclimate studies. Palaeogeography, Palaeoclimatology, Palaeoecology. 280(1):132-142.

Fabbri D, Adamiano A, Falini G, De Marco R, Mancini I. 2012. Analytical pyrolysis of dipeptides containing proline and amino acids with polar side chains. Novel 2, 5-diketopiperazine markers in the pyrolysates of proteins. Journal of analytical and applied pyrolysis. 95:145-155.

Faivre S, Bakran-Petricioli T, Barešić J, Horvatinčić N. 2015. New data on marine radiocarbon reservoir effect in the eastern adriatic based on pre-bomb marine organisms from the intertidal zone and shallow sea. Radiocarbon. 57(4):527-538.

Falini G, Reggi M, Fermani S, Sparla F, Goffredo S, Dubinsky Z, Levi O, Dauphin Y, Cuif J-P. 2013. Control of aragonite deposition in colonial corals by intra-skeletal macromolecules. Journal of Structural Biology. 183(2):226-238.

Ferro-Vázquez C, Kaal J, Arévalo FJS, Boado FC. 2019. Molecular fingerprinting of 14c dated soil organic matter fractions from archaeological settings in nw spain. Radiocarbon. 61(1):101-130.

Gillespie R, Hedges RE, Humm M. 1986. Routine ams dating of bone and shell proteins. Radiocarbon. 28(2A):451-456.

Guzmán N, Dauphin Y, Cuif JP, Denis A, Ortlieb L. 2009. Diagenetic changes in concholepas concholepas shells (gastropoda, muricidae) in the hyper-arid conditions of northern chile – implications for palaeoenvironmental reconstructions. Biogeosciences. 6(2):197-207.

Hadden CS, Loftis KM, Cherkinsky A. 2018. Carbon isotopes (δ13c and δ14c) in shell carbonate, conchiolin, and soft tissues in eastern oyster (crassostrea virginica). Radiocarbon. 60(4):1125-1137.

Hadden CS, Loftis KM, Cherkinsky A, Ritchison BT, Lulewicz IH, Thompson VD. 2019. Radiocarbon in marsh periwinkle (littorina irrorata) conchiolin: Applications for archaeology. Radiocarbon. 61(5):1489-1500.

Hublin J-J. 2012. The earliest modern human colonization of europe. Proceedings of the National Academy of Sciences. 109(34):13471-13472.

Jones DS, Allmon WD. 1995. Records of upwelling, seasonality and growth in stable-isotope profiles of pliocene mollusk shells from florida. Lethaia. 28(1):61-74.

Lindauer S. 2019. Radiocarbon reservoir effects on shells from se arabia in the context of paleoenvironmental studies. PhD thesis - Technical University Darmstadt.

Manne T. 2014. Early upper paleolithic bone processing and insights into small-scale storage of fats at vale boi, southern iberia. Journal of Archaeological Science. 43:111-123.

Manne T, Cascalheira J, Évora M, Marreiros J, Bicho N. 2012. Intensive subsistence practices at vale boi, an upper paleolithic site in southwestern portugal. Quaternary International. 264:83-99.

Marin F, Le Roy N, Marie B. 2012. The formation and mineralization of mollusk shell. Front Biosci. 4(1099):125.

Marreiros J, Bicho N, Gibaja J, Pereira T, Cascalheira J. 2015. Lithic technology from the gravettian of vale boi: New insights into early upper paleolithic human behavior in southern iberian peninsula. Quaternary International. 359-360:479-498.

Milano S, Nehrke G. 2018. Microstructures in relation to temperature-induced aragonite-to-calcite transformation in the marine gastropod phorcus turbinatus. PLoS One. 13(10):e0204577.

Milano S, Schöne BR, González-Morales MR, Gutiérrez-Zugasti I. 2022. Temporal and spatial variability of prehistoric aquatic resource procurement: A case study from mesolithic northern iberia. Scientific Reports. 12(1).

Milano S, Schöne BR, Gutiérrez-Zugasti I. 2020. Oxygen and carbon stable isotopes of mytilus galloprovincialis lamarck, 1819 shells as environmental and provenance proxies. The Holocene. 30(1):65-76.

Nierop KGJ, van Bergen PF. 2002. Clay and ammonium catalyzed reactions of alkanols, alkanoic acids and esters under flash pyrolytic conditions. Journal of Analytical and Applied Pyrolysis. 63(1):197-208.

Ono R, Soegondho S, Yoneda M. 2009. Changing marine exploitation during late pleistocene in northern wallacea: Shell remains from leang sarru rockshelter in talaud islands. Asian Perspectives. 48(2):318-341.

Penkman KEH, Kaufman DS, Maddy D, Collins MJ. 2008. Closed-system behaviour of the intra-crystalline fraction of amino acids in mollusc shells. Quaternary Geochronology. 3(1-2):2-25.

Pereira T, Bicho N, Cascalheira J, Infantini L, Marreiros J, Paixão E, Terradas X. 2016. Territory and abiotic resources between 33 and 15.6 ka at vale boi (sw portugal). Quaternary International. 412:124-134.

Perrin C. 2004. Early diagenesis of carbonate biocrystals : Isomineralogical changes in aragonite coral skeletons. Bulletin de la Société Géologique de France. 175(2):95-106.

Philippsen B. 2013. The freshwater reservoir effect in radiocarbon dating. Heritage Science. 1(1):24.

Pigati JS. 2002. On correcting 14c ages of gastropod shell carbonate for fractionation. Radiocarbon. 44(3):755-760.

Ramos-Muñoz J, Cantillo-Duarte JJ, Bernal-Casasola D, Barrena-Tocino A, Domínguez-Bella S, Vijande-Vila E, Clemente-Conte I, Gutiérrez-Zugasti I, Soriguer-Escofet M, Almisas-Cruz S. 2016. Early use of marine resources by middle/upper pleistocene human societies: The case of benzú rockshelter (northern africa). Quaternary International. 407:6-15.

Reggi M, Fermani S, Landi V, Sparla F, Caroselli E, Gizzi F, Dubinsky Z, Levy O, Cuif J-P, Dauphin Y et al. 2014. Biomineralization in mediterranean corals: The role of the intraskeletal organic matrix. Crystal Growth & Design. 14(9):4310-4320.

Reimer PJ, Reimer RW. 2001. A marine reservoir correction database and on-line interface. Radiocarbon. 43(2A):461-463.

Reimer RW, Reimer PJ. 2017. An online application for δr calculation. Radiocarbon. 59(5):1623-1627.

Russell N, Cook GT, Ascough P, Barrett JH, Dugmore A. 2011. Species specific marine radiocarbon reservoir effect: A comparison of δr values between patella vulgata (limpet) shell carbonate and gadus morhua (atlantic cod) bone collagen. Journal of Archaeological Science. 38(5):1008-1015.

Russo CM, Tripp JA, Douka K, Higham TFJR. 2010. A new radiocarbon pretreatment method for molluscan shell using density fractionation of carbonates in bromoform. 52(3):1301-1311.

Sadler J, Carré M, Azzoug M, Schauer AJ, Ledesma J, Cardenas F, Chase BM, Bentaleb I, Muller SD, Mandeng M et al. 2012. Reconstructing past upwelling intensity and the seasonal dynamics of primary productivity along the peruvian coastline from mollusk shell stable isotopes. Geochemistry, Geophysics, Geosystems. 13(1):n/a-n/a.

Saiz-Jimenez C. 1995. The origin of alkylbenzenes and thiophenes in pyrolysates of geochemical samples. Organic Geochemistry. 23(1):81-85.

Santhanam R. 2018. Biology and ecology of edible marine gastropod molluscs. CRC Press.

Santos GM, Southon JR, Druffel-Rodriguez KC, Griffin S, Mazon M. 2004. Magnesium perchlorate as an alternative water trap in ams graphite sample preparation: A report on sample preparation at kccams at the university of california, irvine. Radiocarbon. 46(1):165-173.

Schöne BR. 2008. The curse of physiology—challenges and opportunities in the interpretation of geochemical data from mollusk shells. Geo-Marine Letters. 28(5-6):269-285.

Schöne BR, Freyre Castro AD, Fiebig J, Houk SD, Oschmann W, Kröncke I. 2004. Sea surface water temperatures over the period 1884–1983 reconstructed from oxygen isotope ratios of a bivalve mollusk shell (arctica islandica, southern north sea). Palaeogeography, Palaeoclimatology, Palaeoecology. 212(3):215-232.

Talamo S, Fewlass H, Maria R, Jaouen K. 2021. “Here we go again”: The inspection of collagen extraction protocols for 14c dating and palaeodietary analysis. STAR: Science & Technology of Archaeological Research. 7(1):62-77.

Talamo S, Richards M. 2011. A comparison of bone pretreatment methods for ams dating of samples >30,000 bp. Radiocarbon. 53(3):443-449.

Tassoni L, Kromer B, Friedrich R, Wacker L, Cattani M, Friedrich M, Paleček D, Pelloni E, Peng K, Thomas E M, Talamo S. (2023, in press) "Safe preparation and delivery of graphite targets for 14C analysis: Procedures of BRAVHO lab at Bologna University". Radiocarbon. 24th Radiocarbon Conference and 10th 14C & Archaeology Conference. Conference Proceeding.

Tátá F, Cascalheira J, Marreiros J, Pereira T, Bicho N. 2014. Shell bead production in the upper paleolithic of vale boi (sw portugal): An experimental perspective. Journal of Archaeological Science. 42:29-41.

Toffolo MB. 2021. The significance of aragonite in the interpretation of the microscopic archaeological record. Geoarchaeology. 36(1):149-169.

Vita-Finzi C, Roberts N. 1984. Selective leaching of shells for 14c dating. Radiocarbon. 26(1):54-58.

Webb GE, Price GJ, Nothdurft LD, Deer L, Rintoul L. 2007. Cryptic meteoric diagenesis in freshwater bivalves: Implications for radiocarbon dating. Geology. 35(9).

Will M, Kandel AW, Conard NJ. 2019. Midden or molehill: The role of coastal adaptations in human evolution and dispersal. Journal of World Prehistory. 32(1):33-72.

Wohlfarth B, Skog, G., Possnert, G., Holmquist, B. 1998. Pitfalls in the ams radiocarbon-dating of terrestrial macrofossils. Journal of Quaternary Science. (13):137–145.

Zilhão J, Angelucci DE, Badal-García E, D'Errico F, Daniel F, Dayet L, Douka K, Higham TFG, Martínez-Sánchez MJ, Montes-Bernárdez R et al. 2010. Symbolic use of marine shells and mineral pigments by iberian neandertals. Proceedings of the National Academy of Sciences. 107(3):1023-1028.

CHAPTER 3 – STABLE ISOTOPES IN THE SHELL ORGANIC MATRIX

3.1. STATE OF THE ART AND PROBLEM STATEMENT

Apart from being a potentially useful material for radiocarbon dating, mollusk shells are often used in paleoenvironmental studies, due to their abundance in the archaeological and paleontological records. The great preservation potential of the calcium carbonate crystalline structure and the frequent and diversified use of shellfish by human populations, throughout the evolutionary history of ours and other human species, contributed to the preservation of these materials in large amount (Bar-Yosef Mayer et al. 2009; Bicho and Haws 2008; Bicho et al. 2010; Cortés-Sánchez et al. 2011; Douka 2011; Douka and Spinapolice 2012; Fa et al. 2016; Joordens et al. 2015; Marean et al. 2007; Peresani et al. 2013; Ramos-Muñoz et al. 2016; Tátá et al. 2014; Wei et al. 2016; Zilhão et al. 2010). Given the difficulty of obtaining reliable radiocarbon dates on shells, as seen in the previous chapter of this thesis, it is important to also develop other approaches in order to obtain information from this material. This chapter will explore the use of mollusk shells for (paleo) environmental reconstruction.

During their lifetime, mollusks incorporate environmental information in the form of shell chemical and physical properties. For instance, the seasonal and sub-seasonal shell growth increments are used to reconstruct changes in environmental conditions with a high temporal and geographical resolution (sclerochronology), similarly to the analysis of annual growth rings in trees (dendrochronology; Andrus 2011; Gillikin et al. 2019; Leng and Lewis 2016; Peharda et al. 2021; Schöne and Fiebig 2009; Yan et al. 2020). In archaeological studies, sclerochronology can help study past environmental changes in connection with human activities and evolution (Andrus 2011). For example, the study of shells from archeological middens allows the determination of the season of collection by past human populations. Therefore, their dietary and foraging habits, site formation and occupation patterns or ritual behavior can be assessed (Andrus 2011; Mannino et al. 2003; Milano et al. 2022).

There are numerous well-known proxies that are used in sclerochronological studies to reconstruct different environmental and biological parameters, which usually consist of stable isotope measurements of different elements (Peharda et al. 2021). Among the different stable isotope ratios, one of the most used and studied is the oxygen $\delta^{18}O$, as an established water (paleo) thermometer (Lécuyer et al. 2004; Leng and Lewis 2016; Mannino et al. 2003; Mannino et al. 2008; Schöne et al. 2003; Schöne et al. 2004; Trofimova et al. 2018). The research so far has been almost exclusively focused on the carbonate fraction of shells (Peharda et al. 2021). However, shells, being biogenic structures, are also composed of a small portion of organic matter

(< 5 wt%) (Kobayashi and Samata 2006; LeBlanc 1989; Marin et al. 2012; Marin et al. 2007; Marin et al. 2013; Suzuki and Nagasawa 2013; Weiner 1979; 1984; Weiner and Hood 1975; Weiner and Traub 1980; Weiner et al. 1983; Wheeler et al. 1988; Wheeler and Sikes 1984). The few available studies on stable isotopes focusing on the organic fraction use $\delta^{13}C$ and $\delta^{15}N$ as proxies for eutrophication and food web reconstruction (Ellis et al. 2014; Misarti et al. 2017; O'Donnell et al. 2007; Whitney et al. 2019). So far, there is only one available study focusing on the potential use of the organic matrix stable isotope ratios for paleoenvironmental studies (Carroll et al. 2006). The advantage of using the organic matrix of the shell is the possibility to measure the hydrogen isotope composition ($\delta^{2}H$), together with the $\delta^{18}O$, which may be influenced by the water chemical composition at the time of shell deposition.

Due to the strong relationship between $\delta^{2}H$ and $\delta^{18}O$ found in meteoric waters (Craig 1961), hydrogen isotopes could offer an additional proxy for the interpretation of paleoenvironments. A global empirical linear relationship for precipitation $\delta^{2}H$ and $\delta^{18}O$ values was established - the GMWL, with a slope of 8 and an intercept of 10 (Craig 1961). The relative fractionations of hydrogen and oxygen isotopes between water vapor and liquid water are partially reflected in the slope and intercept values. Based on the local conditions these values can vary, with the fractionation changing in relative humidity values under 100%, and at different temperatures, creating Local Meteoric Water Lines (Hatvani et al. 2023; Lécuyer et al. 2021; Odezulu 2011; Xiang et al. 2022). The $\delta^{18}O$ of precipitation in places with low slope values had positive correlations to monthly mean air temperatures, and negative correlations to monthly mean precipitations (Lécuyer et al. 2021). Therefore, measuring both $\delta^{2}H$ and $\delta^{18}O$ of the shells and examining their relationship could be useful for paleoenvironmental reconstructions. However, the carbonate mineral phase does not contain hydrogen, thus the shell organic matrix can be used instead. Measurements of $\delta^{2}H$ in the organic matrix of freshwater species in relation to $\delta^{18}O$ of the shell showed promising results for future environmental reconstructions (Carroll et al. 2006). It was shown that the isotopic compositions of the organic matrix reflected the values of the water in which the shells lived. However, the authors did not discriminate between the soluble and the insoluble organic matrix fractions, which were identified and differentiated already in the early studies of the organic matrix composition of mollusk shells (Grégoire 1972; LeBlanc 1989; Lowenstam and Weiner 1989; Weiner 1984; Weiner and Hood 1975; Weiner and Traub 1980; Wheeler et al. 1988; Wheeler and Sikes 1984). Here, we report the results of hydrogen and oxygen stable isotope measurements performed on both the soluble and insoluble organic matrix of modern specimens of *Mytilus galloprovincialis* shells. This species has a wide geographical distribution (Comesaña et al. 1998; Hockey and van Erkom Schurink 1992; Sanjuan et al. 1994; Wonham 2004) and was validated as a reliable species for the estimation of seasonal temperature fluctuations, as well as a potential provenance proxy using the correlation between carbon and oxygen stable isotopes (Milano et al. 2022; Milano et al. 2020). The specimens for this study were collected in three sites along a coast to upper-estuary

gradient in Northern Spain, to evaluate if δ^2H and $\delta^{18}O$ show variation along this gradient. We compare the results among the three sites and with previous $\delta^{18}O$ measurements on carbonates from *M. galloprovincialis* specimens, as well as to water isotope values collected in the same sites (Milano et al. 2020).

3.2. MATERIALS AND METHODS

3.2.1. SHELL COLLECTION AND PREPARATION

A total of 19 *M. galloprovincialis* shells used in this study were collected from three sites in Cantabria, Northern Spain (Fig. 49). Out of these, nine samples were collected from Berria Beach (43°27′54.5″N, 3°27′8.5″W), five from a lower estuarine site near Montehano (43°25′36.4″N, 3°29′27.2″W) and five from an upper estuarine site near Carasa (43°22′22.8″N, 3°28′14″W). After collection the soft tissues were removed immediately, and the shells were air-dried and stored in plastic bags for further analyses. The insoluble and soluble fractions of the organic matrix were extracted in the Bologna Radiocarbon Laboratory devoted to Human Evolution (BRAVHO lab) using the method routinely used on modern shells and coral samples in studies focusing on the organic matrix (Method A; Falini et al. 2013; Reggi et al. 2014). The shell samples were first cleaned with a mechanical drill to remove any sediment that might have been adhered to the shell surface, after which they were further cleaned of impurities by leaving them in a 5% sodium hypochlorite solution overnight. After these cleaning steps, the shells were rinsed in deionized water several times to wash off the sodium hypochlorite and any loose debris and left to air-dry. Samples from Montehano and Carasa were big enough to cut into several subsamples close to 2g, while the samples from Berria were left whole due to size of the shells themselves. The cutting was performed along the growth lines of the shells aiming to obtain information on changes in the isotope composition during shell growth (Figure 49). All samples were hand-crushed to powder in an agate mortar and further crushed in an automatic mill to obtain a finer powder. The obtained powder was sieved with a 150 µm mesh stainless steel sieve and put into labelled glass tubes. The powdered samples were once again left in 5% sodium hypochlorite solution overnight for a thorough removal of exogenous organic material, rinsed three times with deionized water and dried out in the oven for two days at 60°C. The powder was then transferred into regenerated cellulose membranes for dialysis (MWCO = 3.5 kDa) with 5ml of deionized water. The sealed membranes were then put into 1 L of 0.1 M CH_3COOH solution under stirring. The solution was changed every five days until the samples were decalcified, subsequently it was replaced by deionized water to reach a pH value of around 6. The obtained dispersion containing organic matter was centrifuged at 3500 rpm (2301 x g) for 5 min to separate the soluble (liquid) and insoluble (solid) fractions. Both fractions were then lyophilized and weighed before further analysis.

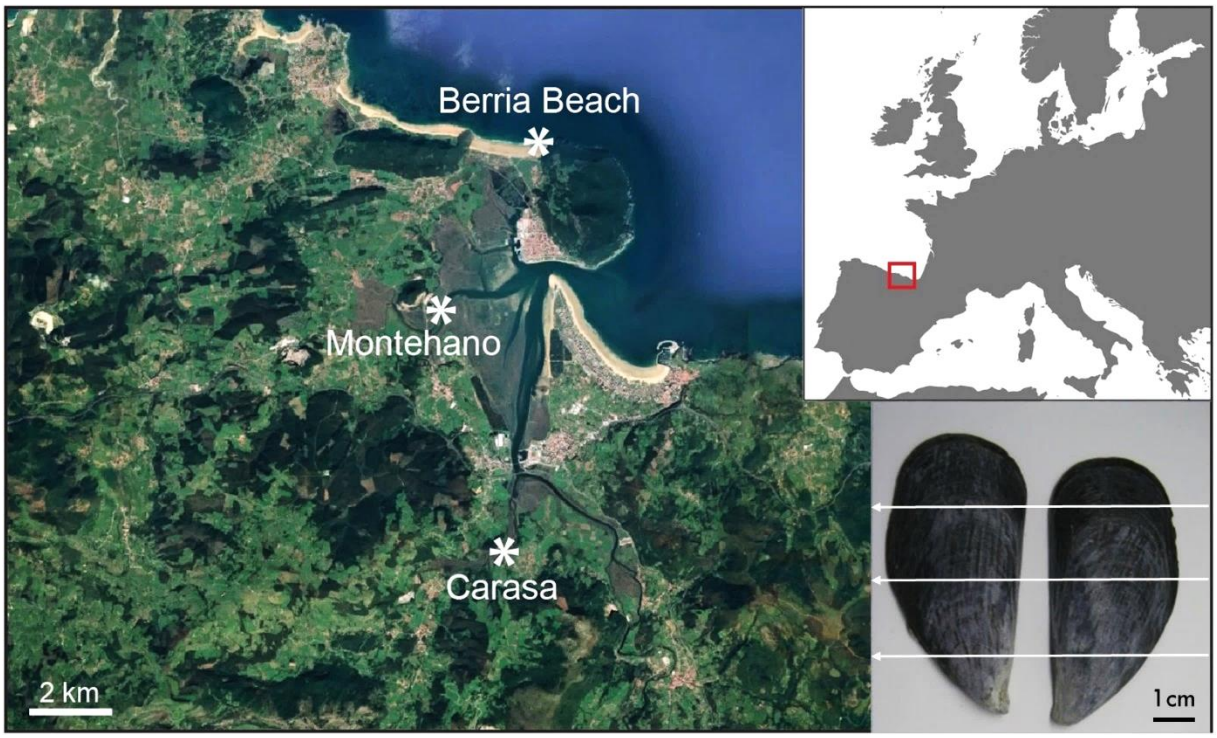

Figure 49. Map of the three localities analyzed in this study: Berria Beach (marine habitat), Montehano (lower estuarine habitat) and Carasa (upper estuarine habitat). In the bottom right an image of a sample from Carasa, with white arrows indicating approximate lines along which the samples were cut, dividing them into 2 to 7 subsamples based on the sample size. Figure modified after Milano et al. (2020).

3.2.2. STABLE ISOTOPE ANALYSIS

Measurements of stable isotope ratios were performed at the Leibniz Institute for Zoo and Wildlife Research (Leibniz IZW) in Berlin. Aliquots of 0.35 ± 0.10 mg from each sample were placed into silver capsules (IVA Analysetechnike.K. Meerbusch, Germany) and then analyzed using a Delta V-Advantage mass spectrometer (Thermo Fisher Scientific, Bremen, Germany) connected via an interface (Conflo IV, Thermo Fisher Scientific, Bremen, Germany) to a High Temperature Conversion Elemental Analyser (TC/EA Thermo Finnigan) and an online temperature-controlled vacuum-equilibration autosampler Uni-Prep (EuroVector; Figure 50). Samples and reference materials were loaded into the autosampler at 60°C. Measurements were performed using the comparative equilibration method to calculate the isotope ratio of the non-exchangeable portion of hydrogen (Wassenaar et al. 2015). After flushing with helium and evacuating the carousel, 20 µl of water of known isotopic composition was injected trough the Uni-Prep septum for equilibration (1 h). The samples were measured together with three in-house keratin standards: sheep wool from Sweden SWE- SHE [$\delta^2H = -111.65$ ‰, $\delta^{18}O = 10.84$ ‰], sheep wool from Spain ESP-SHE [$\delta^2H = -61.54$ ‰, $\delta^{18}O = 16.94$ ‰] and goat wool from Tanzania AFR- GOA [$\delta^2H = -26.44$ ‰, $\delta^{18}O = 22.29$ ‰]. Stable isotope ratios (δ^2H and $\delta^{18}O$) were expressed as deviations from the international reference material Vienna Standard Mean Ocean Water (V-SMOW). Measurement precision was always better than 1 ‰ for δ^2H and $\delta^{18}O$ (1 SD).

3.2.3. DATA ANALYSIS

All statistical data analysis was performed using the PAST 4.12 (PAleontological STatistics) software package (Hammer et al. 2001). For all data, outlier and normality tests were performed prior to further data analysis. To detect differences among the different localities, ANOVA and Kruskal-Wallis tests were used, along with appropriate post-hoc tests when necessary (Tukey's and Mann-Whitney's). Pearson's correlation indices and significances for each of them were determined to demonstrate the presence or absence of correlation between variables.

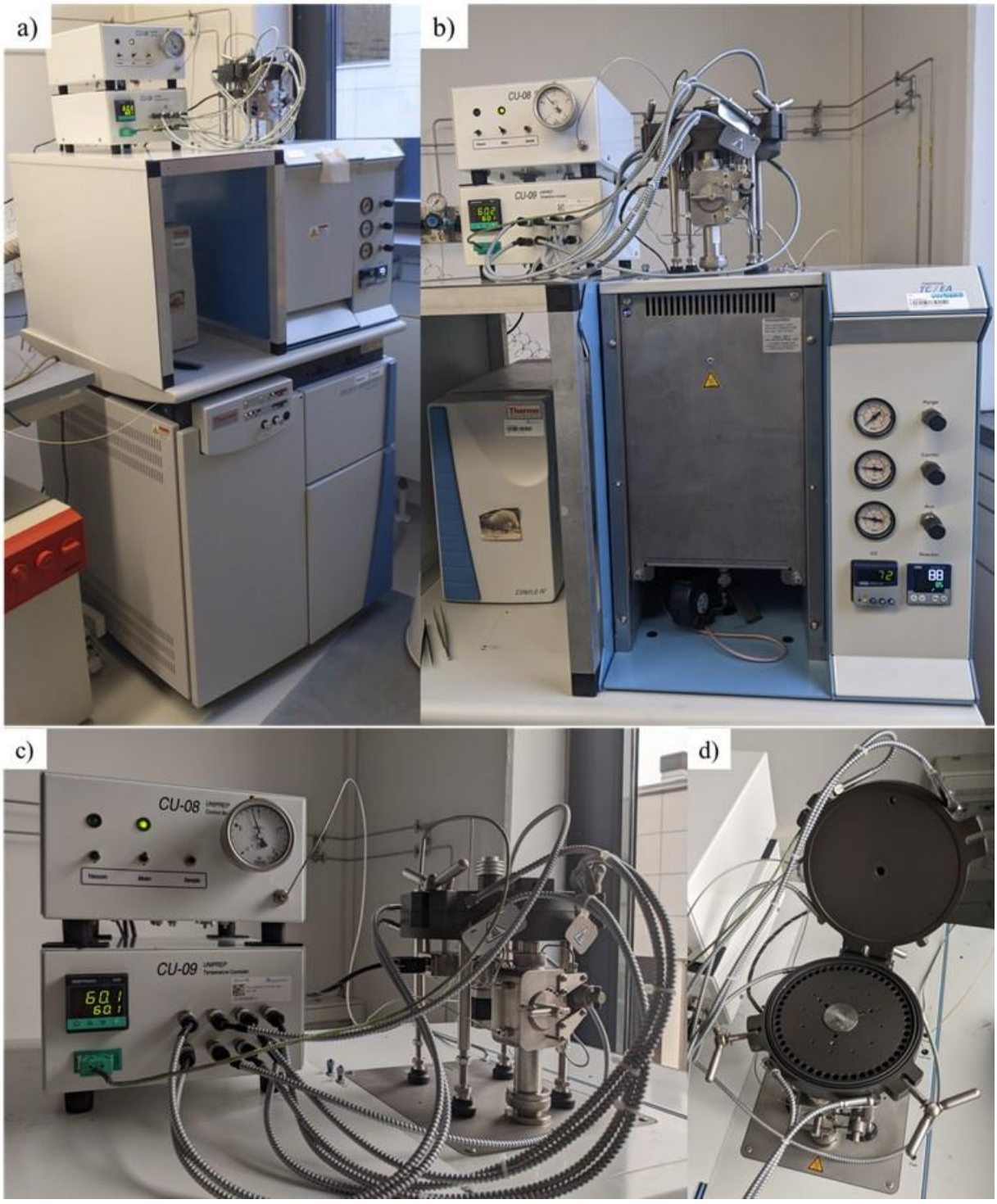

Figure 50. The equipment used for the stable isotope measurements (a) the entire setup of equipment; (b) a closer view of the TC/EA and (c) the Uni-Prep autosampler with (d) the sample slots.

3.3. RESULTS

3.3.1. STABLE ISOTOPE ANALYSIS IN THE SHELL ORGANIC MATRIX

The oxygen and hydrogen stable isotope measurements for the soluble and insoluble fractions of the organic matrix (SOM and IOM, respectively) from all three sites are shown in Table 11. After the identification of one outlier in the IOM and two outliers in the SOM from Carasa and one outlier in the SOM from Berria (italic bold in Table 11), those datapoints were excluded from further data analyses.

SOM - For the SOM, the ranges of δ^2H values are significantly different among the three sites ($p < 0.0001$ Kruskal-Wallis, Figure 51). On the other hand, the $\delta^{18}O$ values of the samples from Berria are significantly different from those from Carasa ($p < 0.05$ ANOVA, Figure 51) while samples from both Berria and Carasa show similar ranges to samples from Montehano ($p > 0.05$ ANOVA, Figure 51). $\delta^{18}O$ and δ^2H values in the SOM show a negligible (Berria) to moderate (Montehano) negative linear relationship (Pearson's R from -0.17 to - 0.5, Figure 52). While for Carasa the $\delta^{18}O$ and δ^2H showed a weak positive correlation (Pearson's R 0.33, Figure 52). However, the correlations were not statistically significant ($p > 0.05$).

Table 11: $\delta^{18}O$ (‰) and $\delta^{2}H$ (‰) values for the SOM and IOM. Missing values were labeled as n/a for samples with insufficient material for the analysis.

	Soluble fraction (SOM)			Insoluble fraction (IOM)		
Site	ID	$\delta^{2}H$	$\delta^{18}O$	ID	$\delta^{2}H$	$\delta^{18}O$
Berria	6005.1.2	-112.7	11.0	6005.1.1	-56.2	22.3
Berria	6006.1.2	-118.0	n/a	6006.1.1	-61.5	17.3
Berria	6007.1.2	-113.2	n/a	6007.1.1	-54.8	20.0
Berria	6008.1.2	-125.2	16.8	6008.1.1	-57.3	22.6
Berria	***6003.1.2***	***-53.8***	***n/a***	6003.1.1	-55.8	20.7
Berria	6004.1.2	-136.7	34.2	6004.1.1	-55.0	22.3
Berria	6009.1.2	-109.9	25.0	6009.1.1	-54.7	21.4
Berria	6010.1.2	-105.3	31.7	6010.1.1	-59.0	22.2
Berria	6011.1.2	-116.5	31.2	6011.1.1	-57.0	23.8
Montehano	5993.1.2	-91.3	29.6	5993.1.1	-55.9	23.6
Montehano	5993.2.2	-54.7	16.7	5993.2.1	-53.5	24.0
Montehano	5993.3.2	-98.6	27.1	5993.3.1	-57.3	22.1
Montehano	5995.1.2	-82.4	23.6	5995.1.1	-58.8	21.7
Montehano	5995.2.2	-81.8	9.3	5995.2.1	-61.6	19.1
Montehano	5995.3.2	-88.5	13.9	5995.3.1	-50.1	19.8
Montehano	5995.4.2	-66.7	14.5	5995.4.1	-55.8	19.3
Montehano	5996.1.2	-62.2	17.2	5996.1.1	-66.4	21.3
Montehano	5996.2.2	-57.7	21.6	5996.2.1	-58.9	23.6
Montehano	5994.1.2	-83.4	29.0	5994.1.1	-61.3	20.8
Montehano	5994.2.2	n/a	n/a	5994.2.1	-49.4	21.0
Montehano	5994.3.2	-67.3	21.3	5994.3.1	-46.3	22.8
Montehano	5997.1.2	-58.5	17.0	5997.1.1	-68.4	20.6
Montehano	5997.2.2	-44.2	12.2	5997.2.1	-55.0	22.9
Carasa	6001.1.2	-56.6	18.3	6001.1.1	-57.8	21.9
Carasa	6001.2.2	-52.2	15.1	6001.2.1	-51.6	22.0
Carasa	6001.3.2	-48.4	19.6	6001.3.1	-53.7	20.3
Carasa	6001.4.2	-44.9	12.2	6001.4.1	-49.3	21.8
Carasa	6001.5.2	-47.1	17.8	6001.5.1	-52.8	20.5
Carasa	6001.6.2	-46.5	17.3	6001.6.1	-46.2	21.5
Carasa	6001.7.2	-35.9	32.0	6001.7.1	-44.4	21.5
Carasa	***5998.1.2***	***-104.2***	***30.6***	5998.1.1	-59.0	21.2
Carasa	5998.2.2	-52.5	20.8	5998.2.1	-54.2	20.1
Carasa	5998.3.2	-44.9	21.6	5998.3.1	-57.5	22.3
Carasa	***5999.1.2***	***-102.7***	***30.3***	***5999.1.1***	***-73.1***	***15.2***
Carasa	5999.2.2	-58.5	20.7	5999.2.1	-57.2	22.4
Carasa	5999.3.2	-52.4	23.8	5999.3.1	-56.9	21.3
Carasa	6000.1.2	-55.6	-2.3	6000.1.1	-59.6	20.7
Carasa	6000.2.2	n/a	n/a	6000.2.1	-54.1	20.5
Carasa	6000.3.2	n/a	n/a	6000.3.1	-57.7	18.8
Carasa	6000.4.2	-46.3	2.4	6000.4.1	-49.7	20.6
Carasa	6002.1.2	-58.8	12.2	6002.1.1	-63.7	19.7
Carasa	6002.2.2	-60.1	15.9	6002.2.1	-61.8	18.0
Carasa	6002.3.2	-53.9	9.9	6002.3.1	-55.6	21.1
Carasa	6002.4.2	-50.6	7.3	6002.4.1	-56.1	21.2

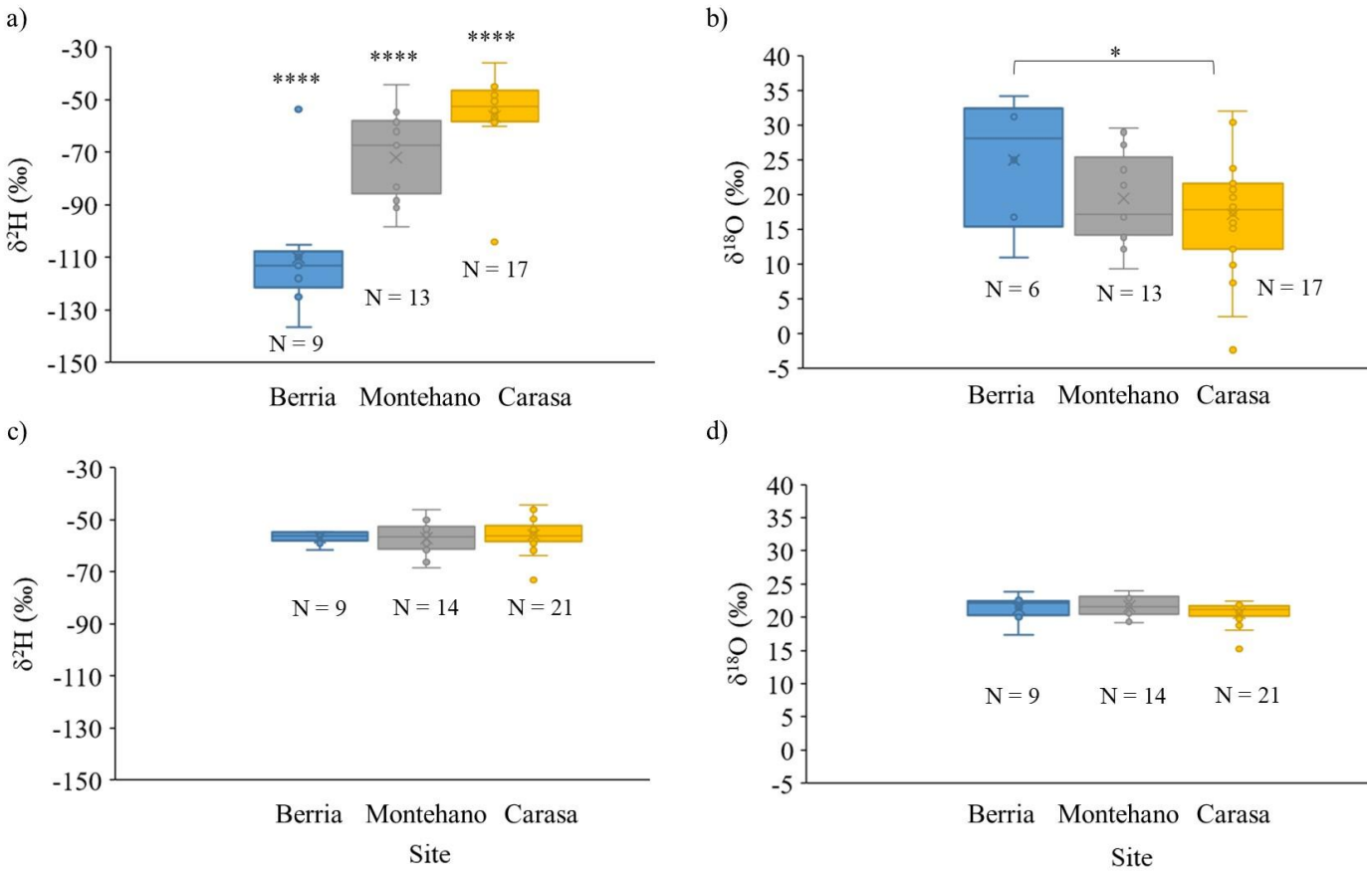

Figure 51: Boxplots showing the ranges of (a) δ^2H of the SOM; (b) the $\delta^{18}O$ of the SOM; (c) the δ^2H of the IOM and (d) the $\delta^{18}O$ of the IOM. The number of samples in each site is indicated as N, **** - $p < 0.0001$; * - $p < 0.05$.

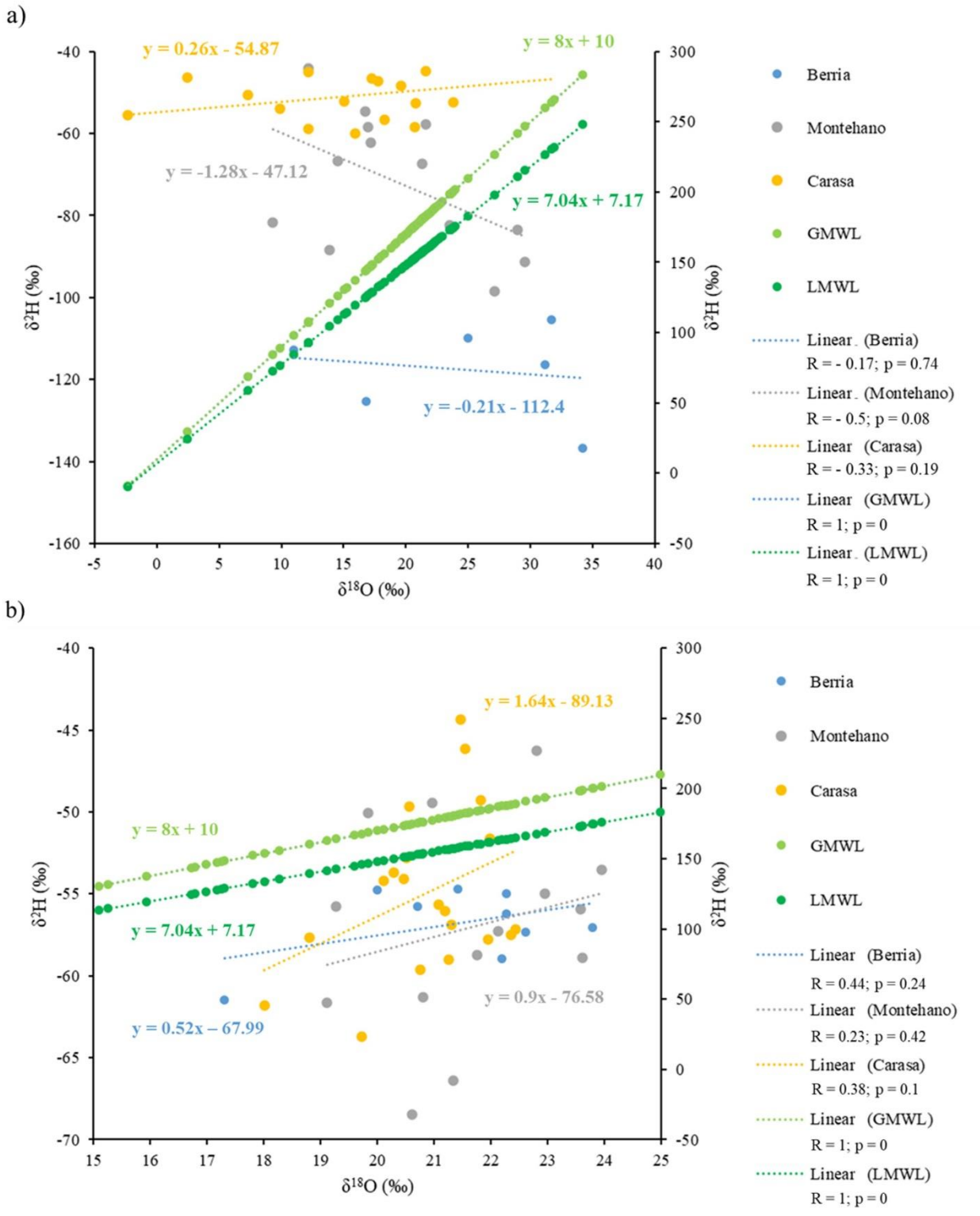

Figure 52: $\delta^{18}O$ and $\delta^{2}H$ of (a) the SOM and (b) IOM compared to the GMWL and LMWL ($\delta^{2}H$ of GMWL and LMWL right Y axis).

IOM - The range of values for both δ^2H and $\delta^{18}O$ in the IOM is similar among the different localities ($p > 0.05$ ANOVA, Figure 51). In terms of correlation between the two isotopes, a weak to moderate linear relationship is observed (Pearson's R from 0.23 to 0.44, Figure 52). The strongest relationship is observed in Carasa (upper estuary) and the weakest in Montehano (lower estuary). However, the correlations were not statistically significant ($p > 0.05$).

Differences between SOM and IOM - The δ^2H values of the SOM were significantly different from the δ^2H values of the IOM in all three sites (t test Berria: $p < 0.0001$; Montehano: $p < 0.01$; Carasa: $p < 0.05$). The $\delta^{18}O$ values of the SOM were significantly different from the $\delta^{18}O$ values of the IOM in Carasa (t test $p < 0.01$), while the $\delta^{18}O$ values of the SOM and IOM in Berria and Montehano were not significantly different (t test $p > 0.05$).

In shells from Montehano and Carasa, which were cut into subsamples, there is a trend from more to less negative values from the umbo towards the edge of the shell for δ^2H in both the SOM and IOM (Table 11; Figure 53). The trend was best observed in the largest sample BRA 6001 from Carasa divided into 7 subsamples. However, it was not as clearly seen for $\delta^{18}O$ (Table 11; Figure 54).

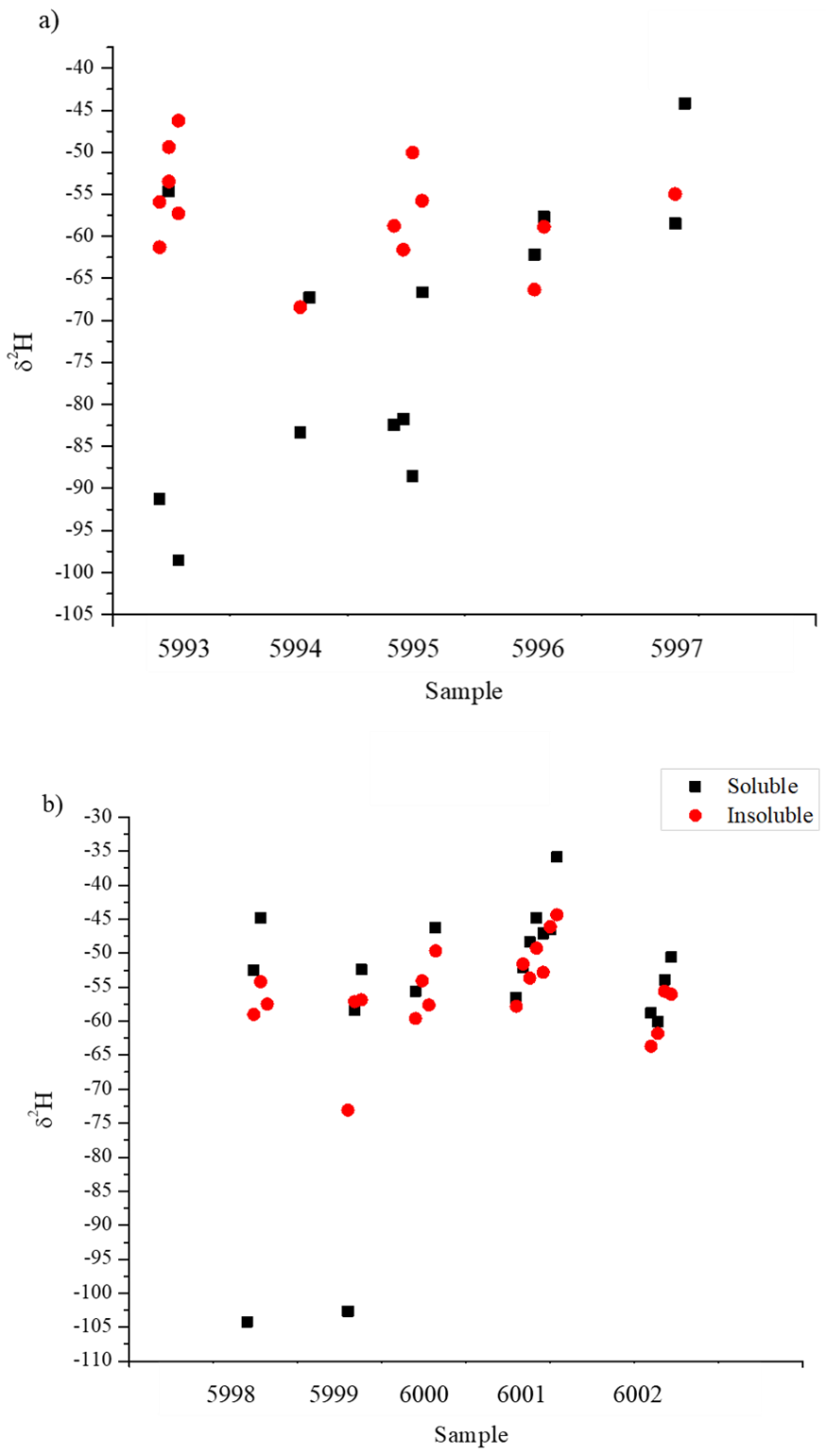

Figure 53: Hydrogen isotope ratios shown for each sample divided into subsamples from (a) Montehano and (b) Carasa.

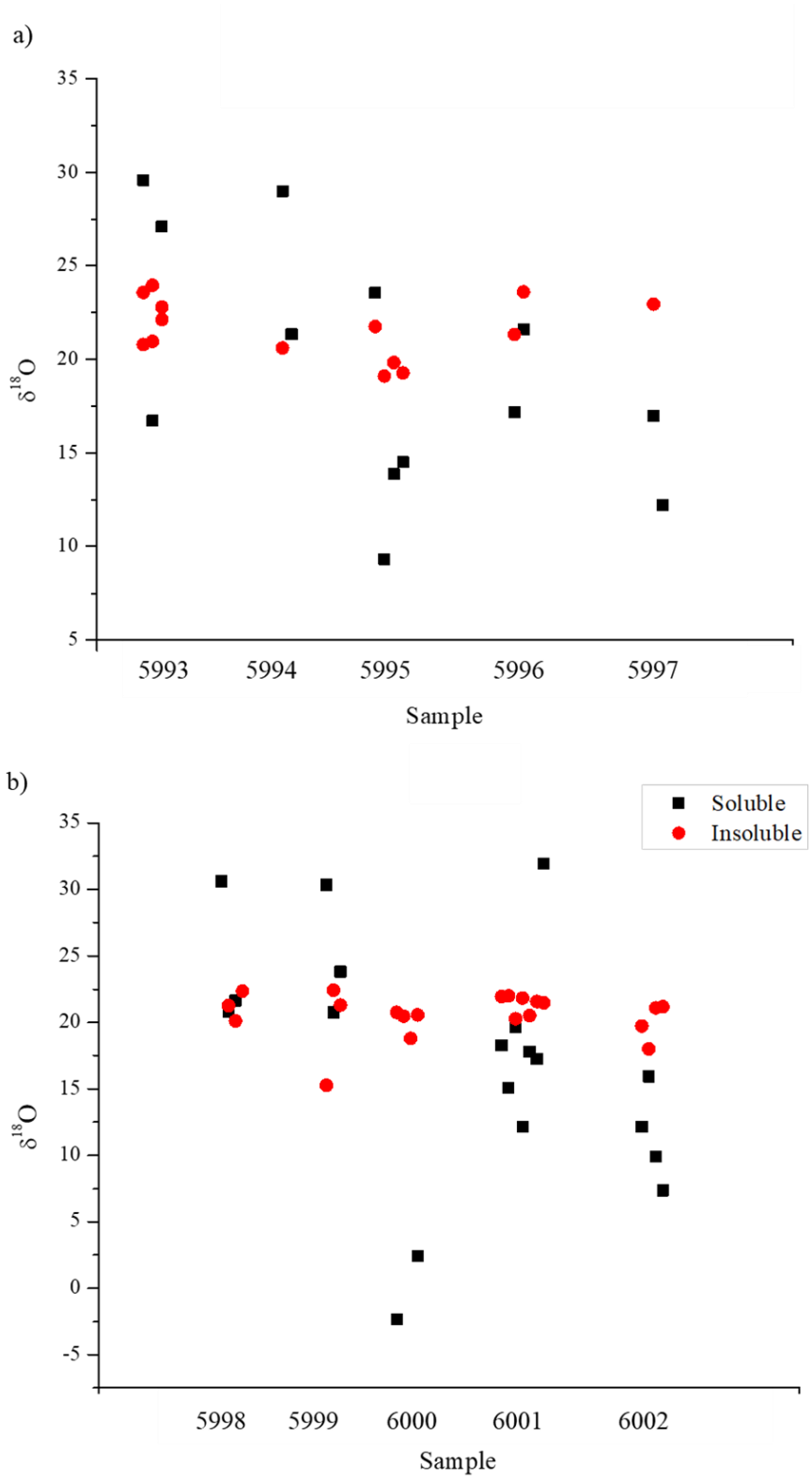

Figure 54. Oxygen isotope ratios shown for each sample divided into subsamples from (a) Montehano and (b) Carasa.

3.3.2. SHELL ORGANIC MATRIX ISOTOPES, GMWL AND LMWL

To graphically represent the relationship between meteoric water $\delta^{18}O$ and $\delta^{2}H$, we used the equation for the GMWL and the LMWL of Santander (ca. 40 km from the study sites), which were calculated using the following formulas:

$$\delta^{2}H = 8 \times \delta^{18}O + 10 \text{ for the GMWL (Craig 1961)}$$

$$\delta^{2}H = 7.04 \times \delta^{18}O + 7.17 \text{ for the LMWL of Santander (Xiang et al. 2022)}$$

SOM - The SOM $\delta^{18}O$ and $\delta^{2}H$ correlations are negative and have an opposite slope compared to the GMWL (Figure 52). The slopes of the relationships in the SOM from the coastal site (Berria) towards the upper estuary (Carasa) do not show clear trends that could be correlated to an environmental or geographical gradient.

IOM - The regression lines of IOM $\delta^{18}O$ and $\delta^{2}H$ are subparallel to the GMWL and LMWL (Figure 52). The value of their slopes increases from the coast (Berria, slope = 0.5), to the lower estuary (Montehano, slope = 0.9) and towards the upper estuary (Carasa, slope = 1.6). The intercepts, on the other hand, show more negative values from the coast (Berria, d = -68), through the lower estuary (Montehano, d = -77) towards the upper estuary (Carasa, d = -89).

3.3.3. SHELL ORGANIC MATRIX ISOTOPES AND WATER ISOTOPES

Unlike the carbonates (Milano et al. 2020), the $\delta^{18}O$ values in both the SOM and IOM were significantly different from respective water $\delta^{18}O$ at each site (Figure 55).

SOM - The SOM $\delta^{18}O$ showed a weak positive correlation with the $\delta^{18}O$ of water in Carasa (Pearson's R = 0.2), while the correlation was negative in Berria (Pearson's R = - 0.1) and Montehano (Pearson's R = - 0.5; Figure 56). However, none of these correlations were statistically significant ($p > 0.05$).

IOM - The IOM $\delta^{18}O$ showed a negligible (Carasa, Pearson's R = 0.1) to moderate (Berria and Montehano, Pearson's R = 0.6 and 0.5 respectively) positive correlation with the $\delta^{18}O$ isotope values of water from the same site (Figure 56). As for the SOM, none of the correlations were statistically significant ($p > 0.05$).

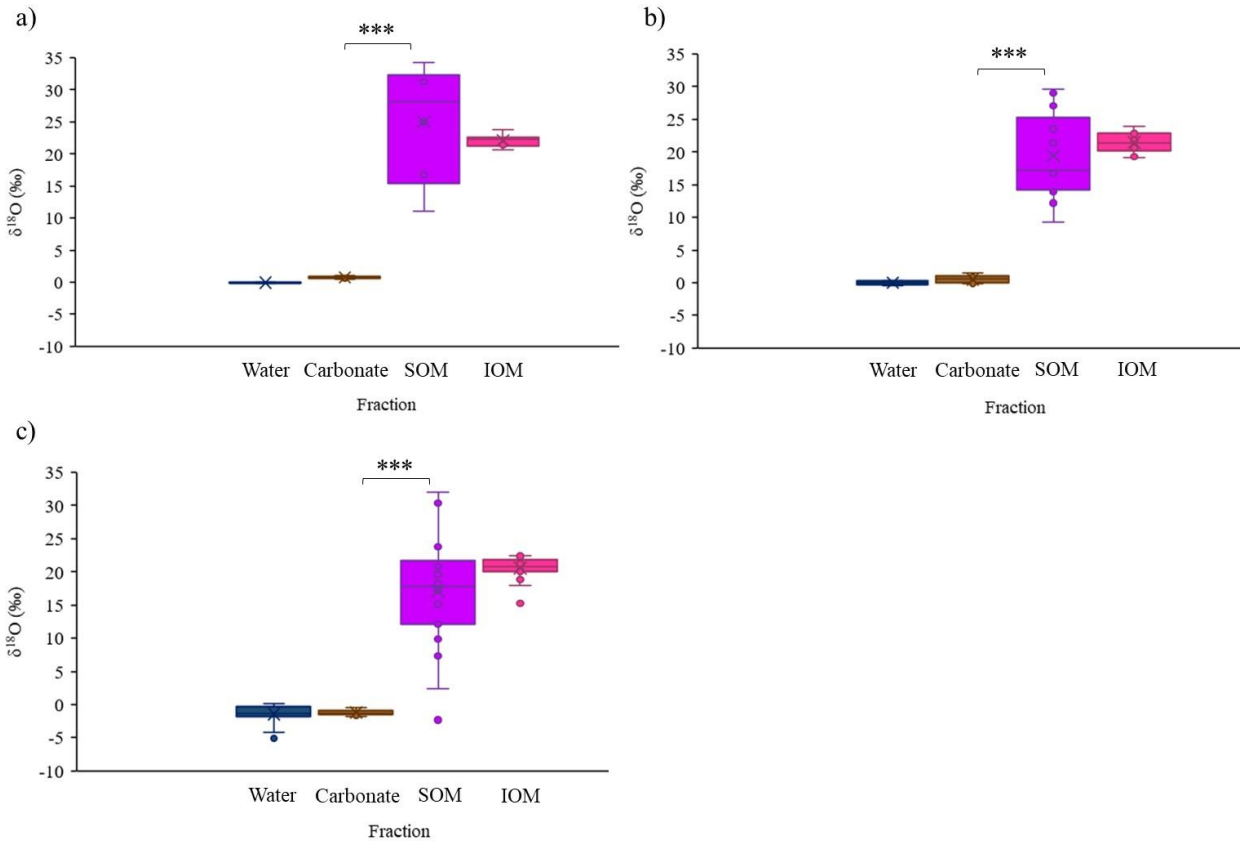

Figure 55: Boxplots showing the $\delta^{18}O$ of the water, the shell carbonate and both IOM and SOM phases for all samples from (a) Berria. N=6; (b) Montehano. N=13; (c) Carasa. N=19. *** - $p < 0.001$. Water and carbonate data from Milano et al. (2020).

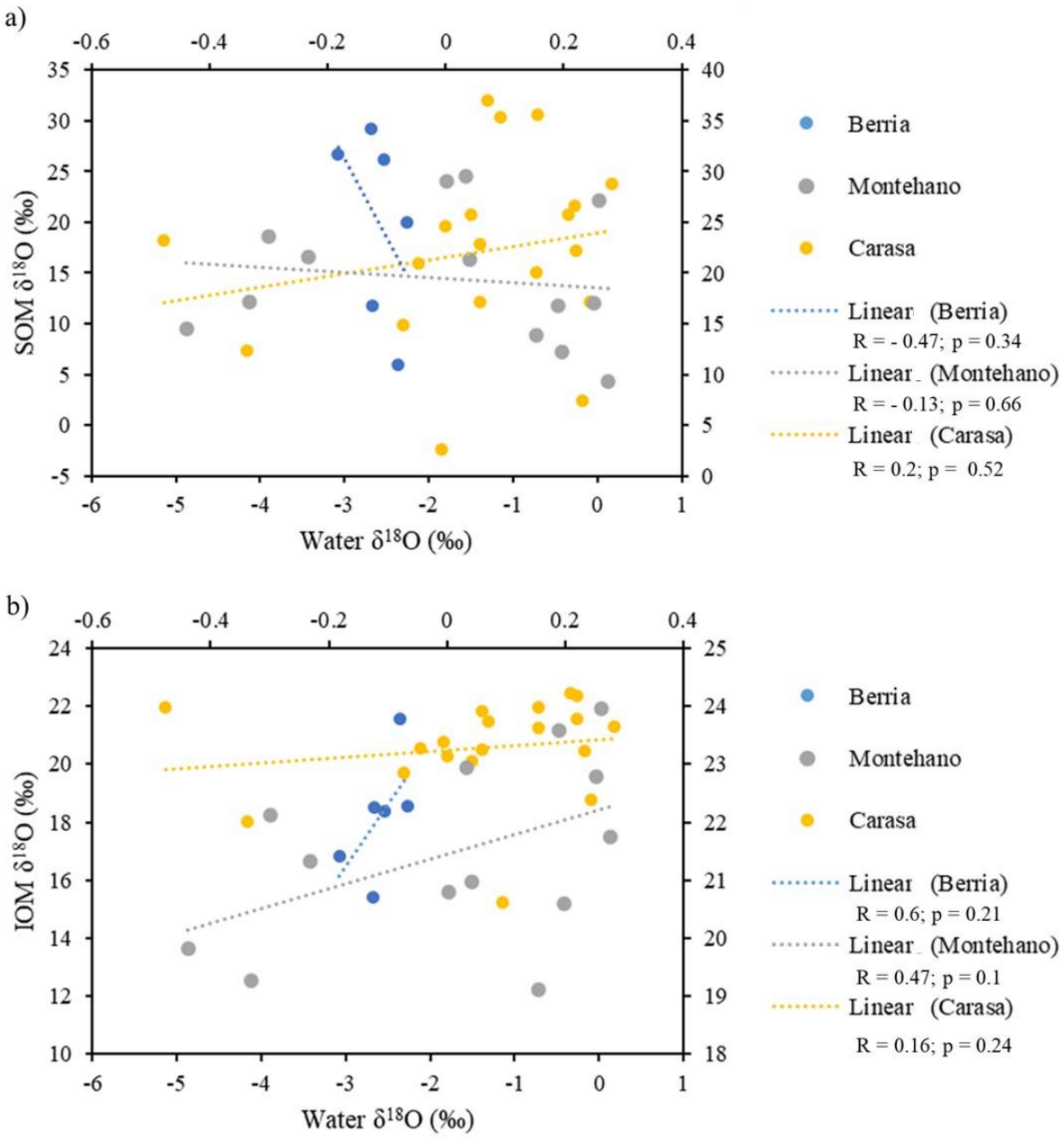

Figure 56: Scatter plot showing the $\delta^{18}O$ of the water, SOM (a) and IOM (b). On the primary axes (bottom and left) the data from Carasa are plotted. On the secondary axes (top and right) the data from Berria and Montehano are plotted. Water data from Milano et al. (2020).

3.4. DISCUSSION

This study, for the first time, analyzed the δ^2H and $\delta^{18}O$ composition of the soluble and insoluble component of the mollusk shell organic matrix. The results indicate that the two fractions have different isotopic signatures, suggesting the involvement of different fractionation mechanisms and therefore different influences from environmental and biological factors.

3.4.1. HYDROGEN AND OXYGEN STABLE ISOTOPE RATIO VALUES IN THE SHELL ORGANIC MATRIX

The δ^2H and $\delta^{18}O$ ratios measured in the organic matrix show values beyond the range of carbonates which are more similar to the water (at least for $\delta^{18}O$). This possibly indicates a substantial isotope fractionation between the shell organic matrix (both IOM and SOM), the carbonates and the water the where the mollusk were growing (Figure 55). The differences in fractionation among the carbonates and the organic matrix are likely due to the formation mechanisms of these two phases. There are different hypotheses on the biomineralization processes in mollusk shells (Addadi et al. 2006; Cölfen and Antonietti 2005; Marin et al. 2012; Rousseau et al. 2005). However, it is generally recognized that the mechanisms behind the deposition of the calcium carbonate and the organic matrix are different and take place successively. The formation of the organic framework precedes the crystallization and is supplied by the calcifying secretory epithelium of the mantle (Marin et al. 2012). Although there are most likely some variations depending on taxon, the general principles that govern the physiology of shell formation are valid for all calcifying mollusks (Marin et al. 2012).

Furthermore, our results show that the δ^2H and $\delta^{18}O$ isotope ranges differ significantly within the organic matrix. For instance, the SOM shows greater variability than IOM (Figure 51). This may suggest that the incorporation of these elements in the two fractions may be influenced by different formation pathways and compositions. Even though it was discovered that the two fractions share several proteins (Marin et al. 2012; Marin et al. 2013; Osuna-Mascaró et al. 2014; Wheeler et al. 1988), the SOM and IOM are biochemically and functionally distinct (Suzuki and Nagasawa 2013; Weiner 1979; 1984; Weiner and Hood 1975; Weiner and Traub 1980; Weiner et al. 1983). The main amino acids composing the proteins which make up the insoluble fraction are glycine, alanine, phenylalanine and tyrosine (Weiner et al. 1983). Furthermore, the cross-linking of proteins by the enzyme phenoloxidase makes this fraction insoluble (Weiner et al. 1983). On the other hand, the proteins of the soluble matrix are rich in aspartic acid and to a lesser extent glutamic acid (Weiner 1979; Weiner et al. 1983). The functions performed by different matrix constituents are still poorly understood, however it is clear that they have important roles in biomineralization (Suzuki and Nagasawa 2013). The insoluble matrix is thought to act as a structural

framework, directing the calcium carbonate mineralization by regulating crystal nucleation, orientation, and polymorphism, while the soluble fraction was found to have a role in the binding of calcium ions regulating crystal growth and morphology (Suzuki and Nagasawa 2013; Weiner and Hood 1975; Weiner and Traub 1980; Weiner et al. 1983).

When considering the SOM, we observe a higher variability in δ^2H values compared to $\delta^{18}O$ (Figure 51 and Figures 53, 54). This could be partially explained by the global natural variation in the isotope ratios of these two elements, which is larger for δ^2H due to the greater mass difference among hydrogen isotopes (Kennedy and Krouse 1990; Odezulu 2011; Xiang et al. 2022). This variation makes it a high-resolution environmental proxy and it is one of the reasons for the frequent use of hydrogen isotope ratios in studies of animal origin and migration (Chamberlain et al. 1997; Cormie et al. 1994; Hobson 1999; Hobson et al. 1999; Kelly et al. 2002; Soto et al. 2013) and more recently food web and trophic level studies (Birchall et al. 2005; Pilecky et al. 2021; Solomon et al. 2009; Soto et al. 2013). In these studies, diet and ambient water are considered the main sources of hydrogen in animal tissues, however the relative contributions of these sources are variable and still not clearly defined. Furthermore, the proportion of dietary versus synthetized lipids and amino acids in animal tissues is uncertain and would have an effect of the tissue δ^2H (Birchall et al. 2005). This is likely true for mollusk shells as well, and as opposed to tissues studied in other animals (i.e., hair, feathers etc.) it would be necessary to use the shell organic matrix. Overall, the observed values and variability of δ^2H in the organic matrix highlight the potential it has as an environmental proxy, but further research will need to assess the impact of metabolic pathways on the δ^2H.

In the SOM, the δ^2H values showed a significant variation among the three sites following the gradient from the coast to the upper estuary (Figure 51), which might be related to the evaporative process and the salinity gradient. In fact, osmoregulation in estuarine mollusk species causes changes in metabolic activities including intracellular enzyme activity and amino acid regulation (Vinu Chandran and Ramachandran 2002). For instance, salinity variations caused changes in $\delta^{13}C$ fractionation during shell formation in *Mytilus edulis* (Wanamaker et al. 2007). The organic matrix of mollusk shells is known to have a key role in biomineralization processes (Nudelman et al. 2006; Weiner 1979; Weiner and Hood 1975) but is also thought to take part in cell signaling, enzymatic (Marin et al. 2012; Marin et al. 2007; Marin et al. 2013) and immunity functions (Arivalagan et al. 2017) which might also affect isotope fractionation. During biomineralization, raw material is transported from the environment to the site of shell deposition, where a series of organic matrix – mediated processes is activated to construct the calcium carbonate mineral (Falini et al. 1996; Weiner and Dove 2003). There are several “vital” or “physiological effects” which are thought to vary among different proxies due to different mechanisms, such as the activity of the carbonic anhydrase enzyme (Weiner and Dove 2003). These enzymes catalyze the reversible hydration of metabolic carbon

dioxide (CO_2) to bicarbonate (HCO^{3-}) requiring protons (H+) (Lindskog and Coleman 1973), thus regulating the formation of calcium carbonate crystals in the shell. Changes in salinity were found to modify the activity of these enzymes thus affecting the regulation of shell biomineralization (Cardoso et al. 2019). The exact location where these processes occur is still unknown, although the activity of these enzymes was observed in the mantle, but also in the shell organic matrix (Marin et al. 2012). Therefore, isotope fractionation in the organic matrix might be affected by this type of enzymatic activity, which in turn depends on the external conditions.

Alternatively, differences among the three sites in the diet and metabolism of the mollusks could be influencing isotope fractionation in the organic matrix. Hydrogen isotope ratios of marine snail soft tissues have been shown to be more influenced by their food source rather than ambient water (Estep and Dabrowski 1980). However, this work was criticized suggesting that isotope fractionation in animal tissues is most likely influenced by multiple factors, including diet and water (DeNiro and Epstein 1981). Metabolic responses to stress caused by external environmental factors (temperature, salinity, nutrient availability) or by internal factors (reproductive stress or disease) can also cause changes in isotope fractionation in animal tissues (Kennedy and Krouse 1990). For example, changes in salinity and temperature have been found to affect the metabolism and stress response in *Mytilus* sp. (Hiebenthal et al. 2012). Furthermore, the biochemical composition of *M. edulis* tissues was found to vary due to different temperatures, phytoplankton availability and reproductive cycle (Fernández et al. 2015). Many bivalve species, including *Mytilus* sp. are filter feeders, acquiring their proteins, lipids, carbohydrates, and other components which are integrated into their tissues mainly from phytoplankton (Alkanani et al. 2007; Fernández et al. 2015; Pettersen et al. 2010). Deuterium depletion in cellular organic matter during the metabolism of carbohydrates into lipids was observed in microalgae phytoplankton (Estep and Hoering 1980). Thus, the consumption of microalgae with variable lipid content and/or the *in-situ* synthesis of lipids might affect the hydrogen isotope fractionation in *Mytilus sp*. Lipids constitute a lesser-known minor portion of the shell organic matrix and are thought to have an important role in biomineralization (De Muizon et al. 2022; Farre and Dauphin 2009; Farre et al. 2008; Marin et al. 2012; Suzuki and Nagasawa 2013). The lipid composition of the organic matrix was found to vary among species and different structures within the shell (i.e., nacreous, and prismatic; Farre and Dauphin 2009; Farre et al. 2008) and their quantity is likely variable and possibly dependent on diet. In fact, the organic matrix has been indicated for studies of the mollusk diet in early research and it showed similar δ^2H values in *M. edulis* flesh and organic matrix (LeBlanc 1989). Consequently, isotope fractionation in the organic matrix of mollusk shells might also be influenced by multiple factors including diet and metabolism. These factors are most likely variable along the coast to upper-estuary gradient due to different environmental conditions and phytoplankton

availability, characteristic of estuarine habitats. For example, a study conducted on the River Pas estuary (ca. 40 km west to localities studied here) showed differences in phytoplankton abundance and diversity between the river mouth and upper estuarine area (Perez and Canteras 1990). Therefore, both the physical and chemical environmental variables and different phytoplankton communities available in the three study sites, might have an influence on the isotopic signatures of the organic matrix of the shells.

3.4.2. HYDROGEN AND OXYGEN STABLE ISOTOPE RATIO CORRELATIONS: WATER LINES AND SHELL ORGANIC MATRIX

A previous study on *M. galloprovincialis* shells from the same three sites considered here, found that the relationship between $\delta^{18}O$ and $\delta^{13}C$ of the carbonate phase could be used as a provenance proxy, showing negative correlations in the marine environment, and positive correlations in the estuarine environment (Milano et al. 2020). A different study found that the $\delta^{2}H$ of the organic matrix and the $\delta^{18}O$ in the mineral fraction of the shell had a positive correlation with a slope subparallel to the GMWL suggesting that the functional relationship between the oxygen and hydrogen isotopes found in meteoric water is maintained in the shell (Carroll et al. 2006).

SOM - Our results for the SOM fraction had a higher variability giving negative relationships between the $\delta^{2}H$ and $\delta^{18}O$ for Berria and Montehano, and a positive relationship for Carasa, yet showing no trends correlated to the environmental gradient (Figure 52). The different relationships are given by the opposite trends of $\delta^{2}H$ and $\delta^{18}O$ along the geographical gradient. Heavy isotope enriched river water can be an effect of increased evaporation (Barrie et al. 2015) and/or the abundance of phytoplankton (Ogrinc et al. 2018; Wehr and Descy 1998). However, the variation of water $\delta^{2}H$ and $\delta^{18}O$ typically follows the same trend for both isotopes, from more to less negative values starting from the source towards the confluence (Barrie et al. 2015; Karim 2002; LeBlanc 1989) or vice versa depending on rainfall and evaporation (Yang and Han 2020). In the three study sites the $\delta^{18}O$ of water is more negative in Carasa and less negative towards Montehano and Berria (Milano et al. 2020). Thus, in the case of SOM, $\delta^{2}H$ values follow a trend that is opposite to what could be expected, supporting the hypothesis that hydrogen incorporation may be metabolic-dependent or diet-dependent, and therefore possibly indirectly related to environmental variables.

IOM - On the other hand, our results for the IOM yielded similar results to those presented in Carroll et al. (2006), with positive correlations and slopes subparallel to the GMWL and LMWL even though the correlation was not statistically significant (Figure 52). This might be due to the limited sample size. However, the slopes and intercepts of the $\delta^{2}H$ and $\delta^{18}O$ relationships in the IOM change following the environmental gradient indicating that they have a potential as an environmental proxy. The hydrogen and

oxygen isotope compositions of meteoric water can form slopes as low as 4 and as high as 9 depending on the geographical position and thus local conditions (Hatvani et al. 2023; Lécuyer et al. 2021). Considering the LMWL for the area of study has a lower slope value of 7.04 and intercept of 7.14 due to the local conditions (Xiang et al. 2022) it is even more similar to the slope obtained for Berria compared to the GMWL (Figure 52). Surface water δ^2H and $\delta^{18}O$ were found to depend mostly on the spatiotemporal variation in precipitation isotope ratios and runoff generation over large geographic areas (Bowen et al. 2011; Ogrinc et al. 2018). However, there were some local deviations from precipitation isotope ratios due to elevation in mountain-fed rivers and due to evaporative effects in small streams (Bowen et al. 2011). For example, surface water in rivers in the British Isles showed a lower slope compared to the GMWL due to evaporative processes causing heavy isotope enrichment (Darling et al. 2003). Thus, in future studies it would be necessary to perform water δ^2H measurements in the study sites, in addition to $\delta^{18}O$. Nonetheless, the differences in slope and intercept values in IOM δ^2H and $\delta^{18}O$ relationships among the three sites indicate that, although the ranges of the single isotope values are limited, their correlation may hold some environmental information. Alternatively, the differences may be due to different food sources in the three sites which in turn influence the organic matrix δ^2H. Hence, we could assume that the differences between the IOM slopes among the three sites depend on the local conditions. It is known that the relationship between water δ^2H and $\delta^{18}O$ can change seasonally (Darling and Talbot 2003). However, seasonal variation in river surface water was shown to be lower than in precipitation, indicating that the isotopic composition of river water was also influenced by the input of groundwater (Ogrinc et al. 2018). Regardless, it would be challenging to obtain seasonal data using the organic matrix from small shells such as *Mytilus* sp., given the high amount of shell material needed for extraction (~ 2g), which results in a lower number of subsamples which can be analyzed compared to isotope analysis of the carbonate phase (Leng and Lewis 2016; Milano et al. 2022; Milano et al. 2020; Trofimova et al. 2018). However, studies on seasonality could target species with larger and thicker shells to obtain more subsamples.

3.5. CONCLUSIONS

To summarize, this study is the first attempt to investigate the variation of stable isotopes along a geographical gradient, using the organic matrix of mollusk shells. The advantage of using the organic matrix fractions as opposed to the carbonate fraction is that it allows for the measurement of not only $\delta^{18}O$, but also $\delta^{2}H$. Furthermore, this is the first study to differentiate the measurements in the SOM and IOM. Our results show that the SOM shows a much higher variability in terms of $\delta^{2}H$ and $\delta^{18}O$ compared to the IOM. Given the differences among the two fractions of the organic matrix, future studies should maintain the division into the SOM and IOM and analyze them separately. For instance, SOM isotope values differ among the three localities, especially the $\delta^{2}H$. We observe a gradient in $\delta^{2}H$ starting from very negative values at the coast towards more positive values in the upper estuary, which is opposite to the variation in $\delta^{18}O$, and opposite to expected water composition depending on Rayleigh fractionation. This indicates that different fractionation processes probably affect hydrogen and oxygen incorporation into the shell organics. They might be related to different dietary inputs, metabolic or enzymatic activity during biomineralization. Therefore, we conclude that $\delta^{2}H$ ratios from the SOM could potentially be a new high-resolution provenance proxy, which might help to disclose information on the hydrographic characteristics of modern and ancient environments. However, further research is needed to better define the biological processes that affect the isotopic composition of the organic matrix. Furthermore, when evaluating $\delta^{2}H$ and $\delta^{18}O$ together, we observe positive correlations in the IOM subparallel to those of GMWL and LMWL and whose slopes follow the coast - estuary gradient, indicating that environmental information might also be encoded in the IOM fraction. We suggest the inclusion of $\delta^{2}H$ and $\delta^{18}O$ measurements of water and phytoplankton isotope ratios in further studies. Our results show an overall potential in using shell organic matrix and more research will be needed to clarify and further develop the application of our observations.

3.6. REFERENCES

Addadi L, Joester D, Nudelman F, Weiner S. 2006. Mollusk shell formation: A source of new concepts for understanding biomineralization processes. Chemistry–A European Journal. 12(4):980-987.

Alkanani T, Parrish CC, Thompson RJ, McKenzie CH. 2007. Role of fatty acids in cultured mussels, mytilus edulis, grown in notre dame bay, newfoundland. Journal of Experimental Marine Biology and Ecology. 348(1):33-45.

Andrus CFT. 2011. Shell midden sclerochronology. Quaternary Science Reviews. 30(21):2892-2905.

Arivalagan J, Yarra T, Marie B, Sleight VA, Duvernois-Berthet E, Clark MS, Marie A, Berland S. 2017. Insights from the shell proteome: Biomineralization to adaptation. Molecular Biology and Evolution. 34(1):66-77.

Bar-Yosef Mayer DE, Vandermeersch B, Bar-Yosef O. 2009. Shells and ochre in middle paleolithic qafzeh cave, israel: Indications for modern behavior. J Hum Evol. 56(3):307-314.

Barrie GM, Worden RH, Barrie CD, Boyce AJ. 2015. Extensive evaporation in a modern temperate estuary: Stable isotopic and compositional evidence. Limnology and Oceanography. 60(4):1241-1250.

Bicho N, Haws J. 2008. At the land's end: Marine resources and the importance of fluctuations in the coastline in the prehistoric hunter–gatherer economy of portugal. Quaternary Science Reviews. 27(23-24):2166-2175.

Bicho N, Umbelino C, Detry C, Pereira T. 2010. The emergence of muge mesolithic shell middens in central portugal and the 8200 cal yr bp cold event. The Journal of Island and Coastal Archaeology. 5(1):86-104.

Birchall J, O'Connell TC, Tim HEH, Robert EMH. 2005. Hydrogen isotope ratios in animal body protein reflect trophic level. Journal of Animal Ecology. 74(5):877-881.

Bowen GJ, Kennedy CD, Liu Z, Stalker J. 2011. Water balance model for mean annual hydrogen and oxygen isotope distributions in surface waters of the contiguous united states. Journal of Geophysical Research: Biogeosciences. 116(G4).

Cardoso JCR, Ferreira V, Zhang X, Anjos L, Félix RC, Batista FM, Power DM. 2019. Evolution and diversity of alpha-carbonic anhydrases in the mantle of the mediterranean mussel (mytilus galloprovincialis). Scientific Reports. 9(1).

Carroll M, Romanek C, Paddock L. 2006. The relationship between the hydrogen and oxygen isotopes of freshwater bivalve shells and their home streams. Chemical Geology. 234(3-4):211-222.

Chamberlain CP, Blum JD, Holmes RT, Feng X, Sherry TW, Graves GR. 1997. The use of isotope tracers for identifying populations of migratory birds. Oecologia. 109(1):132-141.

Cölfen H, Antonietti M. 2005. Mesocrystals: Inorganic superstructures made by highly parallel crystallization and controlled alignment. Angewandte Chemie International Edition. 44(35):5576-5591.

Comesaña AS, Posada D, Sanjuan A. 1998. Mytilus galloprovincialis lmk. In northern africa. Journal of Experimental Marine Biology and Ecology. 223(2):271-283.

Cormie AB, Schwarcz HP, Gray J. 1994. Relation between hydrogen isotopic ratios of bone collagen and rain. Geochimica et Cosmochimica Acta. 58(1):377-391.

Cortés-Sánchez M, Morales-Muñiz A, Simón-Vallejo MD, Lozano-Francisco MC, Vera-Peláez JL, Finlayson C, Rodríguez-Vidal J, Delgado-Huertas A, Jiménez-Espejo FJ, Martínez-Ruiz F et al. 2011. Earliest known use of marine resources by neanderthals. PLoS ONE. 6(9):e24026.

Craig H. 1961. Isotopic variations in meteoric waters. Science. 133(3465):1702-1703.

Darling WG, Bath AH, Talbot JC. 2003. The o and h stable isotope composition of freshwaters in the british isles. 2. Surface waters and groundwater. Hydrology and Earth System Sciences. 7(2):183-195.

Darling WG, Talbot JC. 2003. The o and h stable isotope composition of freshwaters in the british isles. 1. Rainfall. Hydrology and Earth System Sciences. 7(2):163-181.

De Muizon CJ, Iandolo D, Nguyen DK, Al-Mourabit A, Rousseau M. 2022. Organic matrix and secondary metabolites in nacre. Marine Biotechnology. 24(5):831-842.

DeNiro MJ, Epstein S. 1981. Hydrogen isotope ratios of mouse tissues are influenced by a variety of factors other than diet. Science. 214(4527):1374-1376.

Douka K. 2011. An upper palaeolithic shell scraper from ksar akil (lebanon). Journal of Archaeological Science. 38(2):429-437.

Douka K, Spinapolice EE. 2012. Neanderthal shell tool production: Evidence from middle palaeolithic italy and greece. Journal of World Prehistory. 25(2):45-79.

Ellis GS, Herbert G, Hollander D. 2014. Reconstructing carbon sources in a dynamic estuarine ecosystem using oyster amino acid δ¹³c values from shell and tissue. Journal of Shellfish Research. 33(1):217-225, 219.

Estep MF, Dabrowski H. 1980. Tracing food webs with stable hydrogen isotopes. Science. 209(4464):1537-1538.

Estep MF, Hoering TC. 1980. Biogeochemistry of the stable hydrogen isotopes. Geochimica et Cosmochimica Acta. 44(8):1197-1206.

Fa DA, Finlayson JC, Finlayson G, Giles-Pacheco F, Rodríguez-Vidal J, Gutiérrez-López JM. 2016. Marine mollusc exploitation as evidenced by the gorham's cave (gibraltar) excavations 1998–2005: The middle–upper palaeolithic transition. Quaternary International. 407:16-28.

Falini G, Albeck S, Weiner S, Addadi L. 1996. Control of aragonite or calcite polymorphism by mollusk shell macromolecules. Science. 271(5245):67-69.

Falini G, Reggi M, Fermani S, Sparla F, Goffredo S, Dubinsky Z, Levi O, Dauphin Y, Cuif J-P. 2013. Control of aragonite deposition in colonial corals by intra-skeletal macromolecules. Journal of Structural Biology. 183(2):226-238.

Farre B, Dauphin Y. 2009. Lipids from the nacreous and prismatic layers of two pteriomorpha mollusc shells. Comparative Biochemistry and Physiology Part B: Biochemistry and Molecular Biology. 152(2):103-109.

Farre B, Dauphin Y, Cuif JP. 2008 Lipids of the mollusks shells. Conference proceeding, Geophysical Research Abstracts, EGU, 10: 1607-7962.

Fernández A, Grienke U, Soler-Vila A, Guihéneuf F, Stengel DB, Tasdemir D. 2015. Seasonal and geographical variations in the biochemical composition of the blue mussel (mytilus edulis l.) from ireland. Food Chemistry. 177:43-52.

Gillikin DP, Wanamaker AD, Andrus CFT. 2019. Chemical sclerochronology. Chemical Geology. 526:1-6.

Grégoire C. 1972. Structure of the molluscan shell. Chemical zoology. 7:45-102.

Hammer Ø, Harper DA, Ryan PD. 2001. Past: Paleontological statistics software package for education and data analysis. Palaeontologia electronica. 4(1):9.

Hatvani IG, Smati AE, Erdélyi D, Szatmári G, Vreča P, Kern Z. 2023. Modeling the spatial distribution of the meteoric water line of modern precipitation across the broader mediterranean region. Journal of Hydrology. 617:128925.

Hiebenthal C, Philipp E, Eisenhauer A, Wahl M. 2012. Interactive effects of temperature and salinity on shell increment, condition and cellular stress of two bivalve populations, mytilus edulis (l.) and arctica islandica (l.), from the western baltic sea. Aquatic Biology. 14(3):289-298.

Hobson KA. 1999. Tracing origins and migration of wildlife using stable isotopes: A review. Oecologia. 120(3):314-326.

Hobson KA, Wassenaar LI, Taylor OR. 1999. Stable isotopes (δd and δ 13 c) are geographic indicators of natal origins of monarch butterflies in eastern north america. Oecologia. 120(3):397-404.

Hockey PAR, van Erkom Schurink C. 1992. The invasive biology of the mussel mytilus galloprovincialis on the southern african coast. Transactions of the Royal Society of South Africa. 48(1):123-139.

Joordens JC, d'Errico F, Wesselingh FP, Munro S, de Vos J, Wallinga J, Ankjaergaard C, Reimann T, Wijbrans JR, Kuiper KF et al. 2015. Homo erectus at trinil on java used shells for tool production and engraving. Nature. 518(7538):228-231.

Karim A. 2002. Water balance of the indus river basin and moisture source in the karakoram and western himalayas: Implications from hydrogen and oxygen isotopes in river water. Journal of Geophysical Research. 107(D18).

Kelly JF, Atudorei V, Sharp ZD, Finch DM. 2002. Insights into wilson's warbler migration from analyses of hydrogen stable-isotope ratios. Oecologia. 130(2):216-221.

Kennedy BV, Krouse HR. 1990. Isotope fractionation by plants and animals: Implications for nutrition research. Canadian Journal of Physiology and Pharmacology. 68(7):960-972.

Kobayashi I, Samata T. 2006. Bivalve shell structure and organic matrix. Materials Science and Engineering: C. 26(4):692-698.

LeBlanc C. 1989. Terrestrial input to estuarine bivalves as measured by multiple stable isotopes tracers.

Lécuyer C, Bojar A-V, Daux V, Legendre S. 2021. Geographic variations in the slope of the δ 2 h–δ 18 o meteoric water line over europe: A record of increasing continentality. Geological Society, London, Special Publications. 507(1):5-17.

Lécuyer C, Reynard B, Martineau F. 2004. Stable isotope fractionation between mollusc shells and marine waters from martinique island. Chemical Geology. 213(4):293-305.

Leng MJ, Lewis JP. 2016. Oxygen isotopes in molluscan shell: Applications in environmental archaeology. Environmental Archaeology. 21(3):295-306.

Lindskog S, Coleman JE. 1973. The catalytic mechanism of carbonic anhydrase. Proceedings of the National Academy of Sciences. 70(9):2505-2508.

Lowenstam HA, Weiner S. 1989. On biomineralization. Oxford University Press on Demand.

Mannino MA, Spiro BF, Thomas KD. 2003. Sampling shells for seasonality: Oxygen isotope analysis on shell carbonates of the inter-tidal gastropod monodonta lineata (da costa) from populations across its modern range and from a mesolithic site in southern britain. Journal of archaeological science. 30(6):667-679.

Mannino MA, Thomas KD, Leng MJ, Sloane HJ. 2008. Shell growth and oxygen isotopes in the topshell osilinus turbinatus: Resolving past inshore sea surface temperatures. Geo-Marine Letters. 28(5-6):309-325.

Marean CW, Bar-Matthews M, Bernatchez J, Fisher E, Goldberg P, Herries AIR, Jacobs Z, Jerardino A, Karkanas P, Minichillo T et al. 2007. Early human use of marine resources and pigment in south africa during the middle pleistocene. Nature. 449(7164):905-908.

Marin F, Le Roy N, Marie B. 2012. The formation and mineralization of mollusk shell. Front Biosci. 4(1099):125.

Marin F, Luquet G, Marie B, Medakovic D. 2007. Molluscan shell proteins: Primary structure, origin, and evolution. Elsevier. p. 209-276.

Marin F, Marie B, Hamada SB, Ramos-Silva P, Le Roy N, Guichard N, Wolf SE, Montagnani C, Joubert C, Piquemal D. 2013. Shellome': Proteins involved in mollusk shell biomineralization-diversity, functions. Recent advances in pearl research. 149:168.

Milano S, Schöne BR, González-Morales MR, Gutiérrez-Zugasti I. 2022. Temporal and spatial variability of prehistoric aquatic resource procurement: A case study from mesolithic northern iberia. Scientific Reports. 12(1).

Milano S, Schöne BR, Gutiérrez-Zugasti I. 2020. Oxygen and carbon stable isotopes of mytilus galloprovincialis lamarck, 1819 shells as environmental and provenance proxies. The Holocene. 30(1):65-76.

Misarti N, Gier E, Finney B, Barnes K, McCarthy M. 2017. Compound-specific amino acid δ15n values in archaeological shell: Assessing diagenetic integrity and potential for isotopic baseline reconstruction. Rapid Communications in Mass Spectrometry. 31(22):1881-1891.

Nudelman F, Gotliv BA, Addadi L, Weiner S. 2006. Mollusk shell formation: Mapping the distribution of organic matrix components underlying a single aragonitic tablet in nacre. Journal of Structural Biology. 153(2):176-187.

O'Donnell TH, Macko SA, Wehmiller JF. 2007. Stable carbon isotope composition of amino acids in modern and fossil mercenaria. Organic Geochemistry. 38(3):485-498.

Odezulu CI. 2011. Stable hydrogen and oxygen isotopic variations in natural waters in north florida: Implications for hydrological and paleoclimatic studies.

Ogrinc N, Kocman D, Miljević N, Vreča P, Vrzel J, Povinec P. 2018. Distribution of h and o stable isotopes in the surface waters of the sava river, the major tributary of the danube river. Journal of Hydrology. 565:365-373.

Osuna-Mascaró A, Cruz-Bustos T, Benhamada S, Guichard N, Marie B, Plasseraud L, Corneillat M, Alcaraz G, Checa A, Marin F. 2014. The shell organic matrix of the crossed lamellar queen conch shell (strombus gigas). Comparative Biochemistry and Physiology Part B: Biochemistry and Molecular Biology. 168:76-85.

Peharda M, Schoene BR, Black BA, Correge T. 2021. Advances of sclerochronology research in the last decade. Palaeogeography, Palaeoclimatology, Palaeoecology. 570:110371.

Peresani M, Vanhaeren M, Quaggiotto E, Queffelec A, d'Errico F. 2013. An ochered fossil marine shell from the mousterian of fumane cave, italy. PLoS One. 8(7):e68572.

Perez L, Canteras J. 1990. Spatial heterogeneity of phytoplankton in an estuary of cantabria, northern spain. Journal of Coastal Research.157-168.

Pettersen AK, Turchini GM, Jahangard S, Ingram BA, Sherman CDH. 2010. Effects of different dietary microalgae on survival, growth, settlement and fatty acid composition of blue mussel (mytilus galloprovincialis) larvae. Aquaculture. 309(1):115-124.

Pilecky M, Winter K, Wassenaar LI, Kainz MJ. 2021. Compound-specific stable hydrogen isotope (δ 2 h) analyses of fatty acids: A new method and perspectives for trophic and movement ecology. Rapid Communications in Mass Spectrometry. 35(16).

Ramos-Muñoz J, Cantillo-Duarte JJ, Bernal-Casasola D, Barrena-Tocino A, Domínguez-Bella S, Vijande-Vila E, Clemente-Conte I, Gutiérrez-Zugasti I, Soriguer-Escofet M, Almisas-Cruz S. 2016. Early use of marine resources by middle/upper pleistocene human societies: The case of benzú rockshelter (northern africa). Quaternary International. 407:6-15.

Reggi M, Fermani S, Landi V, Sparla F, Caroselli E, Gizzi F, Dubinsky Z, Levy O, Cuif J-P, Dauphin Y et al. 2014. Biomineralization in mediterranean corals: The role of the intraskeletal organic matrix. Crystal Growth & Design. 14(9):4310-4320.

Rousseau M, Lopez E, Stempflé P, Brendlé M, Franke L, Guette A, Naslain R, Bourrat X. 2005. Multiscale structure of sheet nacre. Biomaterials. 26(31):6254-6262.

Sanjuan A, Zapata C, Alvarez G. 1994. Mytilus galloprovincialis and m. Edulis on the coasts of the iberian peninsula. Marine Ecology Progress Series.131-146.

Schöne B, Tanabe K, Dettman D, Sato S. 2003. Environmental controls on shell growth rates and δ 18 o of the shallow-marine bivalve mollusk phacosoma japonicum in japan. Marine Biology. 142:473-485.

Schöne BR, Fiebig J. 2009. Seasonality in the north sea during the allerød and late medieval climate optimum using bivalve sclerochronology. International Journal of Earth Sciences. 98(1):83-98.

Schöne BR, Freyre Castro AD, Fiebig J, Houk SD, Oschmann W, Kröncke I. 2004. Sea surface water temperatures over the period 1884–1983 reconstructed from oxygen isotope ratios of a bivalve

mollusk shell (arctica islandica, southern north sea). Palaeogeography, Palaeoclimatology, Palaeoecology. 212(3):215-232.

Solomon CT, Cole JJ, Doucett RR, Pace ML, Preston ND, Smith LE, Weidel BC. 2009. The influence of environmental water on the hydrogen stable isotope ratio in aquatic consumers. Oecologia. 161(2):313-324.

Soto DX, Wassenaar LI, Hobson KA. 2013. Stable hydrogen and oxygen isotopes in aquatic food webs are tracers of diet and provenance. Functional Ecology. 27(2):535-543.

Suzuki M, Nagasawa H. 2013. Mollusk shell structures and their formation mechanism. Canadian Journal of Zoology. 91(6):349-366.

Tátá F, Cascalheira J, Marreiros J, Pereira T, Bicho N. 2014. Shell bead production in the upper paleolithic of vale boi (sw portugal): An experimental perspective. Journal of Archaeological Science. 42:29-41.

Trofimova T, Milano S, Andersson C, Bonitz FGW, Schöne BR. 2018. Oxygen isotope composition ofarctica islandicaaragonite in the context of shell architectural organization: Implications for paleoclimate reconstructions. Geochemistry, Geophysics, Geosystems. 19(2):453-470.

Vinu Chandran R, Ramachandran R. 2002. Intracellular osmoregulation in the estuarine mollusc villorita cyprinoides var. Cochinensis (mollusca: Bivalvia) hanley. Citeseer.

Wanamaker A, Kreutz K, Borns H, Introne D. 2007. Experimental determination of salinity, temperature, growth, and metabolic effects on shell isotope chemistry of mytilus edulis collected from maine and greenland. Paleoceanography. 22.

Wassenaar LI, Hobson KA, Sisti L. 2015. An online temperature-controlled vacuum-equilibration preparation system for the measurement of δ2h values of non-exchangeable-h and of δ18o values in organic materials by isotope-ratio mass spectrometry. Rapid Communications in Mass Spectrometry. 29(5):397-407.

Wehr JD, Descy JP. 1998. Use of phytoplankton in large river management. Journal of Phycology. 34(5):741-749.

Wei Y, d'Errico F, Vanhaeren M, Li F, Gao X. 2016. An early instance of upper palaeolithic personal ornamentation from china: The freshwater shell bead from shuidonggou 2. PLoS One. 11(5):e0155847.

Weiner S. 1979. Aspartic acid-rich proteins: Major components of the soluble organic matrix of mollusk shells. Calcified Tissue International. 29(1):163-167.

Weiner S. 1984. Organization of organic matrix components in mineralized tissues. American Zoologist. 24(4):945-951.

Weiner S, Dove PM. 2003. An overview of biomineralization processes and the problem of the vital effect. Reviews in mineralogy and geochemistry. 54(1):1-29.

Weiner S, Hood L. 1975. Soluble protein of the organic matrix of mollusk shells: A potential template for shell formation. Science. 190(4218):987-989.

Weiner S, Traub W. 1980. X-ray diffraction study of the insoluble organic matrix of mollusk shells. FEBS letters. 111(2):311-316.

Weiner S, Traub W, Lowenstam H A. 1983. Organic matrix in calcified exoskeletons. Biomineralization and Biological Metal Accumulation: Biological and Geological Perspectives Papers presented at the Fourth International Symposium on Biomineralization, Renesse, The Netherlands, June 2–5, 1982; 1983: Springer.

Wheeler AP, Rusenko KW, Swift DM, Sikes CS. 1988. Regulation of in vitro and in vivo caco3 crystallization by fractions of oyster shell organic matrix. Marine Biology. 98(1):71-80.

Wheeler AP, Sikes CS. 1984. Regulation of carbonate calcification by organic matrix. American Zoologist. 24(4):933-944.

Whitney NM, Johnson BJ, Dostie PT, Luzier K, Wanamaker AD. 2019. Paired bulk organic and individual amino acid δ15n analyses of bivalve shell periostracum: A paleoceanographic proxy for water source variability and nitrogen cycling processes. Geochimica et Cosmochimica Acta. 254:67-85.

Wonham MJ. 2004. Mini-review: Distribution of the mediterranean mussel, mytilus galloprovincialis (bivalvia: Mytilidae), and hybrids in the northeast pacific. Journal of Shellfish Research. 23(2):535-544.

Xiang Q, Liu G, Meng Y, Chen K, Xia C. 2022. Temporal trends of deuterium excess in global precipitation and their environmental controls under a changing climate. Journal of Radioanalytical and Nuclear Chemistry. 331(9):3633-3649.

Yan H, Liu C, An Z, Yang W, Yang Y, Huang P, Qiu S, Zhou P, Zhao N, Fei H et al. 2020. Extreme weather events recorded by daily to hourly resolution biogeochemical proxies of marine giant clam shells. Proc Natl Acad Sci U S A. 117(13):7038-7043.

Yang K, Han G. 2020. Controls over hydrogen and oxygen isotopes of surface water and groundwater in the mun river catchment, northeast thailand: Implications for the water cycle. Hydrogeology Journal. 28(3).

Zilhão J, Angelucci DE, Badal-García E, D'Errico F, Daniel F, Dayet L, Douka K, Higham TFG, Martínez-Sánchez MJ, Montes-Bernárdez R et al. 2010. Symbolic use of marine shells and mineral pigments by iberian neandertals. Proceedings of the National Academy of Sciences. 107(3):1023-1028.

CHAPTER 4 – CONCLUSIONS AND OUTLOOK

The goal this thesis aimed to achieve is to improve the understanding of mollusk shells and their use in the study of human evolution. Archeological mollusk shells represent a valuable resource for archeologists, paleontologists, radiocarbon researchers and sclerochronologists, to name a few. The lack of well-preserved human remains in many archeological sites makes mollusk shells an important material to use for radiocarbon dating and paleoenvironmental reconstructions. This is especially important for the key period of the Middle to Upper Paleolithic transition, when the first *Homo sapiens* populations migrate out of Africa, trough the Levantine corridor and encounter the Neanderthal populations inhabiting Europe. The frequent use of mollusks by human populations of both *Homo sapiens* and Neanderthals in their diet and as tools or ornaments, allows researchers to obtain information on human presence and activity by using shells, even when other materials are unavailable. However, the complexity of the carbonate structure and the many possible confounding factors make it difficult to reliably use mollusk shells for the construction of radiocarbon chronologies. In this thesis, we attempted a new methodological approach, for the first time using the organic fraction of the shell for both radiocarbon dating and (paleo) environmental reconstruction. The results of this thesis provide a starting point for future research, demonstrating the potential of the often-overlooked organic fraction of the shells, underlining potential issues with the extraction method, and recommending advancements for future experimental designs.

For this thesis, several experiments using modern and archeological shells were performed to explore the extent to which the organic matrix of mollusk shells can be used for the study of human evolution. The first part of the PhD project was focused on using this approach for radiocarbon dating. The experiments performed were based on the assumption that the extraction of the organic matrix from the shells could be a potentially useful method for radiocarbon dating, given that the intracrystalline organic matrix of the shell is protected from the surrounding environment in a closed system. To test this hypothesis, we applied two newly proposed methods of organic matrix extraction (Method A and B) to modern and archeological shells, along with two methods from literature (Method C and D) focused on the carbonate fraction. The first set of experiments was performed on modern samples to familiarize with the protocols, evaluate the materials and time necessary for each method and make adjustments where needed. Method A was based on a protocol routinely used on modern shells and coral samples in studies focusing on the intracellular proteins. The advantage of this method is the use of a dialysis membrane, which allows to extract both the soluble and the insoluble organic matrix from the shell and minimize the loss of organic material. The application of this method to modern shells allowed for the estimation of the time needed to dissolve the entire carbonate fraction, while maintaining the organic matrix fraction. The method was performed at different temperatures and with various initial weights of the sample material, to evaluate the effect these

parameters have on the weight yield and adjust them accordingly. Method B followed mostly the same steps as Method A, although it did not include the use of a dialysis membrane. It was developed based on the collagen extraction method routinely used on bone samples for radiocarbon dating. The application of this method on modern shells has allowed to estimate the time needed for the dissolution of the carbonate fraction, similarly to Method A. Method C corresponds to the Carbonate Density Separation (CarDS) protocol, used to separate the aragonite from the calcite in shells and thus allow the removal of the potentially recrystallized calcite portion. The complexity of this method required several trials on pure aragonite and calcite powders, as well as modern shells, to assess the correct proportion of the solutions needed before proceeding with the application to archeological samples. Finally, Method D followed the standard acid etching pretreatment protocol, which serves to remove the outer portion of the shells and is routinely used in many radiocarbon laboratories before dating shells. The application of this method on modern shells served to estimate the time needed to dissolve the outer portion of the samples, without losing too much material.

Once the protocols were established on modern specimens, they were applied to archeological samples from the well-known Upper Paleolithic site of Vale Boi in Portugal. This site is situated between two different environments: the Mediterranean and Atlantic coasts, and it represents the earliest recorded *Homo sapiens* occupation in southwestern Iberia, as attested by the Early Gravettian remains dated to c. 32 ka cal BP. This site has a long stratigraphic sequence spanning from the Early Gravettian to the Magdalenian and was interpreted as a seasonal residential camp for different human populations. Furthermore, the abundance of different mollusk species uncovered throughout the stratigraphic sequence of the site demonstrates the continued use and importance of mollusk shells as an essential resource. The samples for this thesis were selected from one of the three excavated areas of the site - the Terrace, which has the longest and most complete stratigraphic sequence. It spans different time periods starting from Early Gravettian (Layers 8 – 6), Gravettian and Proto-Solutrean (Layer 5), Solutrean (Layer 4) and Epipaleolithic (Layer 3) allowing the application of the methods to samples of different ages. Furthermore, radiocarbon dates on mollusk shells and other materials from this area were already available, allowing for a comparison not only among the four methods but also to previous results.

In this thesis, both methods of organic matrix extraction (Method A and B) resulted in low weight yields for both modern and archeological specimens. This result was expected, given that the organic matrix makes up for less than 5% of the shell weight. Consequently, it is important to take into consideration the large amount of material (~2g) needed to perform the organic matrix extraction compared to the amount needed for the carbonate pretreatment (~100mg). In many archeological sites the amount of material is limited and the samples fragmentary, hence restricting the range of applications of the organic matrix extraction

method. Furthermore, for the archeological specimens from Vale Boi, the carbon yields for these two methods were low as well, and the resulting radiocarbon ages were significantly younger than those from carbonate fractions of the same shell specimens pretreated with Methods C and D. This means that both methods used for organic matrix extraction allowed for the introduction of modern carbon. Further research is needed to explore ways of extracting the organic matrix without the risk of introducing this type of contamination. Therefore, Methods A and B would need to be further developed in terms of contamination prevention and yield increase before they can be considered for routine application in radiocarbon dating.

The CarDS method (Method C) was found to be a difficult to perform, yet useful method for aragonite and calcite separation in shells presenting both calcium carbonate polymorphs in significant amounts, as was the case for modern specimens used in this thesis. However, the X - Ray Diffraction (XRD) analysis showed that most of the archeological samples consisted of one of the two polymorphs and the traces of the other polymorph were difficult to remove. Moreover, the ages obtained on the two fractions resulting from the calcite-aragonite separation were similar, and significantly younger than those obtained from Method D in all the archeological layers except for Layer 4. Therefore, the application of this method did not have enough of an effect to justify the effort of performing the pretreatment. Furthermore, there could be diagenetic effects in the shells that occur without aragonite to calcite transformations, which would not be detected by XRD nor removed by this method. In fact, the results of pyrolysis (Py – GC – MS) performed in this study showed signs of degradation of the organic matter, extracted from the same shell samples which did not show recrystallization in the XRD. This is indicative of diagenesis processes which were not detected in the XRD analyses since they did not cause apparent recrystallization. Therefore, we can conclude that the CarDS method is a complex method, which should be used only in cases where there is a significant amount of recrystallization, and it should ideally be combined with other methods of sample preservation verification other than XRD. Multiple lines of analysis should routinely be performed to determine the state of preservation of archeological shell samples (e.g., XRD, Py-GC-MS, Scanning Electron Microscopy - SEM, Fourier Transform Infra-Red spectroscopy - FTIR etc.) before choosing the appropriate pretreatment protocol to perform (CarDS or acid etching).

Finally, the standard acid etching method (Method D) was the quickest and simplest method performed, and it gave results close to the expected ages for the archeological specimens, compared to the other methods. Thus, so far, it remains the best method to use for mollusk shell pretreatment prior to radiocarbon dating.

When comparing the results of the four methods, the ages obtained on the archeological specimens from the Vale Boi site overlapped only in Layer 3 attributed to the Epipaleolithic. This might be due to the use

of a different species of mollusk shell (*Crassostrea* sp.) in Layer 3 compared to the rest of the archeological sequence analyzed (*Pecten* sp.). This result emphasizes the importance of species selection prior to radiocarbon dating. The phylum Mollusca is an incredibly rich and diverse phylum, and it is important to consider their biology and ecology to better understand how they were collected and used at the archeological site. For example, the species used in this study – *Pecten* sp. is a species that lives at a depth of ~10 - 110m which means it was not collected live, but most likely beached. Thus, it could not have been used as food, rather as a tool or ornament. This means that different shells found in the same layer could have very different ages despite being used and deposited at the site in the same period. We selected this species due to the amount of material needed to perform multiple methods on a single shell for comparison. Other species from the Terrace area of the Vale Boi site, which might have been collected live for consumption, were too fragmentary and small, thus not having enough material to perform all four methods and make the comparison performed in this thesis. Ideally, in an archaeological study dating a site for the first time it would be best to select species which were collected live and used as food, so that there is a tighter connection between the dated event (mollusk death) and the target event (human presence).

When comparing the four methods to previous results and the archeological attributions, the results were inconsistent for the shells analyzed in the Terrace area of Vale Boi. Furthermore, even dates on two bones from Layer 6 gave significantly different ages, suggesting an issue outside of the simple shell pretreatment. Indeed, potential mixing in the stratigraphical sequence at the Vale Boi site was identified in previous work, and some of the inconsistencies in ages obtained from the different layers in this study are likely due to factors not directly linked to dating shells. However, dates obtained from the same individuals using different methods showed significant differences, highlighting the importance of using efficient pretreatment protocols. These results underlined the difficulty of obtaining reliable radiocarbon dates on marine mollusk shells, and the need for additional method improvements for their pretreatment and contamination removal.

To achieve the best results in terms of radiocarbon determinations and interpretations, there is a need for close collaboration between archeologists, (bio - geo) chemists, radiocarbon specialists and malacologists in future studies involving the use of mollusk shells. This way the species and sample selection can be performed so that the confounding factors related to the mollusk biology, the way they were collected and used by the human populations being studied, as well as their stratigraphic/archeological attribution are preferably removed or accounted for in the interpretation of the radiocarbon date. Furthermore, careful sample preservation assessment using different techniques prior to the selection of pretreatment protocol can be undertaken to select the most well-preserved samples and the most appropriate pretreatment method.

The second part of this PhD project focused on the application of the organic matrix extraction method (Method A) to the study of environmental parameters using stable isotopes of mollusk shells. The advantage of using the organic matrix fractions instead of the calcium carbonate, which is typically used for (paleo) environmental studies, is that it allows for the measurement of hydrogen (δ^2H) as well as oxygen ($\delta^{18}O$) stable isotope ratios. Hydrogen and oxygen have a global empirical relationship in precipitation defined as the Global Meteoric Water Line (GMWL). Depending on local environmental conditions this relationship varies forming Local Meteoric Water Lines (LMWL). Comparing these relationships with the ones obtained from the organic matrix can give insight into the amount of environmental signal maintained in the isotopic signature of the organic matrix of mollusk shells. So far, there is only one available study comparing the stable isotope ratios of bulk organic matrix of mollusk shells to the GMWL. The experiments in this thesis were the first to perform stable isotope measurements on the soluble (SOM) and insoluble (IOM) fraction of the organic matrix separately, and compare them to the GMWL, and LMWL of the study area. Furthermore, this was the first time the variation of stable isotopes from the organic matrix was investigated along a geographical gradient from the beach to the upper estuary. The shells used for this study were modern specimens collected from three sites in Cantabria, Northern Spain: Berria beach, Montehano (lower estuary) and Carasa (upper estuary). The results showed a much higher variability in terms of δ^2H and $\delta^{18}O$ in the SOM compared to the IOM. Indeed, the isotope values, especially the δ^2H, differed among the three localities in the SOM. We observed a gradient in δ^2H starting from very negative values at the coast towards more positive values in the upper estuary, which is opposite to the observed variation in $\delta^{18}O$, and opposite to expected water composition depending on Rayleigh fractionation. This indicates that different fractionation processes affect hydrogen and oxygen incorporation into the shell organics. They might be related to different dietary inputs, metabolic or enzymatic activity during biomineralization. More data on modern shells, including phytoplankton and water δ^2H and $\delta^{18}O$ measurements and further research on the lipid content in the soluble and insoluble fraction of the organic matrix might contribute to the understanding of some of the differences in isotope ratios observed in this thesis. Furthermore, there were positive correlations between δ^2H and $\delta^{18}O$ in the IOM subparallel to those of GMWL and LMWL and whose slopes follow the coast - estuary gradient. This indicates that an environmental signal might also be encoded in the IOM fraction. The results obtained for this thesis show an overall potential in using shell organic matrix in (paleo) environmental studies and more research will be needed to clarify and further develop the application of our observations. Given the differences among the two fractions of the organic matrix, future studies should maintain the division into the SOM and IOM and analyze them separately. Once these findings are established on modern specimens, this approach can be applied to archeological specimens in order to reconstruct past environments and elucidate events in prehistory, which could in turn, affect our understanding of human evolution.

The work presented in this thesis shows a state-of-the-art approach to the application of radiocarbon dating and stable isotope analysis, adding a significant contribution to the study of mollusk shells. The results obtained during this Ph.D. project demonstrate the high potential of the organic matrix for radiocarbon dating and stable isotope analyses, opening new directions for research focused on mollusk shells and their use in human evolution and paleoclimate studies. Furthermore, this approach can be applied not only to the study of human evolution but also to other research fields such as climate and environmental studies, and mollusk biomineralization and physiology studies.